Universidad Pública de Navarra
Nafarroako Unibertsitate Publikoa

Public University of Navarre

Electric, Electronical and Communication Engineering Department

Contribution to the development of Optical Fibre Sensors based on Microstructured Optical Fibres to detect gases and Volatile Organic Compounds

PhD Dissertation by

Diego López Torres

Advisors

Dr. César Elosúa Aguado

Prof. Francisco J. Arregui San Martín

Pamplona, July 2019

Universidad Pública de Navarra
Nafarroako Unibertsitate Publikoa

Universidad Pública de Navarra

Departamento de Ingeniería Eléctrica, Electrónica y de Comunicación

Contribución al desarrollo de sensores de fibra óptica basados en fibras micro estructuradas para la detección de gases y compuestos orgánicos volátiles

Memoria de la tesis redactada por

Diego López Torres

Directores de tesis

Dr. César Elosúa Aguado

Prof. Francisco J. Arregui San Martín

Pamplona, Julio 2019

Tesis Doctoral

Contribution to the development of Optical Fibre Sensors based on Microstructured Optical Fibres to detect gases and Volatile Organic Compounds

Autor: Diego López Torres

Directores: Dr. César Elosúa Aguado
Prof. Francisco J. Arregui

Tribunal nombrado para evaluar la citada Tesis Doctoral:

Presidente: _____

Secretario: _____

Vocal: _____

Revisores externos:

_____

_____

Acuerda otorgar la calificación de:

_____

En Pamplona, a _____ de _____ de 20___

A los que me quieren

y me cuidan...

ACKNOWLEDGMENTS

The development of this work has been possible thanks to the economic efforts made by the Public University of Navarra (UPNA) and by the sponsoring of the Spanish Ministry of Economy and Competitiveness, through the investment in the following projects: CYCIT FEDER TEC2013-43679-R and TEC2016-79367-C2-2-R. This work also supported by the Government of Navarre through the Project with reference 2016/PI012 EXCELSEN and by Fundación CAN trough the projects CAN2015-70221 and BINACS. Bio Inspired Nanocoatings for Cellular Scaffolds.

NAITEC must also be acknowledged for the utilization of their facilities and Nadetech Innovations for their technical support, as well.

RECONOCIMIENTOS

La realización de este trabajo ha sido posible gracias a las aportaciones económicas recibidas por parte de la Universidad Pública de Navarra (UPNA), así como del patrocinio de la UPNA y del Ministerio de Economía y Competitividad, a través de los proyectos CICYT fondos TEC2013-43679-R, TEC2016-79367-C2-2-R. Este trabajo fue posible también gracias a los proyectos concedidos por el gobierno de Navarra, con referencia 2016/PI012 EXCELSEN y a la financiación otorgada por la Fundación CAN a través de los proyectos CAN2015-70221 y BINACS: Bio Inspired Nanocoatings for Cellular Scaffolds.

También se quiere agradecer a NAITEC las facilidades prestadas para la utilización de sus equipos, así como a Nadetech Innovations por el servicio técnico prestado.

AGRADECIMIENTOS

Mucho tiempo llevaba esperando a que llegase este momento. El momento de escribir estas líneas y cuando llega… me parecen que son las líneas más difíciles de toda la tesis. Aún me veo, como si fuera ayer, entrando en el despacho de Patxi a preguntarle sobre las opciones que me podía ofrecer para desarrollar mi proyecto *"fin de carrera"*. Unos cuantos años después… aquí sigo. Aquel día me habló de un señor alemán, con una trayectoria súper contrastada como científico, que justo había publicado un "*paper"*, con una teoría que podía dar de qué hablar. Y mirar que si ha dado que aún seguimos trabajando en ella, pero ahora, codo con codo con aquel señor alemán tan importante.

Así que mi primer agradecimiento no puede ser más que para Patxi y César. También recuerdo con mucho cariño, César, un café contigo en la cafetería después de mis primeros 4 meses sin obtener ningún resultado positivo: esto es ciencia me dijiste… luego lo aprendí, pero puede que aquellos minutos fueran el detonante de que ahora esté escribiendo estas frases. Gracias por darme la oportunidad que me habéis dado, de formarme científicamente y humanamente, por creer en mí, por ayudarme siempre que lo necesitaba y, sobre todo, por tener tanta paciencia, que sé que alguna vez os la he puesto a prueba. También quiero hacer extensible este agradecimiento a todo el grupo de *"profes de sensores"*, los cuales siempre han tenido un minuto para mí y ha sido un auténtico placer trabajar a vuestro lado. Gracias Nacho, Jesús, Goico, Miguel, Carlos, Ignacio, Cándido y cómo no, a los nuevos profes Aitor, Abián y Pedrinho… vuestros consejos siempre eran y son bien recibidos.

Especiales quiero, y tienen que ser, mis palabras para mi gente del día a día durante estos años. Ya no somos compañeros, ya somos buenos amigos: gracias Juako por no desesperar con todas las discusiones que hemos tenido hasta las tantas; gracias también a la reina "*reina del Cidec"*… de no hablar más de una hora juntos durante toda universidad y casi matarnos en nuestros primeros meses hasta ahora… al final, creo que no ha salido del todo mal la cosa; gracias a mi JM, sin más palabrería, por ser como eres; y como no, a mi pimuti… poco más que decirte y, aunque a Andy no lo tengas muy contento, dentro de unos pocos días lo celebramos en un día grande ;). No me quiero olvidar de mi despacho. Gracias Paola, Aritz, Vero y especialmente Aitor. Amigo antes de empezar esta

etapa; más amigo al acabarla. Gracias por todas las tardes de discusiones, de pensar en nuevas ideas y también, por qué no decirlo, de risas que nos hemos pegado entre esas cuatro paredes (sigo sin escuchar aún, una risa más contagiosa que la tuya). También quiero acordarme, y aunque no llevemos mucho tiempo juntos, de la nueva hornada del grupo: Desiré, María Elena, Dina y mi comandante Omar. Gracias por transmitirnos la ilusión con la que habéis comenzado. Aprovechad esta oportunidad que tenéis; estoy seguro de que os va a marcar de por vida. Y ya por último, a la pareja de frontenis que más me ha divertido (no creo que haga falta especificar más). Nos hemos conocido tarde, pero tiempo más que suficiente para que nuestra amistad siga creciendo.

Antes de seguir con los agradecimientos más personales, no puedo, ni quiero dejar pasar la oportunidad de agradecer a aquellas personas que, de una forma u otra, han formado parte de mi vida durante este largo camino que ha sido mi tesis. Puede que nunca lean estas líneas, pero yo siempre las tendré muy presentes. Los que sí espero que las lean son mis "*Irish Gudaris*". No sé muy bien que pasó en Dublín, bueno si… ¡¡¡la magia!!! Y supongo que las Guinness… sólo deseo que lo que tenemos ahora siga creciendo al ritmo que lo está haciendo. Gracias de corazón por todos esos momentazos que habéis querido compartir conmigo. También me gustaría agradecer a la Prof. Yuliya Semenova, la oportunidad que me dio de realizar mi estancia de investigación con ella. Fue un auténtico placer. Y cómo no, a mis compis de piso: Mad, Héctor y Javi… gracias por tener siempre esos minutitos conmigo para lo que fuera necesario.

Qué decir también de mi cuadrilla. Un millón de gracias. De verdad que no sabéis lo que valen vuestras risas, vuestras charlas, vuestros consejos… muchas veces no os habréis dado ni cuenta… el Lenny es así, pero de corazón os digo que habéis sido la fuerza que necesitaba para empezar de nuevo el lunes con las pilas cargadas. Una parte de esta tesis también es vuestra.

Y las últimas líneas no pueden ir más que dedicadas a mi familia y en especial, a mis padres. Siempre os digo que ha sido la mejor herencia que me habéis podido dar. No soy una persona de mucha expresividad ni palabras, pero gracias por todo: por la paciencia que tenéis conmigo, por haberme dado esta forma de pensar y de entender el mundo, por dejarme equivocarme para poder aprender… gracias familia por todo el apoyo constante que me habéis dado, por esas video llamadas haciéndome partícipe de vuestra alegría… se OS QUIERE!!!!

Muchas gracias a todos, Diego.

ABSTRACT

Since the first publications related to Microstructured Optical Fibres (MOFs), the development of Optical Fibre Sensors (OFSs), based on this type of fibres, has been increased attracting the interest of many research groups because of the important role that they play in diverse applications. Due to their unique geometric structures and features, MOFs are very useful for optical sensing applications, especially gases and Volatile Organic Compounds (VOC) sensing. Taking it into account, this PhD. work proposes the utilization of MOFs to carry out and to develop new structures and set-ups capable to detect these parameters, gases and VOCs. Moreover, different studies and techniques, such as Fast Fourier Transform (FFT) or WDM multiplexing, have been used with the aim of improving the features of the sensors trying to make the final system as competitive as possible.

RESUMEN

Desde la primera publicación relacionada con las fibras micro estructuradas (MOFs), el desarrollo de sensores basados en fibra óptica (OFSs), que utilizan este tipo de fibras, se ha visto incrementado atrayendo el interés de numerosos grupos de investigación debido al importante papel que juegan en numerosas aplicaciones. Debido a sus propiedades y estructuras únicas, las MOFs son muy útiles en aplicaciones ópticas de sensado, especialmente de gases y compuestos orgánicos volátiles (VOCs). Por estas razones, esta tesis doctoral propone la utilización de este tipo de fibras para generar y desarrollar nuevas estructuras y montajes, capaces de detectar estos parámetros, gases y VOCs. Además, se han realizado diferentes estudios y se han utilizado diferentes técnicas (destacando la transformada rápida de Fourier (FFT) y la multiplexación WDM…), para mejorar las características de los sensores, intentando conseguir de esta manera que el sistema final fuera lo más competitivo posible.

ÍNDICE

Capítulo 1

Introducción: motivación y objetivos para la realización de esta tesis

El este primer capítulo de esta tesis se describen y enumeran los principales factores por los cuales se decidió apostar y realizar este trabajo, basado en fibras micro estructuradas para la detección de gases y VOCs. Se exponen las principales motivaciones y los objetivos planteados, así como un breve resumen de la organización del documento, explicando a grandes rasgos lo que contiene cada uno de los capítulos que forman esta tesis.

1.1. Motivación y objetivos

Un sensor no es más que un dispositivo diseñado para recibir información de una magnitud del exterior y transformarla en otra magnitud. Es decir, los sensores son la herramienta que pone a nuestra disposición la ciencia y la tecnología para poder medir magnitudes o parámetros que se escapan de la percepción humana. La ciencia y tecnología de los sensores han facilitado que haya cada vez más dispositivos a nuestro alrededor, capaces de procesar enormes cantidades de datos para ayudar a mejorar el funcionamiento de las fábricas, el control de procesos productivos, optimizar las cosechas, la detección de terremotos y así se podrían enumerar un sinfín de aplicaciones. En definitiva, intentan mejorar la vida y la sociedad de los seres vivos [1]. Por lo tanto, en la actualidad, existen una gran cantidad de aplicaciones que necesitan de las aportaciones de los sensores en prácticamente cualquier sector de la sociedad.

Desde un punto de vista ingenieril, los sensores se pueden dividir según el tipo de variable medida. Entre ellos se pueden encontrar sensores mecánicos, sensores electrónicos, sensores magnéticos, sensores acústicos, sensores ultrasónicos, sensores químicos, sensores de radiación y sensores ópticos. Respecto a este último grupo, el campo de la fibra óptica ha experimentado en las últimas décadas una importante evolución y los sensores ópticos, han emergido como una solución real y creíble para intentar solventar algunas de las principales limitaciones que presentan otros sensores más convencionales. Por esta razón, el uso de esta tecnología para implementar sensores es muy prometedora porque, por ejemplo, la fibra óptica es químicamente inerte y pasiva electromagnéticamente hablando. Por lo tanto, puede trabajar en entornos explosivos como depósitos de combustible, o con campos eléctricos intensos. Además, la fibra óptica permite obtener una gran cantidad de información de diferentes sensores, los cuales pueden estar separados entre sí por largas distancias de hasta cientos de kilómetros. Otra cualidad importante de los sensores de fibra óptica es que son compactos, pequeños y ligeros. Estas propiedades se han aprovechado en numerosas aplicaciones ópticas con unos resultados muy interesantes [2].

Son varias las estructuras de sensado, basadas en la utilización de la fibra óptica, las cuales han sido propuestas en la última década. Mencionando algunos

ejemplos, existen sensores de fibra óptica basados en redes de *"Fibre Bragg Gratings"* (FBGs, siglas en inglés) [3], en redes *"Long Period Gratings"* (LPGs, siglas en inglés) [4], en interferómetros [5], en resonancias electromagnéticas [6] o en fibras micro estructuradas (MOFs, siglas en inglés) [7], [8].

Las MOFs son un tipo de fibra óptica que presentan nuevas características, más allá de las básicas y generales de las que presentan las fibras ópticas convencionales. Si son utilizadas de forma correcta, pueden ser muy ventajosas para los sensores. Debido a sus estructuras geométricas únicas, las MOFs presentan propiedades y capacidades especiales que les otorgan un potencial excepcional para desarrollar sensores de fibra, especialmente los basados en la detección de gases [9] o compuestos orgánicos volátiles (VOCs, siglas en inglés) [10]. Además, el desarrollo de nuevos materiales sensibles y métodos de deposición, a escala nanométrica, ha significado también una importante mejora en las características finales de los sensores y las aplicaciones.

Pensando en obtener el máximo rendimiento posible de todo el potencial que ofrecen las MOFs, esta tesis propone el desarrollo de nuevas configuraciones y estructuras sensoras, aún no presentes en la literatura, basadas en la utilización de este tipo de fibras. Además, también propone la utilización y deposición de nuevos materiales sobre estas novedosas estructuras, con la intención de mejorar las sensibilidades de los sensores previos utilizados para la detección de gases y VOCs, los cuales pueden llegar a ser perjudiciales y peligrosos para los seres vivos. Estos nuevos retos propuestos se han desarrollado dentro del grupo de "*Comunicaciones Ópticas*" de la Universidad Pública de Navarra (UPNA), teniendo como referencia en determinadas fases de la investigación, estudios previos llevados a cabo por este grupo, como, por ejemplo, los realizados en temas relacionados con la deposición de materiales, las técnicas de post procesado o los montajes utilizados. En resumen, esta tesis propone el desarrollo y optimización de sensores, basados en MOFs, para la detección y análisis de gases y VOCs, intentando crear y desarrollar una nueva vía de investigación para trabajos venideros.

1.2. Organización de la tesis

En esta tesis, se presentan las diferentes contribuciones científicas que se han obtenido durante su proceso de realización. Para facilitar la lectura y comprensión al lector, esta tesis se divide en 5 capítulos, los cuales se exponen de forma progresiva, con una breve introducción previa que intenta contextualizar el porqué de cada una de las decisiones que fueron tomadas. Por lo tanto, cada capítulo no puede ser visto de una forma aislada, ya que sus resultados y conclusiones son la base de los siguientes pasos dados.

El capítulo dos de esta tesis engloba un estudio de las diferentes publicaciones encontradas, hasta la fecha, de sensores que utilizan MOFs para detectar gases y VOCs. La idea es estudiar los métodos de transducción que más se utilizan junto a sus las estructuras, para fijar un punto de partida e intentar introducir cambios para mejorar los resultados obtenidos.

El capítulo tres de la tesis, trata de explicar y mejorar una estructura basada en MOFs, para la medición de humedad. En este caso se propone su optimización cambiando los materiales sensibles depositados y su técnica de deposición. Además, se realiza un comparativa entre varias técnicas de procesado para definir cuál es la más relevante.

En el capítulo cuarto se propone, vistos los buenos resultados obtenidos en el capítulo anterior la mejora y optimización de un sensor de humedad, utilizar el mismo proceso, pero cambiando solo la estructura sensora utilizada, es decir, la MOFs utilizada.

En el capítulo quinto se presentan diferentes estudios realizados para optimizar las sensibilidades obtenidas para detectar gases y VOCs. Parámetros como las dimensiones de las diferentes MOFs utilizadas, la potencia que pueden acoplar cada una de ellas o el efecto del espesor de las películas sensibles en la sensibilidad final son alguno de los que han sido estudiados.

Por último, en el capítulo sexto, se propone la utilización de los sensores desarrollados para aplicaciones reales. Una de ellas se basa en la multiplexación para generar una red de sensores capaz de detectar diferentes parámetros (gases, VOCs, humedad, temperatura…); la otra, es la utilización de un sensor para

medir la humedad de suelos con diferentes propiedades, comparando su comportamiento con un sensor capacitivo.

Para terminar de explicar todos los bloques que componen esta tesis, se presenta también un capítulo con las conclusiones más importantes que se derivan del trabajo realizado, así como el estudio de las propiedades de una pareja de polímeros, poly(sodium phosphate) (PSP) y poly(allylamine hydrochloride) (PAH), los cuales tienen un comportamiento anómalo cuando se depositan bajo unas determinadas condiciones.

Capítulo 2

MOFs utilizadas para la detección de gases y VOCs: estado del arte

Desde las primeras publicaciones relacionadas con las fibras micro estructuradas, el desarrollo de sensores basados en este tipo de fibras ha atraído el interés de numerosos investigadores dadas sus propicias estructuras para el sensado de varios parámetros, entre los que se encuentran los gases y VOCs. Este capítulo trata de proporcionar un estado del arte de las publicaciones más relevantes en las cuales, las fibras micro estructuradas han sido utilizadas para la detección de gases o VOCs.

2.1. Introducción: clasificación de las MOFs

Los sensores de fibra óptica (OFS, siglas en inglés) son utilizados en numerosas aplicaciones relacionadas con el sector industrial, químico y medioambiental [11]–[13]. Estudiando las variaciones en la potencia óptica, los desplazamientos en la fase, en la longitud de onda o en el estado de la polarización, los OFS pueden ser utilizados para medir magnitudes como, temperatura, curvatura, desplazamientos, presión, índices de refracción, campo eléctrico, humedad relativa (RH, siglas en inglés) y gases [14]–[17], entre otros. Comparados con sus homólogos, los sensores electrónicos, los OFS ofrecen numerosas ventajas. Por ejemplo, son pasivos ya que no necesitan de alimentación eléctrica e inmunes a las interferencias que generan los campos electromagnéticos (lo cual hace que sean una alternativa a tener en cuenta para operar en entornos con condiciones ambientales extremas), tienen un peso ligero, presentan muchas menos pérdidas de transmisión y pueden ser multiplexados en longitud de onda [18].

Gracias al esfuerzo realizado por diferentes grupos de investigación desde la década de los 70 [19], [20], un nuevo y prometedor tipo de fibras ópticas, llamado Fibras Ópticas Micro Estructuradas (MOFs, siglas en inglés) fue concebido. Debido a este hecho, el desarrollo de los OFS experimentó una sustancial mejora en términos de sensibilidad, selectividad y tiempos de recuperación o respuesta. La diferencia entre las MOFs y las fibras ópticas de comunicación estándar (fibras monomodo (SMF, siglas en inglés) y fibras multimodo (MMF, siglas en inglés)) es clara: las fibras estándar se basan en un núcleo sólido dopado encerrado por un recubrimiento sólido (en la Figura 2.1 (a) se muestra un ejemplo esquemático de esta estructura). Esta configuración implica una diferencia entre los índices de refracción del núcleo y del recubrimiento que permite que la luz se guíe mediante el mecanismo denominado *"reflexión total interna"* (TIR, siglas en inglés). Por otro lado, la geometría de las MOFs consiste en una serie de agujeros de aire (presentes desde su fabricación), los cuales se encuentran a lo largo de toda su estructura con diferentes dimensiones y patrones dependiendo del tipo de fibra. Tomando como punto de partida las diferentes geometrías, dimensiones, posiciones y formas de los agujeros de aire, hay diferentes criterios para agrupar los tipos de MOFs que existen. Uno de los más aceptados es dividir dichas fibras en dos grandes

familias: fibras de cristal fotónico (PCFs, siglas en inglés) y fibras de núcleo suspendido (SSCs, siglas en inglés).

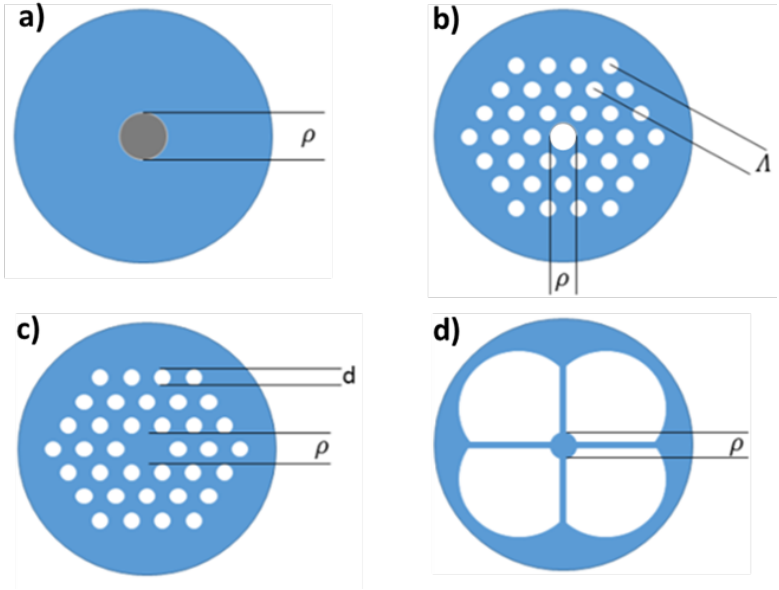

Figura 2. 1 *Dibujo de la sección transversal de una SMF de comunicaciones estándar (a), una fibra de cristal fotónico de núcleo hueco (HC-PCF) (b), una fibra de cristal fotónico de núcleo sólido (SC-PCF) (c) y una fibra de núcleo suspendido (SSC). Los diferentes colores en la figura (azul, negro y blanco) indican las diferentes partes de las fibras: sílice, sílice dopado y agujeros de aire, respectivamente.*

Para facilitar al lector la compresión de esta tesis y la identificación de cada uno de los diferentes tipos de MOFs, a continuación, se muestra un esquema que resume y agrupa todos los tipos que existen en la actualidad (ver Figura 2.2); también se adjunta una foto real de cada una de las secciones transversales de las fibras para que sea más fácil su identificación.

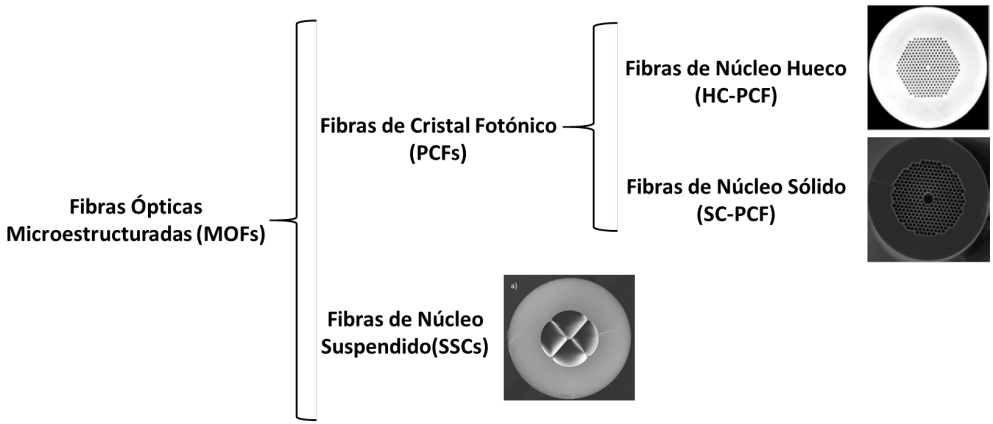

Figura 2. 2 *Esquema y clasificación de los tipos de Fibras Ópticas Micro Estructuradas basada en sus diferentes estructuras.*

La geometría del primer grupo (PCFs), propuesta in 1995 por Russell et al. [19]–[21], se caracteriza por una agrupación periódica de agujeros de aire recorriendo la totalidad de la longitud de la fibra, centrados sobre un núcleo hueco (HC-PCF) o un núcleo sólido (SC-PCF) (ver Figura 2.1 (c)). Es muy importante definir la estructura y geometría del núcleo de estas fibras porque este es el parámetro clave para realizar la subdivisión de las fibras PCFs que esta tesis propone.

Para el diseño de estas fibras es muy importante tener en cuenta estos tres parámetros: el diámetro del núcleo de la fibra (ϱ), el diámetro de los agujeros de aire del recubrimiento (d) y la distancia entre los centros de dos agujeros de aire consecutivos (Λ). Gracias al diseño de estos tres parámetros físicos (se muestran en la Figura 2.1) es posible conseguir distintas distribuciones de los modos de propagación de forma que se puedan confinar en el núcleo o llevar al recubrimiento. Además, debido a la posibilidad de elegir las dimensiones de los agujeros colindantes al núcleo de la fibra, es posible conseguir mayor interacción con el campo evanescente, lo cual es un punto muy interesante para el desarrollo de sensores ópticos. Todos estos factores hacen que las PCFs sean más versátiles que las fibras estándar. Las HC-PCFs (ver Figura 2.3), las cuales presentan una diferencia entre el índice de refracción del núcleo y del revestimiento negativa ($n_{core} < n_{revestimiento}$), no pueden operar vía TIR. Sin embargo, un diseño apropiado de su revestimiento agujereado a lo largo de toda la longitud de la fibra, permite que la luz se guie a través de su núcleo hueco. Las longitudes de

onda ópticas que no se pueden guiar debido a la estructura agujereada de dicho revestimiento, se denominan longitudes de onda prohibidas y son las que se confinan en el núcleo hueco de la fibra. A este nuevo modo de guiado se le denomina *"principio de banda de separación fotónica"* (PBG, siglas en inglés) [22].

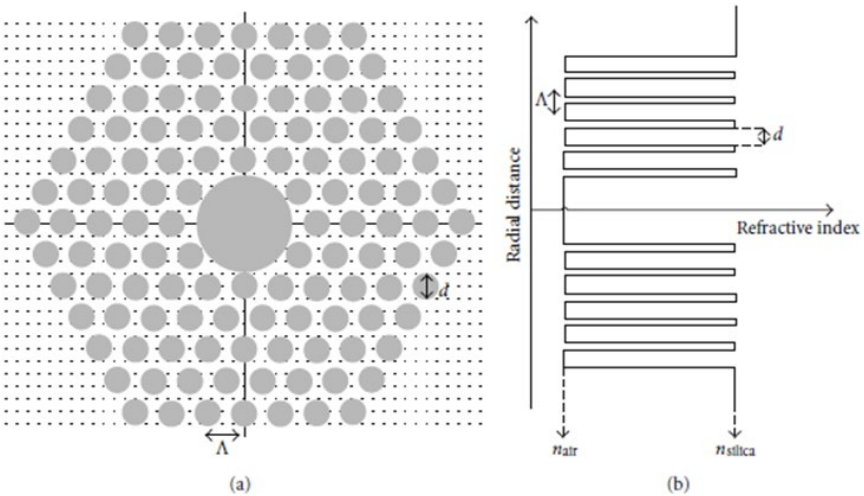

Figura 2. 3 *Ilustración de la sección transversal de una HC-PCF (a) y el respectivo perfil de su índice de refracción; el color gris representa las partes que son aire mientras que el blanco representa las zonas que son sílice. Figura utilizada con los permisos de [13].*

Con respecto a las SC-PCFs, su sección transversal presenta una agrupación periódica de agujeros de aire alrededor de un núcleo sólido, los cuales se extienden a lo largo de toda la longitud de la fibra sin ninguna variación [23]. Además, en las SC-PCFs, el índice de refracción efectivo del recubrimiento varía con la distancia radial, dependiendo de su material y geometría (ver Figura 2.4). Como consecuencia, cuando únicamente se utiliza un material para fabricar la fibra, el valor del índice de refracción efectivo del revestimiento será menor que el del índice de refracción del núcleo, permitiendo que el guiado de la luz sea mediante el principio TIR; de esta manera, se evita tener que dopar el núcleo con otro material para intentar conseguir que su índice de refracción aumente para satisfacer la condición $n_{core} > n_{revestimiento}$. Dado que las propiedades del guiado de la luz en las SC-PCFs no son consecuencia de la composición variable del cristal, como en las SMFs, sino de la agrupación y distanciamiento espacial de los agujeros de aire, el principio de guiado se conoce con el nombre de *"reflexión total interna modificada"* (*modified* TIR, siglas en inglés). Llegados a este punto, es

importante mencionar que, aunque experimentalmente en la mayoría de los casos el guiado de los modos en las SC-PCFs se basa en el mecanismo TIR, bajo unas correctas condiciones determinadas (una alta concentración de agujeros de aire en el recubrimiento), los mecanismos TIR y PBG pueden coexistir en las SC-PCFs [24]; un ejemplo son las fibras que tienen una diferencia positiva entre el índice de refracción del núcleo y el del revestimiento [25].

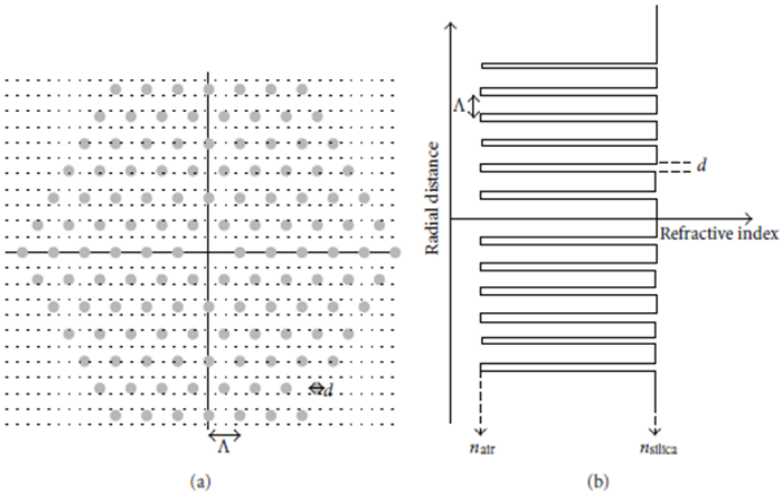

Figura 2. 4 *Ilustración de la sección transversal de una SC-PCF (a) y el respectivo perfil de su índice de refracción; el color gris representa las partes que son aire mientras que el blanco representa las zonas que son sílice. Figura utilizada con los permisos de [23].*

Por otro lado, siguiendo el esquema presentado en la Figura 2.2, el segundo grupo de MOFs es el de las fibras SSCs (ver Figura 1. (d)). El término de SSC es usado para describir las MOFs en las cuales la luz es guiada a través de un núcleo de dimensiones muy pequeñas. Las fibras SSCs suelen presentar agujeros con dimensiones relativamente grandes que rodean su núcleo (típicamente de unas pocas micras de diámetro) que parece estar suspendido a lo largo de la fibra, pero que a su vez está mantenido por unos pequeños puentes. En este tipo de fibras, el confinamiento del campo electromagnético no depende de la periodicidad de los agujeros: no se utiliza ningún efecto derivado del principio PBG para confinar dicho campo. De forma diferente a las PCFs, las propiedades del guiado de la luz se pueden explicar parcialmente gracias a la teoría TIR.

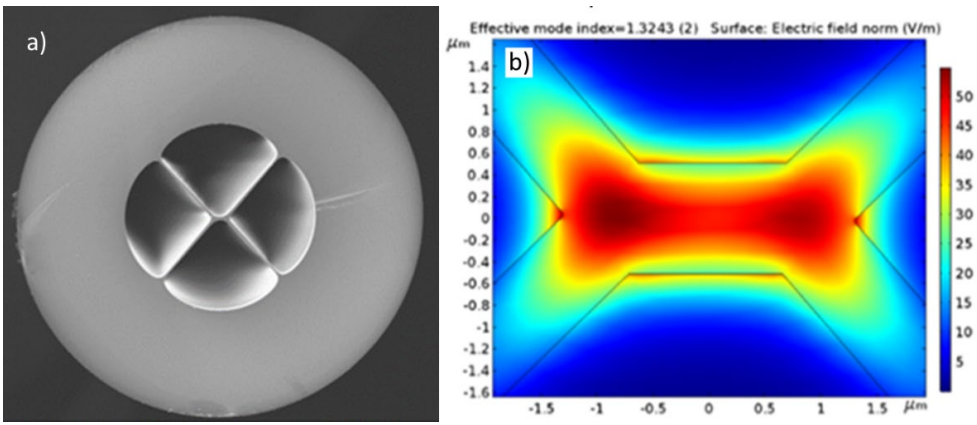

Figura 2. 5 *A la izquierda, detalle de la sección transversal de una SSC (a); a la derecha, la distribución del campo del modo* LP_{01} *(b).*

Las peculiares estructuras de las MOFs pueden proporcionar a los sensores características sin precedentes, lo que las hace especialmente útiles para aplicaciones de sensado basadas en fibras ópticas, en comparación con las SMFs [7], [26], [27]. Por ejemplo, una de las más atractivas e importantes es que debido a su estructura basada en agujeros de aire, se puede controlar y modificar la interacción que se produce entre el campo evanescente de la luz guiada y el medio que rodea a la fibra óptica. En base a las características que ofrecen las MOFs y considerando su alta versatilidad, numerosas contribuciones científicas han demostrado que las MOFs son una buena alternativa para desarrollar sensores capaces de medir algunos de los parámetros físicos y químicos que demanda la sociedad en la que vivimos. Algunos ejemplos son: curvatura [28], tensión [29], temperatura [30], campo eléctrico y magnético [31], [32], torsión [33], índice de refracción [34], vibración [35] y ADN [36], entre otros.

Existen otros dos parámetros detectables muy importantes que no se han mencionado en la anterior enumeración como son los gases y los compuestos orgánicos volátiles (VOCs, siglas en inglés). Dichos parámetros, merecen un apartado especial porque son especialmente interesantes detectarlos utilizando MOFs. La principal razón es que, gracias a la presencia de los agujeros de aire en las MOFs, es posible su detección directa; existe la posibilidad de rellenar los agujeros con el propio gas o VOC en cuestión. Gracias a esta propiedad, las sensibilidades y las características de los sensores previos pueden ser mejoradas,

así como la detección en tiempo real. Por estas razones, el uso de las MOFs para la detección de gases y VOCs atrae el interés de numerosos grupos de investigación.

En la actualidad, y en base a la explicación previamente dada, el desarrollo de aplicaciones relacionadas con la detección de gases o VOCs, utilizando MOFs, está experimentando un considerable crecimiento. A su vez, debido a la gran variedad de clases distintas de MOFs que existen (diferentes núcleos, diferentes dimensiones y patrones de sus agujeros…), el mecanismo de transducción en el que se basan los sensores es distinto y depende en gran medida de la fibra utilizada. Con el fin de clarificar este importante aspecto, el siguiente apartado trata de resumir y explicar los más importantes e interesantes.

2.2. Mecanismos de transducción de los sensores

El término *"mecanismo de transducción de un sensor óptico"* engloba la explicación de cómo la luz que viaja por la fibra óptica se ve alterada por la presencia de un parámetro determinado que se desea medir, en este caso en concreto, con los VOCs o gases. Debido a su presencia, las condiciones del medio en el que se encuentra el sensor cambian y como consecuencia, las propiedades ópticas de los sensores. Dichas propiedades pueden ser medidas de diferentes formas aplicando también distintas técnicas.

Uno de los mecanismos de transducción más utilizados en el desarrollo de sensores ópticos es el basado en las bandas de absorción. Cada elemento químico posee unas determinadas bandas de absorción a unas determinadas longitudes de onda. Es decir que, un espectro óptico aleatorio en presencia de un gas o un VOC, presentará unas pérdidas ópticas concretas en las longitudes de onda de absorción de dicho gas o VOC. Si dichas pérdidas son medidas, es posible la cuantificación e identificación del gas o VOC a medir. Debido a este efecto, la gran mayoría de estos sensores basan sus resultados en cuantificar la diferencia de potencia óptica que se produce en estas bandas en presencia y ausencia del gas o del VOC. Hay que puntualizar que, para que este fenómeno óptico se pueda producir, parte de la potencia óptica que se guía por la fibra tiene que interactuar de algún modo con las moléculas del gas, si no, no es posible realizar la medida.

El otro gran bloque de sensores ópticos que comparten el mismo mecanismo de transducción es el basado en la variación del índice de refracción efectivo del medio que rodea al sensor. Dicha variación, provoca cambios en el espectro óptico (principalmente, desplazamientos en longitudes de onda o desfases) los cuales pueden ser medidos por los sensores aplicando determinadas técnicas (monitorización de una longitud de onda en concreto o la aplicación de la Transformada Rápida de Fourier (FFT, siglas en inglés)). Como sucede en el caso anterior, para que el sensor pueda detectar estos cambios en el índice de refracción, una parte de la potencia óptica guiada por la fibra tiene que interactuar con el medio donde se están produciendo dichos cambios. Un punto que también hay que tener en cuenta es que, los sensores que basan su funcionamiento en este mecanismo de transducción, tienen que tener una huella espectral muy clara y definida, ya que es necesario tomar un punto específico de referencia para poder realizar de forma correcta la medida. Por esta razón, muchos de los sensores pertenecientes a este grupo, son los basados en interferómetros. En este tipo de sensores, es más sencillo encontrar este punto de referencia debido a la forma sinusoidal que tiene su patrón interferométrico.

Comparando ambos métodos, se puede llegar a la conclusión de que el mecanismo de bandas de absorción permite a los sensores ser más selectivos ya que, como se ha comentado anteriormente, cada gas o VOC tiene su particular banda de absorción, previamente conocida. Sin embargo, dichas bandas de absorción corresponden con unas longitudes de onda muy concretas, lo cual implica trabajar con dispositivos ópticos que tengan una alta resolución espectral (por ejemplo, láseres) lo cual puede encarecer el montaje. Por otro lado, los sensores basados en los cambios del índice de refracción no necesitan trabajar con estos dispositivos, pero tienen el hándicap de que muchos factores pueden alterar el índice de refracción efectivo del medio. Por eso, para intentar aumentar la selectividad de los sensores, se suelen depositar películas con sensibilidad específica a ciertos parámetros.

En los siguientes apartados del presente capítulo de la tesis, se va a presentar el estado del arte de todos los OFS encontrados en la bibliografía hasta el momento, los cuales utilizan montajes experimentales basados en MOFs para detectar gases y VOCs.

2.3. Sensores de gases basados en MOFs

En la actualidad, el desarrollo de aplicaciones relacionadas con la detección de gases está experimentando un gran crecimiento debido principalmente a dos razones [37]: primero, ciertos gases son tóxicos para los seres humanos y suponen un peligro para el medio ambiente siendo muy importante su rápida detección; segundo, existen numerosos sectores, como el industrial o químico, los cuales producen gases contaminantes para el medio ambiente y los seres vivos debido a los procesos que desarrollan. Por lo tanto, la medida, la monitorización y la detección de estos es necesaria para prever y evitar situaciones peligrosas y no deseadas.

Las propiedades y características de las MOFs explicadas anteriormente, hacen que este tipo de fibras sean muy atractivas y tengan un gran potencial para desarrollar estos sensores. Las MOFs, más específicamente las HC-PCFs, fueron propuestas para la detección de gases por primera vez en 1999, cuando se demostró y explicó que se podía hacer que una parte significativa de la potencia modal que viajaba a lo largo de una fibra hueca se superpusiera en sus orificios, permitiendo de esta manera, la interacción de la luz con los gases, los líquidos o películas sensibles a través de los efectos del campo evanescente [38]. A partir de entonces, numerosas contribuciones científicas han propuesto la utilización de MOFs para detectar gases.

2.4. Detección de gases basada en sus bandas de absorción

Como ya se ha explicado, el método de transducción basado en las bandas de absorción es muy utilizado para detectar gases debido a que cada uno de ellos tiene definidas de forma muy clara sus bandas propias; de esta forma, es muy sencillo identificar un determinado gas. Pero para que este método funcione, es necesario conseguir que un parte del campo evanescente de la luz guiada por la fibra interactúe con el gas a medir. Es aquí donde el papel de las MOFs cobra mayor importancia, ya que, gracias a su estructura, esto es posible. Por eso, muchos de los sensores que basan su principio de traducción en bandas de absorción, utilizan las MOFs como una celda de gas. De esta manera, cuando el

gas circula por los agujeros, interactúa con el campo evanescente haciendo posible la medida de las pérdidas de potencia óptica en las longitudes de onda asociadas a las bandas de absorción del gas. Pero conseguir la circulación del gas por el interior de las MOFs no es un proceso simple y cada investigador intenta desarrollar su sistema para intentar conseguir que el proceso de difusión sea lo más optimizado posible. Esto se debe a que, la sensibilidad y los tiempos de respuesta y recuperación dependen en gran medida de este parámetro. A continuación, se presentan una serie de contribuciones científicas (agrupadas por el gas que detectan) que basan su funcionamiento en este concepto, utilizando diferentes tipos de MOFs.

El primer gas que se propone es el acetileno, debido al gran número de publicaciones encontradas. Rajesh Thapa et al. propusieron en [39], un sistema basado en espectroscopía de absorción saturada en la banda de absorción del acetileno cercana a 1532 nm. Dos fibras HC-PCFs con diámetros de núcleo de 10 y 20 μm respectivamente, fueron estudiadas basándose en las variaciones de su *"background light transmission"*. La contribución científica concluye que, en la fibra cuyo núcleo es de 20 μm, dichas pérdidas se reducen y la difusión del acetileno en esta estructura, permite una mayor interacción con el campo evanescente y por consiguiente la saturación se obtiene con valores más bajos de potencia. Y.L. Hoo et al. presentaron un estudio en [40] de la difusión del acetileno en una HC-PCF. Un extremo de la fibra HC-PCF estaba alineado con otro de una fibra MMF dentro de una cámara de gas; debido al espacio que quedaba entre ambos extremos, el acetileno era capaz de penetrar en los agujeros de la HC-PCF. La identificación de las diferentes concentraciones de acetileno inyectadas en la cámara de gas fue posible gracias a la medición de las atenuaciones de la luz guiada por la fibra óptica debido a sus bandas de absorción. De nuevo en [39], una HC-PCF fue utilizada como celda de gas al rellenar sus agujeros con acetileno en un sistema basado en interferometría fototérmica. La detección de diferentes concentraciones de acetileno se realizó midiendo el ruido equivalente del coeficiente de absorción (NEA, siglas en inglés) en la banda de absorción de dicho gas a 1530 nm, llegando a un límite de detección equivalente de 2 ppb (partes por billón). En [41], un interferómetro Fabry-Pèrot basado en una HC-PCF, cuya funcionalidad era actuar de nuevo como una celda de gas, fue presentando como sensor para detectar acetileno. En este montaje, la fibra HC-PCF se encontraba entre dos SMFs, cuyos extremos estaban espejados para

conseguir así una alta reflectividad. Cada una de las fibras se insertaban en una férula mecánica cuya función era optimizar el alineamiento entre ellas y garantizar así el acople de la luz; pero de tal manera que existiera un agujero de aire en ambos extremos de los alineamientos HC-PCF-SMF. Así, cuando el sensor se introducía en la cámara de gas, el acetileno podía penetrar y salir de los agujeros de la fibra. El uso de un interferómetro Fabry Pèrot, cuya cavidad era la HC-PCF, reducía significativamente el efecto de la interferencia modal en la detección del gas y mejoraba de esta forma, la sensibilidad del sensor. El sensor fue testado midiendo las variaciones de potencia en la banda de absorción centrada a 1532 nm con un límite de detección de 7.5 ppm.

Las fibras SC-PCFs también fueron utilizadas como celdas de gases en sistemas para medir acetileno; a continuación, se presentan algunos ejemplos. En [42], Shu-Guang Li et al. demostraron la absorción que provoca, en el espectro de transmisión, la presencia del acetileno en una celda de gas formada por una SC-PCF de 16,9 cm de largo. Los autores afirmaron en esta publicación que uno de los factores más importantes a la hora de optimizar los sensores, si el objetivo es mejorar la sensibilidad del sensor, es incrementar la fracción de potencia óptica que se acopla a la cubierta agujerada de una MOF. Por eso, en esta contribución, se estudió este efecto en función de la variación del índice de refracción efectivo de varias SC-PCF (es decir, variando las dimensiones y la geometría de sus agujeros). El resultado final del estudio concluyó que las SC-PCF con menor distancia entre sus agujeros y con una alta proporción de agujeros de aire, eran capaces de acoplar una mayor potencia a los agujeros de la cubierta de la fibra. Intentando cumplir con este propósito, G. Pickrell et al. publicaron en [43], un sensor de fibra óptica basado en una SC-PCF, pero en la cual, sus agujeros no seguían ningún patrón, si no que estaban construidos de una forma aleatoria para aumentar de este modo las zonas de interacción. El mecanismo de transducción del sensor se basaba en las bandas de absorción de los gases cercanos al infrarrojo, las cuales se detectaban a través del campo evanescente de la luz guiada. Siguiendo esta misma idea, y con el objetivo de optimizar la potencia óptica que podía interactuar con los gases a medir, Y.L. Hoo et al. reportaron en [44], una demostración experimental de este hecho con prometedores resultados. El sistema consistía en la alineación de una SMF y una SC-PCF. Para poder insertar el gas en sistema, las fibras se desalineaban y una pequeña parte de la SC-PCF se introducía en una cámara de gas con acetileno.

Después de esto, se volvían a alinear para realizar las pertinentes medidas. El sensor, debido a la geometría especial de las SC-PCFs, permitía una larga interacción, consiguiendo de esta manera obtener una sensibilidad del 6% de la absorción total de la banda del acetileno. Esta sensibilidad, en términos cuantitativos, era 50 veces mejor que la obtenida utilizando fibras pulidas tipo D y 65 veces mejor que utilizando una SMF en los trabajos anteriores. Siguiendo en la misma línea que las dos últimas contribuciones científicas, Guofeng Yan et al. propusieron en [45], un sensor cuya estructura estaba basada en una SC-PCF, en cuyo núcleo, estaba inscrita una rejilla de Bragg y a la que precedía, una SMF con idénticas características. El sensor fue diseñado especialmente para tener un núcleo y una cubierta agujereada fotosensible para la posible detección de gases. De esta forma, los micro agujeros de la SC-PCF, servían como celda de gas donde se producía la interacción moléculas/campo evanescente. La rejilla de Bragg, con un periodo específico, se utilizaba no sólo para hacer que el sensor funcionara en modo reflexión, sino también para determinar la longitud de onda concreta para la detección del gas; así, se podía ajustar con la banda de absorción del acetileno centrada en torno a 1530 nm, que era donde se quería medir. El sensor obtuvo una sensibilidad aproximada de 0.022 dB/%. Ed Austin et al. propusieron en [46], el sistema que se muestra en la Figura 2.6. La difusión del gas se hacía de la siguiente manera: la fibra SC-PCF se empalmaba a una fibra SMF y el otro extremo de la fibra micro estructurada, el extremo libre, se introducía durante varias horas en una celda con acetileno permitiendo la difusión libre del gas y la interacción con la potencia óptica que se acoplaba en los agujeros del revestimiento. Pasado este tiempo, se empalmaba al extremo libre una MMF y se comparaban, en términos de potencia óptica, los espectros obtenidos antes de introducir el gas (espectro de referencia) y el espectro capturado cuando el gas circulaba por los agujeros de la SC-PCF. El sensor pudo distinguir concentraciones de acetileno de hasta 100 ppm.

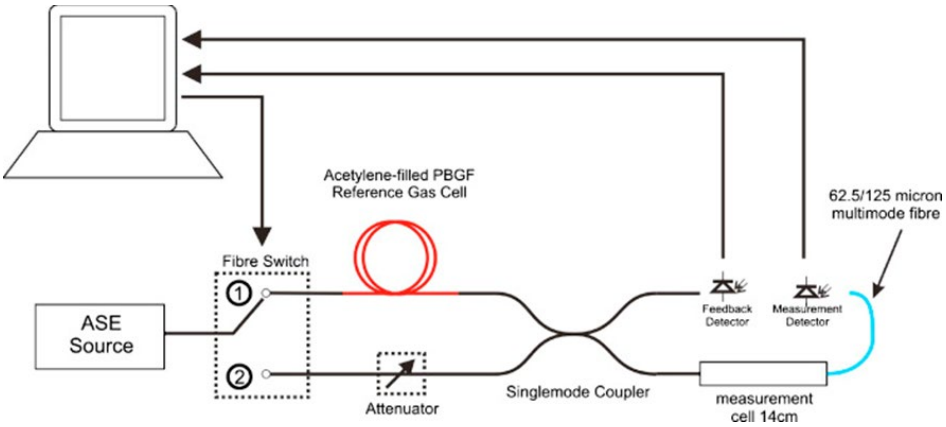

Figura 2. 6 *Montaje experimental de la contribución científica presentada en [40]; láser DFB (láser de retroalimentación distribuida); HC-PCF (fibra de cristal fotónico de núcleo suspendido; en la contribución original se le llama PBGF debido a mecanismo de guiado de la luz); SMF (fibra monomodo); MMF (fibra multimodo); PD (fotodetector); PC (ordenador personal). Figura utilizada con los permisos de* [46].

Otro de los parámetros importantes que debe ser estudiado en este tipo de sensores, es la dinámica de difusión del gas en el interior de la fibra, ya que influye de forma significativa en los tiempos de respuesta y recuperación del sensor, así como en su sensibilidad. Por esta razón, Yeuk L. Hoo et al presentaron en [47] un estudio teórico de este parámetro basado en la periodicidad de los agujeros de aire, dimensiones y distancia entre ellos de una SC-PCF. El sensor fue desarrollado para detectar acetileno y los resultados preliminares de la simulación mostraron que, se podía realizar un sensor de acetileno con un tiempo de respuesta de 1 minuto y un límite de detección aproximado de 6 ppm.

Con el objetivo de mejorar la difusión del gas y la interacción entre luz/gas, A. S. Weeb et al. propusieron en [48] el uso de una SSC para desarrollar un sensor de acetileno. Las SSCs tienen una mayor fracción de aire para ser rellenado con gas si se compara con otras fibras MOFs, lo que a priori las hace ideales para aplicaciones de sensado basadas en la interacción con el campo evanescente de la luz guiada por la fibra. El sistema elegido para introducir el gas fue muy parecido a los ya se han explicado en esta sección: un extremo de la SSC se empalmó a una fibra MMF mientras que el otro se introdujo en una celda, en la cual, se alineó con otra fibra MMF y se inyectó acetileno. El modelado de la fibra mostró que, el solapamiento de interferencia modal fue un 29% más elevado

en comparación con otras MOFs, lo cual es un incremento significativamente importante. En las longitudes de onda correspondientes a las bandas de absorción del acetileno, el espectro óptico resultante presentó unas pérdidas considerables, pero en la contribución científica no fueron cuantificadas.

Otra conclusión que se deriva de estos artículos es que para desarrollar un sensor basado en MOFs con unas buenas características, ciertos parámetros debían ser optimizados: la fabricación de aberturas a lo largo de las MOFs para facilitar el llenado/vaciado del gas en los agujeros de aire o el conexionado entre las SMF/MMF y la MOF utilizada para la detección. Con la intención de dar solución al primero de estos inconvenientes, Sahar Hosseinzadeh Kassani et al. propusieron en [49], un sistema formado por una fibra tipo C y una HC-PCF, cuyo anillo central estaba dopado con germanio, elevando de esta manera, el índice de refracción en el centro de la fibra y mejorando el acople de la luz. La Figura 2.7 muestra un diagrama esquemático del sistema completo propuesto. El segmento de fibra tipo C, empalmado directamente a la HC-PCF, servía para permitir la entrada y salida del gas de una forma más rápida, superando las limitaciones de montajes anteriores y mejorando la respuesta dinámica del sensor. La capacidad de detección del sensor propuesto se investigó experimentalmente detectando y estudiando las bandas de absorción del acetileno, concluyendo que su sensibilidad se incrementaba en un factor 4 comparándolo con los montajes que utilizaban únicamente la HC-PCF.

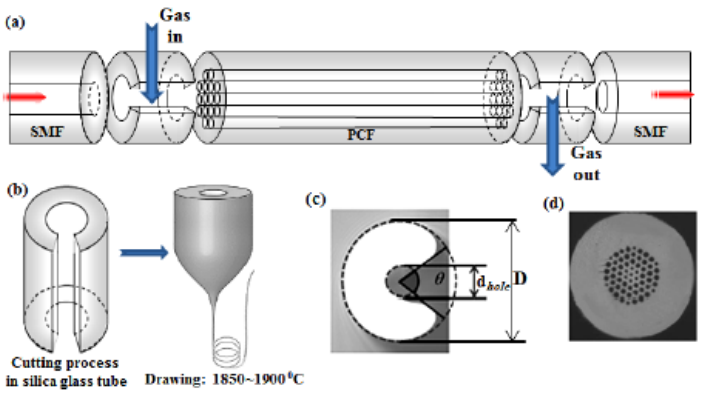

Figura 2. 7 *Montaje propuesto para el sensor de gas formado por una SMF conectada a la fuente de luz y al detector, una HC-PCF y la fibra tipo C como entrada y salida del gas (a); proceso de fabricación de la fibra tipo C (b); sección transversal de la fibra tipo C (c). Figura utilizada con los permisos de* [49] *©2013 Optical Society of America.*

J.P Parry et al. también abordaron esta cuestión en [50]. En este caso, la solución que se propuso para mejorar la difusión del gas fue realizar varias perforaciones a lo largo de la longitud de la HC-PCF (con forma de cono) utilizando un láser óptico, facilitando así, la entrada y salida del gas. El sensor se basaba de nuevo en medir la diferencia de potencia entre las bandas de absorción de los gases cuando el campo evanescente de la luz guiada por la fibra interactuaba con ellos. Los resultados expuestos en esta contribución mostraron que el sensor fue capaz de medir concentraciones de acetileno inferiores al 0.05%.

Otro de los gases, que para su detección se han utilizado MOFs, es el metano. A continuación, se presentan de forma breve, las publicaciones encontradas en la bibliografía, analizando y estudiando sus diferentes bandas de absorción. A.M. Cubillas et al. propusieron en [51], la detección de metano mediante un sensor basado en una HC-PCF y el estudio de su banda de absorción centrada en 1330 nm. El gas penetraba en la fibra gracias a un pequeño espacio de aire que se dejaba entre un extremo de la HC-PCF y otro de la SMF, el cual, estaba angulado para evitar las reflexiones de Fresnel. El mínimo de detección de dicho sensor fue 49 ppmv (partes por millón por volumen). Siguiendo la misma línea de investigación, Y. L. Hoo et al. presentaron en [52], un sensor, cuya respuesta óptica hacia el metano era rápida; el sensor estaba compuesto por una HC-PCF con un patrón de agujeros de aire periódico con dimensiones de micras. Gracias a esta morfología, las pérdidas introducidas en el sistema, por la inclusión de la HC-PCF, eran muy bajas; por esta razón, era posible construir sensores con longitudes de fibra largas, logrando una detección distribuida sin comprometer el tiempo de respuesta del dispositivo. Las mediciones se realizaron esta vez en la banda de absorción del metano cercana a 1670 nm, con un límite de detección de 647 ppm. A. M. Cubillas et al. también propusieron el estudio de dicha banda para desarrollar un sensor de metano, utilizando una HC-PCF de diferente longitud en [53]. En este caso, el mínimo de detección obtenido fue de 10 ppmv. Las dos siguientes contribuciones científicas que se presentan son un estudio de dos estructuras HC-PCF modificadas para intentar mejorar las sensibilidades de los sensores previos: la primera, propuesta en [54], se basaba en una estructura octogonal geométrica de una HC-PCF. Los autores estudiaron numéricamente las propiedades ópticas de la fibra (confinamiento del campo eléctrico guiado, pérdidas de inserción, potencia del campo evanescente acoplado al revestimiento agujereado…), mediante el método

vectorial de elementos finitos (FEM) utilizando el software COMSOL. Todos estos parámetros fueron optimizados para obtener una máximo sensibilidad relativa en la frecuencia de 1670 nm; por otro lado, en [55], se presentó un sensor de metano basado en una HC-PCF helicoidal (ver Figura 2.8). De nuevo, se utilizó el método FEM para realizar un estudio numérico, variando sus parámetros geométricos, para obtener una sensibilidad óptima en frecuencias cercanas a las bandas de absorción del metano; en este caso, el rango variaba de 1 μm hasta 1.8 μm. Para acabar con los sensores de metano, L. Kornaszewski et al. demostraron en [56], la posibilidad de detectarlo en su banda de absorción comprendida entre 3.15-3.35 μm, consiguiendo medir concentraciones inferiores a 0.1%.

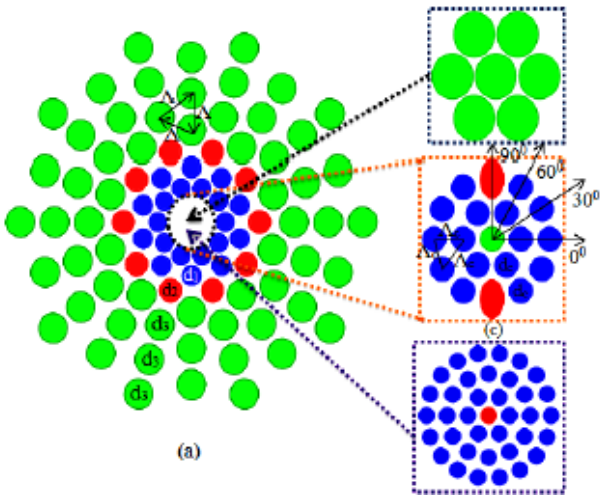

Figura 2. 8 *Sección transversal de la HC-PCF helicoidal propuesta donde se puede observar su estructura. Figura utilizada con los permisos de* [55].

A parte del acetileno y el metano, en la bibliografía se pueden encontrar diversos gases que han sido detectados usando sensores basados en MOFs. Fan Yang and Wei Jin reportaron en [57], un sensor sensible al hidrógeno basado en espectroscopía de ganancia Raman estimulada por una onda continua que, operaba aproximadamente a 1550 nm. Gracias a la luz dispersada por las moléculas de H_2, a ciertas frecuencias se producía una ganancia de potencia óptica que era medida, la cual, dependía de la concentración de dichas partículas. En este trabajo se utilizó una fibra HC-PCF, la cual, nuevamente, funcionaba como celda de gas; el gas se introducía en la fibra mediante una apertura que

existía entre uno de sus extremos y una SMF alineada con ella. El sistema era potencialmente válido para poder detectar niveles de hidrógeno en el rango de 17 ppm. Este mismo montaje y sensor fueron utilizados por Riccardo Pennetta et al. en [58] con la salvedad de que, el empalme entre la fibra SMF y el extremo de la HC-PCF, que no era expuesto directamente a los gases, fue protegido con un cilindro que se fijó térmicamente. En [59], V. P. Minkovich et al. propusieron un nuevo sensor de hidrógeno, pero con una estructura diferente. En este caso, el sistema consistía en el uso de una SC-PCF estrechada; debido a este estrechamiento, los agujeros de aire de la fibra se colapsaban, permitiendo de esta manera la interacción entre el campo evanescente de la luz guiada y las moléculas del gas a detectar (ver Figura 2.9). De esta forma, se producía el fenómeno de la absorción, el cual producía una atenuación en las bandas de absorción del gas. Además, para mejorar la sensibilidad del sensor, una película delgada de paladio se depositó sobre la zona con los agujeros colapsados. Gracias al nuevo sistema propuesto por los autores, la potencia óptica transmitida en este tipo de dispositivos se aumentó en un factor 4, lo cual ampliaba el posible rango de variación de potencia a la hora de la detección del gas.

Otro de los gases detectados con fibras MOFs es el nitrógeno. Michael P. Buric et al. propusieron en [60], el uso de la dispersión Raman espontánea para detectar moléculas de nitrógeno a bajas presiones. Los autores describieron que la detección de gases era posible gracias al uso de una HC-PCF, la cual, al ser usada como celda del gas, aumentaba la zona de interacción de luz con las moléculas del gas que se quería medir y como consecuencia, la potencia final obtenida en las frecuencias asociadas a la retrodispersión Raman; cada gas, dependiendo de sus propiedades, tiene asociada una en concreto. Basándose en esta característica, los mismos autores en [61], utilizaron el mismo sistema para que la luz lanzada interactuara con las moléculas de nitrógeno, las cuales, se encontraban en el interior de los agujeros de la HC-PCF, pudiendo llegar a medir concentraciones de 100 ppm.

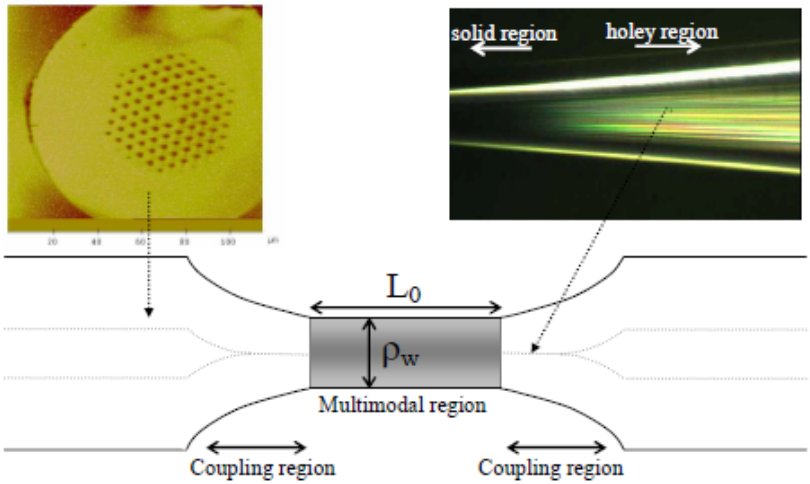

Figura 2. 9 *Imágenes de la sección transversal de la SC-PCF (parte superior izquierda) utilizada para fabricar el estrechamiento y de la zona donde se realizó (parte superior derecha). El dibujo inferior muestra la geometría de la SC-PCF una vez realizado el estrechamiento; el área sombreada muestra la delgada película de paladio depositada. El* L_0 *es la sección de la longitud multimodal y* ρ_w *es el diámetro de la cintura del estrechamiento. Figura utilizada con los permisos de* [59].

El oxígeno es otro de los gases que los investigadores han podido detectar utilizando MOFs; Xinghua Yang et al. propusieron por primera vez en [62], un novedoso tipo de sensores de oxígeno utilizando un optrodo cuyo material sensible para responder al analito era fluoróforo, el cual, se depositó dentro de los micro agujeros de aire de la SC-PCF. A su vez, las moléculas del fluoróforo eran excitadas midiendo la fluorescencia emitida en el segmento de la SC-PCF.

Hui Ding et al. consiguieron detectar monóxido de carbono utilizando MOFs en [63]. Esta publicación tiene cierta importancia debido a la toxicidad y peligrosidad del gas detectado para los seres humanos. El sistema propuesto para el sensado consistía en una HC-PCF, en cuyos extremos, se alineaban una SMF y una MMF, dejando en ambos casos un hueco de aire entre ellas; por el espacio de aire formado entre la SMF y la HC-PCF se insertaba el gas, mientras que el otro, se utilizaba para vaciar el sistema. Las propiedades del montaje experimental fueron demostradas para la detección de monóxido de carbono y acetileno, obteniendo aproximadamente una relación lineal entre la respuesta del sistema y la concentración del gas detectado. Ambos gases pudieron ser medidos

ya que el láser sintonizable utilizado barría las frecuencias donde estos gases tienen sus bandas de absorción. El sensor pudo detectar concentraciones de 300 ppm para el monóxido de carbono y de 5 ppm para el acetileno. Como se ha explicado en la contribución científica anterior, varios gases pueden ser detectados con el mismo sensor. Las siguientes publicaciones también son un ejemplo de ello. De nuevo el acetileno fue detectado, junto al cianuro de hidrógeno ($H^{13}CN$) en [64]. La idea de utilizar una HC-PCF como celda de gas se mantuvo, para medir las variaciones de potencia que se producían en las frecuencias asociadas a las bandas de absorción de ambos gases próximas a 1530 nm. Un nuevo ejemplo de detección múltiple de gases es la publicación de T. Ritari et al. [65]. Propusieron la detección de metanol, amoniaco, cianuro de hidrógeno y acetileno. De nuevo, un extremo de una HC-PCF, que actuaba como celda de gas, se empalmó a una SMF, mientras que el otro se alineó con una MMF dejando un espacio entre ambos para la entrada y salida del gas a medir. Este sistema era válido para detectar varios gases ya que los autores utilizaron como fuente de luz un LED, pudiendo estudiar de esta forma un espectro óptico más ancho; consecuentemente, más bandas de absorción de diferentes gases pudieron ser detectadas (sus frecuencias).

Al igual que en el caso del acetileno, en la bibliografía también se han encontrado varias contribuciones científicas que proponen sistemas para la detección de gases basados en modificaciones de las estructuras de las MOFs, para un rango determinado de frecuencias. En alguno de los casos, para comprobar el buen funcionamiento del sistema, se evalúa con un gas en concreto. Un ejemplo es la contribución científica presentada por Bikash Kumar Paul et al. en [66] (ver Figura 2.10). El objetivo de esta publicación fue proponer una estructura que mejorase las propiedades de los sensores previos, en términos de pérdidas de confinamiento o de empalmes, no linealidades de las fibras y sensibilidad. Para conseguirlo, los autores realizaron un riguroso estudio numérico en un amplio rango de longitudes de onda (desde 1.30 μm hasta 2.0 μm, cerca de la región infrarroja) utilizando el método FEM. El estudio concluyó que, una buena solución era realizar varias ranuras sobre el núcleo de la SC-PCF; los resultados se comprobaron y confirmaron exponiendo el sensor a diazeno. Yang Hao et al. propusieron en [67], un novedoso diseño basado en una HC-PCF anti resonante para el sensado de gases, la cual, podía permitir la difusión de los gases (entrada y salida) debido a una apertura en el revestimiento de la misma,

en cuestión de segundos; de esta forma, la respuesta dinámica del sensor también mejoraba. Las propiedades de la HC-PCF anti resonante y sus ventajas fueron investigadas y discutidas en detalle, así como, su potencial para aplicaciones relacionadas con la detección de gases.

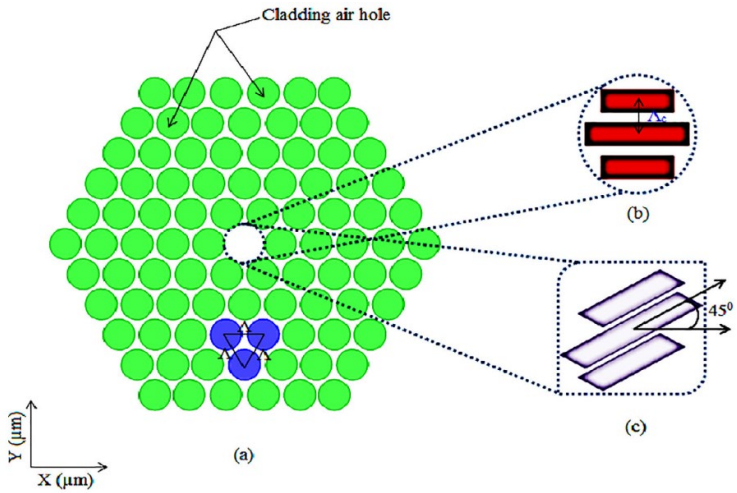

Figura 2. 10 *Esquemático del extremo de la HC-PCF propuesta (a); geometría del núcleo ranurado con 0° de rotación (b) y con 45° de rotación (c). Figura utilizada con los permisos de* [66].

Jinendra K. Ranka et al. analizaron en [68], las propiedades de una MOF, más concretamente de una SC-PCF, formada por un núcleo de sílice, rodeado de un anillo simple de largos agujeros de aire, pensados para la detección de gases (ver Figura 2.11). Los resultados mostraron que la SC-PCF podía soportar numerosos modos espaciales transversales pero que, la diferencia en el índice de refracción efectivo de los modos de orden más bajo, podría ser bastante significativa, impidiendo el acoplamiento de estos a la región agujereada de la fibra, lo cual hacía que la potencia del campo evanescente no fuera la óptima. Otra nueva micro estructura fue presentada en [69] por Sayed Asaduzzaman et al; los autores propusieron el desarrollo de un núcleo micro estructurado dentro del propio núcleo de una SC-PCF, con la finalidad de utilizar dicho sensor en aplicaciones de sensado de gases. El núcleo descrito anteriormente estaba formado por un patrón de agujeros dispuestos verticalmente para mejorar de esta manera la sensiblidad final del sensor; además, las dimensiones geométricas

de la estructura de la SC-PCF, habían sido estudiadas para optimizar todos las parámetros descritos en la contribución anterior.

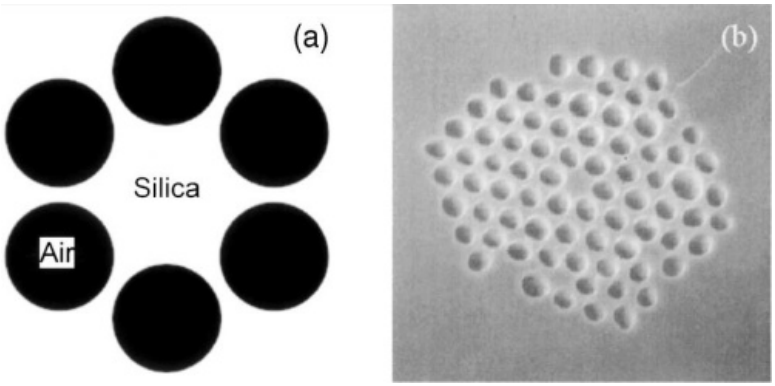

Figura 2. 11 *Patrón del núcleo de la SC-PCF rodeado del anillo formado por agujeros de aire (a). Imagen obtenida del Š Electron del revestimiento agujereado y del núcleo de la SC-PCF. Figura utilizada con los permisos de* [68].

Para finalizar este apartado de la tesis, una contribución científica muy interesante fue la escrita por Hartmut Lehmann et al. en [70]: la usabilidad y las ventajas y limitaciones de las fibras SSCs y las HC-PCFs, cuando son utilizadas para el sensado de gases, en la región cercana al infrarrojo. Fibras SSCs, con diferentes geometrías y HC-PCFs con diferentes propiedades de transmisión, fueron estudiadas y analizadas en base a sus sensibilidades relativas y anchos de banda disponible, detectando diferentes gases como el nitrógeno, el metano o el acetileno. Las conclusiones que se derivaron del estudio fueron las siguientes: ambos tipos de fibra pueden ser utilizadas en aplicaciones de detección de gases pero el funcionamiento de las HC-PCFs, puede considerarse como un celda de transmisión convencional, lo que las hace especialmente útiles para detectar concentraciones de gas muy pequeñas, en las cuales se trabaja con longitudes de fibra relativamente cortas (pocos metros); por otro lado, el comportamiento de las fibras SSC hace que su uso sea más ventajoso para detectar altas concentraciones de gas y/o para sensores con longitudes más largas, como por ejemplo, para el desarrollo de sensores distribuidos en aplicaciones industriales o ambientales.

2.4.1. Detección de gases basada en cambios del índice de refracción efectivo del medio

Aunque en la detección de gases, la inmensa mayoría de los sensores encontrados en la bibliografía, basan su mecanismo de transducción en sus bandas de absorción, también se pueden encontrar sistemas, en los cuales, sus sensores utilizan MOFs y basan su funcionamiento en los cambios del índice de refracción efectivo del medio que rodea al sensor. En el siguiente párrafo, se detallan los datos más relevantes de los encontrados en la bibliografía.

Hai Liu et al. propusieron en [71], la detección simultánea de hidrógeno y metano cuando se encontraban mezclados, gracias a una estructura especial basada en una SC-PCF; 6 pequeños agujeros de aire se ordenaban a lo largo del ángulo de 45° y de 135°, tomando como referencia el núcleo de la fibra y 4 agujeros de aire, con mayores dimensiones, se distribuían en el eje vertical y horizontal (ver Figura 2.12). Una capa de oro se depositaba en los agujeros de la fibra para generar *"Resonancias de Plasmón Superficial"* (SPR, siglas en inglés). Además, sobre esta capa, en los agujeros superiores de la izquierda, se depositaban los siguientes materiales: en el primero, una delgada película de Pd-WO_3, la cual, era sensible a las moléculas de hidrógeno; en el segundo, se depositaba, mediante la técnica de "*dip coating*", un fluoro siloxano sensible al metano. Estas películas son sensibles a las moléculas de los gases que se quieren medir, y en presencia de ellas, su índice de refracción efectivo varía, provocando un desplazamiento, en longitud de onda, de la resonancia generada. El sensor propuesto mostró una sensibilidad de −1.99 nm/% para el metano y de −0.19 nm/% para el hidrógeno.

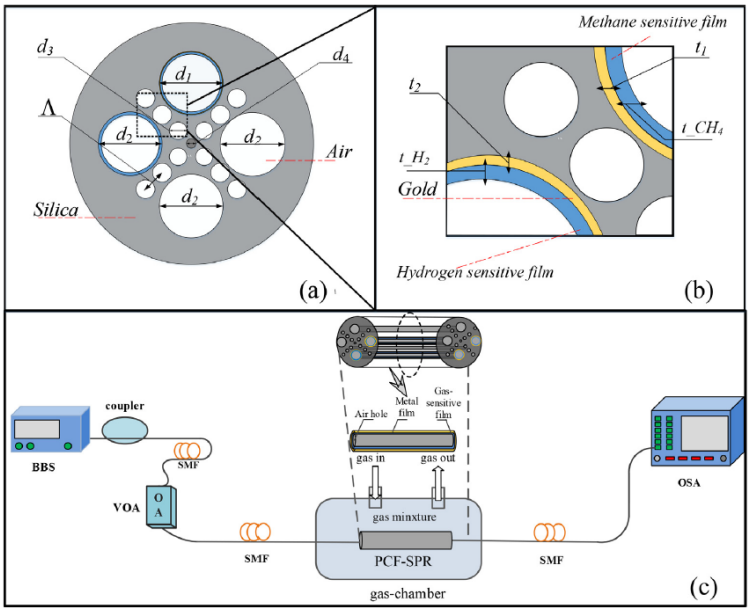

Figura 2. 12 *Dibujo y sección transversal del sensor basado en HC-PCF (a), sus parámetros estructurales (b) y montaje utilizado (c). Figura utilizada con los permisos de* [71].

Un refractómetro, utilizando una novedosa SC-PCF ranurada, se desarrolló en [72], para la medición de las variaciones en el índice de refracción provocadas por ciertos gases. El sensor consistía en una porción de fibra SC-PCF con 6 orificios de aire con forma ovalada que rodeaban su núcleo sólido y en cuyos extremos se habían empalmado dos SMFs; al realizar ambos empalmes, los agujeros de aire se colapsaban, generando un interferómetro Mach-Zehnder. Uno de los agujeros de la SC-PCF se perforó creando dos pequeñas micro ranuras, utilizando un láser de femtosegundo, sin comprometer las propiedades ópticas de la guía onda; de esta manera, el sensor podía ser expuesto a muestras de gases externas como, por ejemplo, de nitrógeno. Cuando este gas llenaba el agujero ranurado, se producía un solapamiento entre el campo evanescente de la luz guiada por la fibra y el gas en cuestión, el cual, con su presencia, alteraba el índice de refracción efectivo de dicho agujero. El sensor mostró una sensibilidad de −827.94 dB/RIU. El mismo montaje, fue usado por Anand M. Shrivastav et al., para generar de nuevo un interferómetro Mach-Zehnder, en [73]. Pero con una salvedad, la estructura del revestimiento de la SC-PCF estaba formada por un

patrón periódico de agujeros de aire y una película sensible (PANI@SnO_2) al gas que se quería detectar (amoniaco). El sensor pudo detectar concentraciones de hasta 8.09 ppt (47.59 fM).

2.5. Sensores de humedad basados en MOFs

La humedad relativa (RH, siglas en inglés) es un parámetro importante y su medida es un valor que se utiliza comúnmente en varios aspectos de la vida diaria de los seres humanos, en la agricultura, en los pronósticos del tiempo, en la atención médica o en el control de procesos químicos. El concepto de RH se puede definir como la proporción entre la cantidad de vapor de agua que tiene una masa de aire y la máxima que podría tener [74]. Por lo tanto, la medida de la RH puede ser considerada también como un "*gas*", pero dado el elevado número de publicaciones encontradas en la bibliografía que hacen referencia a este parámetro, se ha decido exponerlas en un nuevo apartado.

2.5.1. Detección de humedad basada en cambios del índice de refracción efectivo del medio

De forma contraria al caso de la detección de gases, el método de transducción más utilizado para desarrollar sensores de fibra óptica, capaces de detectar variaciones en la humedad, es el basado en los cambios del índice de refracción del medio que rodea al sensor. Como se ha comentado anteriormente, para desarrollar este tipo de sensores, una de las posibilidades que existen es trabajar con interferómetros, principalmente, Mach-Zehnder o Fabry-Pèrot, dependiendo de la configuración con la que trabaje el sensor, bien sea en modo transmisión o en reflexión.

En esta primera parte, se van a exponer los sensores basados en interferómetros Mach-Zehnder, cuya configuración más utilizada y sencilla, es en transmisión. Brevemente, un interferómetro Mach-Zehnder se genera al empalmar entre si distintos tipos de fibra, en este caso en concreto, dos SMFs a ambos extremos de una SC-PCF. Los empalmes se llevan a cabo de tal manera que los agujeros de aire de la SC-PCF se colapsan en una pequeña región; cuando el haz de luz llega a la primera de estas regiones, se difracta y parte de la potencia óptica pasa a viajar por la región agujereada del revestimiento de la

fibra, dividiendo el haz de luz en dos caminos ópticos. En el revestimiento agujereado de la SC-PCF, las constantes de propagación son distintas y, por lo tanto, los modos que viajan por esta parte de la fibra acumulan un cierto desfase. Cuando estos modos alcanzan la segunda región colapsada, interfieren con el modo fundamental que viaja por el núcleo de la fibra, generando una respuesta interferométrica. Un dibujo esquemático de esta explicación se muestra en la siguiente figura.

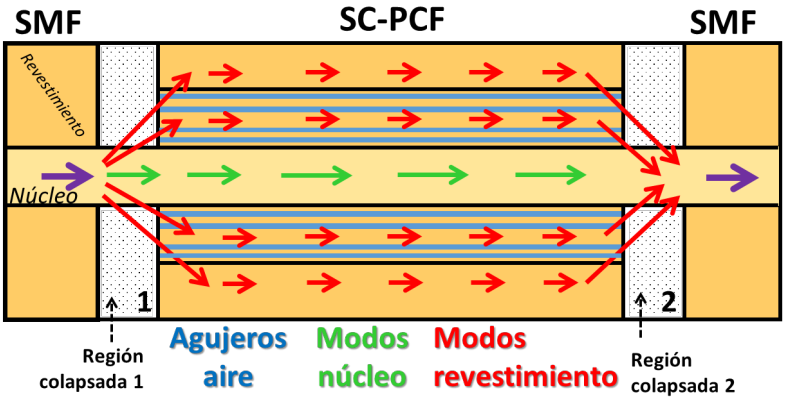

Figura 2. 13 *Mecanismo de operación de un interferómetro Mach-Zehnder utilizando una SC-PCF. Las flechas muestran el comportamiento de los modos que viajan por el revestimiento y el núcleo de la fibra; las líneas azules hacen referencia a los agujeros de aire mientras que las zonas punteadas son aquellas en las que los agujeros han sido colapsados.*

Basándose en esta estructura, M Y Mohd Noor et al. propusieron en [75], un sensor para detectar cambios en la humedad relativa. Gracias al efecto de la región colapsada, cierta parte del campo evanescente de la luz guiada por la fibra podía interactuar con las moléculas de agua, las cuales, alteraban el índice de refracción efectivo del medio. Midiendo el desplazamiento de uno de los picos (en longitud de onda) que generaba el interferómetro, se obtuvo que la sensibilidad del sensor era de 60.3 pm/%RH en el rango de 60–80%RH y de 188.3 pm/%RH en la región comprendida entre 80 y 95%RH; además, el sensor exhibió una muy baja sensibilidad cruzada a la temperatura, 0.5 pm/°C. Con la intención de mejorar la sensibilidad hacia la humedad obtenida en la publicación anterior, sin alterar el montaje del sensor, varios investigadores propusieron depositar películas delgadas higroscópicas, formadas por diferentes materiales y

depositadas utilizando diferentes técnicas como, por ejemplo: "*dip coating*" o "*capa a capa*" (LbL, siglas en inglés). Uno de ellos fue Tao Li, quien propuso recubrir la sección de la SC-PCF, con una capa de alcohol polivinílico (PVA) en [76]. Los resultados experimentales mostraron una sensibilidad de 40.9 pm/%RH, en un rango de humedad comprendido entre 20 y 95 %RH. De la misma manera, Piaopiao Wang et al. propusieron el uso de una película de metilcelulosa en [77], obteniendo un desplazamiento, en longitud de onda, de 10 nm para un cambio de humedad del 55%RH. Siguiendo de nuevo con la misma idea, Shuqin Zhang et al. presentaron en [78], la posibilidad de medir simultáneamente humedad relativa y temperatura; la única diferencia con la publicación anterior fue que, el sensor tenía una estructura en cascada de la siguiente manera: SMF-SC-PCF-FBG (la FBG se utilizaba como sensor de temperatura) (ver Figura 2.14). Debido a que, en el espectro óptico, el patrón interferométrico del Mach-Zehnder y la frecuencia de trabajo de la FBG se identificaban claramente, se pudo medir de forma independiente ambos parámetros. La resolución del sensor frente a la humedad fue de 0.13%RH (rango de humedad: 30%-95%) mientras que para la temperatura fue de 1.0°C.

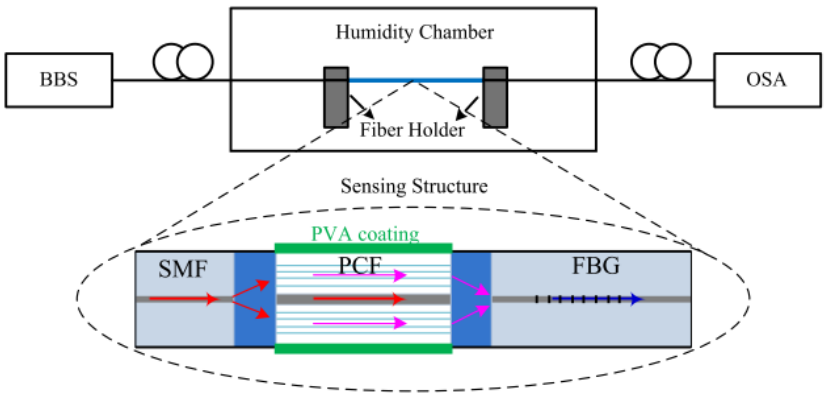

Figura 2. 14 *Dibujo esquemático del montaje experimental utilizado con los diferentes tipos de fibra óptica utilizados: SMF-SC-PCF (interferómetro Mach-Zehnder)-FBG. Figura utilizada con los permisos de* [78].

Sin alterar el montaje de los sensores anteriores, Jinesh Mathew et al. propusieron en [79] y [80] depositar un nuevo material a lo largo de la longitud de la SC-PCF, utilizando la técnica de deposición "*dip coating*": el material elegido

fue la agarosa. En [79], el sensor mostró un desplazamiento en longitud de onda de aproximadamente 56 nm para un cambio total en la humedad del 56% y una resolución de humedad de 0.017%RH (en el rango comprendido entre 40% y 80%RH) y una más alta resolución, de 0.007%RH, en el rango 80%-95%RH.

Las siguientes publicaciones que se presentan, aunque se siguen basando principalmente en interferómetros Mach-Zehnder utilizando SC-PCF, incluyen en sus montajes ciertas variaciones que las hacen peculiares. Por ejemplo, Pan Zhang et al. propusieron en [81], un interferómetro Mach-Zehnder para la realización de medidas de humedad relativa y temperatura. El montaje que se presentó en este trabajo era idéntico al descrito en [72], con la salvedad de que, en el primer empalme, entre la SMF y el extremo de la SC-PCF, se introducía un segmento de una MMF (ver Figura 2.15).

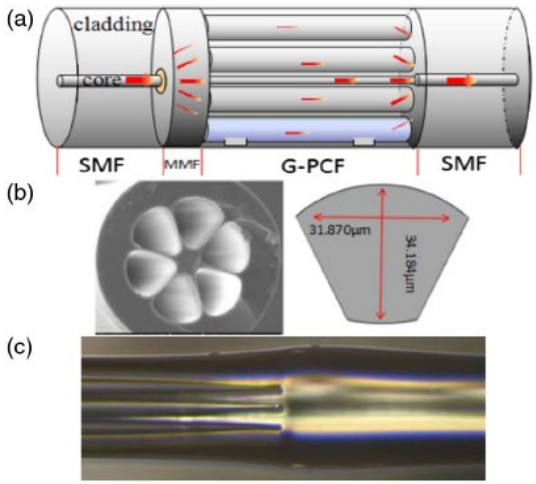

Figura 2. 15 *Diagrama esquemático del interferómetro en el que se basa el sensor de humedad (a); sección transversal de la SC-PCF utilizada (b); los agujeros de la SC-PCF quedan completamente colapsados en la región del empalme con la SMF. Figura utilizada con los permisos de* [81] *©2018 Optical Society of America.*

Gracias a este segmento, era posible excitar los modos de mayor orden y facilitar el acople de estos a los agujeros de aire, intentando mejorar de esta manera la sensibilidad final. La sensibilidad del sensor frente a la humedad fue de −0.077 dB/%RH, en un rango de 25%-80%RH. Ran Gao et al. propusieron en [82], una nueva alternativa para desarrollar un sensor de humedad. El sensor fue

construido rellenando con gel de agarosa un pequeño espacio de aire que se dejó entre la SMF y la SC-PCF. Debido a las variaciones del espesor de la película de agarosa depositada, cuando el índice de refracción efectivo del medio cambiaba (debido a los cambios de RH), el diámetro del campo modal de la luz propagada también lo hacía, produciendo una diferencia en la proporción de la luz que se acoplaba entre la SC-PCF y la SMF. Los resultados experimentales mostraron que la sensibilidad del sensor podía llegar hasta 2.2 dB/%RH. La variación que propuso Rui-jie Tong et al. en [83], fue la inclusión de dos dilataciones en las SMFs, antes y después de las regiones colapsadas, (ver Figura 2.16). La primera de estas imperfecciones actuaba como un divisor, dividiendo el haz de luz en dos: uno que se acoplaba al revestimiento de la SC-PCF y el otro que se acoplaba a su núcleo; la segunda imperfección tenía un comportamiento inverso, haciendo que los modos que viajaban por el revestimiento se acoplaran al núcleo, generando, de esta manera, una interferencia. El sensor, fue recubierto por películas de diferentes espesores, compuestas de *"Graphene quantum Dots"* (GQDs, siglas en inglés) y PVA, para estudiar su efecto. Concretamente los espesores utilizados fueron: 2.48 μm, 3.72 μm, 4.45 μm, 5.96μm, 7.42 μm and 8.17 μm. El objetivo era estudiar el efecto del espesor en la sensibilidad final del sensor; las sensibilidades obtenidas fueron: 0.0901 nm/%RH, −0.0797 nm/%RH, -0.0337 nm/%RH, 0.0586 nm/%RH, 0.0539 nm/%RH y 0.0313 nm/%RH, respectivamente. Estos resultados revelaron que, cuando una película de diferente espesor era depositada, la sensibilidad del sensor se veía alterada; en otras palabras, que el espesor era uno de los parámetros clave en el proceso de optimización de la sensibilidad de un sensor ya que de él dependía el porcentaje de campo evanescente que interactuaba con dicha película. Por esta razón, Jinesh Mathew et al. publicaron en [84] un estudio del efecto que producía, en la sensibilidad final del sensor frente a la humedad, recubrir la SC-PCF con películas de agarosa de diferentes espesores. De nuevo, la conclusión fue que la sensibilidad del sensor tenía una significativa dependencia del espesor de la película depositada.

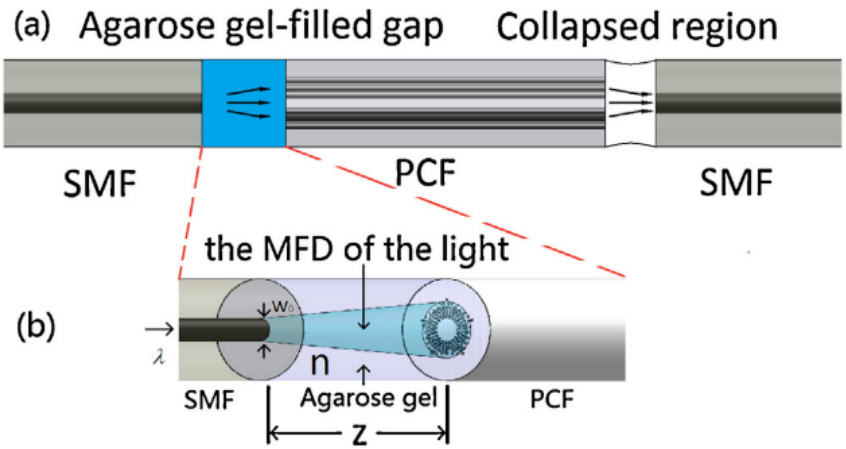

Figura 2. 16 *Dibujo esquemático del sensor de humedad propuesto basado en una SC-PCF (a) y el diámetro del campo modal de la luz en la deposición de agarosa (b). Figura utilizada con los permisos de* [82].

Las SC-PCFs en montajes en reflexión también fueron utilizadas en varias contribuciones científicas para el sensado de la humedad relativa. Esta configuración consistía en hacer el mismo empalme entre las fibras (SMF y SC-PCF) que, en artículos anteriores, pero ahora, el otro extremo de la SC-PCF se cortaba para que se comportase como un espejo. De esta manera, los agujeros de dicha fibra se dejaban abiertos y en contacto con la atmósfera ambiental. Al llegar al espejo, tanto los modos que viajaban por la cubierta, como los que viajaban por el núcleo, se reflejaban y cuando alcanzaban de nuevo la región colapsada, se volvían a recombinar como un sólo modo en el núcleo de la SMF, generando así un interferómetro Michelson. Llegados a este punto, es necesario aclarar que este montaje descrito operaba de forma correcta gracias a la inclusión de un circulador óptico. S S Hindal y H J Taher presentaron en [85], un novedoso método para la detección de humedad basado en esta configuración: la fabricación del sensor era simple, ya que sólo implicaba el corte y la fusión del empalme. Además, el sensor presentaba la ventaja de que no requería el uso de ningún material higroscópico. La sensibilidad final del sensor obtenida fue de 2.41 pm/%RH para humedades comprendidas entre el 27% y 85%RH. Variando únicamente la longitud de la SC-PCF utilizada y disminuyendo las pérdidas introducidas en el montaje, debido a los empalmes y al corte realizado en el extremo de la MOF, Jinesh Mathew et al. consiguieron en [74] y [86], mejorar la

sensibilidad final del sensor; en el rango de humedad comprendido entre el 40-70%RH, la sensibilidad obtenida fue de 5.6 pm/%RH, mientras que para humedades superiores al 70%RH, la sensibilidad fue de 24 pm/%RH. Al comprobar el buen comportamiento del sensor, los mismo autores propusieron en [87] depositar un material higroscópico (agarosa) en el interior de los agujeros de la SC-PCF intentando mejorar de esta manera la sensibilidad. El sensor mostró una alta sensibilidad a las variaciones de la humedad relativa, con un cambio en su potencia reflejada de aproximadamente 12 dB, para una variación de humedad del 84%RH, mejorando los resultados obtenidos en trabajos anteriores. Al igual que en las configuraciones previas, también fue posible la detección de humedad y temperatura de forma simultánea: Jinesh Mathew et al. lo propusieron y demostraron en [88]. El dispositivo estaba formado por una FBG y una SC-PCF en reflexión, en cuyos agujeros se había depositado agarosa. Gracias a la agarosa, era posible monitorizar los cambios de humedad, mientas que los de temperatura se realizaban mediante la FBG. La temperatura era medida estudiando el desplazamiento de la longitud de onda de la FBG y la humedad era medida monitorizando los cambios en la potencia óptica en el espectro reflejado. La sensibilidad del sensor frente a la temperatura fue de 9.8 pm/°C y la variación de la potencia óptica fue superior a 7 dB, para un cambio de RH del 75%, mostrando una baja sensibilidad cruzada.

Una mezcla entre los dos montajes utilizados por los dos últimos bloques de sensores presentados es lo que utilizaba el siguiente grupo de sensores para desarrollar medidas de humedad relativa. En este caso, el montaje era muy parecido al basado en un interferómetro Michelson, pero el extremo de la SC-PCF, que se dejaba libre a la atmosfera ambiental, ahora se convertía en una nueva región colapsada, a la que no se le empalmaba ninguna SMF: es decir, la nueva configuración de los sensores en reflexión incluía dos regiones con los agujeros colapsados. Más detalladamente, Joel Villatoro et al. expusieron en [89] todo el montaje: los sensores eran fabricados colapsando ambos extremos de la SC-PC. La primera región colapsada tenía la misma función que en los anteriores casos y la segunda, ahora actuaba como espejo, reflejando los modos que viajaban por el revestimiento, que luego se volvían a juntar en un único modo, cuando llegaban a la primera región colapsada. En la contribución científica también se estudiaron parámetros como la longitud y geometría de la SC-PCF utilizada, así como los picos interferométricos obtenidos en el espectro resultante,

concluyendo que este sensor podía ser utilizado para medir cambios en la humedad relativa. Tomando esta idea, Muhammad Yusof Mohd Noor et al. presentaron en [90], el primer sensor de humedad basado en este montaje. Debido a la absorción y desorción de las moléculas de agua a lo largo de la longitud de la SC-PCF, el sensor era capaz de detectar un cambio en el índice de refracción efectivo del medio y, como consecuencia de ello, se producía un cambio en longitud de onda en el patrón interferente resultante. El sensor mostró una sensibilidad de 20.3 y 61.6 pm/%RH en los rangos de humedad comprendidos entre 60%–80%RH y 80%–95%RH, respectivamente. Utilizando los resultados de esta publicación, y con el propósito de hacer más sensible el sensor hacia la humedad, Wei Chang Wong et al. propusieron en [91] y [92], recubrir dicho sensor con un material higroscópico afín a la humedad como es el PVA (ver Figura 2.17); el sensor mostró una sensibilidad de 0.60 nm/%RH, para un rango de humedad comprendido entre 30% y 90%RH, mejorando así el resultado anterior. Dado el potencial que se vio que podían ofrecer los sensores basados en este montaje, Fernando C. Favero et al. propusieron en [93], su uso en aplicaciones donde los sensores electrónicos podían fallar o no eran muy recomendadas. También se pensó que podían ser útiles en la evaluación de la salud: el dispositivo se utilizó para controlar la respiración de una persona independientemente de su frecuencia respiratoria. Además, los autores explicaron que todos los componentes del sensor eran (o podían ser) materiales dieléctricos, lo cual implicaba que podía ser utilizado durante resonancias magnéticas o en algunos tratamientos oncológicos.

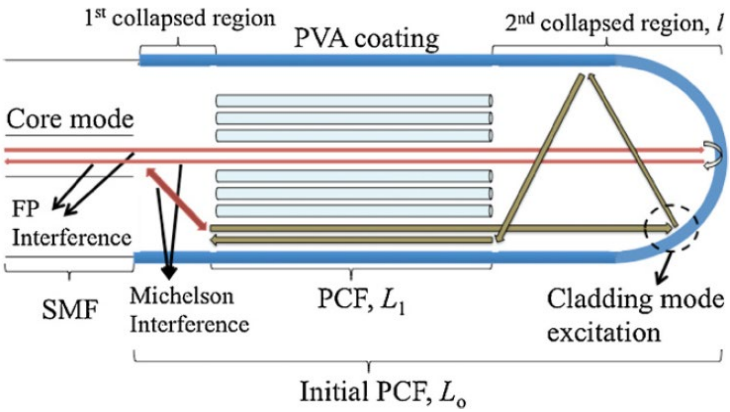

Figura 2. 17 *Representación del sensor SC-PCF, en la que se muestra su mecanismo de trabajo. Figura utilizada con los permisos de* [91].

Para acabar esta sección, se presenta una nueva estructura que fue desarrollada por Shijie Zheng et al. en [94] y [95]: el uso de "*Long Period Gratings*" (LPG, siglas en inglés), en montajes en reflexión. La LPG fue inscrita en la sección de SC-PCF utilizada para realizar el sensor. Además, los agujeros de la SC-PCF-LPG fueron recubiertos con dos tipos de nano recubrimientos poliméricos; el primero formado por PAH/PAA, con la intención de mejorar la sensibilidad del sensor hacia el índice de refracción del agua; y el segundo, formado por Al_2O_3/PSS, para intentar mejorar la selectividad del sensor y que sólo fuera sensible al parámetro a medir. El sensor mostró una sensibilidad final de 0.058nm/%RH y una variación de potencia óptica en el espectro de transmisión de 2 dB en un intervalo de humedad entre 20%-54%RH.

Como era de esperar, también se han encontrado en la bibliografía, publicaciones científicas en las cuales se usan HC-PCFs para desarrollar sensores de humedad. La configuración más utilizada por los investigadores es en reflexión, debido a su arquitectura, generando de esta forma un interferómetro Fabry-Pèrot. Dicho interferómetro se forma al empalmar una sección de una HC-PCF con una SMF sin colapsar sus agujeros durante el empalme. Además, en algunas de las publicaciones que se han encontrado, el otro extremo de la fibra HC-PCF se recubre con un polímero higroscópico. De esta forma, se generan 3 superficies reflectantes, debido a las diferencias en los índices de refracción: SMF/HC-PCF, HC-PCF/polímero higroscópico y polímero higroscópico/aire. La luz emitida por la fuente de luz se refleja en estas tres interfaces y los rayos reflejados interfiere entre sí debido a los diferentes retardos de fase provocados por los distintos caminos ópticos que describen. Basándose en esta explicación, Hao Sun et al. propusieron y demostraron experimentalmente en [96], un sensor para la medición simultánea de humedad y temperatura. El material utilizado para recubrir el extremo final de la HC-PCF fue PVA. Los resultados experimentales demostraron que el sensor propuesto era capaz de medir cambios en la humedad relativa y la temperatura, demodulando las variaciones en la potencia óptica y los desplazamientos en longitud de onda del espectro de reflexión, con un error de 1.47% y 0.0032%, respectivamente. El sensor mostró un desplazamiento máximo en longitud de onda de 5 nm, para unas variaciones de humedad comprendidas entre 35%-95%RH. Intentando mejorar la sensibilidad de este sensor, Xiaohui Liu et al. utilizaron la misma configuración en [97], pero depositando esta vez chitosan (ver Figura 2.18). El sensor mostró un máximo de

sensibilidad cuando la humedad relativa estaba en un valor cercano al 90%RH de 0.28 nm/%RH.

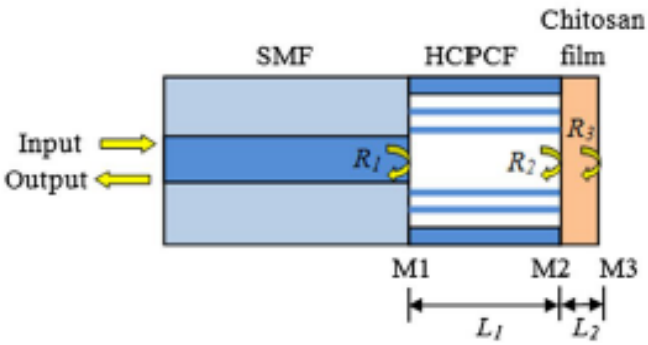

Figura 2. 18 *Estructura del sensor propuesto basado en un interferómetro Fabry-Pèrot recubierto con una película de chitosan. Figura utilizada con los permisos de* [97].

Una nueva idea fue propuesta y desarrollada por Qingmei Sui et al. en [98]: consistía en un sensor de humedad basado en dos interferómetros Fabry-Pèrot en cascada. Se construyó empalmando una sección de una HC-PCF entre dos SMFs. Además, utilizando la técnica de deposición *"LbL"*, se depositó una película en la interfaz final del sensor intrínseco formada por poly(sodium-p-styrenesulfonate)/(PSS) poly(allyamine hydrochloride) (PAH). Debido a los cambios de humedad, el índice de refracción efectivo del medio variaba y como consecuencia, la potencia óptica reflejada. El sensor mostró una sensibilidad final de 0.008 dB/%RH en un rango de humedad comprendido entre el 5%-90%RH. Con el objetivo de mejorar esta sensibilidad, Yong Zhao et al. propusieron en [99] introducir algunos cambios en la configuración del sensor. El interferómetro fue construido realizando dos empalmes: el primero, formado por una SMF y una SC-PCF y el segundo, formado por el extremo libre de la SC-PCF y una HC-PCF (ver Figura 2.19). En este caso, la película depositada en los agujeros de la HC-PCF estaba formada por GQDs y PVA, pero con una salvedad: dicha película no sé depositó en la totalidad de la longitud de los agujeros. La sensibilidad del sensor obtenida fue de 0.456 nm/%RH con variaciones en la humedad comprendidas entre 19.63%RH to 78.86%RH.

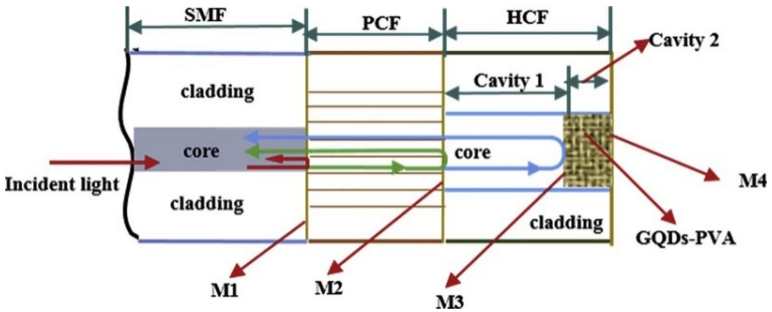

Figura 2. 19 *Estructura del interferómetro Fabry-Pèrot desarrollado en la publicación [96], empalmando una SMF y un HC-PCF (HCF en la figura) a ambos extremos de una SC-PCF (PCF en la figura). Figura utilizada con los permisos de* [99].

Finalmente, el uso de HC-PCFs para el desarrollo de sensores de humedad, fue analizado por Tao Li et al. en [100]. Estos autores propusieron una nueva estructura: utilizar una HC-PCF estrechada como elemento sensible a la humedad. La fibra consistía en un núcleo hueco dopado de germanio con 5 largos agujeros de aire a su alrededor, los cuales habían sido recubiertos con un hidrogel. Gracias al estrechamiento, el modo del núcleo era muy sensible a cualquier cambio en el índice de refracción del revestimiento debido a la gran interacción que existía entre el campo modal y los agujeros de aire. Los cambios de humedad modificaban el índice de refracción efectivo del material, lo que llevaba a cambios en la potencia óptica reflejada. Los resultados de las simulaciones teóricas mostraron que las pérdidas en la potencia óptica variaban de 0.063dB/cm a 75.847dB/cm cuando la humedad cambiaba desde 0 hasta 95%RH.

Para finalizar esta sección, se presenta la única publicación encontrada en la bibliografía que utilizó una fibra SSC para desarrollar un sensor de humedad. El sensor, presentado por Chengliang Wang et al. en [101], estaba formado por dos segmentos. El primero, era un pequeño segmento de una SSC formada por 4 grandes agujeros alrededor de su núcleo suspendido y el segundo, un recubrimiento formado por un adhesivo óptico higroscópico (ver Figura 2.20). De esta forma, se generaba un interferómetro Fabry-Pèrot con tres diferentes interfaces: SMF/SSC, SSC/adhesivo óptico y adhesivo óptico/aire. Debido a las diferentes sensibilidades de las cavidades Fabry-Pèrot hacia los cambios de humedad y de temperatura, ambos parámetros pudieron ser medidos

simultáneamente monitorizando los desplazamientos de la fase al aplicar la FFT. En el rango comprendido entre 15%-90%RH, el sensor mostró una sensibilidad máxima de -0.042 rad/%RH.

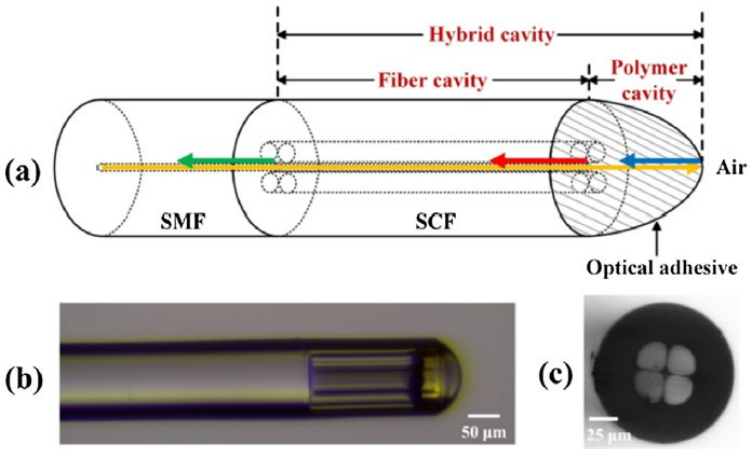

Figura 2. 20 *Esquema de las diferentes partes del sensor. La cavidad híbrida está formada por: la cavidad de la fibra, formada por la SSC (SCF en la figura) y por la cavidad del polímero, formada por el adhesivo óptico (a). Imagen obtenida con el microscopio del sensor desarrollado (b). Sección transversal de la SSC de 4 agujeros (c). Figura utilizada con los permisos de* [101].

2.5.2. Detección de humedad basada en sus bandas de absorción.

En menor medida que en la sección anterior de los gases, ya que sólo se encontró una contribución científica en la bibliografía, las MOFs también se utilizaron como *"celda de humedad"*, basando su mecanismo de transducción en las bandas de absorción. Tomando esta idea como referencia, M. Y. Mohd Noor et al. propusieron en [102], [103], un nuevo sensor para medir variaciones en la humedad utilizando una HC-PCF como celda de humedad. El nivel de humedad se determinaba analizando la diferencia de potencia óptica entre una señal previamente definida y la potencia óptica del sensor medida, en un momento determinado, en el pico de absorción del vapor de agua centrado en 1368.59 nm. Las moléculas de agua penetraban en los agujeros de la HC-PCF, gracias a dos pequeños espacios de aire que se dejaban a ambos extremos de esta fibra, cuando se alineaba con dos SMFs. De esta manera, las moléculas de agua interactuaban con el campo evanescente de la luz guiada por los agujeros de aire. La resolución

del sensor frente a la humedad fue de 0.2%RH en un rango de humedad de 0%-90%RH.

2.6. Sensores de VOCs basados en MOFs

En la actualidad, la detección de compuestos orgánicos volátiles (VOCs, siglas en inglés), juega un papel muy importante debido a que determinados VOCs pueden ser una amenaza significativa para la salud humana, así como para el equilibrio ecológico. Hay un considerable número de aplicaciones potenciales basadas en la detección de VOCs como, por ejemplo, la monitorización de las condiciones ambientales, la regulación de procesos en la industria química o alimenticia… sólo por mencionar algunos [10]. Los OFS desarrollados para la detección de VOCs ofrecen nuevas e interesantes propiedades gracias a las cuales pueden superar algunos de los inconvenientes encontrados en los sistemas para detección de VOCs tradicionales los cuales están basados principalmente en mecanismos eléctricos, electroquímicos o en materiales poliméricos pesados.

Haciendo referencia a los datos presentados en [9], en términos de micro y nano ingeniería de fibra óptica, las PCFs (ambas, SC-PCF y HC-PCF), las fibras SSC o los estrechamientos micro/nano de las fibras son muy buenas alternativas para desarrollar sensores para la detección de VOCs; en este apartado de la tesis, se va a presentar el estado del arte de las MOFs utilizadas para este fin.

Al igual que sucedía en el caso de la detección de gases, las MOFs son especialmente útiles para el sensado de VOCs debido a su micro estructura, la cual permite el paso a través de ella de las moléculas del VOC a detectar, actuando como una *"celda para VOCs"*. Una de las principales diferencias en comparación con la detección de gases es que los VOCs no tienen unas bandas de absorción tan definidas, por lo que su mecanismo de transducción se basa, principalmente, en detectar los cambios en el índice de refracción efectivo del medio. Teniendo esto en cuenta, Joel Villatoro et al. presentaron en [104] y [105], un sensor en reflexión utilizando una fibra SC-PCF, a la cual se le empalmaba una SMF. En el empalme, los agujeros de la fibra SC-PCF se colapsaban, haciendo que cierta parte del haz de luz viajara por el revestimiento, excitando de esta forma modos de más alto orden y permitiendo también, la interacción de estos modos con las moléculas del VOC (ver Figura 2.21); además, cuando estas

moléculas penetraban en los agujeros de la SC-PCF, el índice de refracción del medio variaba, lo que producía un desplazamiento en longitud de onda en el espectro interferométrico del sensor. Los autores afirmaron que el sensor podía medir deferentes VOCs como metanol (CH_3OH), acetonitrilo (CH_3CN), isopropanol (C_3H_6OH) o tetrahidrofurano (THF). Las pruebas experimentales se realizaron para tetrahidrofurano y acetonitrilo (inyectando un volumen de 600 pL en la celda de medida donde se evaporaba el VOC y se introducía el sensor) obteniendo un desplazamiento máximo de 700 y 500 pm, respectivamente.

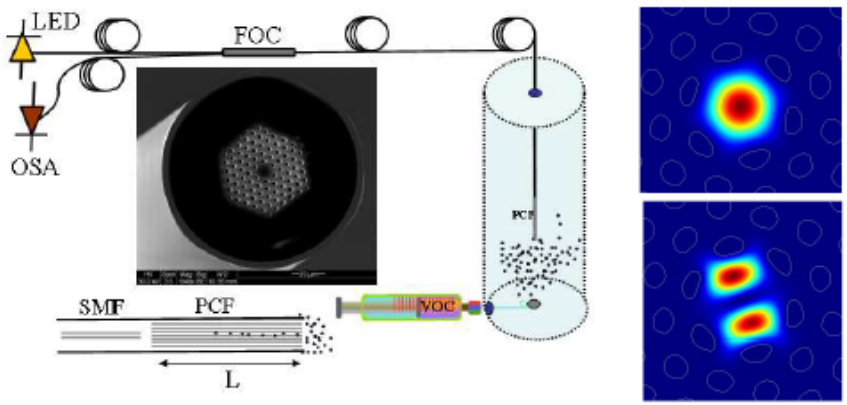

Figura 2. 21 *A la izquierda, esquema del montaje experimental con una imagen de la sección transversal de la SC-PCF utilizada para desarrollar el sensor. L es la longitud de la sección de dicha fibra. LED es la fuente óptica utilizada, OSA (siglas en inglés) es el analizador de espectros y FOC (siglas en inglés) es el circulador óptico utilizado en el montaje. A la derecha, las distribuciones del campo eléctrico de los modos LP_{01} y LP_{11}* [105].

Utilizando también una HC-PCF en reflexión, Bongkyun Kim et al. presentaron en [106] el siguiente montaje: un extremo de una sección de una fibra capilar fue empalmada a una SMF, mientras que el otro extremo se empalmó a una SC-PCF; de esta forma, se generaba un interferómetro Fabry-Pèrot, debido a las 3 interfaces con diferentes índices de reflexión que existían. El patrón interferométrico resultante de la señal reflejada se desplazaba, en longitud de onda, cuando en los agujeros de la SC-PCF se infiltraban las moléculas de los VOCs. Para analizar la sensibilidad del sensor, se empleó la técnica de la FFT, evaporando en la celda de medida 2 μL de acetona. El sensor mostró un desplazamiento de 1.3 rad.

Las HC-PCF también se propusieron para desarrollar sensores capaces de detectar VOCs, pero utilizando montajes en transmisión. Luo Niu et al. en [107], presentaron un sensor para la detección de etanol, basado en el efecto de la dispersión Rayleigh. Ambos extremos de la HC-PCF se alineaban con dos SMFs, dejando un pequeño espacio de aire entre ellas, lo que permitía la difusión de las moléculas de etanol. Conforme la concentración de etanol en la celda de medida se incrementa, las moléculas de etanol empezaban a penetrar en los agujeros de aire de la HC-PCF, lo que provocaba una excitación del efecto de la dispersión Rayleigh y pérdidas en la potencia óptica transmitida. Cuando la luz alcanzaba la segunda SMF, los modos se recombinaban en uno sólo, simulando su funcionamiento al de un interferómetro Mach-Zehnder. Los resultados experimentales mostraron una sensibilidad del sensor hacia el etanol de 0.022 dB/ppm. Los mismos autores, volvieron a proponer la medida de etanol, utilizando el mismo montaje, pero en este caso midiendo el desplazamiento en longitud de onda que se producía en el espectro de luz reflejada. El rango de concentración medido fue de 250 ppm hasta 100 ppm de etanol y el desplazamiento de 1542.96 nm (cuando el sensor se expuso a 250 ppm) hasta 1545.52 nm (cuando el sensor se expuso a 1000 ppm). Siguiendo con el uso de las HC-PCF, Jason M. Kriesel et al. describieron en [108], un sistema versátil de espectroscopía en el infrarrojo medio para poder medir diferentes concentraciones de una amplia gama de VOCs, utilizando un volumen de muestra pequeño, del orden de los pL. El sistema combinaba un láser de características muy concretas, el cual permitía barrer un ancho espectro óptico, con una HC-PCF que hacía la función de celda de gas. Dicho láser, tenía suficiente resolución espectral para medir VOCs como aldehídos o cetonas. Gracias a los agujeros de la HC-PCF, el rayo del láser era capaz de interactuar con las diferentes moléculas de los VOCs. Partiendo de este sistema, Christy Charlton et al. presentaron en [109], un sensor para detectar cloroetano, mostrando una sensibilidad de 30 ppbv.

Respecto a las fibras SSCs, en la bibliografía, no se ha encontrado ningún sensor que las utilice en sus montajes, pero, viendo el potencial que pueden tener en aplicaciones para la detección de VOCs, a lo largo de esta tesis doctoral se decidió apostar por ellas y en los capítulos siguientes, se presentan algunos experimentos y trabajos en los que sí que fueron utilizadas, obteniendo unos resultados muy interesantes y prometedores.

2.7. Conclusiones

Como se ha visto a lo largo de este capítulo, son muchos los montajes en los que se han utilizado algún tipo de MOFs para desarrollar sensores que sean capaces de detectar gases o VOCs.

El atractivo de utilizar MOFs es debido a poder elegir la estructura que más se adecúa para una aplicación final determinada. Debido a la estructura agujerada de las PCFs o a los agujeros que rodean el núcleo de las SSCs, la interacción entre la luz guiada por la fibra (bien sea, por el campo evanescente o por los modos de mayor orden) y las moléculas del gas o VOC a detectar es posible.

Los dos principales mecanismos de transducción de las MOFs son: la absorción de cierta potencia óptica en las bandas de absorción de los gases y en la variación del índice de refracción efectivo del medio que rodea al sensor debido a la presencia de las moléculas de gases o VOCs, que se desean medir. Dichas variaciones provocan cambios en las señales transmitidas o reflejadas que, pueden ser medidas, utilizando diferentes técnicas (midiendo el desplazamiento en longitud de onda o midiendo la diferencia de potencia óptica entre dos señales, aplicando la FFT…).

Si a la cantidad de gases y VOCs que pueden ser medidos, obteniendo unos resultados óptimos, se le suma las diferentes estructuras y configuraciones de MOFs que aún quedan por estudiar, el resultado anima a fomentar estudios para desarrollar sensores, ya que pueden ofrecer un enorme potencial en el campo de los sensores de fibra óptica.

Capítulo 3

Desarrollo de sensores de humedad basados en interferómetros MZ y SC-PCF

En este tercer capítulo de la tesis, se describen dos sensores de humedad basados en interferómetros Mach-Zehnder (MZ) y SC-PCF. Diferentes parámetros han sido estudiados y optimizados con la intención de conseguir mejorar las características finales de los sensores. Enumerándolos son: técnicas de deposición utilizadas, materiales sensibles elegidos para ser depositados y espesores de las nano películas de estos materiales cuando son depositados sobre la fibra óptica micro estructurada.

3.1. Introducción

La humedad es una de las magnitudes químicas más importantes en la vida de los seres vivos y en especial de los seres humanos. Está presenta en innumerables procesos industriales como los relacionados con el campo de la electrónica, de la agricultura, de la industria alimenticia, farmacéutica, papelera, textil o de la automoción e incluso, puede llegar a tener un papel clave en alguna aplicación médica como puede ser la monitorización de la respiración humana en pacientes enfermos. Por esta razón, su control y parametrización tiene un valor muy importante.

En las últimas décadas, una nueva clase de sensores de humedad está atrayendo el interés de números grupos de investigación debido a las ventajas que ofrece sobre los sensores más convencionales (típicamente sensores electrónicos): estos son los sensores de humedad basados en fibra óptica (OFHS, siglas en inglés). Este tipo de sensores presenta varias ventajas importantes con respecto a los sensores electrónicos como, por ejemplo, su pequeño tamaño, su durabilidad, la posibilidad de trabajar en entornos inflamables o con humedades y temperaturas altas, con distintos rangos de presión e incluso con riesgo de explosión… Pero, probablemente, la más interesante sea su inmunidad electromagnética. Por todas estas cualidades expuestas, los sensores de fibra óptica pueden soportar condiciones exigentes como las que se dan en los procesos industriales previamente citados, haciéndolos de esta forma unos buenos candidatos para su utilización en estos entornos.

Gracias a lo expuesto en el párrafo anterior, el desarrollo de los OFHS creció exponencialmente, y con ello, el número de contribuciones científicas. Una manera de poder clasificar todos los sensores publicados hasta la fecha es basándose en su principio de transducción y en las diferentes estructuras que se usan para el sensado. El primero grupo de la clasificación puede considerarse el basado en la absorción óptica de ciertos materiales sensibles, que a su vez fue el primero que se investigó por la comunidad científica [110]; el siguiente grupo sería el formado por los sensores basados en "*Fibre Bragg Gratings*" (FBG, siglas en inglés); otra posibilidad para desarrollar OFHS sería la utilización de interferometría, la cual puede generar diferentes tipos de interferómetros: Fabry-Pèrot, Sagnac, Mach-Zehnder, Michelson e interferómetros modales; el cuarto grupo sería el que agrupa a los OFHS que basan su mecanismo de transducción

en micro estructuras o deformaciones de la fibra como por ejemplo: "*tapers*", anillos, así como los sensores basados en "*whispering galleries modes*" (WGM, siglas en inglés); por último, el grupo basado en resonancias electromagnéticas, más específicamente "*lossy mode resonances*" (LMRs, siglas en inglés). Un esquema con la clasificación propuesta se presenta a continuación.

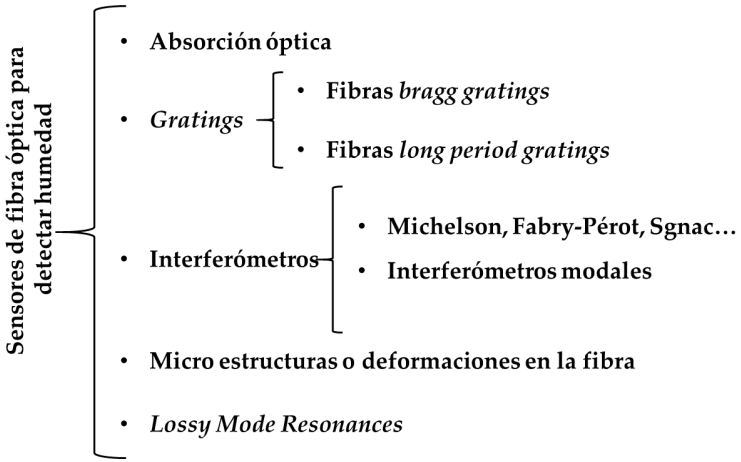

Figura 1. 1 *Clasificación de los diferentes tipos de sensores de humedad basados en la utilización de fibra óptica.*

Dentro de los sensores interferométricos, existen diferentes formas de generar dicha interferometría: una de ellas es la utilización de fibras ópticas micro estructuradas. Dichas fibras son un excelente candidato para desarrollar este tipo de sensores debido a su estructura, la cual favorece la interacción entre el campo evanescente generado por la luz que viaja guiada a través de ellas y el medio que rodea a la fibra.

3.2. Interferometría Mach-Zehnder y SC-PCF

Una de las principales conclusiones que se puede deducir del estudio realizado en el primer capítulo de esta tesis es que la generación de un interferómetro MZ utilizando SC-PCF es una de las mejores alternativas para desarrollar sensores de humedad debido a las sensibilidades obtenidas.

De forma breve, el interferómetro Mach-Zehnder se consigue al empalmar dos latiguillos SMF a ambos extremos de una SC-PCF, generando de esta forma

dos regiones colapsadas (los agujeros de la SC-PCF se colapsan en dos pequeñas regiones próximas a los empalmes debido al efecto de las descargas que se producen al realizarlos). Pero para entender cómo el interferómetro trabaja es necesario analizar el comportamiento del haz de luz guiado cuando atraviesa estas dos regiones colapsadas. El modo fundamental de la SMF se difracta cuando entra en contacto con la primera región colapsada. Debido a esta difracción, los modos del revestimiento, en el segmento de la SC-PC, se excitan; de esta manera, el haz de luz se divide en dos componentes: una que viaja por el núcleo de la SC-PCF y otra que viaja a lo largo de la cubierta de la fibra. Las constantes de propagación de los distintos modos excitados son distintas y, por consiguiente, ciertos modos acumulan una diferencia de fase conforme se propagan a lo largo de la sección de SC-PCF. Cuando se alcanza la segunda región colapsada, ambas componentes se recombinan en el núcleo de la segunda SMF empalmada describiendo un patrón interferométrico.

Un factor importante y que hay que tener en cuenta a la hora de desarrollar un sensor, es el material sensible elegido para detectar los cambios de humedad; no todos los materiales son igual de sensibles. Las propiedades y características de este material sensible, al interactuar con las moléculas de agua, determinarán si un sensor es más sensible o menos sensible. Tomando como referencia la publicación encontrada en la bibliografía con mejor sensibilidad, utilizando fibras SC-PCF para generar un interferómetro Mach-Zehnder [84], se consideró la posibilidad de mejorar dicha sensibilidad empleando otro material sensible y otra técnica de deposición. Es aquí donde nace la idea para desarrollar la primera contribución de esta tesis.

3.2.1. Deposición de polímeros higroscópicos utilizando la técnica de deposición *"Layer-by-Layer" (LbL)*

La agarosa fue utilizada en [84] como material sensible. Es un polímero higroscópico que, en presencia de moléculas de H_2O, es capaz de interactuar con ellas debido a un fenómeno denominado absorción y desorción (provocando los efectos de *"swelling"* y "*deswelling*"). De esta manera, los posibles cambios de humedad en el medio que rodean al sensor pueden ser detectados. La técnica utilizada para depositar la agarosa en esta contribución científica fue la de *"dip coating"*. Dicha técnica, sumada a la morfología viscosa del material, generaban

ciertas limitaciones en términos de reproducibilidad, así como en el control del espesor depositado. El control de este parámetro es de vital importancia para la sensibilidad del sensor y su optimización, por lo tanto, conduce a una mejora de ella. Por estas razones, en la primera contribución que se deriva de esta tesis, se propuso la mejora de la sensibilidad de los sensores previamente publicados, utilizando una nueva técnica de deposición (Layer-by-Layer nanoassembly, LbL) y una nueva pareja de polímeros sensibles a la humedad (poly(allylamine hydrochloride, PAH y poly(acrylic acid, PAA) que permitieran tener un control del espesor depositado. La construcción de un recubrimiento utilizando esta técnica (LbL), se basa en el ensamblaje de las partículas cargadas con signo opuesto, es decir, de un polímero con carga positiva (policatión: PAH) y de otro con carga negativa (polianión: PAA). Las partículas con una determinada carga se adhieren al sustrato (en este caso la fibra óptica) atraídas por las partículas de carga opuesta, bien de una pareja de capas inicial o bien de la última capa depositada, para ir formando lo que se conoce con el nombre de pareja de capas, de una forma parecida a la que ilustra la siguiente imagen.

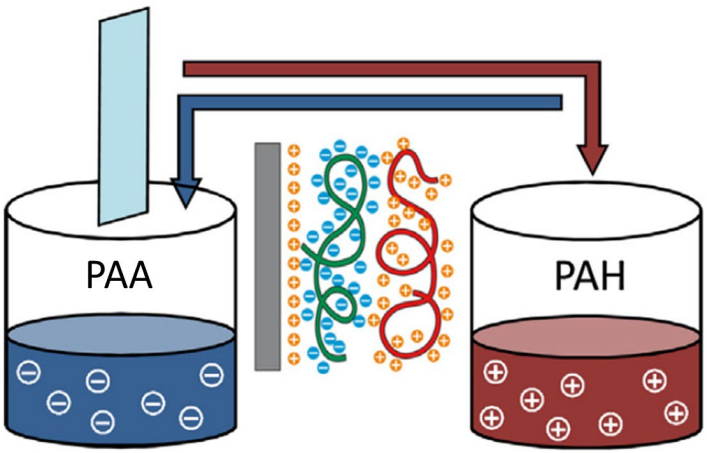

Figura 1. 2 *Esquema de los pasaos utilizados para la deposición de una película polimérica utilizando la técnica de deposición LbL.*

Por último, y como novedad con respecto a los artículos previamente publicados en este campo de investigación, en esta primera contribución se realizó una comparativa entre la técnica utilizada en la gran mayoría de los artículos para dar el dato de la sensibilidad del sensor (medir el desplazamiento

de un pico del patrón interferente en longitud de onda) y una técnica basada en la transforma rápida de Fourier (FFT). Esta técnica consiste en monitorizar los cambios en fase de la frecuencia fundamental del patrón interferométrico del sensor. Los resultados obtenidos se muestran en la siguiente publicación de la revista "*Sensors and Actuators B: Chemical*", que lleva por título: "*Photonic crystal fibre interferometer coated with a PAH/PAA nanolayer as humidity sensor*".

Sensors and Actuators B 242 (2017) 1065–1072

Contents lists available at ScienceDirect

Sensors and Actuators B: Chemical

journal homepage: www.elsevier.com/locate/snb

Photonic crystal fiber interferometer coated with a PAH/PAA nanolayer as humidity sensor

Diego Lopez-Torres[a,*], Cesar Elosua[a,b], Joel Villatoro[c,d], Joseba Zubia[c], Manfred Rothhardt[e], Kay Schuster[e], Francisco J. Arregui[a,b]

[a] Nanostructured Optical Devices Laboratory, Electric and Electronic Engineering Department, Public University of Navarre, Edif. Los Tejos, Campus Arrosadía, 31006 Pamplona, Spain
[b] Institute Of Smart Cities (ISC), Centro Jerónimo de Ayanz, Campus Arrosadia, 31006 Pamplona, Spain
[c] Department of Communications Engineering, Escuela Técnica Superior de Ingeniería de Bilbao, University of the Basque Country, Bilbao 48049, Spain
[d] IKERBASQUE, Basque Foundation for Science, Bilbao, Spain
[e] Leibniz Institute of Photonic Technology (IPHT), Albert-Einstein-Strasse 9, 07745 Jena, Germany

ARTICLE INFO

Article history:
Received 30 June 2016
Received in revised form
21 September 2016
Accepted 23 September 2016
Available online 25 September 2016

Keywords:
Photonic crystal fiber
Interferometer
Layer-by-layer nanoassembly
Humidity sensor
Fast Fourier transform

ABSTRACT

In this paper, an optical fiber interferometric humidity sensor is presented. The device consists of 1 cm-long segment of photonic crystal fiber (PCF) spliced to standard single mode fibers (SMFs), forming an interferometer: the two collapsed interfaces between PCF and SMF segments produce the excitation and recombination of core and cladding modes. The latter interact with a poly(allylamine hydrochloride) (PAH) and poly(acrylic acid) (PAA) polymeric nanocoating deposited on the PCF by the well-established layer-by-layer nano assembly (LbL) technique. Humidity modifies the index of the polymeric nanolayer which in turns alters the cladding modes along the PCF segment and causes a detectable shift to the interference pattern. A study of different nanocoting thicknesses is presented in order to obtain the best possible sensibility for the sensor. Furthermore, the interrogation of the humidity sensor is presented not only by the conventional study of the spectrum shift amplitude, but also making use of the Fast Fourier Transform (FFT), which yields a linearization of the device response. The sensor here presented is reproducible, can resolve 0.074% of relative humidity (RH) and operates in the 20–95% RH range. Moreover, it exhibits response time of 0.3 s, a negligible cross sensitivity to temperature as well as long term stability.

1. Introduction

A large number of papers have been published in the field of optical fiber sensors in the last decades [1–4]. These devices can benefit from advantage of the electromagnetic immunity, light weight, low transmission losses in the communication windows, low cost or wavelength multiplexing. The utilization of optical fiber sensors for measurement of different magnitudes such as temperature [5], humidity [6], gases [7] or pHs [8] has been described by different authors in the literature using a wide range of interrogation techniques i.e. interferometry, long-period gratings or resonances.

In the past decade, new optical fibers have been developed in order to get lower nonlinearity, lower attenuation, and unique wave-guiding properties. This is the case of Photonic Crystal Fibers (PCFs), proposed in 1995 by Russell et al. [9] which contain arrays of tiny air holes along their structure allowing the development of new applications and the fabrication of new optical fiber sensors. If a portion of PCF is spliced between two segments of single mode fibers, then a Photonic Crystal Fiber Interferometer (PCF-I) is obtained. In such devices, the fundamental mode guided in the core of the single mode fiber, when reaches the interface with the PCF, can excite cladding modes of the PCF. In this manner, the light signal is divided in two components: one traveling through the core of the PCF and the other one along its cladding. At the end of the PCF segment, the both modes are recombined in the core of the second

Abbreviations: LbL, layer-by-layer; PCF, photonic crystal fiber; KOH, potassium hydroxide; PAH, poly(allylamine hydrochloride); PAA, poly(acrylic acid); RH, relative humidity; FFT, fast Fourier transform; OSA, optical spectrum analyzer; SNR, signal to noise ratio.

* Corresponding author.
E-mail addresses: diego.lopez@unavarra.es (D. Lopez-Torres), cesar.elosua@unavarra.es (C. Elosua), agustinjoel.villatoro@ehu.eus (J. Villatoro), joseba.zubia@ehu.es (J. Zubia), manfred.rothhardt@leibniz-ipht.de (M. Rothhardt), kay.schuster@leibniz-ipht.de (K. Schuster), parregui@unavarra.es (F.J. Arregui).

http://dx.doi.org/10.1016/j.snb.2016.09.144
0925-4005/

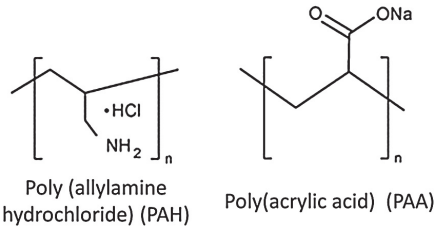

Fig 1. Chemical structures of the hydrogels (PAH/PAA).

single mode fiber: it produces an oscillatory spectral response of an interferometer. These devices are used to implement sensors: the transduction is based on depositing a sensing material along the PCF segment: the cladding modes are affected by the external medium surrounding the PCF and, therefore, the interferometric pattern is altered.

In order to create a humidity fiber sensor, the utilization of PCF-I combined with an agarose coating sensitive to humidity and deposited by dip-coating has been presented in previous works [10]. However, due to the limitations of the deposition technique, these sensors present some drawbacks such as the reproducibility in the fabrication of the nanocoating as well as the limitation to control the thickness of the coating on the nanometer scale [11].

The current work proposes the use of two polymers (poly(allylamine hydrochloride) (PAH) and poly(acrylic acid) (PAA)) deposited by layer-by-layer nanoassembly (LbL) on a Photonic Crystal Fiber Interferometer (Fig. 1 shows the chemical structures of the hydrogels) (PAH/PAA). Based on [12], absorption (swelling and deswelling) is the mainly mechanism of interaction between water molecules and [PAH/PAA] nanofilm. At lower humidity (RH values up to ≈60%), the nanofilm shows a low swellability and it can be physically explained by strong interchain H-bonding between COOH groups. At higher humidity, however, water penetrates the structure, mitigates interchain H-bonding, and permits rapid swelling as the COOH groups ionize and are forced apart. Working at the nanometer scale with the humidity sensing coating should overcome the limitations seen in previous works. Furthermore, since the thickness of the coatings is below the penetration depth of the evanescent field, the sensing coating cannot be considered as an infinitum medium. Due to this, besides the sensitivity to the refractive index of the sensing coating, the sensitivity to the coating thickness could also play an important role [13].

In addition, the studied humidity sensors were interrogated not only studying the spectrum shift but also making use of the Fast Fourier Transform (FFT) for monitoring the spectrum phase variations. The FFT is calculated by the software MATLAB through the command fft. A script in MATALB was programmed in order to obtain the phase sensor response using the recorded data obtained by the OSA and the command mentioned above (fft). This method does not depend of the signal amplitude and also avoids the necessity of tracking the wavelength evolution in the spectrum; moreover, it is applicable to networks that require narrow band sensors, allowing high multiplexing rates. The proposed sensor is characterized following the spectral shift and FFT approaches, comparing them in terms of sensitivity and linearity [14].

To our knowledge, this is the first time that a nanocoating has been deposited by means of LBL on a PCF-I to achieve a humidity sensor and moreover, the first time FFT is used to characterize this type of configuration.

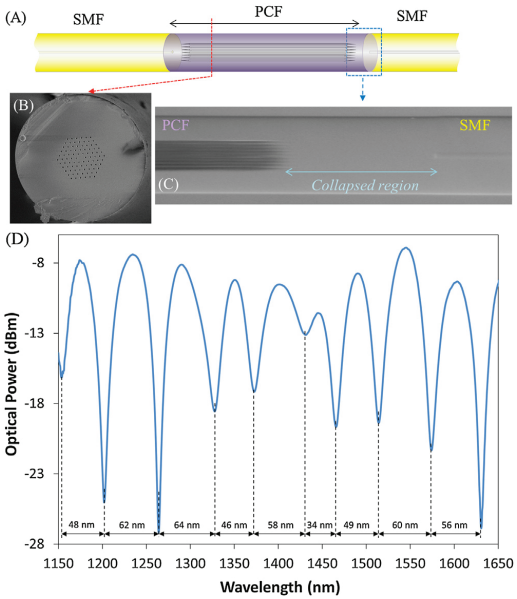

Fig. 2. (A) Schematic representation of the photonic crystal fiber interferometer (PCF-I); (B) Micrograph of the PCF-SMF juntionc showing the collapsed region of the PCF; (C) Cross section of the PCF used to build up the interferometer; (D) Transmission spectrum of the PCF-I.

2. Experimental details

2.1. Chemical reagents

Two different polymers have been used for the construction of the nanocoating: poly(allylamine hydrochloride) (PAH) (Mw ~15,000) and poly(acrylic acid) (PAA) (Mw ~15,000) 35 wt% solution in water. The cleaning and the generation of a superficial electrical charge on the optical fiber were performed by 10% Potassium Hydroxide (KOH) solutions. The pH of the different mixtures was measured by an electronic pH-metter (Crimson INC). The acidity of the polymeric solutions was adjusted to pH 4.4 by Hydrochloridric acid (HCl) and Sodium Hydroxide (NaOH). The entire set of reagents were supplied by Sigma–Aldrich and they were used without further purification. All solutions were prepared using ultrapure water with a resistivity of 18.2 MΩ cm (Diamond RO D12671).

2.2. Construction of the nanocoating

Prior to the deposition of the nanocoating, one centimeter of standard PCF (LMA-8 Crystal Fiber A/S) was spliced to Corning SMF-28 (standard fiber optic) with a conventional splicing machine. The splicing was carried out in such a way that the voids of the PCF collapsed completely over a short region (generally less than 300 micrometers long) [15]. At this point, the PCF-I was attached to a U-shaped holder in order to prevent undesired bending or possible breakages and, in addition, to facilitate the coating deposition. Fig. 2 shows a schematic representation of the resulting interferometer, detailing the PCF microstructure and the collapsed region interface.

The technique used for the deposition of the humidity sensitive coating was LbL nanoassembly technique. The method was proposed by Decher [16] as a simple and automatable method

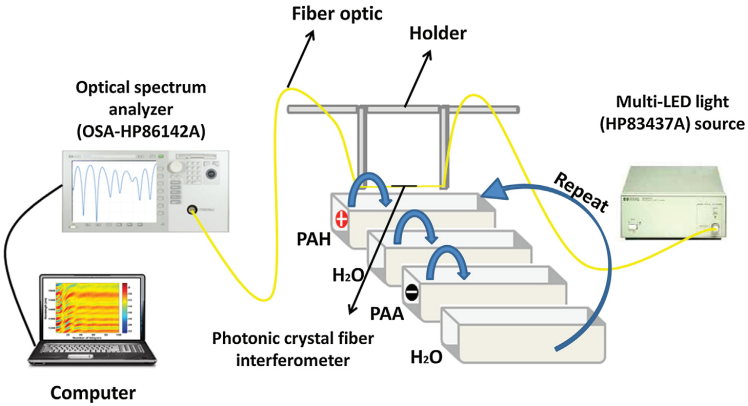

Fig. 3. Transmission set up used to monitor de deposition process based on LbL nano assembly method.

to fabricate films at the nanometer scale. LbL technique consists of the assembly of oppositely electrically charged polyelectrolytes (polycation and polyanion respectively) forming a bilayer [17]. LbL procedure is not limited by the shape or the size of substrates, which a remarkable feature for optical fiber sensors [18]. First of all, PCF-I was immersed for ten minutes into a 1 M potassium hydroxide (KOH) aqueous solution in order to induce a negative electrical superficial charge. Thereafter, the PCF-I was cleaned up in ultrapure water. The nanocoating was prepared dipping the PCF alternatively into the 10 mM polyelectrolyte solutions: first, the fiber was immersed into the polycationic solution (PAH) for two minutes and then it was washed with ultrapure water for 1 min to remove the not properly assembled chains; then, the device was dipped into the polyanionic (PAA), rinsing it again with ultrapure water for another minute. In this manner, a bilayer with the structure [PAH/PAA] was conformed. This process was repeated as many times as required. The method was automated by using a robotic arm (acquired from Nadetech Innovations S.L.), ensuring its reproducibility.

2.3. Characterization setup

The transmission setup used in this work is shown in Fig. 3. The transmission configuration has advantages when it is compared with the reflection one used in previous works [19,20]: the collapsed voids interface cannot be contaminated by dust or unwanted particles causing an erroneous measurement; moreover, the use of the fiber optic circulator is not required. The PCF sensor device was interrogated with a multi-LED light (HP83437A) source whose emission spectrum span was between 1150 and 1650 nm allowing the spectra behavior of the PCF interferometer to be studied in a higher spectra range; the sensing signal was acquired by an optical spectrum analyzer (OSA-HP86142A). To calculate the interferometric response, the signal obtained with a SMF pigtail connecting the light source and the spectrometer was considered as reference. Once the interferometer was included to the setup, the interferometric response was evaluated comparing the different signals with the reference. In this manner, changes in the interferometric pattern were observable. This set up was used to monitor both the growth of the nanocoating and its response with RH changes in terms of wavelength shifts.

The influence of the length of the PCF segment on the fringe spacing of a transmission-type PCF interferometer was investigated [21]. It was shown an inversely proportional relation between the fringe spacing and the length of the PCF section. In order to facilitate the study of the PCF-I humidity response and to increase the measurement range of relative humidity, a large fringe spacing for the interferometer was required. The length of the PCF was 10 mm: the resulting averaged fringe spacing was ~53 nm (see Fig. 2D), which allowed the construction process to be optimized in terms of maximum sensitivity as well as to characterize the sensor.

3. Study of thickness effect on the sensor sensitivity

The fabrication of the nanocoating was monitored using the setup described in Fig. 3. As it was mentioned in the introduction section, the evanescent field along the PCF section interacts with the surrounding media a distance known as penetration depth, which is below 1 μm. The thickness of the sensing coating deposited by LbL method is in the nanometrical scale: as more bilayers get deposited, their interaction with the evanescent field changes, and in this manner, so does the interferometric pattern. In terms of the spectral shape, it was observed a red shift as the number of bilayers increased. Furthermore, the sensing coating behaves as and hydrogel, so that the interaction between [PAH/PAA] nanofilm and water molecules causes the effect of swelling and deswelling. Consequently, an increase in the nanofilm thickness occurs when the relative humidity is increased [12]. And according to Fig. 5, an increase in the nanofilm thickness results in a redshift (always working below the penetration depth of the evanescent field, where the effect of the thickness change plays a dominant role with respect to the contribution of the refractive index variation). Thus, a decrease in the nanofilm thickness gives a blueshift. Therefore, the construction process should show an optimal point at which variations in RH would produce significant spectral shifts: actually, this point would show the highest slope (in terms of spectral shift).

The effect of the nanocoating thickness (firstly expressed as the number of bilayers) was studied by monitoring the interferometric pattern for a 100 bilayers nano construction. The resulting spectrum after the deposition of each bilayer was recorded: all of them are displayed in 2D graphs (Fig. 4A): every spectrum is represented in the vertical axis, and their respective magnitudes (expressed in dB) are indicated by a color map. It can be observed that there are 3 sections along the construction process that show different slopes in terms of spectral shift: they are marked with dashed squares in Fig. 4A. Actually, the slope gets lower as the number of bilayers is increased: in fact, there is almost no shift once 60 bilayers are deposited. It is a consequence of the coating thickness: above 60 bilayers, this parameter is thicker than the penetration depth of

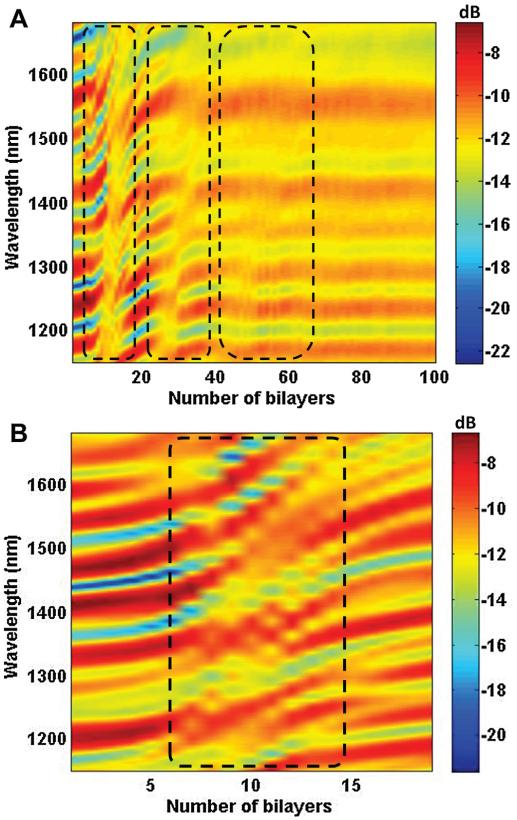

Fig. 4. (A) Transmission spectra that were recorded after the deposition of every single layer: the dashed squares highlight the areas with a remarkable spectral red shift; (B) Detailed representation of the spectra registered from the deposition of the first 20 bilayers: the dashed line frames the spectra that show a significant red shift (For interpretation of the references to color in this figure legend, the reader is referred to the web version of this article.).

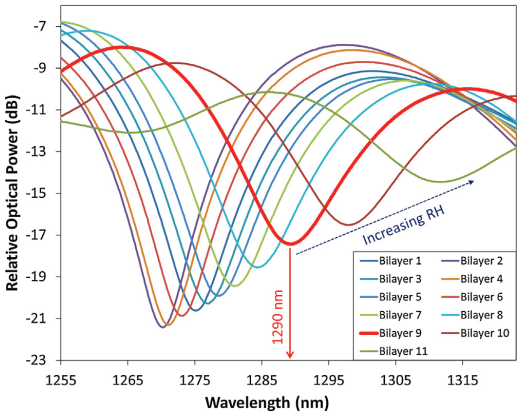

Fig. 5. (A) Spectral red shift observed along the construction process from 1225 nm and 1325 nm. After 9 layers are deposited, the transmission valley is centered at 1290 nm: its spectral shift when RH is increased is supposed to show the optimal sensitivity, following the trending pointed in the graph (For interpretation of the references to color in this figure legend, the reader is referred to the web version of this article.).

the evanescent, so that any increase above this point produces no variation in the interaction between the coating and this propagating mode. What is more, the evanescent field decays exponentially from the cladding, which explains why the slope of the shift is lower as more layers are deposited. Fig. 4B displays a detailed representation of the spectra from the first 20 bilayers: it can be observed that for 10 bilayers the slope is maximum, so that to get the optimal sensitivity, the construction process was to be stopped for 9 bilayers. Fig. 5 shows in detail the spectral shift for the transmission valley initially located at 1270 nm, verifying that for that number of bilayers the sensitivity should be optimal. Therefore, once another sensor was prepared with just 9 bilayers, the location of the spectral valley to monitor was 1290 nm. In order to not affect the coating deposition, the thickness of the sensor was only measured at the end of the fabrication process. Due to this, in our work we only measured the thickness of the coating at the end of the process, the sensor with 9 bilayers. The thickness of the deposited coating was measured by a Scanning Electronic Microscope: the resulting value was 240 ± 20 nm (below the penetration depth of the evanescent field) and, moreover, the images shown a uniform coating morphology (Appendix A Supplementary data, Fig. S1 in the online version, at http://dx.doi.org/10.1016/j.snb.2016.09.144). These data are in accordance with [22], where the thickness of the PAH/PAA polymeric coating is estimated as a function of the number of bilayers, from 0 to 100 bilayers.

4. Results and discussion

The relative humidity (RH) response of a PAH/PAA nanocoated PCF-I was studied with the set up shown in Fig. 6: the sensor was placed inside a climatic chamber (Angelantoni, CH 250). Several experiments were implemented changing the relative humidity from 20% to 95% at $25\,^{\circ}C \pm 2\,^{\circ}C$ at room atmospheric pressure. The sensor response was firstly characterized following the red shift of the transmission valley that shown the highest sensitivity: as it was mentioned in the previous section, it was located at 1290 nm once the construction process was over. This type of characterization is typically performed for sensors based on interferometers, but it has two remarkable drawbacks: on one hand, the wider the transmission valley (or peak) is, the less accurate is its wavelength location; on the other hand, in the case of several peaks are recorded, only the information of one of them is used, so the rest of the spectrum becomes useless, reducing the potential robustness of the sensor. In this context, it is possible to take advantage of the whole spectrum by applying an analysis based on FFT: as an interferometric response, the magnitude of the resulting FFT spectrum is not supposed to change, but the phase one should show the spectral shifts. In this manner, the sensor response can be studied following the most significant components of the phase spectrum obtained from FFT analysis of the sensor signal. Another relevant feature is that SNR is not as restrictive as in the case of wavelength shift based measurements and moreover, it is applicable to narrow band sensors, which allows working with high multiplexation rates [23].

In order to compare the wavelength shift and the FFT methods, the sensor was exposed to 20%–95% increasing/decreasing cycles (temperature was kept constant at $25\,^{\circ}C$). The spectra were recorded every minute, and they were processed following both approaches: the results are plotted in Fig. 7. As it can be observed in Fig. 7A, there is no a linear relationship between the wavelength shift and the RH: the total shift is 61 nm, which is higher than the one reported in previous works [21] (56 nm). The relationship between the shift and RH is not lineal along the entire range of

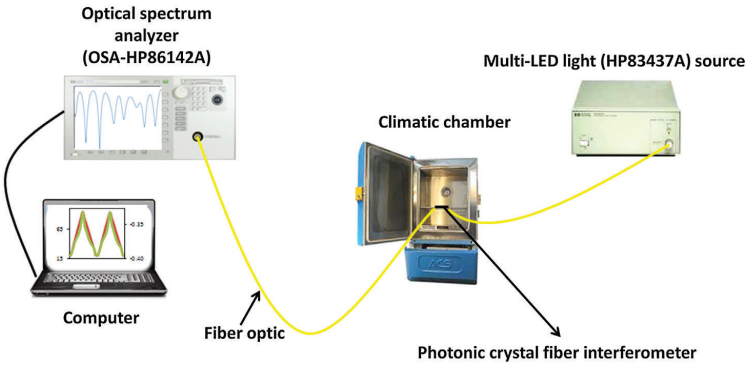

Fig. 6. Set up used to study the response of the sensor to RH variations: it is located inside a climatic chamber where humidity and temperature are controlled.

RH: for lower humidity values (20%–75%), an almost linear behavior linear behavior is observed, with a sensitivity of 0.29 nm/% RH; in contrast between 75%–95%, the response is exponential, with an estimated sensitivity of 2.35 nm/% RH. The resolution for each RH segment is 0.21% RH and 0.025% RH respectively and the humidity resolution for the entire range, 20–95% RH, is 0.074% RH. Other feature of the sensor is that the signal is very stable when the RH is constant at 20% (at the beginning and at the end of the measurement, as well as between every cycle). In order to clarify these dates, Table 1. compares the [PAH/PAA] PCF-I resolution with the earlier devices published [21] and confirms that the total resolution of the [PAH/PAA] PCF-I resolution is the highest, to our knowledge, for a relative humidity change from 20% to 95% RH.

The results obtained when applying FFT are displayed in Fig. 7B. The response with this method is more linear and less noisy than the study of the spectrum shift focused on a specific peak. This improvement can be associated to work only with the most significant component of the FFT module. FFT technique can be applied due to the existence of a series of periodic maxima and minima in the transmission spectra of the PCF-I, but it is not ideally periodic; moreover, no-linear components appear in the spectrum. The interferometric response changes due to phase variations of the pattern: in the case of wavelength shift, they follow a non linear mathematical expression, but for FFT, just the phase component of this expression is considered, which is linear (the non linear components of the spectrum produce the deviation from the linear approach). Considering the response as linear (in the range 20%–95% RH), the sensitivity is 0.86 mrad/% RH (0.16°/% RH) and the total phase shift is 0.065 rad (12°).

The resulting characterizations for both approaches are also plotted in Fig. 8A (wavelength shift) and 8 B (phase shift): in both graphs, the response registered with increasing and decreasing RH is displayed in order to check hysteresis. In the case of the wavelength shift based analysis, the remarked non linear response for RH values above 80% is observable; on the contrary, when the FFT analysis is applied, the behavior of the sensor is more linear. Two fitting lines have been calculated in order to confirm this assumption. The R^2 of the wavelength analysis (Fig. 8A) is 0.992 when the relative humidity is increased from 20% to 75% RH and 0.9047 when the relative humidity is increased from 75% to 95% RH. For the case of FFT analysis (Fig. 8B), the R^2 is 0.9936 in the first range and 0.9862 in the second range. In both cases, the R^2 is higher when the FFT is applied. This difference is because the shift of the interferometric pattern depends linearly on the phase component of its FFT spectrum. It is also remarkable that the hysteresis of the sensor is below 5%.

In order to study the influence of temperature in the $[PAH/PAA]_9$ nanocoated PCF-I, cycles with different temperatures (from 15 °C to 45 °C) were performed. Fig. 9 shows the phase variation along these cycles. The sensitivity of the PCI interferometer in the range of 15 °C–45 °C is 5.23×10^{-5} rad/°C (0.003°/°C). This sensitivity (0.003°/°C) is much lower than the sensitivity obtained in the humidity cycles (0.18°/% RH): it can be concluded that the PCF-I sen-

Table 1
Comparison between [PAH/PAA] PCF-I resolution and earlier devices published [21] where a humidity sensor based on an Agorose-coated was carried out.

PAH/PAA PCF-I (OSA resolution: 0.06 nm)	PAH/PAA PCF-I (OSA resolution: 0.01 nm)	Earlier published, Ref [21] Agarose (OSA resolution: 0.01 nm)
Total wavelength for a RH change of 75% RH → 61 nm	Total wavelength for a RH change of 75% RH → 61 nm	Total wavelength for a RH change of 60% RH → 56 nm
Resolution in the lineal range for a RH change of 55% RH → 0.21% RH	Resolution in the lineal range for a RH change of 55% RH → 0.035% RH	Resolution in the lineal range for a RH change of 40% RH → 0.017% RH
Resolution in the lineal range for a RH change of 20% RH → 0.025% RH	Resolution in the lineal range for a RH change of 20% RH → 0.004% RH	Resolution in the lineal range for a RH change of 20% RH → 0.007% RH
Total resolution for a RH change of 75% RH → 0.07% RH	Total resolution for a RH change of 75% RH → 0.01% RH	Total resolution for a RH change of 60% RH → 0.01% RH

The resolution of each RH segment is determined as follows:

1. First of all, we calculate the wavelength shift in each segment (~16 nm for the first area, humidity values from 20% to 75% RH and ~45 nm for the second area, humidity values from 75% to 95% RH).
2. Secondly, we divide these wavelength shifts by the relative humidity range of each segment. In the first case, 55% RH (from 20% to 75% RH) and in the second case 20% RH (from 75% to 95% RH). In this manner, we obtain the sensitivity of each segment: 0.29 nm/% HR and 2.35 nm/% HR.
3. Finally, we only have to divide the OSA resolution (in our case 0.06 nm) by the results of point 2. The result of this division is the resolution of each segment.

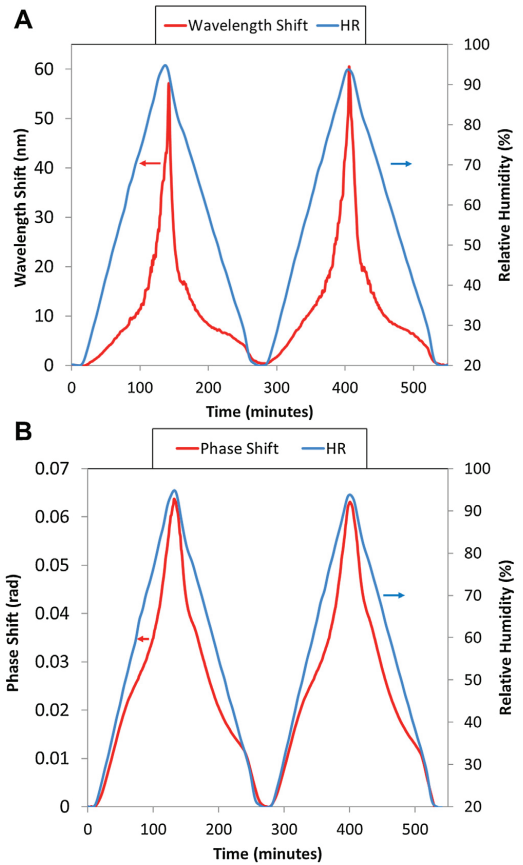

Fig. 7. Spectral shifts from the transmission valley located at 1290 nm once the deposition process was completed: (A) RH values are represented on the right hand axis, whereas the wavelength shift is indicated in the left hand one; (B) Phase shift observed once the FFT is applied to the transmission spectrum along the humidity cycles.

sor has a negligible cross correlation with temperature [24], which is a relevant feature in relative humidity sensing applications.

The kinetics of the sensor were also studied. The set up used was the same one shown in Fig. 3 but OSA was set to mode "Zero Span": in this manner, the intensity of the sensing signal at a specific wavelength (1285 nm) was monitored. Humidity changes were performed using the human breath towards the sensor. This experiment consists of inhaling and exhaling several times placing the sensor close to the mouth, so that quick RH variations are produced by breathing. The shift in the spectrum of transmission was studied at a room temperature of 20 °C and RH of 55%. Roughly, the maximum value reached by human breath exhale is 90%: therefore, the approximate range of RH in this experiment is 55%–90%. The temporal response of the sensor is shown in Fig. 10. In every cycle, the response recovered the baseline and the observed signal variations confirmed the repeatability of its response. The average response time of the PDF-I is below 300 miliseconds, whereas the recovery time was found shorter than 270 miliseconds. The test was repeated three weeks later and the results obtained were similar (see Fig. 10), so that the temporal stability of the sensor is verified.

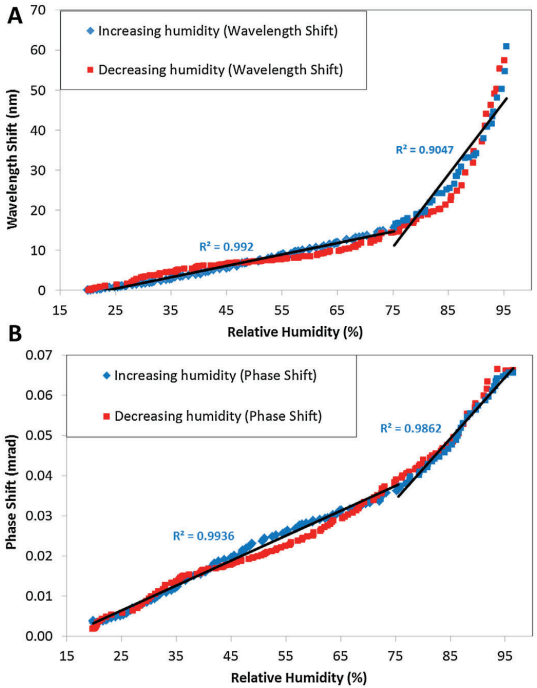

Fig. 8. Characterization of the sensor response as a function of the relative humidity expressed in (A) wavelength shift and (B) FFT phase shift.

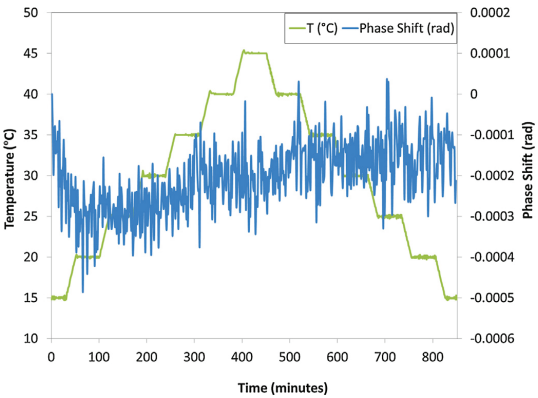

Fig. 9. Study of the effect of temperature on the phase shift.

5. Conclusions

A sensor based on PCF-I to measure RH is presented in this work. The transduction is produced by the interaction of the evanescent field along the PCF section and the sensing layer coated along it, which behaves as a hydrogel. The final sensitivity of the sensor can be optimized by adjusting the thickness of the coating (following LbL method): any variation in its value produced by changes in relative humidity will produce the highest spectral shift. In any case, the total thickness of the sensing coating has to be below the penetration depth of the evanescent field to ensure an

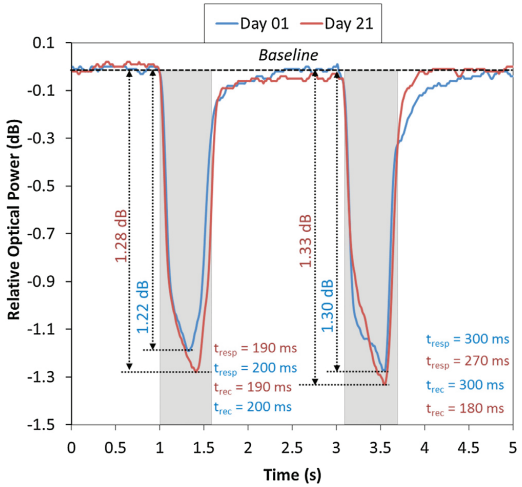

Fig. 10. Optical power at 1270 nm when the sensor is exposed to human breath. Inset, data about the signal change and kinetics are detailed; the gray areas indicate the exhalation and the white ones the inhalation.

optimal response. The sensitivity reported from PCF-I sensors prepared with hydrogels deposited with dip coating technique is lower than the obtained from the optimized sensor. The guarantied reproducibility by LbL method, as well as the just mentioned sensitivity optimization, makes this construction procedure more interesting than the traditional ones such as dip coating. Moreover, LbL technique achieves high reproducibility and a precise control in the thickness of the nanocoating allowing to work at the nanometer scale where the thickness of nanocoating is below the penetration depth of the evanescent field. At this scale the sensibility of the sensor depends mainly on the nanocoating thickness instead of the refractive index of the sensing coating.

The response of the sensor has been analyzed applying two different techniques. The first one is based on the traditional approach of following the shift of remarkable points of the interferometric spectral response, such a transmission valley. The resulting characterization is non linear for RH values above 80%. As an alternative, a method based on the FFT is proposed: the interferometric spectrum shift can be monitored by the phase component of its FFT. This approach enhances the performance of PCF-I based sensors because the resulting characterization is more linear and less noisy than the ones based on wavelength monitoring.

Temperature has a negligible effect on the sensor response and furthermore, the response of the sensor is preserved unaltered after at least 3 weeks. Regarding to its kinetics, the nanometric thickness of the coating easies the transduction, so that response and recovery times below 1 s were observed. All these features are a consequence of the synergy between the PCF-I transmission configuration, LbL method and FFT signal processing: the resulting sensor improves the results reported from previous works, making it possible to use it in applications where linear behavior is required.

Competing interests

The authors declare that they have no competing interests.

Acknowledgments

This work was supported by the Spanish Economy and Competitivity Ministry-FEDER TEC2013-43679-R. The authors would like to express their gratitude to Nadetech Inc. for the design, fabrication and tune-up of the robot used for the deposition of the nanocoatings.

References

[1] F.J. Arregui, I.R. Matías, I. Del Villar, J.M. Corres, J. Goicoechea, Optical fiber sensors based on nanostructured coatings, III Jornadas Hisp. IBERNAM-CMC2. 2015 (2006).
[2] F.J. Arregui, I.R. Matias, J.M. Corres, I. Del Villar, J. Goicoechea, C.R. Zamarreño, M. Hernáez, R.O. Claus, Optical fiber sensors based on layer-by-layer nanostructured films, Procedia Eng. 5 (2010) 1087–1090.
[3] C. Elosua, N. De Acha, I.R. Matias, F.J. Arregui, ScienceDirect luminescent optical fiber oxygen sensor following layer-by-layer method, Procedia Eng. (2014) 3.
[4] J. Ascorbe, J.M. Corres, F.J. Arregui, I.R. Matias, Optical fiber current transducer using lossy mode resonances for high voltage networks, J. Lightwave Technol. 33 (2015) 2504–2510.
[5] S.M. Chandani, N.A.F. Jaeger, Fiber-optic temperature sensor using evanescent fields in D fibers, IEEE Photonics Technol. Lett. 17 (2005) 2706–2708.
[6] M. Hernaez, D. Lopez-Torres, C. Elosua, I.R. Matias, F.J. Arregui, Sensitivity enhancement of a humidity sensor based on poly(sodium phosphate) and poly(allylamine hydrochloride), IEEE Sens. (2013) 1–4.
[7] C. Elosua, N. de Acha, M. Hernaez, I.R. Matias, F.J. Arregui, Layer-by-layer assembly of a water-insoluble platinum complex for optical fiber oxygen sensors, Sens. Actuators B: Chem. 207 (2015) 683–689.
[8] P. Zubiate, C.R. Zamarreño, I. Del Villar, I.R. Matias, F.J. Arregui, Tunable optical fiber pH sensors based on TE and TM lossy mode resonances (LMRs), Sens. Actuators B: Chem. 231 (2016) 484–490.
[9] D.M. Atkin, T.J. Shepherd, T.A. Birks, P.S.J. Russell, P.J. Roberts, Full 2-D photonic bandgaps in silica/air structures, Electron. Lett. 31 (1995) 1941–1943.
[10] J. Mathew, Y. Semenova, G. Farrell, A high sensitivity humidity sensor based on an agarose coated photonic crystal fiber interferometer, Int. Soc. Opt. Eng. 8421 (2012), 842177-842177-4.
[11] J. Mathew, Y. Semenova, G. Farrell, Effect of coating thickness on the sensitivity of a humidity sensor based on an agarose coated photonic crystal fiber interferometer, Opt. Express 21 (2013) 6313–6320.
[12] K.E. Secrist, A.J. Nolte, Humidity swelling/deswelling hysteresis in a polyelectrolyte multilayer film, Macromolecules (2011) 2859–2865.
[13] F.J. Arregui, Sensors Based on Nanostructured Materials, New York (2009).
[14] D. Leandro, M. Bravo Acha, A. Ortigosa, M. Lopez-Amo, Real-time FFT analysis for interferometric sensors multiplexing, J. Lightwave Technol. 8724 (2015) 1.
[15] J. Villatoro, M.P. Kreuzer, R. Jha, V.P. Minkovich, V. Finazzi, G. Badenes, V. Pruneri, Photonic crystal fiber interferometer for chemical vapor detection with high sensitivity, Opt. Express 17 (2009) 1447.
[16] G. Decher, Fuzzy nanoassemblies: toward layered polymeric multicomposites, Science 277 (1997) 1232–1237.
[17] F. Surre, W.B. Lyons, T. Sun, K.T.V. Grattan, S. O'Keeffe, E. Lewis, C. Elosua, M. Hernaez, C. Barian, U-bend fibre optic pH sensors using layer-by-layer electrostatic self-assembly technique, J. Phys. Conf. Ser. 178 (2009) 012046.
[18] D. Lopez-Torres, C. Elosua, M. Hernaez, J. Goicoechea, F.J. Arregui, From superhydrophilic to superhydrophobic surfaces by means of polymeric layer-by-layer films, Appl. Surf. Sci. 351 (2015) 1081–1086.
[19] J. Mathew, Y. Semenova, G. Farrell, Photonic crystal fiber interferometer for dew detection, J. Lightwave Technol. 30 (2012) 1150–1155.
[20] J. Mathew, Y. Semenova, G. Farrell, Relative humidity sensor based on an agarose-infiltrated photonic crystal fiber interferometer, IEEE J. Sel. Top. Quantum Electron. 18 (2012) 1553–1559.
[21] J. Mathew, Y. Semenova, G. Farrell, Experimental demonstration of a high-sensitivity humidity sensor based on an agarose-coated transmission-type photonic crystal fiber interferometer, Appl. Opt. 52 (2013) 3884–3890.
[22] C.R. Zamarreño, M. Hernáez, I. Del Villar, I.R. Matías, F.J. Arregui, Optical fiber pH sensor based on lossy-mode resonances by means of thin polymeric coatings, Sens. Actuators B: Chem. 155 (2011) 290–297.
[23] S. Rota-Rodrigo, R. Pérez-Herrera, A. Lopez-Aldaba, M.C. López Bautista, O. Esteban, M. López-Amo, Nanowire humidity optical sensor system based on fast Fourier transform technique, in: H.J. Kalinowski, J.L. Fabris, W.J. Bock (Eds.), Proc. SPIE—Int. Soc. Opt. Eng., SPIE, 2015, p. 96342H.
[24] M.F. Durstock, M.F. Rubner, Dielectric properties of polyelectrolyte multilayers, Langmuir 17 (2001) 7865–7872.

Biographies

Diego López-Torres received the M.S. degree in electrical and electronic engineering and the master's degree in communications from the Public University of Navarra

(UPNA), Pamplona, Spain, in 2013 and 2014, respectively. Since 2014, he has been working as a Researcher at the UPNA. In 2105, he obtained a scholarship from this university. His research interest includes optical fiber sensors, photonic crystal fiber and nanostructured materials.

Cesar Elosúa Aguado received his MS degree in electrical and electronic engineering from the Public University of Navarre (UPNA, Pamplona, Spain) in 2004. In the same year, he obtained a scholarship from the Science and Technology Spanish Ministry and he joined the optical fiber sensor group at UPNA. During 2008, he was a visiting Ph.D. student at the University of Limerick and at the City University of London. He became a lecturer of this department in 2009, receiving his PhD degree in the next year. His research interests include optical fiber sensors and networks, organometallic chemistry and data mining techniques.

Joel Villatoro received the M.Sc. and Ph.D. degrees in optics from the National Institute for Astrophysics, Optics, and Electronics, Puebla, Mexico, in 1995 and 1999, respectively. He is currently Ikerbasque Research Professor at the University of the Basque Country, Spain. Prior to that, he worked for the Aston Institute of Photonic Technologies (UK) and the world-famous ICFO—Institute of Photonic Sciences (Spain), among others. He is the author of nearly 100 scientific publications and of 6 patents. His contributions to his field are acknowledged by the internationally community as reflected by a large number of citations and several invited talks.

Joseba Zubia received a degree in solid-state physics in 1988 and the PhD degree in physics from the University of the Basque Country, in 1993. His PhD work focused on optical properties of ferroelectric liquid crystals. He is a full professor at the Telecommunications Engineering School (University of the Basque Country, Bilbao, Spain). He has more than 8 years of experience doing basic research in the field of plastic optical fibers. At present, he is involved in research projects in collaboration with universities and companies from Spain and other countries in the field of plastic optical fibers, fiber-optic sensors, and liquid crystals. Prof. Zubia won a special award for best thesis in 1995.

Manfred Rothhardt received his diploma degree from the Physics faculty of the Friedrich-Schiller-University, Jena, Germany in 1984. From 1984 to 1991 he was a scientific assistant in the research center of Carl-Zeiss-Jena GmbH. From 1991 to 1995 he was with Jenoptik AG leading a R&D group developing interferometric measurement systems. Since 1995 he is with Institute of Photonic Technology, Jena. His research interest includes applications of fibre Bragg gratings and planar lightwave circuits in sensors, biophotonics, fiber lasers and telecommunication.

Kay Schuster holds the group leader position of the Optical Fibres Technology Group within the Fibre Optics Division of the Leibniz Institute of Photonic Technology (IPHT Jena). He obtained his PhD in inorganic chemistry 1995 at the University of Karlsruhe (Research University). Dr. Kay Schuster is engaged for many years in preparation of specialty fibres, based on heavy metal oxide glasses, chalcogenide glasses and high purity silica. The recent activities of Dr. Schuster are concentrated on design and preparation of special functionalized microstructured fibres for passive, active and remote sensing applications. Beside the fabrication of specialty microstructured fibres the group is intensively engaged in material science as well as preform and fibre manufacturing for high power fibre lasers and FBG and Raman based sensing applications. He has coauthored/authored 82 articles in refereed journals, 2 book chapters and holds 3 patents.

Francisco J.Arregui (M'01) is a Full Professor at the Public University of Navarre, Pamplona, Spain. He was part of the team that fabricated the first optical fiber sensor by means of the Layer-by-Layer assembly method at Virginia Tech, Blacksburg, VA, USA, in 1998. He is the author of around 300 scientific journal and conference publications. He has been an Associate Editor of "IEEE Sensors Journal", "Journal of Sensors" (founded by Prof, Arregui in 2007), and "International Journal on Smart Sensing and Intelligent Systems". He is also the editor of the books entitled Sensors-Based on Nanostructured Materials and Optochemical Nanosensors.

3.3. Estudio de factores para la mejora de la sensibilidad de los señores frente a la humedad

Dados los prometedores resultados presentados en la primera publicación expuesta en esta tesis, en la cual la sensibilidad de los sensores de humedad basados en interferometría MZ y fibras SC-PCF fue mejorada, se propuso de nuevo intentar mejorarla optimizando otra vez los dos parámetros anteriores: el material sensible seleccionado y la técnica usada para su deposición.

3.3.1. Material sensible: óxidos metálicos

Los óxidos metálicos son unos materiales prometedores para desarrollar sensores. Gracias a su naturaleza son térmica y mecánicamente robustos, sus propiedades no se ven afectadas por el paso del tiempo y además tienen una buena resistencia a la degradación química. Estos materiales han sido utilizados previamente, con muy buenos resultados, para desarrollar sensores electrónicos de diferentes tipos debido a las reacciones de oxidación/reducción (redox), las cuales producen cambios en la conductividad eléctrica del propio material medibles de una forma muy sencilla. Pero para que esto se produzca, los óxidos metálicos deben ser calentados a temperaturas superiores a 100 grados Celsius lo que en alguna ocasión puede ser no muy deseable según los entornos de trabajo. Sin embargo, si se consigue evitar esta necesidad, como fue la intención de esta segunda contribución científica, son un candidato idóneo para desarrollar sensores de humedad. El óxido metálico elegido fue el dióxido de estaño (SnO_2) ya que los sensores de humedad electrónicos que lo utilizaban mostraron en la bibliografía los mejores tiempos de respuesta y sensibilidades más altas. Este óxido metálico, en presencia de humedad (moléculas de H_2O) sufre una reacción redox (se oxida) y como consecuencia, se produce un intercambio de electrones, lo cual provoca una alteración en las propiedades del material, y más concretamente en su índice de refracción efectivo.

3.3.2. Técnica de deposición: "*sputtering*"

Una vez elegido el material sensible, fue necesario escoger una técnica de deposición la cual permitiera depositar dicho material de formar sencilla pero que a su vez permitiera controlar el espesor de dicho material con un alto grado

de precisión. De esta manera, se podría conseguir una optimización de la sensibilidad del sensor.

Por esta razón, se pensó en utilizar una técnica de deposición llamada "*sputtering" o "pulverización catódica*" basada en alto vacío las cuáles mejora sustancialmente el grado de organización de la estructura interna del material depositado. Esta técnica se basa en la evaporación de un compuesto (en este caso un óxido metálico, SnO_2) y su posterior condensación sobre el sustrato a recubrir (SC-PCF). En otras palabras, el *sputtering* es un fenómeno en el que los átomos de un material sólido se desprenden debido a un bombardeo de partículas provocado por la aplicación de un gran campo eléctrico. A pesar de que las condiciones necesarias para su correcto funcionamiento son muy exigentes, principalmente por el alto vacío que hay que realizar, los recubrimientos finales obtenidos sobre la fibra óptica pueden son altamente homogéneos.

Los planteamientos que se propusieron originalmente en esta segunda contribución (cambio del material sensible y de la técnica de deposición) con la premisa de mejorar la sensibilidad obtenida frente a la humedad en la contribución previa, fueron acertados. Como consecuencia, se consiguió publicar en la revista "*Sensors and Actuators B: Chemical*" un nuevo artículo científico que se pasa a presentar ahora con el título de: "*Enhancing sensitivity of photonic crystal fibre interferometrichumidity sensor by the thickness of SnO_2 thin films".*

Sensors and Actuators B 251 (2017) 1059–1067

Contents lists available at ScienceDirect

Sensors and Actuators B: Chemical

journal homepage: www.elsevier.com/locate/snb

Enhancing sensitivity of photonic crystal fiber interferometric humidity sensor by the thickness of SnO_2 thin films

Diego Lopez-Torres[a,*], Cesar Elosua[a,b], Joel Villatoro[c,d], Joseba Zubia[c], Manfred Rothhardt[e], Kay Schuster[e], Francisco J. Arregui[a,b]

[a] Nanostructured Optical Devices Laboratory, Electric and Electronic Engineering Department, Public University of Navarre, Edif. Los Tejos, Campus Arrosadía, 31006 Pamplona, Spain
[b] Institute Of Smart Cities (ISC), Centro Jerónimo de Ayanz, Campus Arrosadia, 31006 Pamplona, Spain
[c] Department of Communications Engineering, Escuela Técnica Superior de Ingeniería de Bilbao, University of the Basque Country, Bilbao 48049, Spain
[d] IKERBASQUE, Basque Foundation for Science, Bilbao, Spain
[e] Leibniz Institute of Photonic Technology (IPHT), Albert-Einstein-Strasse 9, 07745 Jena, Germany

ARTICLE INFO

Article history:
Received 15 October 2016
Received in revised form 19 May 2017
Accepted 23 May 2017
Available online 25 May 2017

Keywords:
Photonic crystal fiber
Interferometer
Sputtering
Thickness
Humidity sensor
Evanescent field

ABSTRACT

In order to improve the sensitivity of an interferometric humidity sensor based on a photonic crystal fiber with a sputtered SnO_2 nanocoating, a study of the effect of its thickness on the sensitivity is presented in this paper. Sensors with coatings of different thickness were performed by applying distinct sputtering times in order to obtain an optimal thickness: the resulting nanofilms ranged from 470 to 1800 nm. Sensors were tested increasing the relative humidity from 20% to 90%, finding that the thickness was a key parameter which has to be optimized at nanometer scale to get the best sensitivity. The study points that there is an optimal thickness and higher or lower thicknesses worsen the sensitivity of the sensor. The optimal sensor showed a humidity resolution of 0.067%HR, a wavelength shift of 67 nm and a negligible sensitivity with the temperature.

1. Introduction

A high number of papers have been published in the field of optical fiber optics in the last decades. This fact is due to that fiber optic sensors have several advantages over other devices such as electromagnetic immunity, light weight, low transmission losses in the communication window, low cost or wavelength multiplexing, making very interesting its use in many applications [1–4].

In this context, new optical fibers have been developed in order to improve the characteristics of the traditional fibers such as the guidance of the polarization, unprecedented dispersion or non-linear properties. It is the case of Photonic Crystal Fibers (PCFs), also called holey fibers, which contain arrays of tiny air holes along their structure [5–7]. This kind of fibers has attracted an intense research activity because of the possibility of fabricating new optical fiber sensors; devices based on the evanescent field interaction in the holes inside these microstructured fibers is an example [8].

The holey structure of photonic crystal fiber (PCF) allows to detect many parameters such as gases [6], volatile organic compounds (VOCs) [9], temperature [10], strain [11] or humidity [12]. To enable the interaction, the holes of the PCF are collapsed making possible that the modes of the fiber can interact with the evanescent field and with the environments [13]. Previous papers show interesting results in these fields which encourage to work in them as is the case of humidity sensors [14,15]. The measurement of humidity is required in a range of areas, including meteorological services, chemical or medicine industry, food and beverages processing industry, civil engineering, air-conditioning, horticulture, and electronic processing [16,17]. These sensors, compared with their conventional electronic counterparts, offer specific advantages such as the possibility to work at high relative humidity values avoiding the risk of short circuit or corrosion resistance, among others mentioned above.

Most of these fiber optic humidity sensors work on the basis of a hygroscopic material coated over the optical fiber to modulate the

Abbreviations: PCF, photonic crystal fiber; PCF-I, photonic crystal fiber interferometer; SMF, single mode fiber; LMR, Lossy mode resonances; RH, relative humidity; OSA, optical spectrum analyzer.

* Corresponding author.
E-mail addresses: diego.lopez@unavarra.es (D. Lopez-Torres), cesar.elosua@unavarra.es (C. Elosua), agustinjoel.villatoro@ehu.eus (J. Villatoro), joseba.zubia@ehu.es (J. Zubia), kay.schuster@leibniz-ipht.de (K. Schuster), parregui@unavarra.es (F.J. Arregui).

http://dx.doi.org/10.1016/j.snb.2017.05.125
0925-4005/

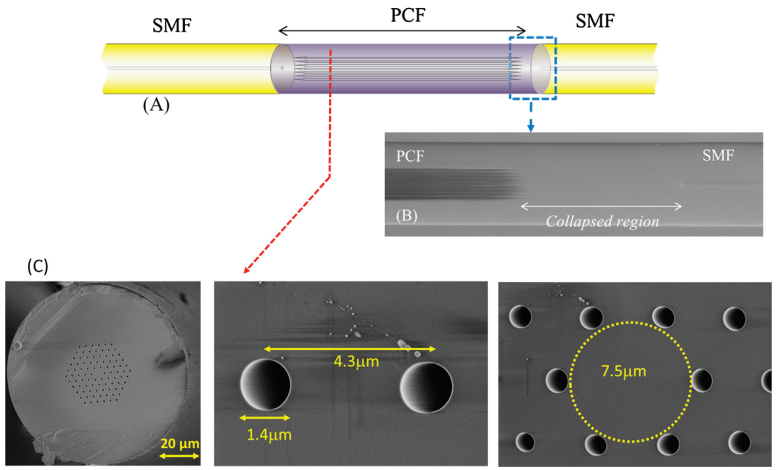

Fig. 1. (A) Scheme of the photonic crystal fiber interferometer (PCF-I): (B) Detail of the splice between PCF and SMF showing the collapsed region of the PCF: (C) Cross section, geometry and dimensions of the PCF used in this work.

light propagating through the fiber. In [18], a relative humidity sensor based on an agarose coating is reported. This study shows that the technique used to deposit this type of materials, dip-coated, does not ensure a repeatable coating in different sensors. Because of this, it is necessary to monitor the spectral shift during the coating process to achieve an optimal thickness for the coating. For this reason, in this paper the use of a hygroscopic material that can be deposited by an electrostatic self-assembly onto the fiber with a repeatable thickness is proposed as a good alternative in the future. In [19], this subject is tackled with very interesting results using the Layer-by-Layer nanoassembly technique [20].

With the aim to improve the sensitivity of previous devices, the current work proposes an interferometric humidity sensor based on a PCF with a sputtered semiconductor nanocoating (tin oxide, SnO_2) [21]. SnO_2 is highly sensitive to changes on the humidity [22] and, when used onto optical fiber, it does not have to be heated to operate. Among different methods to deposit it, sputtering technique allows nanofilms to be fabricated with a high uniformity, reproducibility and with short construction times [23]. Furthermore, the nanofilm thickness can be controlled at nanometer scale. This feature is critical in the case of sensors based on the interaction of the evanescent field with the coating because the thickness should be always below its penetration depth [18,19]. Moreover, thanks to the interferometric nature of the proposed device, the growing of the coating can be monitored on real time by registering the transmission spectra of the sensor and observing any red or blue shift. The resulting sensor characterization can be also expressed in terms of spectral shift, which is more robust than intensity based measurements.

The sensor developed in this paper improves the sensitivity and the wavelength shift of previous works, has a good repeatability and it is relatively easy to made. Also, to our knowledge this is the first time that a SnO_2 nanocoated has been deposited by means of sputtering technique on a PCF as humidity sensor.

2. Experimental details

2.1. Sensing material

SnO_2 has various specific and unique properties, which make this material very useful for many applications [24]. The structure of SnO_2 is an isotropic polar crystal which crystallises in tetragonal rutile structure. The unit cell contains six atoms (2-tin and 4-oxygen, respectively). Each tin atom is at the center of six oxygen atoms placed at the corners of a regular slightly deformed octahedron [25,26]. Thanks to this geometry, the interaction with water molecules is possible but in different ways depending on the temperature. The majority of metallic oxides need to work at temperatures higher than 150 °C [27] but this paper proposes to perform the study at room temperature (25 °C). At this temperature, below 60 °C, water molecules interact with SnO_2 by means of physisorption (the adsorption with the least possible interaction due to the dipole/dipole interactions) [26]. Based on these properties and knowing that SnO_2 is highly sensitive to relative humidity changes, chemically stable and it can be deposited by sputtering technique, it was chosen as sensing material.

2.2. Theoretical background of the PCF-I

The dimensions of the PCF used are shown in (Fig. 1). The air holes pattern are distributed in a hexagon (with a radius of 20 µm) centered at core fiber: each hole has a diameter of 7.5 and the distance between two neighbor holes is 4.3 µm (Fig. 1C). The interferometric sensor was built by splicing 1 cm of PCF between two standard single mode fibers (SMF) (Fig. 1A). Due to the splicing, the voids of the PCF were collapsed completely along the two transitions SMF-PFC-SMF [28]. These transitions were named micro-hole collapsed region (Fig. 1B).

To understand how the interferometer works, it is necessary to analyze the optical signal when it gets into the interface between SMF and PCF and vice versa. At this point, part of the fundamental SMF mode is coupled to the PCF cladding modes which are affected by the external refractive index. The propagation constants of PCF cladding modes are different and consequently, the cladding modes accumulate a phase difference as they propagate along the PCF section. Once these cladding modes reach the second PFC-SMF transition, they interfere with the remaining fundamental SMF mode, producing an interferometric response. Fig. 2 shows a design of the light beam to make easier the understanding. This is the transduction mechanisms of the device and it is based on a Mach Zehnder interferometer [29].

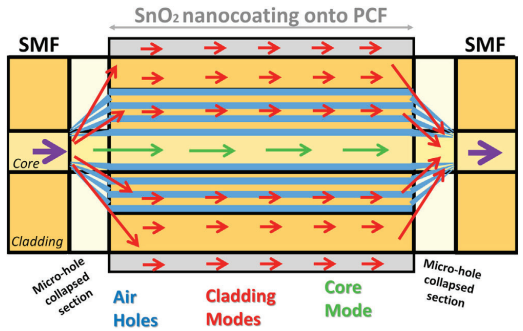

Fig. 2. Operating mechanic of the PCF-I. The arrows show the behavior of the cladding and core modes trough the PCF; in blue are drawn the holes of the PCF and in black the micro-hole collapsed sections; along the PCF the SnO_2 nanocoating is represented with a grey rectangle. (For interpretation of the references to colour in this figure legend, the reader is referred to the web version of this article.)

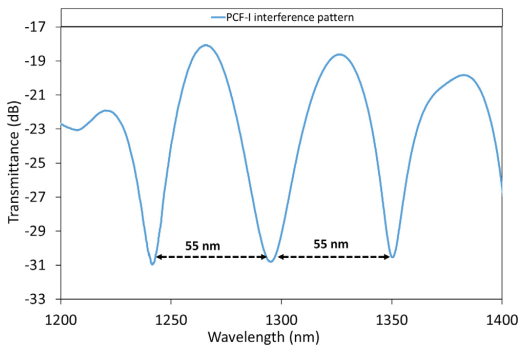

Fig. 3. Interference pattern of the PCF-I from 1200 nm to 1400 nm with a difference between peaks of 55 nm.

Fig. 3 shows the interferometric response obtained before the deposition of the SnO_2 thin film. It can be seen that the transmission of the PCF-I exhibits a series of periodic maxima and minima with a period of 55 nm. The transmission spectrum of the interferometric pattern can be expressed with the next mathematical formula [30]:

$$T(\lambda) = I_{co}(\lambda) + I_{cl}(\lambda) + 2[I_{co}(\lambda) I_{cl}(\lambda)]^{1/2} + \cos\left(2\pi \Delta n_{ef} L/\lambda\right)$$

where I_{co} and I_{cl} are the intensities of the cladding and core modes, L is the length of the PCF-I segment and λ is the wavelength of the guided light. These parameters are constant but the term $\cos(2\pi Dn_{ef} L/\lambda)$ changes, specifically Δn_{ef}: this parameter is the difference between the refractive index of core and the effective refractive index of cladding modes. In our case, the effective refractive index of cladding modes is influenced by the change in the effective refractive index of the nanofilm as well as by the working wavelength. This theory can be applied if the nanofilm thickness is below the penetration depth of the evanescent field: otherwise, the nanofilm acts as an infinite medium because any thickness increase does not modify the effective refractive index of the cladding. Due to this fact, it is necessary to make a study with different nanofilm thicknesses in order to obtain an optimal value.

2.3. Experimental set up and instrumentation

As it can be observed in Fig. 4, the set up used for the construction of the SnO_2 thin film was performed in transmission mode. A multi-LED light (HP83437A) source was used to illuminate a standard SMF (Corning SMF-28) whose emission spectrum range was from 1200 nm to 1600 nm. A Pulsed DC-Sputtering System (Nadetech Inc.) was used to fabricate the SnO_2 thin film and an optical spectrum analyzer (OSA-HP86142), controlled by a computer, was used to analyze the PCF-I interferometric response during the construction process as well as during the characterization of the sensor.

Fig. 4 also shows the set up used to the interrogation of the humidity response of the sensor. This set up was similar to the previous one only replacing the Pulsed DC-Sputtering System instead of the climatic chamber (Angelantoni, CH 250) where de PCF-I was located. The sensor humidity response was performed placing the PCF-I into the climatic chamber where the humidity was increased/decreased from 20% to 90% RH at a constant temperature of 25 °C.

2.4. Construction of the nanofilm

The PCF-I was placed into the vacuum chamber of the sputtering machine, where it was coated with SnO_2. An advantage to use a DC-Sputtering System is that the material is deposited homogenously around the entire surface of the fiber avoiding the necessity to rotate it. The two SMF pigtails were placed in the sputtering machine through wall bushings which ensured the vacuum, so that the transmission spectrum could be tracked in real time. In this way, an increase in the nanofilm thickness should produce a red shift in the interference pattern, making possible to follow the growing as well as preparing PCF-I in a reproducible manner.

The SnO_2 target, 99.99% of purity, was purchased from ZhongNuo Advanced Material Technology Co. The sputtering machine was set to a power of 90 mW, a current of 140 mA and a chamber pressure of 6×10^{-2} mbar. Four sensors were carried out with different thin films and different construction times: in every case, the distance between the SnO_2 target and the PCF-I was 5 centimeters. The resulting thickness of the nanofilm is determined by the construction time in such a way that the thickness increases as the time passes. In order to confirm that the nanofilm construction process is reproducible, three different constructions (with a deposition time of 5 min) were carried out on three different days with the same construction parameters mentioned above. The resulting nanofilm thicknesses (337 nm, 334 nm and 328 nm, respectively) were measured with a quartz crystal microbalance (QCM) located at a 9 cm from the SnO2 target. Consequently, a standard deviation of 3.74 nm (less than 1.15%) was obtained, confirming in this manner that the sputtering technique can be considered highly reproducible. Several authors have studied the effect of post processing in metallic oxide, such as heat curing, with interesting results but this effect will be studied in future works due to the main objective of this paper is to study the feasibility of the humidity sensor [31].

3. Study of the optimal nanofilm thickness

First of all, a sputtering construction of 100 min was carried out with the intention of studying the behavior of the PCF-I during construction in terms of the wavelength shift. Fig. 5A shows the evolution of the PCF-I peaks along the construction time. The resulting spectrums during the 100 min sputtering were recorded every minute: all of them were displayed in a 2D graph. Every spectrum was represented in the vertical axis and their respective magnitudes (expressed in dB) were indicated by a color map. Each peak of

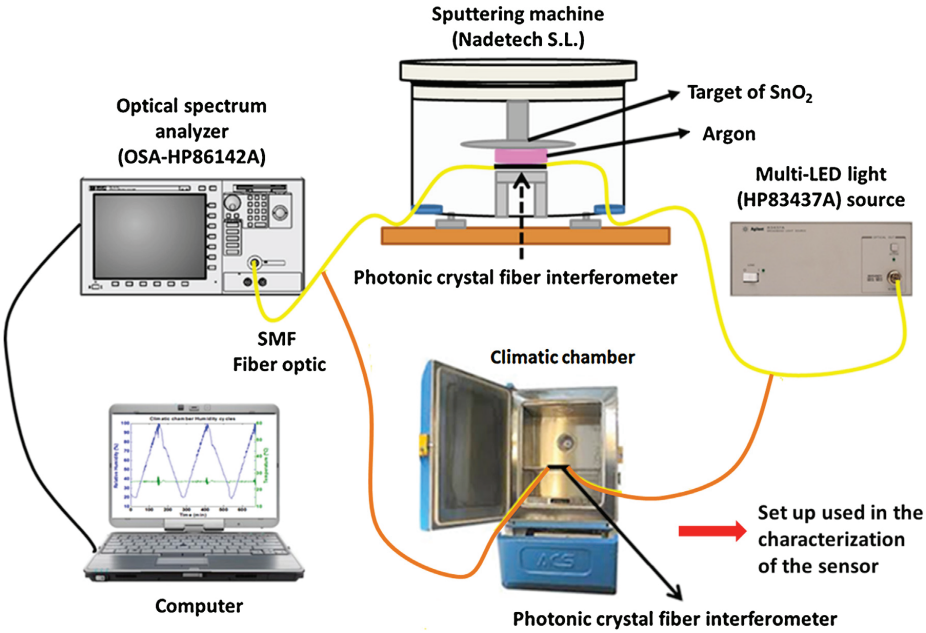

Fig. 4. In yellow, the transmission set up used to monitor the deposition process based on sputtering method; in orange, the transmission set up used to characterize the response of the sensor towards humidity. (For interpretation of the references to colour in this figure legend, the reader is referred to the web version of this article.)

the interference pattern has associated a wavelength shift. For certain areas for the graph, the shifts describe a slope: this parameter can be used to determine the optimum point to stop the construction [19]. At the point where the slope is high, small changes in the refractive index of the coating will give high spectrum shifts, or in other words, will yield into a high sensitivity.

As it can also be appreciated in Fig. 5A, there are zones (indicated by dashed black circles) where the interference pattern disappears. It is due to the presence of a certain electromagnetic resonance known as Lossy Mode Resonance (LMR) [32]. Briefly, an LMR consists of the coupling of the light traveling through the core to the cladding when certain boundary conditions (related with the refractive index and the thickness of the coating) happen. In the case of the PCF-I, when these conditions are fulfilled, the core mode along the PCF segment loses its intensity, in such a way the interference between cladding modes and it is negligible at the second collapsed region [33]. As it can be noticed in Fig. 5B, LMRs appear at 20 min, 40 min, 60 min and 80 min during the sputtering process. It is critical to avoid this phenomenon to obtain a proper interferometric pattern. In light of these results, the sputtering time was limited to 20 min.

It is also noticeable that there is not slope change and therefore no wavelength shift when the construction last longer than 40 min. This is because sputtering times above this value yield to a thickness higher that the penetration depth of the evanescent field: in this manner, the coating acts as infinity medium. As a consequence, no shift in the interferometric pattern is observed beyond this time.

With the aim to locate the point which the highest peak slope, the evolution of the spectral shift during the first 20 min of construction process were studied in details. To make its evaluation easier, three different sections were considered (they are delimited in Fig. 5B with a vertical dashed black line), each one with a specific slope (red shift in every case):

- Up to the first 10 min the total shift is 25 nm, and it is the lowest observed.
- Between 10 and 15 min the slope of the peaks shift was increased up to 53 nm
- Beyond 15 min the total wavelength shift is 79 nm but as the deposition time gets close to 20 min, the amplitude of the peaks tends to decrease and finally, the interferometric pattern disappears. It is due to the presence of a zone where the interference pattern disappears, and consequently this period of time is not the best option to stop the construction

Taking these considerations about the sputtering time into account, four sensors were performed with different times: the first two sensors with a construction time of 5 and 10 min, the third one with 15 min and the last one with 20 min. The corresponding thicknesses for each one were measured by Scanning Electronic Microscope (SEM): 470 nm, 800 nm, 1150 nm and 1800 nm, respectively.

As it can be seen in Fig. 5C, the spectrum of the PCF-I showed several peaks with different amplitudes and transmittances. To make the study easier, only one peak of them was selected although every peak had its own wavelength shift; the peak centered at 1295 nm (in Fig. 5C is highlighted by a red circle). This peak was selected because it was the narrowest and had the highest dynamic range. The spectral shifts of this peak with the four different thicknesses are showed in Fig. 6. In each case, initial pattern is plotted in blue (left vertical axis) and the shifted one is drawn in orange (right vertical axis). The sensor with a construction time of 20 min showed the highest wavelength shift but it had some drawbacks: as it can be seen in Fig. 6.D, the dynamic range of this peak was reduced considerably because of the proximity of the LMR. Due to this fact, a small red wavelength shift when it was exposed towards humidity changes would cause the loss of the interference pattern. Taking it

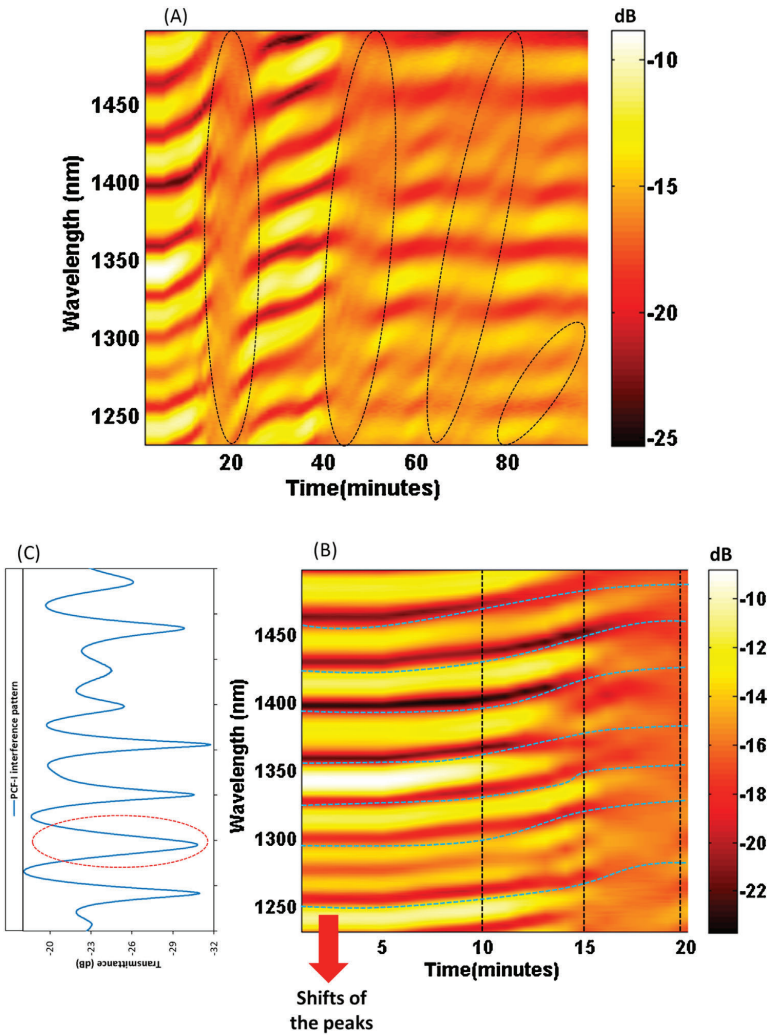

Fig. 5. (A) Spectra red shift observed along the construction process of the nanofilm: a black dashed circle indicates the zones where the interference pattern disappears: (B) Detail of the first 20 min to show three different sections with distinct spectral shifts: the dashed turquoise blue lines show the wavelength shifts of the different peaks of the PCF-I spectrum along the first 20 min of the construction process (C) Transmission spectra of the PCF-I which the peak selected for the study in a red dashed circle. (For interpretation of the references to colour in this figure legend, the reader is referred to the web version of this article.)

into consideration, it was decided to choose the sensor prepared with 15 min sputtering time (and a 1150 nm coating thickness): the shift produced by the coating is 53 nm and at that point, the high slope and the narrower and deeper valley guaranteed a high sensitivity and a better way to register spectral shifts.

4. Results and discussion

The behavior of the four sensors towards humidity was studied by placing them in a climatic chamber where relative humidity was varied from 20% to 90% RH while the temperature was kept constant to 25 °C. The shifts observed for the peak initially located at 1295 nm for each sensor are displayed in Fig. 7A. It can be observed that the highest shift is obtained for the sensor with a thickness of 1150 nm, specifically, 67 nm: it confirms the hypothesis exposed before about the optimal sputtering time. To our knowledge, this wavelength shift improves the previous results reported in other papers [34,35]. These experimental results showed a sensitivity of 0.96 nm/HR% for this sensor and a relative humidity resolution of 0.067%HR (with an OSA resolution of 0.06 nm). Lower sensitivities were obtained for the rest of thicknesses, 0.23 nm/HR% (480 nm); 0.31 nm/HR% (800 nm); and 0.19 nm/HR% (1800 nm), respectively. It is remarkable that for a lower thickness, the total spectra shift was lower (16 nm and 22 nm, respectively); this is because of the nanofilm thickness is thinner than the one of the optimized sensor and a smaller part of the evanescent field interact with it. Regarding to the sensor with a thickness of 1800 nm, the wavelength shift was 13 nm. The reason of the low wavelength shift has been exposed

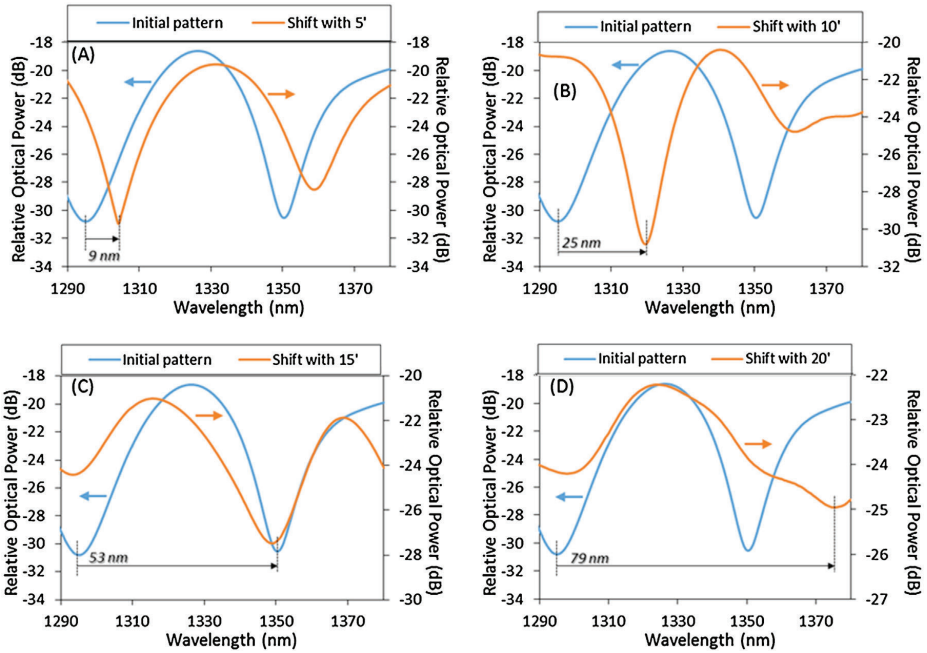

Fig. 6. Spectral red shift of an interferometric valley centered at 1295 nm along the sputtering: (A) 5′, (B) 10′, (C) 15′ and (D) 20′. In each case, initial pattern is in blue (left vertical axis) and the shifted one in orange (right vertical axis). (For interpretation of the references to colour in this figure legend, the reader is referred to the web version of this article.)

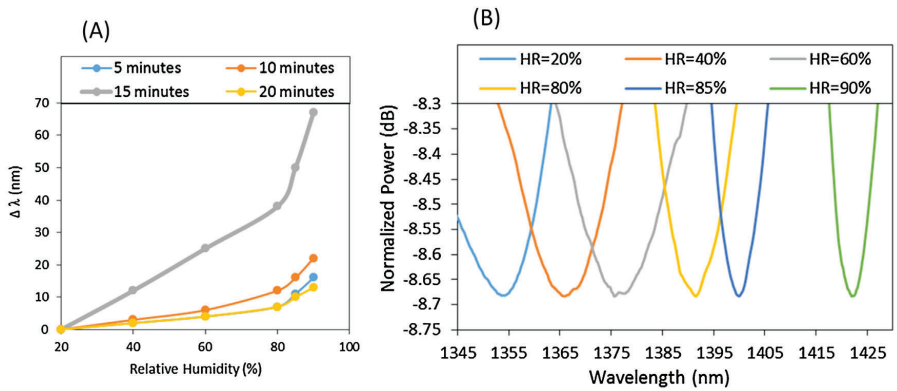

Fig. 7. (A) Wavelength shift for different relative humidity registered from the optimized sensor; (B) Detailed red shift of a certain transmission valley from the sensor with the highest sensitivity. All the spectra are normalized for the sake of clarity. (For interpretation of the references to colour in this figure legend, the reader is referred to the web version of this article.)

above and it is due to the nearby presence of LMR which makes the interference pattern disappear, worsening the response of the sensor. Taking into account that the main phenomenon of interaction between SnO_2 and H_2O molecules is the physisorption [27] and as it is explained and studied in [36], the response and recovery times of sensors with thinnest films are supposed to be faster.

Fig. 7B shows the detailed spectra centered at the transmission valley used as reference of the best sensor obtained for different values of RH. The sensor showed a red shift due to the effect of the humidity on the thin film [37]. All the spectra in the figure were normalized for the sake of clarity. Furthermore, it can be appreciated that when the RH is high, close to 80%, the spectra shift was also higher (with a sensitivity of 3 nm/%HR) than the spectra shift at lower RH values (from 20% to 80% HR the sensitivity was ~1 nm/%HR). In the range 80% –90% HR, the behavior of the sensor can be considered as exponential behavior. This result is very interesting because the sensor can be used in applications which a high

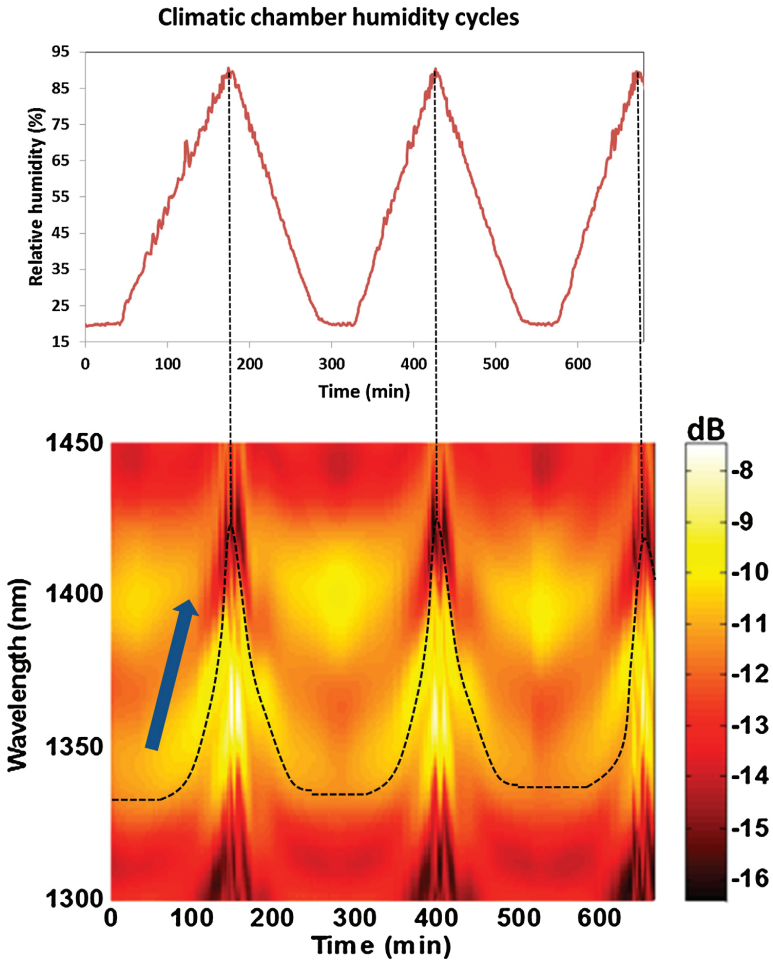

Fig. 8. (Up) Humidity cycles performed by the climatic chamber which the relative humidity is increased from 20% to 90% RH; (Down) Transmission spectra of the sensor when it was placed in the climatic chamber. The Y axis represented wavelength and the X axis time. The black dashed line represents the wavelength shift of the sensor with a nanofilm thickness of 1150 nm.

relative humidity is required to work. Also, due to the features of the sensor, the risk of short circuit with these conditions is avoided.

The response of the optimized sensor was studied with more detail by plotting the complete spectral evolution during different humidity conditions on real time by sampling the transmission spectra every minute: specifically, the device was exposed to changes between 20% and 90% HR three times. The results obtained are displayed in Fig. 8: the graph above shows the temporal evolution of relative humidity, whereas the spectra registered along the test are shown in the graph below. In this manner, the horizontal axis of the spectra graph, although expressed in time units, is directly related with the relative humidity value. It can be observed how the spectral shift follows the change in humidity along time: actually, the higher sensitivity above 80% is also noticeable. Furthermore, no hysteresis is observed and what is more, the response of the sensor is repetitive and stable in time (there is no shift when relative humidity is 20% between the cycles).

The temperature effect on the sensor under study was also checked: it has been studied using the same climatic chamber as before but was increased from 15 °C to 40 °C, setting the RH at 40%. Furthermore, the stability of the sensor towards temperature was studied with a cycle of 200 min at constant temperature (40 °C) once this value was reached. As it can be observed in Fig. 9, the wavelength shift of the peak was below 1 nm, which can be mathematically compensated.

5. Conclusions

Thanks to the study that it has been carried out in this paper, these conclusions can be derived. Firstly, oxide metallic (in our case SnO_2) can be use as sensing material in sensors based on an interferometric pattern. Also, this kind of materials can be work at room temperature which is a high advantage over other devices such as electronic sensors.

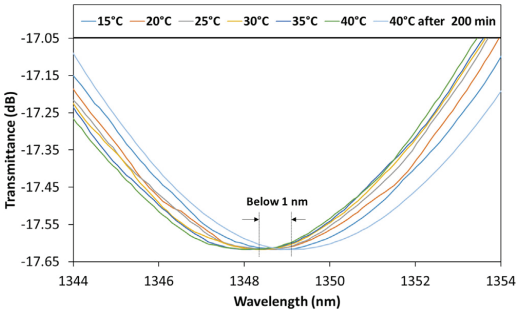

Fig. 9. Study of the wavelength shift of the selected peak of the sensor with a nanofilm of 1150 nm when it was exposed to different temperatures.

Whit the aim to obtain the best sensitivity for the sensors, it has been confirmed that the nanofilm thickness is the key parameter in this process. But to achieve it, it is necessary to work at nanometer scale, where nanofilm thickness is below the penetration depth of the evanescent field. The sputtering technique allows to work at this scale making very interesting its use in this work.

The operating mechanism of the sensor is based on the interaction between cladding modes and the SnO_2 nanofilm. To make it possible, a suitable nanofilm has to be deposited along the PCF-I. This study concludes that there is an optimal thickness, 1150 nm, and higher or lower thicknesses worsen the sensitivity of the sensor. It has been found that there is a tradeoff related with this parameter: as it increases, the interaction between cladding modes and nanofilm also increases but when the thickness reaches the value of the evanescent field, the device loses sensibility as the film grows. Moreover, during the construction process of the nanofilm another phenomenon occurs, the presence of magnetic resonances (LMR) which have to be avoided.

Due to the features of the PCF-I spectrum, the sensors were characterized by following the wavelength shifts. These measurements were robust and they allowed to control the nanofilm construction process as well as the characterization of the sensor.

To summarize, the resulting sensor offers a repeatable response, good repeatability in terms of thickness, low hysteresis, long-term stability and a humidity resolution of 0.067%HR. Taking these results account, this paper encourages to continue studying the construction of nanofilms based on metallic oxide to develop fiber optic sensors.

Competing interests

The authors declare that they have no competing interests.

Acknowledgments

This work was supported by the Spanish Economy and Competitivity Ministry-FEDERTEC2013-43679-R as well as Public University of Navarre grant program. The authors would like to express their gratitude to Nadetech Inc. for the design, fabrication and tune-up of the robot used for the deposition of the nanocoatings.

References

[1] R.C. Jorgenson, S.S. Yee, A fiber-optic chemical sensor based on surface plasmon resonance, Sens. Actuators B: Chem. 12 (1993) 213–220, http://dx.doi.org/10.1016/0925-4005(93)80021-3.
[2] B. Lee, Review of the present status of optical fiber sensors, Opt. Fiber Technol. 9 (2003) 57–79, http://dx.doi.org/10.1016/S1068-5200(02)00527-8.
[3] J. Ascorbe, J.M. Corres, F.J. Arregui, I.R. Matias, Optical fiber current transducer using lossy mode resonances for high voltage networks, J. Light Technol. 33 (2015) 2504–2510, http://dx.doi.org/10.1109/JLT.2015.2396353.
[4] P. Zubiate, C.R. Zamarre, I. Del Villar, I.R. Matias, S. Member, F.J. Arregui, Experimental Study and Sensing Applications of Polarization-Dependent Lossy Mode Resonances Generated by D-Shape Coated Optical Fibers, J. Lightwave Technol. 33 (2015) 2412–2418.
[5] P. Russell, Photonic crystal fibers, Science 80 (2003) 299 (358 LP-362) http://science.sciencemag.org/content/299/5605/358.abstract.
[6] Y.L. Hoo, W. Jin, C. Shi, H.L. Ho, D.N. Wang, S.C. Ruan, Design and modeling of a photonic crystal fiber gas sensor, Appl. Opt. 42 (2003) 3509, http://dx.doi.org/10.1364/ao.42.003509.
[7] K. Suzuki, H. Kubota, S. Kawanishi, M. Tanaka, M. Fujita, Optical properties of a low-loss polarization-maintaining photonic crystal fiber, Opt. Express 9 (2001) 676–680, http://dx.doi.org/10.1364/OE.9.000676.
[8] J.B. Jensen, L.H. Pedersen, P.E. Hoiby, L.B. Nielsen, T.P. Hansen, J.R. Folkenberg, J. Riishede, D. Noordegraaf, K. Nielsen, A. Carlsen, A. Bjarklev, Photonic crystal fiber based evanescent-wave sensor for detection of biomolecules in aqueous solutions, Opt. Lett. 29 (2004) 1974–1976, http://dx.doi.org/10.1364/OL.29.001974.
[9] J. Villatoro, M.P. Kreuzer, R. Jha, V.P. Minkovich, V. Finazzi, G. Badenes, V. Pruneri, Photonic crystal fiber interferometer for chemical vapor detection with high sensitivity, Opt. Express 17 (2009) 1447, http://dx.doi.org/10.1364/oe.17.001447.
[10] A. Lopez-Aldaba, A. Pinto, M. Lopez-Amo, O. Frazão, J. Santos, J. Baptista, H. Baierl, J.-L. Auguste, R. Jamier, P. Roy, Experimental and numerical characterization of a hybrid Fabry-Pérot cavity for temperature sensing, Sensors 15 (2015) 8042–8053, http://dx.doi.org/10.3390/s150408042.
[11] J. Villatoro, V. Finazzi, V.P. Minkovich, V. Pruneri, G. Badenes, Temperature-insensitive photonic crystal fiber interferometer for absolute strain sensing, Appl. Phys. Lett. 91 (2007) 89–92, http://dx.doi.org/10.1063/1.2775326.
[12] P. Hu, X. Dong, K. Ni, L.H. Chen, W.C. Wong, C.C. Chan, Sensitivity-enhanced Michelson interferometric humidity sensor with waist-enlarged fiber bitaper, Sens. Actuators B: Chem. 194 (2014) 180–184, http://dx.doi.org/10.1016/j.snb.2013.12.081.
[13] Y. Song, M. Hu, C. Wang, Z. Tian, Q. Xing, L. Chai, C. Wang, Environmentally Stable, High Pulse Energy Laser Operating in the Soliton-Like Regime, IEEE Photonics Technol. Lett. 20 (2008) 1088–1090.
[14] J. Shi, V.K.S. Hsiao, T.R. Walker, T.J. Huang, Humidity sensing based on nanoporous polymeric photonic crystals, Sens. Actuators B: Chem. 129 (2008) 391–396, http://dx.doi.org/10.1016/j.snb.2007.08.037.
[15] S. Zheng, Y. Zhu, S. Krishnaswamy, Fiber humidity sensors with high sensitivity and selectivity based on interior nanofilm-coated photonic crystal fiber long-period gratings, Sens. Actuators B: Chem. 176 (2013) 264–274, http://dx.doi.org/10.1016/j.snb.2012.09.098.
[16] W.H. Reeves, D.V. Skryabin, F. Biancalana, J.C. Knight, P.S.J. Russell, F.G. Omenetto, a Efimov, a J. Taylor, Transformation and control of ultra-short pulses in dispersion-engineered photonic crystal fibres, Nature 424 (2003) 511–515, http://dx.doi.org/10.1038/nature01798.
[17] L. Rindorf, J.B. Jensen, M. Dufva, L.H. Pedersen, P.E. Høiby, O. Bang, Photonic crystal fiber long-period gratings for biochemical sensing, Opt. Express 14 (2006) 8224–8231, http://dx.doi.org/10.1364/OE.14.008224.
[18] J. Mathew, Y. Semenova, G. Farrell, Experimental demonstration of a high-sensitivity humidity sensor based on an Agarose-coated transmission-type photonic crystal fiber interferometer, Appl. Opt. 52 (2013) 3884–3890, http://dx.doi.org/10.1364/AO.52.003884.
[19] D. Lopez-Torres, C. Elosua, J. Villatoro, J. Zubia, M. Rothhardt, K. Schuster, F.J. Arregui, Photonic crystal fiber interferometer coated with a PAH/PAA nanolayer as humidity sensor, Sens. Actuators B: Chem (2016), http://dx.doi.org/10.1016/j.snb.2016.09.144.
[20] D. Lopez-Torres, C. Elosua, M. Hernaez, J. Goicoechea, F.J. Arregui, From superhydrophilic to superhydrophobic surfaces by means of polymeric layer-by-layer films, Appl. Surf. Sci. 351 (2015) 1081–1086, http://dx.doi.org/10.1016/j.apsusc.2015.06.004.
[21] B. Jaffe, R.S. Roth, S. Marzullo, Properties of piezoelectric ceramics in the solid-solution series lead titanate-lead zirconate-lead oxide: tin oxide and lead titanate-lead hafnate, J. Res. Natl. Bur. Stand. 1934 55 (1955) 239–254, http://dx.doi.org/10.6028/jres.055.028.
[22] Q. Kuang, C. Lao, L.W. Zhong, Z. Xie, L. Zheng, High-sensitivity humidity sensor based on a single SnO2 nanowire, J. Am. Chem. Soc. 129 (2007) 6070–6071, http://dx.doi.org/10.1021/ja070788m.
[23] J. Ascorbe, C. Sanz, J.M. Corres, F.J. Arregui, I.R. Matias, S.C. Mukhopadhyay, High sensitivity extrinsic Fabry-Pèrot interferometer for humidity sensing, Proc. Int. Conf. Sens. Technol. (2016) 143–146, http://dx.doi.org/10.1109/ICSensT.2015.7438380, ICST. 2016–March (2016).
[24] E. Shanthi, V. Dutta, A. Banerjee, K.L. Chopra, Electrical and optical properties of undoped and antimony-doped tin oxide films, J. Appl. Phys. 51 (1980) 6243–6251, http://dx.doi.org/10.1063/1.327610.
[25] K. Maier, A. Helwig, G. Müller, P. Hille, M. Eickhoff, Effect of water vapor and surface morphology on the low temperature response of metal oxide semiconductor gas sensors, Mater. (Basel) 8 (2015) 6570–6588, http://dx.doi.org/10.3390/ma8095323.
[26] W. Schmid, Consumption Measurements on SnO 2 Sensors in Low and Normal Oxygen Concentration, Diss. Am Inst. Für Chemie Und Pharm. Der Eberhard-Karls- Univ. Tübingen, 2004.

[27] W.E. Pickett, Electronic structure of the high-temperature oxide superconductors, Rev. Mod. Phys. 61 (1989) 433–512, http://dx.doi.org/10.1103/RevModPhys.61.433.
[28] J. Mathew, Y. Semenova, G. Rajan, G. Farrell, Humidity sensor based on photonic crystal fibre interferometer, Electron. Lett. 46 (2010) 1341, http://dx.doi.org/10.1049/el.2010.2080.
[29] E. Udd, W.B. Spillman, Fiber Optic Sensors Fiber Optic Sensors An Introduction for Engineers and Scientists, A John Wiley Sons, Ltd Publ., 2011, pp. 498.
[30] O. Letters, Refractometry based on a photonic crystal ber interferometer, Opt. Lett. 34 (2009) 617–619.
[31] I. Del Villar, C.R. Zamarreño, M. Hernaez, P. Sanchez, F.J. Arregui, I.R. Matias, Generation of surface plasmon resonance and lossy mode resonance by thermal treatment of ITO thin-films, Opt. Laser Technol. 69 (2015) 1–7, http://dx.doi.org/10.1016/j.optlastec.2014.12.012.
[32] C.R. Zamarreño, M. Hernáez, I. Del Villar, I.R. Matías, F.J. Arregui, Optical fiber pH sensor based on lossy-mode resonances by means of thin polymeric coatings, Sens. Actuators B: Chem. 155 (2011) 290–297, http://dx.doi.org/10.1016/j.snb.2010.12.037.
[33] P. Zubiate, C.R. Zamarreño, I. Del Villar, I.R. Matias, F.J. Arregui, High sensitive refractometers based on lossy mode resonances (LMRs) supported by ITO coated D-shaped optical fibers, Opt. Express 23 (2015) 8045, http://dx.doi.org/10.1364/oe.23.008045.
[34] J. Mathew, Y. Semenova, G. Farrell, Effect of coating thickness on the sensitivity of a humidity sensor based on an Agarose coated photonic crystal fiber interferometer, Opt. Express 21 (2013) 6313–6320, http://dx.doi.org/10.1364/OE.21.006313.
[35] J. Mathew, Y. Semenova, G. Farrell, A high sensitivity humidity sensor based on an Agarose coated photonic crystal fiber interferometer, Proceedings of SPIE, 8421 (2012) 842177–842177-4, 10.1117/12.975153.
[36] C. Liewhiran, S. Phanichphant, Influence of thickness on ethanol sensing characteristics of doctor-bladed thick film from flame-made ZnO nanoparticles, Sensors 7 (2007) 185–201, http://dx.doi.org/10.3390/s7020185.
[37] J. Ascorbe, J.M. Corres, I.R. Matias, F. Arregui, High sensitivity humidity sensor based on cladding-etched optical fiber and lossy mode resonances, Sens. Actuators B: Chem. 233 (2016) 7–16, http://dx.doi.org/10.1016/j.snb.2016.04.045.

Biographies

Diego López-Torres received the M.S. degree in electrical and electronic engineering and the master's degree in communications from the Public University of Navarra (UPNA), Pamplona, Spain, in 2013 and 2014, respectively. Since 2014, he has been working as a Researcher at the UPNA. In 2105, he obtained a scholarship from this university. His research interest includes optical fiber sensors, photonic crystal fiber and nanostructured materials.

Cesar Elosúa Aguado received his MS degree in electrical and electronic engineering from the Public University of Navarre (UPNA, Pamplona, Spain) in 2004. In the same year, he obtained a scholarship from the Science and Technology Spanish Ministry and he joined the optical fiber sensor group at UPNA. During 2008, he was a visiting Ph.D. student at the University of Limerick and at the City University of London. He became a lecturer of this department in 2009, receiving his PhD degree in the next year. His research interests include optical fiber sensors and networks, organometallic chemistry and data mining techniques.

Joel Villatoro received the M.Sc. and Ph.D. degrees in optics from the National Institute for Astrophysics, Optics, and Electronics, Puebla, Mexico, in 1995 and 1999, respectively. He is currently Ikerbasque Research Professor at the University of the Basque Country, Spain. Prior to that, he worked for the Aston Institute of Photonic Technologies (UK) and the world-famous ICFO –Institute of Photonic Sciences (Spain), among others. He is the author of nearly 100 scientific publications and of 6 patents. His contributions to his field are acknowledged by the internationally community as reflected by a large number of citations and several invited talks.

Joseba Zubia received a degree in solid-state physics in 1988 and the PhD degree in physics from the University of the Basque Country, in 1993. His PhD work focused on optical properties of ferroelectric liquid crystals. He is a full professor at the Telecommunications Engineering School (University of the Basque Country, Bilbao, Spain). He has more than 8 years of experience doing basic research in the field of plastic optical fibers. At present, he is involved in research projects in collaboration with universities and companies from Spain and other countries in the field of plastic optical fibers, fiber-optic sensors, and liquid crystals. Prof. Zubia won a special award for best thesis in 1995.

Manfred Rothhardt received his diploma degree from the Physics faculty of the Friedrich-Schiller-University, Jena, Germany in 1984. From 1984–1991 he was a scientific assistant in the research center of Carl-Zeiss-Jena GmbH. From 1991–1995 he was with Jenoptik AG leading a R&D group developing interferometric measurement systems. Since 1995 he is with Institute of Photonic Technology, Jena. His research interest includes applications of fiber Bragg gratings and planar lightwave circuits in sensors, biophotonics, fiber lasers and telecommunication.

Kay Schuster holds the group leader position of the Optical Fibres Technology Group within the Fibre Optics Division of the Leibniz Institute of Photonic Technology (IPHT Jena). He obtained his PhD in inorganic chemistry 1995 at the University of Karlsruhe (Research University). Dr. Kay Schuster is engaged for many years in preparation of specialty fibers, based on heavy metal oxide glasses, chalcogenide glasses and high purity silica. The recent activities of Dr. Schuster are concentrated on design and preparation of special functionalized microstructured fibers for passive, active and remote sensing applications. Beside the fabrication of specialty microstructured fibers the group is intensively engaged in material science as well as preform and fiber manufacturing for high power fiber lasers and FBG and Raman based sensing applications. He has coauthored/authored 82 articles in refereed journals, 2 book chapters and holds 3 patents.

Francisco J. Arregui (M'01) is a Full Professor at the Public University of Navarre, Pamplona, Spain. He was part of the team that fabricated the first optical fiber sensor by means of the Layer-by-Layer assembly method at Virginia Tech, Blacksburg, VA, USA, in 1998. He is the author of around 300 scientific journal and conference publications. He has been an Associate Editor of "IEEE Sensors Journal", "Journal of Sensors" (founded by Prof, Arregui in 2007), and "International Journal on Smart Sensing and Intelligent Systems". He is also the editor of the books entitled Sensors-Based on Nanostructured Materials and Optochemical Nanosensors.

3.4. Conclusiones

La utilización de SC-PCF para generar interferometría MZ, a la hora de desarrollar sensores de humedad, es una prometedora elección debido a la posibilidad que ofrecen de que el campo evanescente de la luz guiada por la fibra óptica pueda interactuar con las películas depositadas de material sensible.

La elección de una técnica de deposición que permita controlar el espesor de la película depositada es de vital importancia ya que es un parámetro que hay que optimizar si el objetivo es conseguir la mayor sensibilidad posible para el sensor final.

Las técnicas de deposición *LbL* y *sputtering* garantizan la construcción de nano películas uniformes siempre que los parámetros iniciales de construcción se mantengan inalterados.

También se ha comprobado que todos los materiales no son igual de sensibles a la humedad y que, por lo tanto, a la hora de optimizar la sensibilidad de un sensor o dependiendo de la aplicación final en la que vaya a ser utilizado, su elección hay que tenerla muy presente. Por ejemplo, dependiendo de si la respuesta dinámica del sensor es importante, es conveniente elegir un material u ya que esta dependerá de su mecanismo de interacción con las moléculas de agua, o si por ejemplo la película sensible va a estar mucho tiempo expuesta al desgaste de agentes externos, igual hay que pensar en materiales que tengan propiedades más resistivas a estos agentes.

Capítulo 4

Optimización de la sensibilidad de sensores de humedad utilizando SSC

En este capítulo de la tesis se desarrolló un nuevo sensor de fibra óptica basado en un interferómetro Fabry-Pèrot utilizando SSC para detectar cambios de humedad. La idea de utilizar un nuevo tipo de MOF fue debido a la posibilidad de mejorar la sensibilidad de los sensores previos. Gracias a la estructura que presentan estas fibras, es posible acoplar a la zona donde se deposita la película de material sensible, más potencia óptica aumentando de esta manera, la sensibilidad final del sensor.

4.1. Introducción

Tomando como referencia los resultados de las publicaciones presentadas en el capítulo previo, se puede afirmar que a la hora de desarrollar un sensor de fibra óptica existen varios factores clave para lograr una sensibilidad óptima. Por esta razón, la técnica de deposición elegida, el material sensible utilizado y su espesor depositado, deben ser estudiados y analizados. Es innegable que estos factores influyen en la sensibilidad final del sensor, pero no son los únicos. Existe otro parámetro que también tiene una importancia capital y no se tuvo en cuenta en las contribuciones presentadas anteriormente: este es, la geometría de la MOF de la que se parte para desarrollar dicho sensor.

Cabe recordar que, el punto de partida de esta tesis es el artículo científico publicado por Jinesh Mathew et al. [84]. Se tomó como referencia la estructura desarrollada en este trabajo (SC-PCF utilizadas para generar un interferómetro Match-Zehnder) debido a que, la sensibilidad final obtenida, era el mejor resultado encontrado entre todas las publicaciones científicas basadas en MOFs para detectar cambios en la humedad. Por esta razón, sólo fueron optimizados los parámetros descritos en el párrafo anterior, concluyendo que, la mejor sensibilidad se obtiene depositando SnO_2 mediante la técnica de *sputtering*. En este punto de la investigación, se pensó que una nueva vía a explotar para mejorar la sensibilidad de los sensores basados en MOF podría ser proponer una nueva estructura sensora en la que se depositara SnO_2 mediante *sputtering*. Gracias a su estructura, las fibras SSC permiten depositar películas de materiales sensibles a la humedad en las paredes de sus agujeros y, además, es posible acoplar a la zona donde se deposita dicha película, más potencia óptica; de esta manera, la sensibilidad final del sensor debería aumenta. Teniendo en cuenta todas estas teorías, se propuso la idea que dio origen a la contribución científica que se presenta en este capítulo.

4.2. Sensores de humedad basados en SSC

El potencial de las MOF para detectar cambios de humedad ha sido explicado con detalle en la introducción de esta tesis. Gracias a las diferentes dimensiones que ofrecen sus estructuras, concretamente en el tamaño de sus agujeros y sus núcleos, pueden ser utilizadas de forma ventajosa para mejorar las

propiedades y sensibilidades de los sensores. Un ejemplo es el posible incremento de la zona de interacción entre el campo evanescente de la luz guiada por el interior de la fibra y el medio que la rodea o la película de material sensible depositada; a su vez, también pueden favorecer las reacciones químicas que se producen entre las moléculas de H_2O y las películas depositadas, solo por mencionar algunas. Teniendo en cuenta todas estas ideas, se pensó que, dentro de los diferentes tipos de MOF, las SSC podían ser una buena opción ya que cumplen con todas las condiciones anteriormente enumeradas. Más concretamente, la fibra que se eligió fue una *"four-bridge double-Y-shape-core SSC"*. En particular, esta estructura tiene unas interesantes propiedades para el sensado de la humedad debido a la presencia de 4 agujeros longitudinales que están directamente en contacto con el núcleo de la fibra. Debido a esto, parte de la luz guiada por el núcleo de la fibra se acopla con facilidad al campo evanescente, interactuando esta señal, por medio de los agujeros, con el medio circundante. De la misma manera, gracias a la técnica de deposición elegida, el SnO_2 puede ser depositado en el interior de los agujeros permitiendo su interacción directa con el campo evanescente de la luz guiada y, por consiguiente, una mejora en la sensibilidad final del sensor. Por otro lado, también gracias a las dimensiones de los agujeros, las moléculas de H_2O se difunden por ellos y son adsorbidas por la película de SnO_2 lo que facilita las reacciones redox entre ellos.

4.2.1. Utilización de SSC para la generación de interferómetros Fabry-Pèrot

Una vez elegida el tipo de fibra óptica que se quería utilizar, era necesario definir la configuración del sensor. Para poder cumplir con la idea expuesta en el apartado anterior, se optó por una configuración en reflexión. De haberse elegido la configuración del sensor en transmisión, no hubiera sido posible depositar el SnO_2 en el interior de los agujeros y se habría perdido también la ventaja de que las moléculas de H_2O penetraran en dichos agujeros. Esta es una de las principales diferencias en comparación con los sensores SC-PCF basados en interferómetros Mach-Zehnder.

Por lo tanto, la configuración final del sensor se desarrolló empalmando una SMF (Corning SMF-28) a una sección de SSC. De este modo, dos espejos de baja reflectividad se forman en ambos extremos de la SSC: el primero, en la

interfaz SMF-SSC debido a la discontinuidad en el índice de refracción entre ambas fibras y el segundo, en la interfaz SSC-aire debido también a la alta discontinuidad en el índice de refracción, lo cual provocó una reflexión Fresnel. El comportamiento de un haz de luz al llegar a ambos interfaces, sería parecido al que describe un haz de luz en un interferómetro Fabry-Pèrot, donde la cavidad Fabry-Pèrot (FP) pasa a ser la longitud de la sección SSC utilizada.

4.2.2. Optimización del espesor de la película depositada

Habiendo fijado con anterioridad el material a sensible a depositar (SnO_2) y la técnica utilizada para ello (*sputtering*) era necesario volver a realizar un estudio con diferentes espesores para determinar cuál era el óptimo y alcanzar de esta forma, la mejor sensibilidad posible. Una vez optimizado, se comprobó también un factor muy interesante: se había conseguido, gracias a la técnica de deposición elegida, que la película de SnO_2 estuviera depositada en una longitud importante de los agujeros de la SSC (570 μm de los aproximadamente 700 μm que media la cavidad), aumentando en gran medida la zona de interacción del campo evanescente de la luz guiada con la película depositada. Una conclusión directa de esta circunstancia fue la mejora en la sensibilidad final del sensor de humedad.

La sensibilidad final obtenida con este sensor frente a la humedad fue de 0.14 rad/% en un rango de humedad comprendido entre 20% y 90% frente a los 0.001 rad/% obtenidos con el sensor reportado en el capítulo anterior. Este resultado, junto a todas las hipótesis formuladas para llegar a él, fueron recogidas y descritas en la contribución científica: "*SnO_2-MOF-Fabry-Pèrot optical sensor for relative humidity measurements*" que fue publicada en la revista "*Sensors and Actuators B: Chemical*". Dicha contribución, la tercera que se deriva de esta tesis, se expone a continuación.

Sensors and Actuators B 257 (2018) 189–199

Contents lists available at ScienceDirect

Sensors and Actuators B: Chemical

journal homepage: www.elsevier.com/locate/snb

Research Paper

SnO_2-MOF-Fabry-Perot optical sensor for relative humidity measurements

A. Lopez Aldaba[a,*], D. Lopez-Torres[a], C. Elosua[a], J.-L. Auguste[b], R. Jamier[b], P. Roy[b], F.J. Arregui[a], M. Lopez-Amo[a]

[a] Universidad Pública de Navarra, Dept. of Electrical and Electronic Engineering, Institute of Smart Cities (ISC), and IDISNA, Campus Arrosadia, 31006, Pamplona, Spain
[b] Xlim, Fibre Photonics Department, UMR CNRS/University of Limoges 7252, 123 Avenue Albert Thomas, 87060 Limoges Cedex, France

ARTICLE INFO

Article history:
Received 5 July 2017
Received in revised form 3 October 2017
Accepted 25 October 2017
Available online 28 October 2017

Keywords:
Photonic crystal fiber
Microstructured optical fiber
Fiber sensor
Humidity sensing
Breathe sensing
Fast Fourier transform

ABSTRACT

In this paper, a new optical fiber sensor for relative humidity measurements is presented and characterized. The sensor is based on a SnO_2 sputtering deposition on a microstructured optical fiber (MOF) low-finesse Fabry-Pérot (FP) sensing head. The feasibility of the device as a breathing sensor is also experimentally demonstrated. The interrogation of the sensing head is carried out by monitoring the Fast Fourier Transform phase variations of the FP interference frequency. This method substitutes the necessity of tracking the optical spectrum peaks or valleys, which can be a handicap when noise or multiple contributions are present: therefore, it is low-sensitive to noise and to artifacts signal amplitude. The sensor shows a linear behavior in a wide relative humidity range (20%–90% relative humidity) in which the sensitivity is 0.14 rad/%; the maximum observed instability is 0.007 rad, whereas the highest hysteresis is 5% RH. The cross correlation with temperature is also considered and a method to lower its influence is proposed. For human breathing measurement, the registered rising and recovery times are 370 ms and 380 ms respectively.

1. Introduction

Optical fiber based sensors have shown great features to measure different parameters such as temperature, curvature, displacement, pressure, refractive index, electric field, relative humidity and gases, among others. Many types of optical fibers have been used for sensing along the time: standard silica based, plastic, doped, and photonic crystal fibers are some examples. Since the first experiments with microstructured optical fibers (MOFs), they have shown relevant improved characteristics compared to conventional optical fibers as well as a great potential for sensing applications, overcoming some of the standard optical fiber limitations [1–3]. Different geometries have been proposed for this kind of fibers. Among them, suspended-core MOFs present relatively large air holes surrounding a small core (typically a few microns diameter) that seems to be suspended along the fiber length but maintained by thin silica bridges. Distinct pure silica suspended-core fibers have been applied for instance in temperature and curvature sensing [4], gas sensing [5] or micro-displacement measurements [6]. One of the most important type of MOF sensors are the ones based on evanescent field. These sensors have been used for different applications: simultaneous measurement of humidity and mechanical vibration [7], detection of biomolecules in aqueous solutions [8] as well as organic pollutants [9] or hydrogen detection [10–12] have been reported using such a kind of transducers.

Fiber based optical Fabry-Pérot (FP) interferometers are a common sensor configuration due to their compactness, simple configuration, design flexibility and dynamic range. A fiber based FP sensor is most of the times fabricated by splicing a section of a waveguide, which acts as cavity, to a standard optical fiber segment. This structure presents robustness and multiplexing capability. The FP cavity output signal consists of an interference pattern which is a function of the cavity length and of the refractive index of the cavity, or more precisely, the effective indices of the different modes supported by the fiber interferometer. FP cavities based on MOFs are also common structures. For instance, a hybrid structure that used a MOF as the guiding fiber, in combination with a hollow-core fiber and a single mode fiber (SMF), for high-temperature sensing, was demonstrated in [13]. Nitrogen sensors [14], chitosan based ones for relative humidity (RH) [15] as well as strain, temperature and pressure FP devices [16,17] have been also reported. Other fiber based sensors were implemented by fusing a small length of PCF to the end of a cleaved SMF for relative humidity ranged 40%-95% RH [18] or by chemical deposition of polymers [19].

* Corresponding author.
E-mail address: aitor.lopez@unavara.es (A. Lopez Aldaba).

https://doi.org/10.1016/j.snb.2017.10.149
0925-4005/

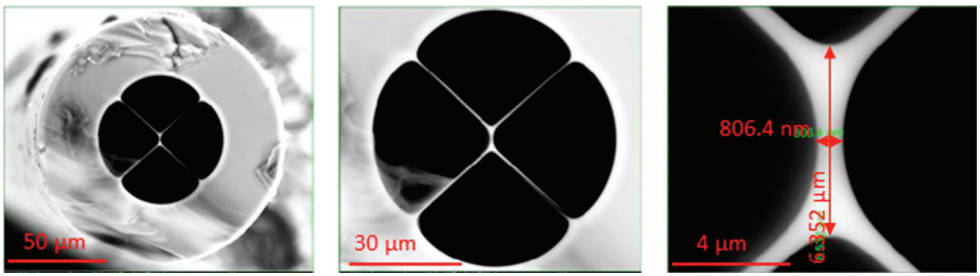

Fig. 1. Microscope photograph of the microstructured optical fiber (MOF)'s cross section.

Among optical fiber sensors, those based on nanocoatings have recently experienced a significant development [20]. Furthermore, new chemical deposition techniques, such as sputtering [21], allow the morphology of the deposited coatings to be controlled with high accuracy: as a consequence, the final features of the sensor (sensitivity, kinetics) are enhanced. SnO_2 depositions have shown great properties for sensing applications such as high sensitivity H_2S sensors [22], ethanol sensors [23], CO and NO_2 sensors [24] or smoke sensors [25]. There are several methods to prepare SnO_2 sensitive layers. To create a homogeneous layer on the surface of a pure silica optical fiber, sputtering depositions are commonly used [26–28].

Several relative humidity sensors using optical fiber substrates have already been reported: agarose gel layers on tapered fibers [29], hygroscopic layers on hetero-core based fibers [30], nano Fabry-Perot cavity sensors [31] and coatings on long-period and standard FBGs [32,33] are some remarkable examples. One of the most studied applications for the relative humidity sensors in the field of bio medical engineering is breathing monitoring. Fast response and recovery time are critical for this kind of measurements. Different types of breathing sensors have been experimentally reported: the most relevant ones are devices based on microstructured fiber [34], macrobending [35], medical textiles in which Bragg and time reflectometry sensors are embedded [36], devices based on nanostructured fibers [37] or plastic optical fiber (POF) [38].

A SnO_2 Fabry-Pérot interferometer implemented with a four-bridge dual highly coupled cores microstructured optical fiber is presented and characterized in this work. By monitoring the Fast Fourier Transform (FFT) phase variations of the FP interference frequency, an experimental study of this cavity's response towards relative humidity changes is described.

In a previous study, an initial characterization of the relative humidity sensor was performed by the FFT technique, showing the independence of the signal amplitude and avoiding the necessity of tracking the wavelength evolution in the spectrum, which makes the measurements more robust [39]. Furthermore, relevant factors such the optimization of sputtering thickness, an analysis of the response vs temperature variations, hysteresis error measurements, and a novel study though the optical backscatter reflectometer in order to observe the propagation of light and sputtering depth inside the MOF are studied in detail. Finally, an application for human breath monitoring on real time is proposed and validated.

2. Experimental

2.1. Microstructured optical fiber

A sample of a "four-bridge double-Y-shape-core MOF" was developed and fabricated using the stack and draw process. It presents four large air holes divided by four thin bridges (~800 nm), showing a suspended core of 6.5 µm by 806 nm and exhibiting a double Y shape, as can be seen in the SEM pictures shown in Fig. 1. This MOF presents multimodal and birefringence features [40]. Birefringence in the 1550 nm region was theoretically estimated in $\sim 6.8 \times 10^{-3}$ with a beat length of 350 µm.

This particular structure has interesting properties for gas sensing and chemical deposition processes: the presence of the four longitudinal air holes directly in contact with the fiber core allows the light guided in the core and the surrounding medium to interact directly through the evanescent field. Moreover, the reduced dimensions of the MOF core and the high numerical aperture (due to the effective refractive index difference between the core and air cladding) increases the evanescent field as it has been previously reported [41,42]. The air holes dimensions also allows different chemical compounds to be deposited, which leads to high sensitive layers.

2.2. Fabry-Perot cavity

The low-finesse Fabry-Pérot interferometer was fabricated by splicing a single mode fiber (Corning SMF-28) to ~700 µm of the four-bridge MOF, whose end was perpendicularly cleaved, as it is shown in Fig. 2. This delicate splice was made through a custom splice program due to the fragility of the MOF fiber, especially given by the bridge thickness. There is a trade-off between the cavity robustness and the MOFís structural stability once the splicing arc is applied. The splice was made with a Fitel S175 fusion splicer with a custom developed program for this MOF and manual operation for its alignment. Results were obtained repeatedly as shown in [39,40].

By splicing a piece of MOF to a SMF, two low-reflectivity mirrors are formed at both ends of the MOF: one in the interface SMF-MOF due to the discontinuity in refractive index between both fibers; the other one is located at the interface MOF-air because this high discontinuity provides a Fresnel reflection (3.3%). Light is coupled from the SMF to the MOF, reflected at the MOF's end and then coupled back in the SMF. In this manner, a low-finesse Fabry-Pérot interferometer is created when a light beam reaches the cavity (MOF) and it is reflected several times between the two interfaces. Each beam has a certain phase difference with respect to the preceding one: this shift corresponds to the extra path length travelled inside the cavity. Due to the high loss of the MOF and the low reflectivity of the air-glass interface, high order reflections inside the cavity are neglected and therefore a low-finesse scenario is assumed which approximates a two-beam Fabry-Perot [43].

Assuming a two beam Fabry-Perot, the reflected signal obtained should follow equation (1), where $\Delta\lambda$ is the optical spectrum wavelength spacing, λ is the working wavelength, n is the refractive

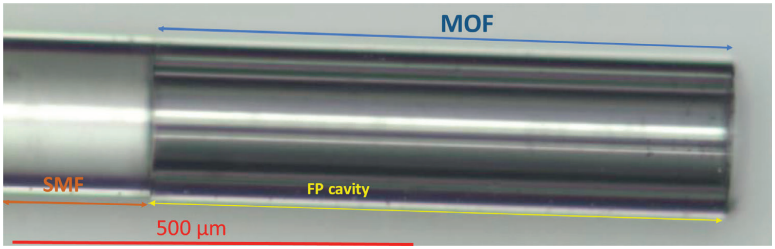

Fig. 2. Microscope photograph of the low-finesse Fabry-Pérot cavity.

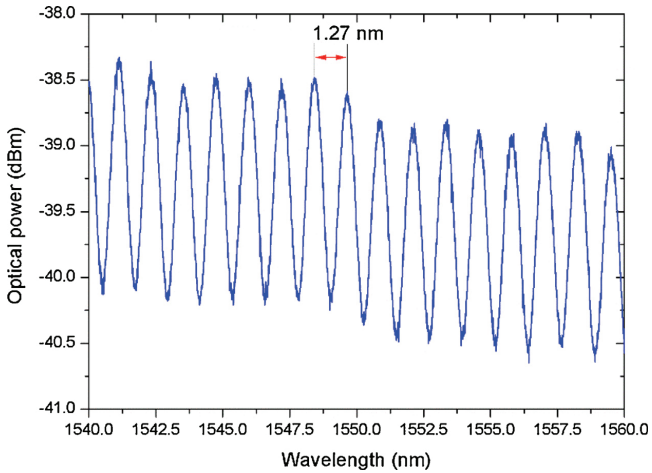

Fig. 3. Low-finesse FP reflected spectrum.

index and d is the MOF cavity length. Experimentally, λ = 1550 nm, d = 690 µm and n_{eff} = 1.37 [40].

$$\Delta\lambda = \frac{\lambda^2}{2nd} \quad (1)$$

As a result, the experimental reflected spectrum is shown in Fig. 3.

2.3. Experimental setup

Fig. 4 presents the experimental set-up used to characterize the resulting sensor. Two commercial interrogating sensor devices were used to illuminate the sensing head and also to analyze the spectra of the signal guided back from the sensor. It should be noticed that in addition to their original purpose as FBG interrogators, this equipment can be used to interrogate other type if sensors in real time. The optical interrogators are remotely controlled by a MATLAB script which also computes the FFT real time analysis. The sensing head was placed into a climatic chamber where relative humidity ranges from 20% to 90% were applied at a constant temperature of 25 °C ± 1 °C to evaluate its response.

Experimental measurements were carried out with two different optical interrogators showing dissimilar sample rates and spectral resolutions. A Micron Optics SM 125 optical sensing interrogator with a resolution of 5 pm and a maximum scan frequency of 1 Hz [44] was used to perform the characterization of the sensing head inside the climatic chamber (Angelantoni CH 250). For human breath measurements, higher sample rates were required, so that a Micron Optics si155 with a maximum sample rate of 1 kHz and 10 pm of resolution was employed. The sample rate was set to 10 Hz for breathing measurements.

A multi-LED light source (HP83437A) and Optical Spectrum Analyzer (OSA-HP86142A) combined with an optical circulator were used to monitor the interference pattern shift along the sputtering process as well as to test the sensor (as Fig. 5 illustrates).

Finally, to monitor the SnO_2 final deposition depth inside the MOF an Optical Backscatter Reflectometer (OBR 4600 Luna Technologies) with a spatial resolution of 10 µm was used in reflexive configuration (same as Fig. 4).

2.4. Sensing material

Several papers have shown very interesting results when tin dioxide (SnO_2) was deposited in different types of optical fibers to prepare relative humidity sensors [45,46]. Due to the structure of the MOF used in this work, SnO_2 can be deposited on the walls of the air holes of the short section of the MOF as well as on the top of the sensor head, which improves the sensitivity of previous devices. For this reason, the combination of MOF and SnO_2 is very interesting for sensing applications. The interaction between SnO_2 and H_2O molecules is due to the phenomena called physisorption by means of the adsorption/desorption of these molecules [47]. The molecules of water interact just with the surface of the deposited film.

A SnO_2 (the sputtering target was purchased in ZhongNuo Advanced Material Techonology Co) thin film was deposited onto

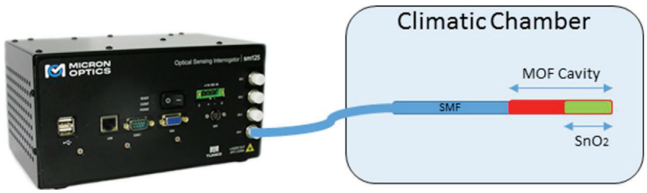

Fig. 4. Experimental setup for RH characterization.

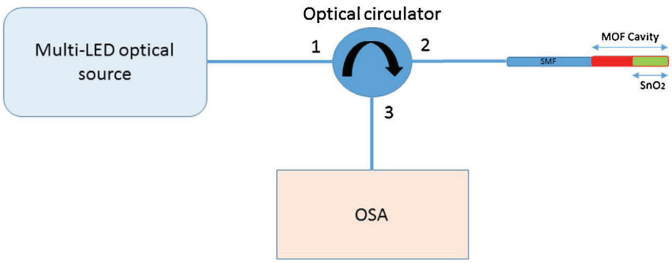

Fig. 5. Experimental setup for SnO_2 construction and breathe measurements.

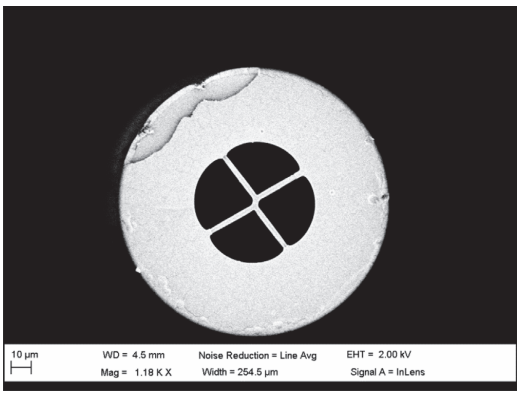

Fig. 6. Fiber cross section after deposition.

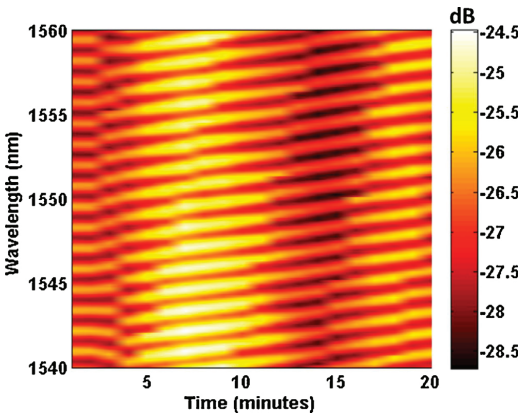

Fig. 7. Spectral (1540–1560 nm) evolution of the SnO_2 thin film MOF sensor transfer function during the sputtering process.

the low-finesse FP interferometer sensor head using a sputtering machine (Pulsed DC sputtering System, Nadetech Innovations). The sputtering process was performed with a partial pressure of Argon of 5×10^{-2} mb, a current of 160 mA and a voltage of 190 V. The distance between the sensor head and the SnO_2 target was set to 2 cm. Sputtering technique was selected because it is a reproducible process which allows a homogeneous thickness to be achieved, as it can be observed in Fig. 6. The nanofilm thickness is to be optimized because it is a critical parameter that determines the sensitivity of sensor.

2.5. Optimization of the thin film thickness

In Section 2.1, it has been mentioned that the presence of air holes in the fiber core allows a direct interaction between the light guided in the core and the surrounding medium through the evanescent field. Based on this explanation, when an optimal thickness of SnO_2 is sputtered on the walls of the MOF air holes, the interaction between the evanescent field of the guided light and the thin film is possible: it is the transduction mechanism, in which the thin film thickness is critical for the sensitivity. When the sensor is exposed to different relative humidity values, the refractive index of the surrounding medium changes shifting the interference pattern.

In order to achieve the optimal SnO_2 thin film that maximizes the sensitivity of the sensor, a 20 min long sputtering process was performed. Fig. 7 illustrates the evolution of the interference pattern peaks of the cavity during the sputtering process. The recorded shift depends on the deposition thickness and therefore the thin film effect can be studied by analyzing these data. In previous papers [48], it was found that the optimal point to stop the construction is when little thickness changes generate high wavelength shifts in the spectrum. In the current work, as it can be observed in Fig. 7, when the thickness of the sensor is increased the wavelength shift of every peak is roughly the same and consequently, the slope of each of them is apparently the same. This is an important result of the sputtering process which means that the spectrum continues shifting during the whole deposition time but the sensitivity can be compromised. As Ref. [49] explains, if an unsuitable thick-

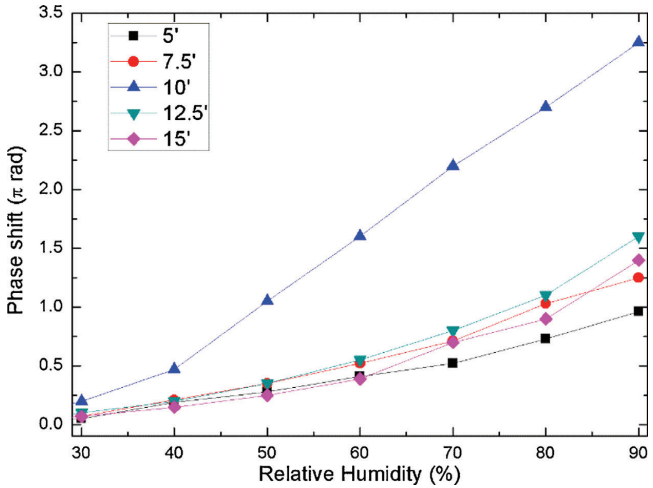

Fig. 8. Phase shift of sensors with different deposition times towards relative humidity.

ness is deposited onto the sensor, there are two different scenarios regarding to the sensor sensitivity: firstly, if the nanofilm thickness deposited is very thin, only a small part of the evanescent field interacts whit it; secondly, if the nanofilm thickness deposited is too high, the interaction between the evanescent field and the nanofilm that has adsorpted the eater molecules is not possible. In both of cases, the sensitivity of the sensor is not the optimal one.

To analyze this problem and achieve the thin film thickness that optimizes the sensitivity of the sensor, five different devices were performed with distinct construction times. The times selected were 5′, 7.5′, 10′, 12.5′ and 15 min respectively. The sputtering time determines the thin film thickness and therefore the sensors' sensitivity as it can be seen in Fig. 8. All the resulting sensors where tested within 20%-90% relative humidity ranges showing different sensitivities. Starting from a 5 min deposition, the sensitivity is gradually increased showing the best sensitivity at 10 min (0.014π rad/%, 0.018π rad/%, and 0.047π rad/% for 5′, 7.5′ and 10′ respectively). Beyond 10 min, the SnO_2 thin film becomes thicker than the evanescent field penetration and consequently, the sensitivity decreases (0.023π rad/% and 0.02π rad/% for 12.5′ and 15′ respectively). The thickness for each case was estimated by comparing SEM images of the sensing head's cross section before and after deposition (Figs. 1 and 4 respectively). The 10 min deposited sensor presents a thin film thickness of 1.10 μm ± 0.09 μm.

After the sputtering deposition, a precise study of the results achieved inside the MOF cavity was carried out through the Optical Backscatter Reflectometer LUNA 4600. This device performs spatial measurements with resolution of 10 μm and allows the orthogonal polarizations states of light S and P to be analyzed. Fig. 9a) shows the Luna backscatter results for the MOF cavity before the sputtering deposition whereas Fig. 9b) represents the same MOF cavity after the deposition.

Two main reflections are observable in Fig. 9a): the first one (set as reference) located at 0.0 mm corresponds to the splice between the SMF and the MOF fibers and it produces a light reflection of −17.6 dBr; the second relevant reflection is located at 0.690 mm and corresponds to the cleaved end of the MOF cavity giving a reflection power of −10 dBr. It must be also noticed that although there is a difference in the optical power reflected by the different polarization states: this difference is almost the same one along the whole MOF cavity (3.46 dB).

After the deposition, as Fig. 9b) illustrates, the splice location remains at the same point, but the cavity end is shifted 10 μm. This length increase is due to the SnO_2 deposition on the second interface of the fiber cavity, although it is not a precise measurement because of the LUNA resolution limit; furthermore, a new reflection peak appears located at 0.130 mm. This new peak means that at this point, there is something affecting the light propagation along the core in the MOF cavity: the SnO_2 deposition depth limit. From this point towards the cleaved cavity end, the whole reflected light has changed. This effect is even easier to appreciate on the polarization states: polarization P is severely affected by the SnO_2 presence giving strong differences in relation to polarization S behavior. By measuring the distance from the cavity end to the new reflection point it can be assumed that the deposition depth inside the cavity is about 570 μm which means 130 μm before the cavity physical length limit. The SnO_2 deposition inside the MOF cavity in addition to the deposition on the top of the fiber ensure the interaction zone between the evanescent field of the guided light and the deposited thin film. As far as authors know it is the first time that an OBR is used in order to determine a sputtering thickness at the end of the fiber and it complements perfectly the results obtained from the SEM pictures' analysis. Moreover it is also the first time that an OBR is used to provide information of how a chemical deposition affects light inside a MOF.

2.6. Interrogation method

The interrogation technique is based on the Fast Fourier Transform of the sensor's optical spectrum. By monitoring the Fast Fourier Transform phase, wavelength shifts in the optical spectrum can be monitored without the noise influence or signal amplitude variations and enabling multiplexing several sensors within a single interrogator's channel as it will be explained in Section 3.4. Optical spectrum signal amplitude undesired variations lead to changes in the FFT module amplitude but do not affect the FFT phase.

A theoretically perfect periodical sinusoidal signal (such as the low finesse Fabry-Pérot response) in the optical spectrum domain presents two main components in the transformed domain (one in the positive part and its equivalent in the negative part) as can be seen in Fig. 10 (only positive part of the FFT module is shown).

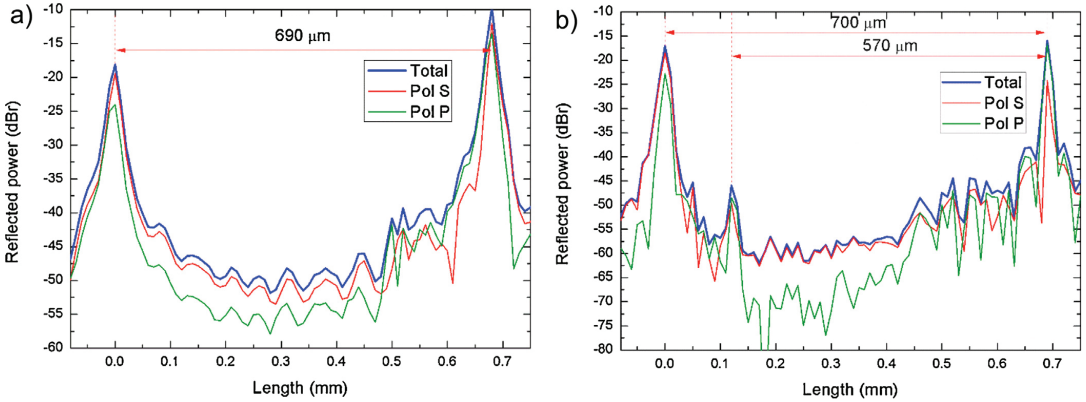

Fig. 9. Luna backscatter optical power of the MOF cavity and orthogonal polarization states: a) before sputtering deposition and b) after it.

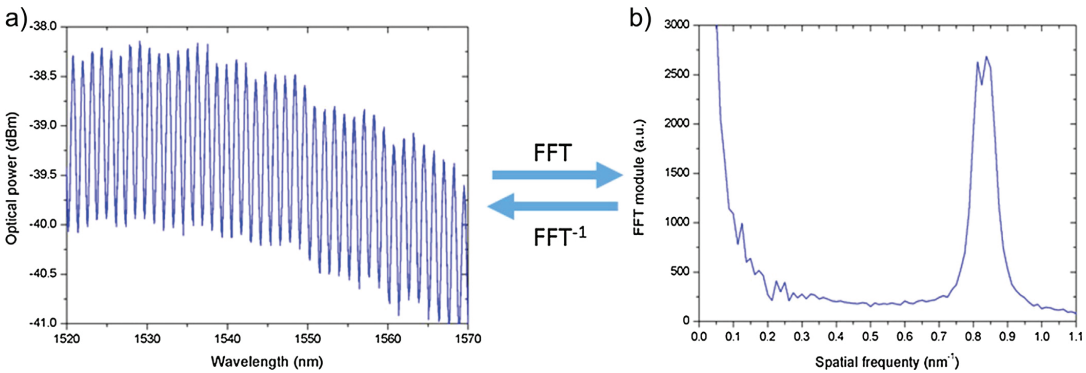

Fig. 10. Optical spectrum and its FFT.

Real optical signals present some dispersion around the main transformed component due to the resolution of the optical interrogator but they can be assumed as a single contribution. Noise present in the optical spectrum is present in the transformed domain as high spatial frequency contributions and it can be neglected.

Wavelength shifts in the optical domain lead to phase shifts in the Fast Fourier Transform domain while the FFT module stays unaltered. By tracking the phase of the spatial frequency component (located in 0.8375 nm^{-1} in Fig. 10) the evolution of the optical spectrum and therefore the sensor can be monitored. Through this technique sensors can be monitored without the influence of signal amplitude noise or amplitude fluctuations and furthermore, it provides a useful multiplexing instrument.

3. Results and discussion

3.1. RH sensing

To verify the sensing head performance (and the influence of the SnO_2 deposition) with relative humidity variations, the fiber sensor was placed into the climatic chamber, and several experiments were implemented with RH variations from 20% to 90% at a constant 25 °C ± 1 °C temperature and at atmospheric pressure. The sensor response was measured tracking the FFT phase corresponding to spatial frequency located at 0.8375 nm^{-1}. Three increasing/decreasing relative humidity cycles were performed in each case to assure the time-stability of the sensor. Data were recorded using the Micron Optics SM 125 every 30 s and they were processed following the FFT algorithm. Furthermore, this device allows real time measurements to be recorded, although a sensorís calibration is required. Fig. 11 presents the results of the MOF-FP cavity towards relative humidity cycles before and after SnO_2 deposition.

On the one hand, as can be noticed from Fig. 11 (green line) the MOF cavity itself, without the SnO_2 layer presents negligible response to relative humidity variations. Direct guided light evanescent field interaction with the external medium do not show high variations giving a maximum shift of 0.015π rad from 20% to 90% RH. Furthermore, as it was previously commented, the high loss of the fiber and the low reflectivity of its core-air interface only allows a single round trip, which supposes a low capability to measure directly the surrounding medium.

On the other hand, Fig. 11(blue line) presents the MOF-FP-SnO_2 sensing head response after the sputtering deposition. It can be noticed that the sensitivity is improved, which sets maximum phase variation between 20% and 90% of 3.29π rad. Typically, the sensitivity of relative humidity sensors is different depending on the relative humidity range [18] showing 2–3 different regions with different sensitivities, but in our case, the sensor response shows a linear behavior in the whole measured relative humidity range with a constant sensitivity of 0.047π rad/% RH and a resolution of 0.0026% RH. In this manner, continous measures in the range 20%-

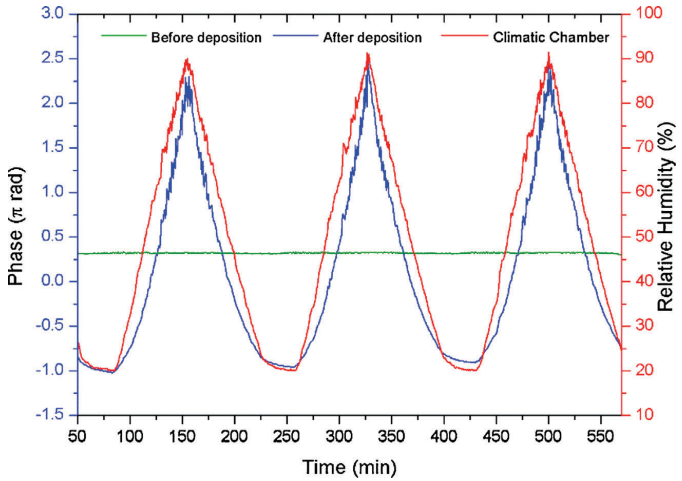

Fig. 11. Sensor's phase response: before deposition and after SnO_2 deposition. (For interpretation of the references to colour in the text, the reader is referred to the web version of this article.)

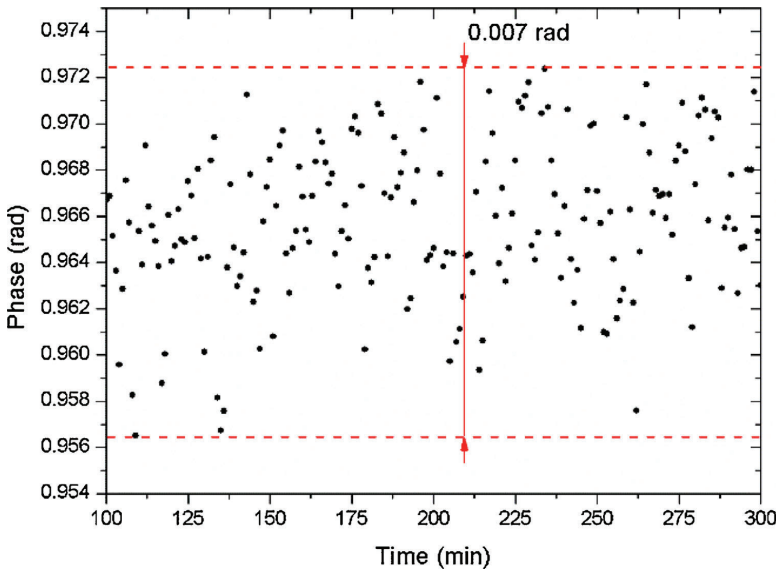

Fig. 12. MOF-FP-SnO_2 sensor's stability.

90% RH can be performed without further callibrations. The sensor was tested repeatedly along two weeks to assure its repetibility, showing the same results in all cases.

3.2. Stability

One important feature of this type of sensors is its phase stability during time. To measure this parameter, the sensing head was placed in the climatic chamber at constant 40% RH and 25 °C for 300 min and a sample was registered every minute. Fig. 12 shows the stability results with a maximum instability of 0.007 rad which implies an error of 5%.

At this point, the influence of birefringence must be remarked. As the low-finesse Fabry-Pérot is highly birefringent, polarization affects its optical spectrum, showing important differences in the FFT module but slightly ones in the FFT phase. To reduce its influence, a polarizer and a stable optical bench were used during all the measurements.

3.3. Hysteresis

Another key feature in RH sensors is the hysteresis error. Usually metal oxide sensitive layers present low hysteresis effects in comparison with the polymeric ones [50]. In the MOF-FP-SnO_2 this tendency is also followed.

The sensor presents low hysteresis with a maximum deviation of 5.03% RH showed in the high relative humidity region as Fig. 13

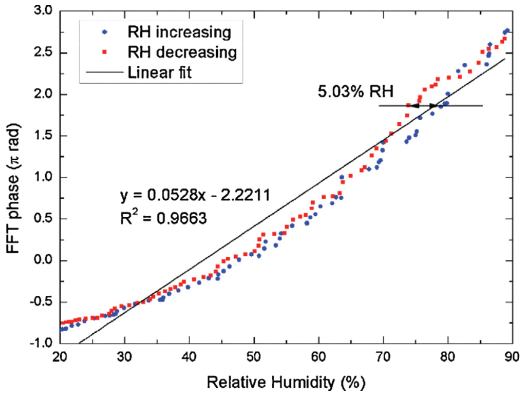

Fig. 13. Sensor's hysteresis.

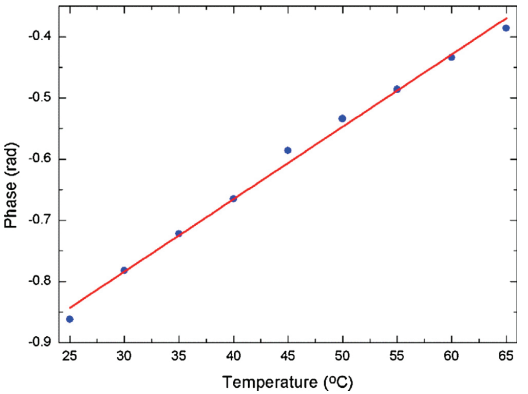

Fig. 14. MOF-FP-SnO_2 sensor's response to temperature.

illustrates. This result agrees with the error produced due to the signal phase instability and can be influenced by it.

3.4. Multiplexing capability

As it was previously commented in Section 2.2, the MOF cavity optical spectrum is directly influenced by its length (1). Varying appropriately the MOF length fused to the SMF it is possible to achieve different sensing heads with interferometric spectrums whose FFT modules do not overlap with each other. This way, if the main spatial component of each sensor in the FFT module is isolated, by tracking its FFT phase it is possible to measure independently avoiding crosstalk with the other sensors.

This FFT feature enables multiplexing high number of sensors within a single channel of the optical interrogator, reducing proportionally the economic cost of each sensor. Experimentally, authors have previously reported 3 multiplexed sensors [51] and successfully multiplexed up to 5 MOF-FP sensors with no crosstalk between measurements (work still not published) but theoretically it can be increased up to 10 without amplification needed. Furthermore, MOF-FP sensing heads with different sensitive layers can be multiplexed simultaneously increasing the versatility of the system becoming a multi-parameter and multi-point real-time monitoring system.

3.5. Temperature cross correlation

The influence of temperature variations on the MOF-FP-SnO_2 sensing head was experimentally tested. The performance of a MOF-FP cavity was previously tested by the authors [40] but not with the SnO_2 sensitive layer.

As Fig. 14 shows, the sensing head presents linear response to temperature variations with a sensitivity of 0.012 rad/°C. This temperature influence is lower than the one reported from previous works [52] but it can produce crosstalk with RH measurements, although its effect can be compensated taking advantage of the system multiplexing capability: with a proper selection of MOF lengths, a MOF-FP-SnO_2 sensing head for RH measurements and a MOF-FP sensing head for temperature variations can be multiplexed. With the MOF-FP, temperature can be monitored independently of the RH and therefore it can be used as a reference for the others RH sensing head.

3.6. Breath measurements

In addition to the sensor sensitivity to RH variations, it presents two additional advantageous features: fast response and reversibility. These features make the MOF-FP-SnO_2 sensor suitable to be a real time human breath sensor. For this purpose, two differ-

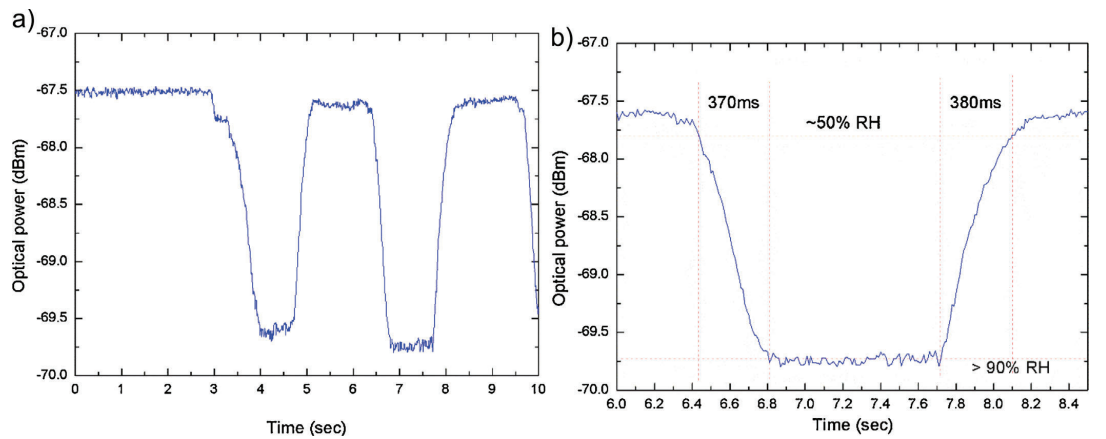

Fig. 15. a) Sensor's response to human breath using a zero span in the OSA and b) detail of one breath cycle.

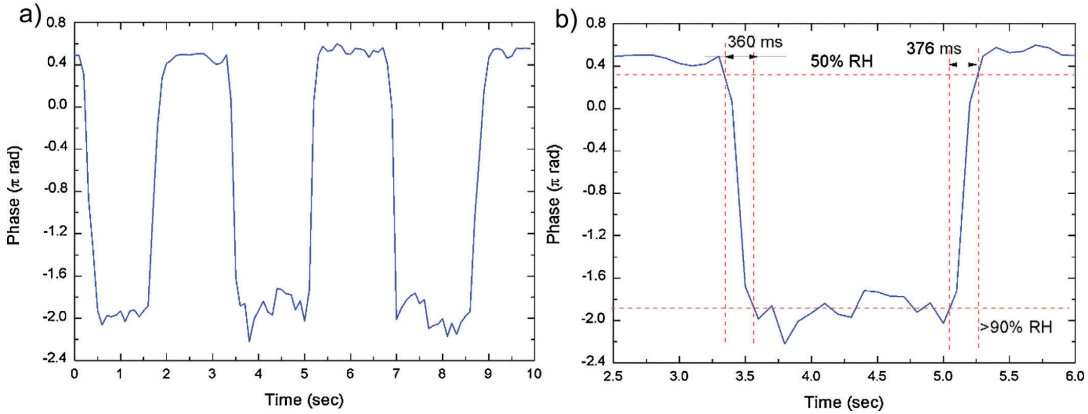

Fig. 16. a) Sensor's response to human breath using the si55 optical interrogator and b) detail of one breath cycle.

ent scenarios have been implemented with different devices and interrogating methods.

On the one hand the MOF-FP-SnO_2 sensing head was interrogated with a multi-LED source an analyzed in an OSA with a zero-spam method. Within this set up, the optical power temporal evolution at a certain wavelength of the optical spectrum was monitored. The OSA provides a sampling rate of 100 Hz with a maximum continuous measured period of 10 s and the results are shown in Fig. 15. The sensing head was placed close to the mouth of the target person and the RH variations produced by the exhalation were measured.

The sensor responds continuously to human exhalation showing a response time of 370 ms, a recovery time of 380 ms: moreover, no baseline drift is observed.

On the other hand, additional measurements were performed with the optical interrogator Micron Optics si155 with a sample frequency of 10 Hz. With this device, RH can be tracked continuously and determined unambiguously in the whole range, as Fig. 16 illustrates.

Once again, MOF-FP-SnO2 sensor shows similar rise and recovery time with full recovery of the baseline as it was expected. The difference between both interrogating methods lies on the capability of the second method (with the optical interrogator) to follow slow RH alterations during the exhalation period and the suitability of multiplexing several sensors at the same time. Furthermore, the recording and processing time of the system can be reduced using a high features computer.

4. Conclusions

A new sensor system for relative humidity measurements based on its interaction with a SnO_2 thin film sputtered on a MOF-Fabry-Pérot cavity has been proposed and experimentally demonstrated. The interrogation of the sensing head has been carried out through the FFT analysis. By monitoring the FFT phase variations of the low-finesse FP interference frequencies the optical spectrum can be tracked unambiguously. This method is low-dependent of the signal amplitude and avoids the necessity of tracking the wavelength evolution of maxima or minima of the spectrum, which can be a handicap when noise is present; it also allows several sensors to be multiplexed, which reduces the economic cost of the system and improves its versatility. The sensor has been operated within a wide relative humidity range (20%–90% RH), obtaining a maximum sensitivity achieved of 0.14 rad/% RH a resolution of 0.0026% RH and a phase standard deviation of 0.007 rad which presents an error of ±5%. Furthermore, FFT based signal processing makes the sensor response linear and along the entire RH range. The temperature influence can be real-time-compensated due to the multiplexing suitability of the interrogation technique. The SnO_2 MOF-FP sensor presents high-speed response, reversibility, high repeatability rate, robust and compact features. Furthermore, the baseline is always recovered without deviations, so that the device can be used for a real time applications such as breath monitoring.

Acknowledgments

The authors are grateful to A. Ortigosa, D. Erro, Dr. M. Bravo and Dr. R.A. Perez-Herrera. We also thank the Spanish Government projectsTEC2013-47264-C2-2-R, TEC 2016-76021-C2-1-R, TEC2016-78047-R, TEC2016-79367-C2-2-R, Innocampus and the Cost Action MP 1401, as well as to the AEI/FEDER Funds.

References

[1] A.M.R. Pinto, M. Lopez-Amo, Photonic crystal fibers for sensing applications, J. Sens. 21 (2012).
[2] T.M. Monro, S. Warren-Smith, E.P. Schartner, A. François, S. Heng, H. Ebendorff-Heidepriem, S. Afshar, Sensing with suspended-core optical fibers, Opt. Fiber Technol. 16 (6) (2010) 343–356.
[3] O. Frazao, J.L. Santos, F.M. Araújo, L.A. Ferreira, Optical sensing with photonic crystal fibers, Laser Photon. Rev. 2 (6) (2008) 449–459.
[4] O. Frazao, S.F.O. Silva, J. Viegas, J.M. Baptista, J.L. Santos, J. Kobelke, K. Schuster, All fiber Mach-Zehnder interferometer based on suspended twin-Core fiber, IEEE Photon. Technol. Lett. 22 (2010) 1300–1302.
[5] A.S. Webb, F. Poletti, D.J. Richardson, J.K. Sahu, Suspended-core holey fiber for evanescent-field sensing, Opt. Eng. 46 (2007), 010503-010503-010503.
[6] M. Bravo, A.M.R. Pinto, M. Lopez-Amo, J. Kobelke, K. Schuster, High precision micro-displacement fiber sensor through a suspended-core Sagnac interferometer, Opt. Lett. 37 (2) (2012) 202–204.
[7] S. Rota-Rodrigo, A. López-Aldaba, R.A. Pérez-Herrera, M.D.C.L. Bautista, Ó. Esteban, M. López-Amo, Simultaneous measurement of humidity and vibration based on a microwire sensor system using fast fourier transform technique, J. Lightwave Technol. 34 (19) (2016) 4525–4530.
[8] J.B. Jensen, L.H. Pedersen, P.E. Hoiby, L.B. Nielsen, T.P. Hansen, J.R. Folkenberg, J. Riishede, D. Noordegraaf, K. Nielsen, A. Carlsen, A. Bjarklev, Photonic crystal fiber based evanescent-wave sensor for detection of biomolecules in aqueous solutions, Opt. Lett. 29 (17) (2004) 1974–1976.
[9] J. Bürck, J.P. Conzen, H.J. Ache, A fiber optic evanescent field absorption sensor for monitoring organic contaminants in water, Fresenius' J. Anal. Chem. 342 (4–5) (1992) 394–400.
[10] M. Tabib-Azar, B. Sutapun, R. Petrick, A. Kazemi, Highly sensitive hydrogen sensors using palladium coated fiber optics with exposed cores and evanescent field interactions, Sens. Actuators B: Chem. 56 (1) (1999) 158–163.
[11] S. Sekimoto, H. Nakagawa, S. Okazaki, K. Fukuda, S. Asakura, T. Shigemori, S. Takahashi, A fiber-optic evanescent-wave hydrogen gas sensor using

palladium-supported tungsten oxide, Sens. Actuators B: Chem. 66 (1) (2000) 142–145.
[12] A.S. Webb, F. Poletti, D.J. Richardson, J.K. Sahu, Suspended-core holey fiber for evanescent-field sensing, Opt. Eng. 46 (1) (2007), 010503–010503.
[13] H. Choi, K. Park, S. Park, U. Paek, B. Lee, E. Choi, Miniature fiber-optic high temperature sensor based on a hybrid structured Fabry-Perot interferometer, Opt. Lett. (2008) 2455–2457.
[14] G.Z. Xiao, A. Adnet, Z. Zhang, F.G. Sun, C.P. Grover, Monitoring changes in the refractive index of gases by means of a fiber optic Fabry-Perot interferometer sensor, Sensor Actuators A: Phys. 118 (2) (2005) 177–182.
[15] L.H. Chen, T. Li, C.C. Chan, R. Menon, P. Balamurali, M. Shaillender, B. Neu, X.M. Ang, P. Zu, K.C. Leong, Chitosan based fiber-optic Fabry–Perot humidity sensor, Sens. Actuators B: Chem. 169 (2012) 167–172.
[16] O. Frazao, S.H. Aref, J.M. Baptista, J.L. Santos, H. Latifi, F. Farahi, J. Kobelke, K. Schuster, Fabry–Pérot cavity based on a suspended-core fiber for strain and temperature measurement, IEEE Photon. Technol. Lett. 21 (17) (2009) 1229–1231.
[17] M.J. Gander, W.N. MacPherson, J.S. Barton, R.L. Reuben, J.D. Jones, R. Stevens, K.S. Chana, S.J. Anderson, T.V. Jones, Embedded micromachined fiber-optic Fabry-Perot pressure sensors in aerodynamics applications, IEEE Sens. J. 3 (1) (2003) 102–107.
[18] J. Mathew, Y. Semenova, G. Rajan, G. Farrell, Humidity sensor based on photonic crystal fibre interferometer, Electron. Lett. 3 (19) (2010) 1341–1343.
[19] M. Hernaez, D. Lopez-Torres, C. Elosua, I.R. Matias, F.J. Arregui, Sensitivity Enhancement of a Humidity Sensor Based on poly (sodium phosphate) and poly (allylamine hydrochloride), Sensors 13 (2012), 1930–0395.
[20] F.J. Arregui, Sensors Based on Nanostructured Materials, Springer, New York (NY), 2009.
[21] M. Stowell, J. Müller, M. Ruske, M. Lutz, T. Linz, RFsuperimposed DC and pulsed DC sputtering for deposition of transparent conductive oxides, Thin Solid Films (2007) 7654–7657.
[22] G.S. Devi, S. Manorama, V.J. Rao, High sensitivity and selectivity of an SnO2 sensor to H2S at around 100 °C, Sens. Actuators B: Chem. 28 (1) (1995) 31–37.
[23] R.N. Mariammal, K. Ramachandran, B. Renganathan, D. Sastikumar, On the enhancement of ethanol sensing by CuO modified SnO 2 nanoparticles using fiber-optic sensor, Sens. Actuators B: Chem. 169 (2012) 199–207.
[24] H.E. Endres, W. Göttler, R. Hartinger, S. Drost, W. Hellmich, G. Müller, Ch.B. Braunmühl, A. Krenkow, C. Perego, G. Sberveglieri, A thin-film SnO2 sensor system for simultaneous detection of CO and NO2 with neural signal evaluation, Sens. Actuators B: Chem. 36 (1–3) (1996) 353–357.
[25] J. Mizsei, Response pattern of SnO2 sensor system for smoke of different origins, Sens. Actuators B: Chem. 18 (1–3) (1994) 264–267.
[26] J.Z. Ou, M.H. Yaacob, J.L. Campbell, M. Breedon, K. Kalantar-zadeh, W. Wlodarski, H 2 sensing performance of optical fiber coated with nano-platelet WO 3 film, Sens. Actuators B: Chem. 166 (2012) 1–6.
[27] J. Dai, M. Yang, X. Yu, H. Lu, Optical hydrogen sensor based on etched fiber Bragg grating sputtered with Pd/Ag composite film, Opt. Fiber Technol. 19 (1) (2013) 26–30.
[28] N. Cennamo, D. Massarotti, L. Conte, L. Zeni, Low cost sensors based on SPR in a plastic optical fiber for biosensor implementation, Sensors 11 (12) (2011) 11752–11760.
[29] C. Bariain, I.R. Matıías, F.J. Arregui, M. Lopez-Amo, Experimental results towards development of humidity sensors by using a hygroscopic material on biconically tapered optical fibre, Proc. of SPIE 3555 (1998) 95–105.
[30] S. Akita, H. Sasaki, K. Watanabe, A. Seki, A humidity sensor based on a hetero-core optical fiber, Sens. Actuators B: Chem. 147 (2) (2010) 385–391.
[31] F.J. Arregui, Y. Liu, I.R. Matias, R.O. Claus, Optical fiber humidity sensor using a nano Fabry–Perot cavity formed by the ionic self-assembly method, Sens. Actuators B: Chem. 59 (1) (1999) 54–59.
[32] M. Konstantaki, S. Pissadakis, S. Pispas, N. Madamopoulos, N.A. Vainos, Optical fiber long-period grating humidity sensor with poly (ethylene oxide)/cobalt chloride coating, Appl. Opt. 45 (19) (2006) 4567–4571.
[33] P. Kronenberg, P.K. Rastogi, P. Giaccari, H.G. Limberger, Relative humidity sensor with optical fiber Bragg gratings, Opt. Lett. 27 (16) (2002) 1385–1387.
[34] F.C. Favero, J. Villatoro, V. Pruneri, Microstructured optical fiber interferometric breathing sensor, J. Biomed. Opt. 17 (3) (2012) 0370061–0370065.
[35] J. Witt, F. Narbonneau, M. Schukar, K. Krebber, J. De Jonckheere, M. Jeanne, D. Kinet, B. Paquet, A. Depré, L.T. DÁngelo, T. Thiel, R. Logier, Medical textiles with embedded fiber optic sensors for monitoring of respiratory movement, IEEE Sens. J. 12 (1) (2012) 246–254.
[36] A. Grillet, D. Kinet, J. Witt, M. Schukar, K. Krebber, F. Pirotte, A. Depré, Optical fiber sensors embedded into medical textiles for healthcare monitoring, IEEE Sens. J. 8 (7) (2008) 1215–1222.
[37] Y. Kang, H. Ruan, Y. Wang, F.J. Arregui, I.R. Matias, R.O. Claus, Nanostructured optical fibre sensors for breathing airflow monitoring, Meas. Sci. Technol. 17 (5) (2006) 1207.
[38] S. Muto, O. Suzuki, T. Amano, M. Morisawa, A plastic optical fibre sensor for real-time humidity monitoring, Meas. Sci. Technol. 14 (6) (2003) 746.
[39] A. Lopez-Aldaba, D. Lopez-Torres, J. Ascorbe, S. Rota-Rodrigo, C. Elosua, M. Lopez-Amo, F.J. Arregui, J.M. Corres, J.-L. Auguste, R. Jamier, P. Roy, SnO2-MOF-Fabry-Pérot humidity optical sensor system based on fast Fourier transform technique, in: Sixth European Workshop on Optical Fibre Sensors, International Society for Optics and Photonics, 2016 (pp. 99161T–99161T).
[40] A. Lopez-Aldaba, A.M.R. Pinto, M. Lopez-Amo, O. Frazão, J.L. Santos, J.M. Baptista, H. Baierl, J.L. Auguste, R. Jamier, P. Roy, Experimental and numerical characterization of a hybrid Fabry-Pérot cavity for temperature sensing, Sensors 15 (2015) 8042–8053.
[41] B.D. Gupta, C.D. Singh, Fiber-optic evanescent field absorption sensor: a theoretical evaluation, Fiber Integr. Opt. 13 (4) (1994) 433–443.
[42] S.K. Khijwania, B.D. Gupta, Fiber optic evanescent field absorption sensor: effect of fiber parameters and geometry of the probe, Opt. Quantum. Electron. 31 (8) (1999) 625–636.
[43] J.L. Santos, A.P. Leite, D.A. Jackson, Optical fiber sensing with a low-finesse Fabry–Perot cavity, Appl. Opt. 31 (34) (1992) 7361–7366.
[44] D. Leandro, M. Bravo, A. Ortigosa, M. Lopez-Amo, Real-time FFT analysis for interferometric sensors multiplexing, J. Lightwave Technol. 33 (2) (2015) 354–360.
[45] J. Ascorbe, J.M. Corres, I.R. Matias, F.J. Arregui, High sensitivity humidity sensor based on cladding-etched optical fiber and lossy mode resonances, Sens. Actuators B: Chem. 233 (2016) 7–16.
[46] J. Ascorbe, J.M. Corres, F.J. Arregui, I.R. Matias, Humidity sensor based on bragg gratings developed on the end facet of an optical fiber by sputtering of one single material, Sensors 17 (5) (2017) 991.
[47] W. Schmid, Consumption Measurements on SnO2 Sensors in Low and Normal Oxygen Concentration (Doctoral Dissertation), Universität Tübingen, 2004.
[48] D. Lopez-Torres, C. Elosua, J. Villatoro, J. Zubia, M. Rothhardt, K. Schuster, F.J. Arregui, Photonic crystal fiber interferometer coated with a PAH/PAA nanolayer as humidity sensor, Sens. Actuators B: Chem. 242 (2017) 1065–1072.
[49] D. Lopez-Torres, C. Elosua, J. Villatoro, J. Zubia, M. Rothhardt, K. Schuster, F.J. Arregui, Enhancing sensitivity of photonic crystal fiber interferometric humidity sensor by the thickness of SnO2 thin films, Sens. Actuators B: Chem. 251 (2017) 1059–1067.
[50] C. Massaroni, M.A. Caponero, R. D'Amato, D. Lo Presti, E. Schena, Fiber bragg grating measuring system for simultaneous monitoring of temperature and humidity in mechanical ventilation, Sensors 17 (4) (2017) 749.
[51] A. Lopez-Aldaba, D. Lopez-Torres, C. Elosua, J.-L. Auguste, R. Jamier, P. Roy, F.J. Arregui, M. Lopez-Amo, Relative humidity multi-point optical sensors system based on fast Fourier multiplexing technique, in: 25th International Conference on Optical Fiber Sensors, International Society for Optics and Photonics, 2017 (pp. 103233L–103233L).
[52] J. Mathew, Y. Semenova, G. Farrell, Experimental demonstration of a high-sensitivity humidity sensor based on an Agarose-coated transmission-type photonic crystal fiber interferometer, Appl. Opt. 52 (16) (2013) 3884–3890.

Biographies

Aitor Lopez-Aldaba was born in Navarra, Spain, in July 1988. He received the, Telecommunication Engineering degree from the Universidad Pública de Navarra, Navarra, in 2014. In 2013, he joined the Optical Communications Group, Department of Electrical and Electronic Engineering, Universidad Pública de Navarra. His research interests include fiber optic lasers, optical amplifiers, optical fiber sensor networks, photonic crystal fibers and chemical fiber optic sensors.

Diego López-Torres received the M.S. degree in electrical and electronic engineering and the master's degree in communications from the Public University of Navarra (UPNA), Pamplona, Spain, in 2013 and 2014, respectively. Since 2014, he has been working as a Researcher at the UPNA. In 2105, he obtained a scholarship from this university. His research interest includes optical fiber sensors, photonic crystal fiber and nanostructured materials.

Cesar Elosúa Aguado received his MS degree in electrical and electronic engineering from the Public University of Navarre (UPNA, Pamplona, Spain) in 2004. In the same year, he obtained a scholarship from the Science and Technology Spanish Ministry and he joined the optical fiber sensor group at UPNA. During 2008, he was a visiting Ph.D. student at the University of Limerick and at the City University of London. He became a lecturer of this department in 2009, receiving his PhD degree in the next year. His research interests include optical fiber sensors and networks, organometallic chemistry and data mining techniques.

Jean-Louis Auguste received a PhD degree in Optical and High Frequency of Telecommunications from the University of Limoges (France) in 2001. During his thesis, the main areas of activity have been involved theory, design and experimental investigation on optical fibres and more particularly on a design and fabrication of high negative chromatic dispersion fibre. Since December 2000, he is a CNRS Engineer at Xlim research institute where he was, until 2012, in charge (Process Manager) of the research and development around fabrication of optical fibres – guide structure (PCF) and materials for optical fibres with recent developments around glass synthesis thanks to a European project (VORTEX) that he manages. He works in strong collaboration with researchers of the Fibre Group and is associated to ANR and other European Projects like researcher from Ceramic Laboratory to develop new topics mixing optical glass development and optical fibre applications. By this way in collaboration with researcher from SPCTS (Ceramic Laboratory) he manages a new research project at Xlim around 'original glasses for optical fibre applications'. He has authored or co-authored 45 publications in international journals with referees and 43 papers in international conferences with referees including several invited papers and international seminars plus 4 patent applications. In 2010, he has obtained the degree of HDR, highest diploma of University and giving him the

possibility to be Research Director for PhD students. A part of his activity is dedicated to teaching and training students from University and school engineering.

Raphael Jamier was born in Périgueux, France, in 1981. He received the Ph.D. degree in 2007 from the University of Limoges, France. Since 2008, he has been an Assistant professor at XLIM research institute/University of Limoges, where he has been engaged in design, fabrication and characterisation of specialty optical fibers. His current research activities include the design, fabrication and characterization of photonic crystal fibers for high-power generation at unconventional spectral domains (in particular in the mid-infrared wavelengths). He is also the Deputy Director of the Physics Department of the University of Limoges since 2012. – He has 27 articles as co-author/author in refereed journals, 58 papers in internationally recognized conferences with peer-review system and 2 patents.

Philippe Roy was born in May 1971 in Bellac (France) and received his Ph Degree in Microwave Electronics and Optoelectronics (speciality Photonics and Electronics Systems) in 1997 in the University of Limoges. He is now a CNRS senior researcher and head of Fibre Photonics group at XLIM, which is a mixed laboratory of University of LIMOGES and CNRS. Since 1998, he is involved in design, fabrication and characterisation of Photonic Crystal fibres (PCFs). More recently, he developed specialty and composite fibres mainly dedicated to advanced fibre sensor systems and to very high power fibre lasers. He develops rare earth doped fibre with complex structure based on an aperiodic design to reach higher power levels without modal instabilities and/or non-conventional emitted spectrum, from visible to THz domain.

Francisco J.Arregui (M'01) is a Full Professor at the Public University of Navarre, Pamplona, Spain. He was part of the team that fabricated the first optical fiber sensor by means of the Layer-by-Layer assembly method at Virginia Tech, Blacksburg, VA, USA, in 1998. He is the author of around 300 scientific journal and conference publications. He has been an Associate Editor of "IEEE Sensors Journal", "Journal of Sensors" (founded by Prof, Arregui in 2007), and "International Journal on Smart Sensing and Intelligent Systems". He is also the editor of the books entitled Sensors-Based on Nanostructured Materials and Optochemical Nanosensors.

Manuel López-Amo (M'91–SM'98) was born in Madrid, Spain, in 1960. He received the Telecommunications Engineering and Ph.D. degrees from the Universidad Politécnica de Madrid, Madrid, in 1985 and 1989, respectively. From 1985 to 1996, he belonged to the Photonic Technology Department, Universidad Politécnica de Madrid, where, in 1990, he became an Associate Professor. In 1996, he moved to the Electrical and Electronic Engineering Department, Public University of Navarra, Pamplona, Spain, where he became a Full Professor and is currently the Head of the Optical Communications Group. He has been the Chairman of the Optoelectronic Committee of Spain. He has been the leader of more than 40 research projects and he has coauthored more than 250 works in international refereed journals and conferences related with fiber-optic networks, optical amplifiers, fiber-optic sensors, and integrated optics. He is a member of the technical committees of the International Conference on Fiber Optic Sensors and the European Workshop on Optical Fiber Sensors, among others. He is a senior member of the IEEE and member of the Optical Society of America.

4.3. Conclusiones

En comparación con las SC-PCF, las SSC poseen una estructura más interesante para desarrollar y optimizar sensores de humedad. En el caso que se propone en esta tesis, gracias a sus 4 agujeros, los cuales están directamente conectados con el núcleo, se fuerza a que una mayor parte de la luz, que es guiada por la fibra, se acople al campo evanescente. Por consiguiente, la potencia óptica que interactúa con el medio que rodea al sensor, tiene una mayor magnitud y es capaz de detectar menores variaciones en el índice de refracción efectivo de este medio

Si una película de un material sensible a la humedad es depositada en el interior de los agujeros de SSC, dicha película podrá interactuar con el campo evanescente del haz de luz guiado por la fibra. Por lo tanto, la sensibilidad del sensor mejorará, siendo posible detectar cambios más pequeños de humedad.

La técnica de interrogación utilizada, la FFT, ha demostrado ser una buena elección en este tipo de sensores, cuya respuesta óptica en el espectro es una onda sinusoidal. Se ha comprobado que este método no depende de la amplitud de la señal reflejada y que elimina la necesidad de monitorizar una longitud de onda concreta, lo cual puede ser problemático si la señal contiene una alta componente de ruido. Además, gracias al módulo de la FFT obtenido, se puede considerar multiplexar, en futuros trabajos, varios sensores.

Capítulo 5

Desarrollo de sensores basados en fibras SSC para la detección de gases y VOCs

En el presente capítulo se describen sensores para detectar gases y VOCs basados en fibras SSC. El objetivo marcado fue encontrar las dimensiones de un núcleo que optimizase la sensibilidad del sensor. Por esta razón, varias fibras con núcleos distintos fueron analizadas y estudiadas. Para reforzar las hipótesis que se podían derivar de los resultados, el comportamiento de la luz a través de las diferentes estructuras fue analizado teóricamente con el software COMSOL©.

5.1. Introducción

Partiendo de los resultados obtenidos en el capítulo anterior cuando el sensor fue expuesto a diferentes valores de humedad relativa, se consideró poder utilizar la misma configuración para desarrollar sensores que fueran sensibles a otras magnitudes (usar fibra SSC en reflexión para generar interferómetros FP).

Los óxidos metálicos, como ya se ha demostrado anteriormente, son sensibles a los cambios en el índice de refracción del medio que les rodea. Por esta razón, son unos buenos candidatos para detectar cualquier magnitud que altere de alguna manera determinada dicho índice. Esta condición la pueden cumplir determinados gases, que son capaces de variar el índice de refracción del medio que les rodea con su mera presencia. No hay que olvidar tampoco que, gracias a la estructura de la fibra SSC, la interacción entre una película de material sensible depositada y las moléculas del gas a detectar puede producirse de una manera más sencilla y efectiva, mejorando de esta manera la sensibilidad del sensor.

Otra de las principales causas por las que se propuso desarrollar un sensor capaz de detectar gases fue el desarrollo de la sociedad y la industria en la actualidad. Numerosas actividades realizadas por el ser humano como la combustión de combustibles fósiles (petróleo, carbón…) o la utilización de pesticidas e insecticidas producen la emisión de un gran número de gases a la atmósfera. Algunos de estos gases pueden ser perjudiciales para la salud humana o el medio ambiente debido a su toxicidad y por eso, su pronta detección es un factor importante. El amoniaco puede considerarse uno de esos gases (NH_3).

Por lo tanto, y a modo de resumen, teniendo en cuenta las características de las SSC y de los óxidos metálicos explicadas con anterioridad, se propuso la combinación de ambos elementos para desarrollar un sensor de amoniaco. Además, se consideró interesante realizar una comparativa entre SnO_2 (previamente utilizado) e ITO, con el fin de estudiar sus sensibilidades. El ITO fue elegido por las buenas sensibilidades obtenidas en trabajos científicos previos cuando se utilizó para la detección de gases con sensores electrónicos.

5.2. Influencia del espesor en la sensibilidad del sensor: análisis teórico

En todos los sensores desarrollados en esta tesis, se ha comprobado de una forma clara, que la influencia del espesor de la película depositada bien sea de polímeros o de óxidos metálicos, juega un papel fundamental en la sensibilidad final del sensor. Anteriormente, el estudio de optimización del grosor se basaba en depositar varios espesores y exponerlos a los mismos cambios de humedad y determinar cuál de ellos obtenía la mejor sensibilidad. A partir de ahí, se exponían una serie de hipótesis para intentar explicar por qué depositando un determinado espesor se obtenía la mejor sensibilidad. Por eso, llegados a este punto, se pensó en reforzar las teorías que se podían derivar realizando un estudio teórico de la influencia de los diferentes espesores de las películas de los óxidos metálicos depositados. Los parámetros a estudiar serían la potencia óptica acoplada a la película sensible depositada, la interacción entre el campo evanescente de la luz guiada y dicha película, la sensibilidad final obtenida y los tiempos de respuesta del sensor.

Un estudio teórico y numérico fue desarrollado para entender mejor la interacción del campo evanescente de la luz guiada por la fibra con la película depositada y el efecto de incrementar su espesor, utilizando un software COMSOL©. El estudio se desarrolló en un rango de espesores entre 0.1 to 11 μm, ya que se tomó como referencia el espesor de la película con la que se obtuvo la mejor sensibilidad en el capítulo anterior.

Los resultados de este estudio aportan una conclusión muy interesante. Conforme el espesor de la película del óxido metálico depositado aumenta, la potencia óptica deja de estar guiada por la fibra óptica para acoplarse y ser guiada por la película depositada, hasta un determinado espesor. Por lo tanto, cuando esta nueva guía onda está formada por espesores más gruesos, es posible guiar más potencia óptica, y como consecuencia, generar un campo evanescente más potente. Si ningún otro parámetro influyera en la sensibilidad del sensor, estos espesores deberían ser los óptimos (en el caso estudiado en esta tesis, aproximadamente 10 μm). Pero hay otro parámetro que debe ser considerado y es la variación del índice de refracción debido a la penetración de las moléculas de gas en la película sensora por su la difusión. Para optimizar el sensor, es

necesario llegar a un compromiso entre estos dos parámetros. Todas estas hipótesis, explicaciones y resultados fueron publicados y argumentados de una forma más extensa en la siguiente contribución científica: "*Sensitivity Optimization of a Microstructured Optical Fibre Ammonia Gas Sensor by means of Tuning the Thickness of a Metal Oxide nano-Coating"* la cual fue publicada en la revista "*Sensors*".

D. López-Torres *et al*., "Sensitivity Optimization of a Microstructured Optical Fiber Ammonia Gas Sensor by Means of Tuning the Thickness of a Metal Oxide Nano-Coating," in *IEEE Sensors Journal*, vol. 19, no. 13, pp. 4982-4991, 1 July1, 2019. DOI: 10.1109/JSEN.2019.2901361

5.3. Respuesta del sensor a diferentes gases

Debido al buen comportamiento del sensor frente al amoniaco y teniendo en cuenta que el mínimo de detección obtenido no se debía a las limitaciones del sensor si no a las del sistema, se planteó la idea de detectar otros gases peligrosos para el ser humano y el medio ambiente. Este hecho puede ser posible debido a la baja selectividad que ofrecen los óxidos metálicos. Pero como se expone en varias de las contribuciones de esta tesis, esta característica no tiene por qué ser tomada como una desventaja ya que existen técnicas de post procesado que son capaces de identificar mezclas complejas de gases. También existe la posibilidad de funcionalizar la película sensora depositada en el sensor, haciéndola de esta manera solamente sensible a un determinado gas [111], [112].

El primer gas al que se expuso el sensor fue el CO_2 (dióxido de carbono). Como bien es sabido, el dióxido de carbono es el principal causante del efecto invernadero y como consecuencia, del calentamiento global del planeta. Así pues, son importantísimos todos los esfuerzos que se hacen para reducir su emisión y llegar así al equilibrio entre "producción y eliminación" de este gas. El sensor fue expuesto a diferentes ciclos, disminuyendo la concentración de dicho gas hasta llegar al 8%. En comparación con la respuesta del sensor frente al amoniaco, en esta ocasión, las variaciones obtenidas no son tan elevada y su comportamiento conforme la concentración de CO_2 disminuye no es tan lineal. Este hecho se ve más claramente reflejado en la concentración mínima (8%) (ver Figura 5.1).

El siguiente gas que se intentó detectar fue CO (monóxido de carbono). Se eligió este gas porque su inhalación puede producir al ser humano dolores de cabeza, mareos, náuseas o pérdida de conocimiento. Además, una exposición prolongada a este gas puede ser particularmente peligrosa ya que los seres humanos pueden sufrir daño cerebral irreversible o, incluso, la muerte. Por eso, su rápida detección es de vital importancia. En este caso, como prueba de concepto, el sensor fue expuesto durante dos ciclos seguidos a 10 ppm, que es el valor mínimo que puede ofrecer el sistema con el que se realizaron los experimentos (ver Figura 5.2). El sensor mostró unos tiempos de respuesta en torno a 70 segundos, mientras que los tiempos de recuperación fueron de escasos segundos. En ambos casos, la línea base se alcanzó sin dificultad y de formo estable.

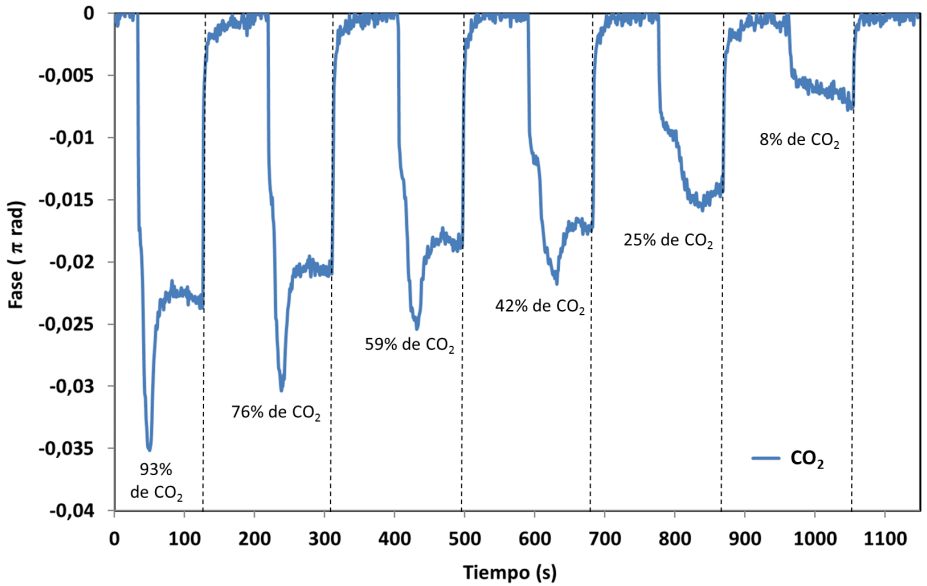

Figura 5. 1 *Respuesta del sensor cuando fue expuesto a diferentes concentraciones de CO2. Como se puede apreciar, en cada uno de los casos el sensor alcanza la línea base.*

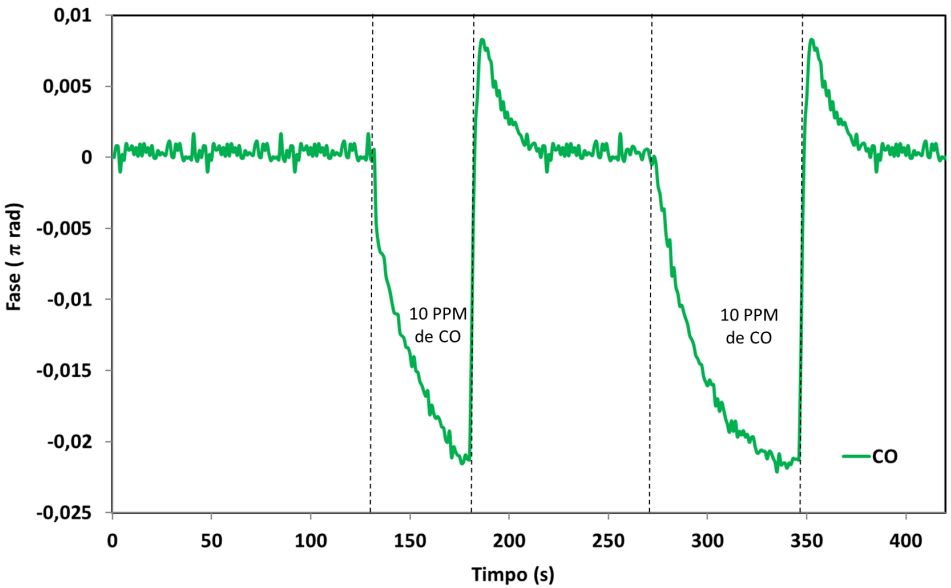

Figura 5. 2 *Respuesta del sensor cuando fue expuesto a dos ciclos de 10 ppm de CO. Como se puede apreciar, en cada uno de los casos el sensor alcanza la línea base.*

Por último, el sensor fue expuesto a diferentes concentraciones de O_2 (oxígeno). La detección de oxígeno es la línea principal de trabajo de muchos grupos de investigación debido a las numerosas aplicaciones que la requieren. Algunas de las más relevantes son las asociadas al campo de la biomedicina, a la industria alimentaria, a la calidad del aire o a la seguridad en el trabajo. El sensor se comportó de una forma similar a cuando fue expuesto a CO_2. Si bien es cierto que a concentraciones altas de O_2 se cumple la premisa de que el desplazamiento de la fase es mayor que a bajas concentraciones, su comportamiento no es lineal. Es más, entre el desplazamiento de fase obtenido para el 85% y el 69% no se observa demasiada diferencia en la variación de la fase (ver Figura 5.3). Esto pudo ser debido a que no se dejó suficiente tiempo de recuperación al sensor. Como consecuencia pudiera ser que aún existieran moléculas de O_2 en la película sensible. Lo que sí es destacable es que el sensor alcanzó la línea base en cada uno de los ciclos a los que se expuso. Además, el desplazamiento de fase alcanzado para la concentración menor (7% de O_2) anima a pensar que ese no es el límite mínimo de detección del sensor y, por lo tanto, una concentración más baja podría ser detectada.

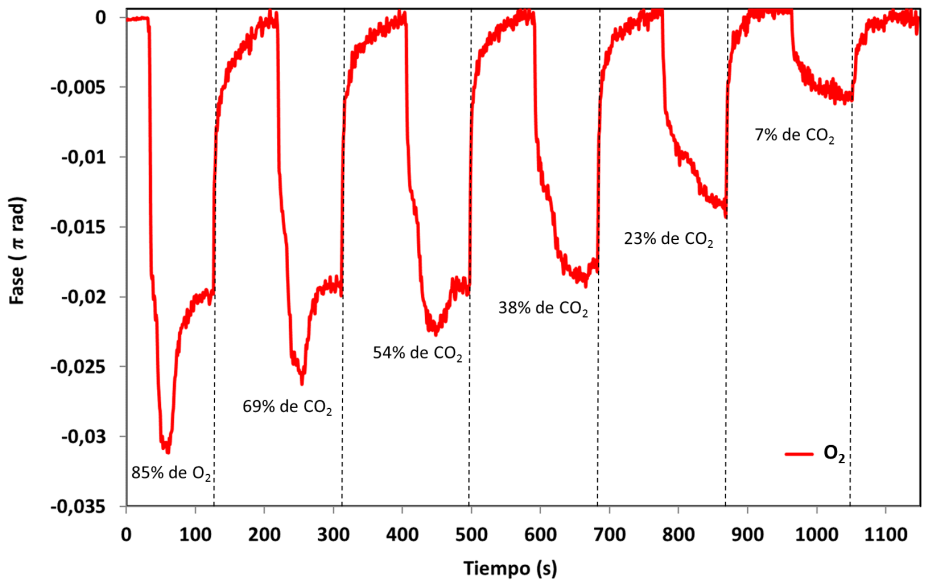

Figura 5. 3 *Respuesta del sensor cuando fue expuesto a diferentes concentraciones de O2. Como se puede apreciar, en cada uno de los casos el sensor alcanza la línea base.*

Para concluir, y antes de empezar un nuevo apartado, es necesario comentar que estas medidas no han sido incluidas en ninguna contribución científica. Deben ser aun optimizadas, sobre todo en lo relacionado con la respuesta dinámica del sensor (tiempos de respuesta y recuperación), pero se ha considerado que los resultados obtenidos, como prueba de concepto inicial para futuros trabajos, son interesantes y animan a seguir trabajando con ellos. El punto a mejorar del sistema sería detectar por qué el sensor tiene esas derivas que presenta cuando se expone a las diferentes concentraciones de los gases para intentar desarrollar una respuesta dinámica más estable y lineal.

5.4. Optimización de la sensibilidad de sensores basados en SSC e interferómetros FP mediante su estructura

El software de trabajo COMSOL©, como se ha visto en el apartado anterior, es una herramienta muy potente de trabajo debido a la información que se puede extraer de los análisis y estudios teóricos de las estructuras que se pueden realizar. Dada la gran relevancia que se descubrió que tiene el depositar una película de material sensible sobre la fibra SSC, se propuso realizar simulaciones teóricas de este tipo de MOF variando las dimensiones de sus núcleos y agujeros. De esta manera, se podría analizar de una forma más rigurosa el efecto de estas variaciones en términos de potencia óptica acoplada, campo evanescente y sensibilidad. Por lo tanto, y debido a que la principal idea era estudiar exclusivamente este efecto, se decidió depositar la misma película de material sensible en todos los sensores estudiados, para reducir al máximo el efecto de esta. Se depositó una película de ITO de aproximadamente 500 nm que fue el espesor óptimo obtenido en la contribución anterior para este óxido metálico.

5.4.1. Análisis teórico de las diferentes SSC utilizadas

Para realizar el análisis teórico se decidió elegir 3 fibras SSC cuyas dimensiones fueron las siguientes: la primera fibra SSC estaba formada por un núcleo sólido rectangular con unas dimensiones de 2.62x1.02 μm mientras que la segunda tenía un núcleo de 3.1x4.4 μm; por último, la tercera fibra elegida mostraba un núcleo rectangular de 2.73x4.2 μm, pero incluía un defecto en su núcleo: un agujero de diámetro 761 nm. En la contribución científica asociada a este trabajo, los sensores fabricados a partir de cada una de estas fibras se nombraron de la siguiente manera: MOF-1, MOF-2 y MOF-3, respectivamente.

Se realizaron dos tandas de simulaciones: una antes de depositar la película de material sensible y otra después de depositarla, para así determinar de forma más exacta el efecto que tenía. De los resultados obtenidos antes de depositar la película se deriva que debido a las dimensiones (más pequeñas) del núcleo de la fibra MOF-1, la potencia guiada por ella es muy baja en comparación con la fibra MOF-2 (7 veces menor). Sin embargo, esta potencia viaja menos confinada, lo que genera que una mayor parte de esta potencia pase a formar parte del campo evanescente. Con respecto a la fibra MOF-3, el efecto del agujero provocó una

reducción de la potencia óptica acoplada, pero a la vez también produjo que esta potencia viajara menos confinada, produciendo un incremento de los valores del campo evanescente. Estos dos resultados obtenidos hacían prever que esta fibra en particular tuviera interesantes características para el desarrollo de sensores.

Los resultados obtenidos una vez depositada la película de ITO son análogos a los explicados en la contribución anterior: la película depositada pasa a ser la nueva guía onda donde se acopla la luz. En este caso, debido al efecto que produce el agujero en el núcleo de la fibra MOF-3, los valores de potencia óptica y campo evanescente alcanzados para esta fibra fueron máximos. Por esta razón, esta fibra era la candidata óptima para obtener la mejor sensibilidad final, confirmando la hipótesis lanzada tras el primer análisis teórico.

5.4.2. Detección de etanol mediante sensores basados en SSC

Como prueba de concepto para confirmar que las dimensiones y la estructura de la fibra MOF-3 eran las óptimas para desarrollar un sensor de fibra óptica, se pensó en probar a detectar Compuestos Orgánicos Volátiles (VOCs, siglas en inglés). En este caso, las tres SSC estudiadas fueron expuestas a atmósferas saturadas de etanol y la mejor respuesta se obtuvo, como se esperaba, con la fibra MOF-3. Como dato a añadir, decir que la sensibilidad de la MOF-3 mejoraba en un factor 5 la sensibilidad de la MOF-2, que fue el sensor con la segunda mejor sensibilidad. Todas estas simulaciones teóricas, resultados y conclusiones fueron presentados en la contribución científica que se presenta a continuación: *"Comparison between Different Structures of Suspended-Core Microstructured Optical Fibres for Volatiles Sensing"* publicada en la revista *"Sensors"*.

sensors

MDPI

Article

Comparison between Different Structures of Suspended-Core Microstructured Optical Fibers for Volatiles Sensing

Diego Lopez-Torres [1,*], Aitor Lopez-Aldaba [1,2], Cesar Elosua [1,2], Jean L. Auguste [3], Rapahel Jamier [3], Philippe Roy [3], Manuel Lopez-Amo [1,2] and Francisco J. Arregui [1,2]

1 Electric and Electronic Engineering Department, Universidad Publica de Navarra, Edif. Los Tejos, Campus Arrosadía, 31006 Pamplona, Spain; aitor.lopez@unavarra.es (A.L.-A.); cesar.elosua@unavarra.es (C.E.); mla@unavarra.es (M.L.-A.); parregui@unavarra.es (F.J.A.)
2 Institute of Smart Cities (ISC), Universidad Publica de Navarra. Campus Arrosadia, 31006 Pamplona, Spain
3 XLIM Photonics Department, UMR 7252, University of Limoges, CNRS, F-87000 Limoges, France; jean-louis.auguste@xlim.fr (J.L.A.) raphael.jamier@xlim.fr (R.J.); philippe.roy@xlim.fr (P.R.)
* Correspondence: diego.lopez@unavarra.es; Tel.: +34-948-169-841

Received: 6 June 2018; Accepted: 31 July 2018; Published: 2 August 2018

Abstract: In this paper, different core structures of microstructured optical fibers (MOFs) for low-finesse Fabry–Pérot (FP) sensors are experimentally compared to get the highest sensitivity. These devices are designed for volatile organic compounds (VOCs) measurements. Indium tin oxide (ITO) thin films were deposited by sputtering on the MOFs and different optical fast Fourier transform (FFT) phase responses from the FP were measured for saturated atmospheres of ethanol. It has been demonstrated that the sensitivities of the developed sensors depend strongly on the geometry and the dimensions of the MOF-cores. The sensors show recovery times shorter than 100 s and the baselines are fully recovered after every exposure to ethanol vapors.

Keywords: microstructured optical fiber (MOF); low-finesse Fabry–Pérot (FP); volatile organic compounds (VOCs); indium tin oxide (ITO); evanescent field

1. Introduction

Nowadays, the development of sensors based on fiber optics is experiencing considerable growth due to the relevance of the different applications where they are involved [1–3]. Another important factor in this growth is the advantages that optical fiber sensors offer over other kinds of sensors (for example, electronic sensors): small size, light weight, low cost, multiplexing or distributed measurements, remote monitoring, immunity to electromagnetic field interference, or no electrical biasing are some of them [4,5].

One specific type of fiber optic sensors is sensors based on microstructured optical fibers (MOFs) [6]. The geometry of MOFs is characterized by a periodic arrangement of air holes running along the entire length of the fiber, centered on a solid or hollow core [7]. The biggest attraction in these fibers is that by varying the size and location of the cladding holes or the core, the fiber transmission spectrum, mode shape, nonlinearity, dispersion, air filling fraction, and birefringence, among others, can be tuned to reach values that are not achievable with conventional optical fibers. Moreover, the existence of air holes gives the possibility of light propagation in air, or alternatively provides the ability to insert liquids or gases into the air holes. For these reasons, MOFs exhibit improved characteristics over conventional optical fibers and great potential for sensing applications [8].

As it has been mentioned in the previous paragraph, due to the geometry of MOFs, they can be divided into two different types: single material solid-core MOFs and hollow-core MOFs. More concretely, solid-core MOFs include one specific group of fiber named suspended-core MOFs. These fibers present relatively large air holes surrounding a small core (typically a few μms in diameter) which seem to be suspended along the fiber length but are maintained by small silica bridges. Due to the innate features of suspended-core MOFs, they have awakened the interest of many scientific groups and several papers have been published using them as curvature/bend sensors [9,10], displacement/strain sensors [11,12], pressure sensors [13,14], or temperature sensors [15,16], just to mention some. But in other cases, a sensing material is required to make the optical structure sensitive or aims to improve its MOF sensitivity [17]; this is the case of volatile organic compounds (VOCs) [18]. Suspended-core MOFs are a good option to detect VOCs because their specific geometry facilitates the absorption and desorption of VOC molecules and increases the evanescent field of the guided light: both effects enhance the total interaction of the optical signal with the analyte, improving the final sensitivity.

Regarding sensing materials, metallic oxides, such as indium tin oxide (ITO), have been used in previous works to develop optical fiber optic sensors because they are able to detect organic vapors [19,20]. Metallic oxides and more concretely ITO, show reversible changes in their optical properties (refractive index, optical absorption) in the presence of VOCs [21,22]. In most cases, the operating mechanism of the sensors is based on intensity changes or wavelength shifts [23]. In this paper, the authors propose a reflection system for VOC measurements based on an ITO thin film deposited onto a microstructured optical fiber (MOF) low-finesse Fabry–Pérot (FP) using the fast Fourier transform (FFT) as the method of characterization of the sensor response [24,25]. FFT has been used in other works as an alternative method for the calibration and analysis of the sensor response: compared with spectral shifts of amplitude measurements, this one is more robust against artifacts and the resulting calibration is more linear [26].

Another important factor to be considered is that most of devices based on metallic oxides need to work at temperatures higher than 150 °C to obtain a proper sensitivity [27,28], but this paper proposes to perform the study at room temperature (25 °C). At this temperature, the interaction between ITO thin film and VOCs is due to the oxidation and reduction (chemisorption) reactions because of the presence of external agents (oxygen) that produce conductivity changes, as explained in References [29,30]. Both phenomena are transduced to a phase shift between the modes traveling through the core and the ones that are coupled to the evanescent field: in this manner spectral shifts in the interferometric pattern can be used to characterize the sensor response.

In brief, the synergy resulting from the combination of suspended-core MOF used to implement FP cavities together with metallic oxides is clear. One of the most important factors on the sensor sensitivity is the geometry of the MOF section as it determines the coupling to the evanescent field, and therefore, the interaction with the sensing material [31]. Considering this context, the authors propose (for the first time to our knowledge) to give an explanation, based on a new theoretical analysis and an experimental study, of why and how it is possible to improve the sensitivity and kinetics of previously published sensors by studying the effect of the different suspended-core MOFs geometries (MOFs with different cores and hole dimensions, and even introducing a hole in the center of the MOF core) on the final sensor sensitivity. As proof of concept and in order to verify this assumption, the different MOF structures were exposed to saturated atmospheres of a concrete VOC, ethanol.

2. Materials and Methods

2.1. Suspended-Core MOF Sensor Fabrication

Three different sensors were fabricated by splicing a single mode optical fiber (Corning SMF-28) to a segment, from 0.3 mm to 1 mm, of three new rectangular-shaped suspended-core MOFs to prepare low-finesse Fabry–Pérot interferometers: each one showing distinct geometries in terms of silica bridges and core. The suspended-core MOFs were fabricated using the stack and draw process [32].

Three different MOFs were employed: they are all formed by four large air holes divided by four bridges from the cladding to a rectangular core, but there are differences between them: MOF-1 showed a solid rectangle core of 2.62 μm by 1.02 μm (Figure 1A) whereas MOF-2 has a 3.1 μm by 4.4 μm core (Figure 1B); finally, MOF-3 also showed a rectangle core (2.73 μm by 4.2 μm) and a hole (with a diameter of 761.1 nm, Figure 1C) in its center. From now on, the fiber optic sensors will be named in the same way as the MOFs with which they have been made of, in order to identify them easily.

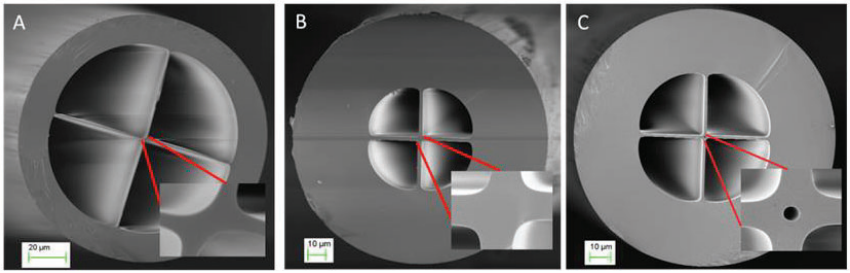

Figure 1. MOF-1 (**A**), MOF-2 (**B**), and MOF-3 (**C**) cross section. In every figure, the detail of the core geometry can be appreciated and especially in (C), the hole located in the center of the optical fiber. MOF = microstructured optical fibers.

The low-finesse Fabry–Pérot cavities were made by splicing a single mode fiber to the MOF fibers. The MOFs were cleaved at the other end, creating the cavity with a length of ~500 μm. The splices were made using a commercial arc-electric fusion splicer machine, in manual mode. Since these MOF have a high air filling fraction, the typical arc power and duration used for single mode fibers fusion induces the MOF to collapse. Thus, a study was made on the arc power and duration settings in order to develop a new adapted program. This program allowed splicing the SMF and MOF without collapsing the MOF. To ensure that the SMF and MOF cores were aligned before splicing, the manual approximation of both fibers were made while illuminating the SMF and retrieving the signal at the MOF's opposite end. Through the output at the MOF, it was possible to observe the amount of light transmitted from one core to the other.

A low-finesse Fabry–Pérot interferometer consists of two mirrors separated by a cavity with a length d. This cavity can be made by a MOF since its core refractive index is different from the SMF's core refractive index. When splicing a piece of MOF to a SMF, two mirrors are formed at both ends of the MOF: (1) in the interface SMF–MOF due to the discontinuity in refractive index between both fibers and (2) at the interface MOF–air, since this high discontinuity provides Fresnel reflection (3.3%). The low-finesse Fabry–Pérot interferometer is created when a light beam enters the cavity (MOF) and is reflected between the interfaces (1) and (2). Each beam has a fixed phase difference with respect to the preceding one, and this phase difference corresponds to the extra path length travelled in the cavity. The interferometric signal of this cavity has a period corresponding to $\Delta\lambda = \lambda 2/(2nd)$, where λ is the wavelength of operation and n is the cavity refractive index.

2.2. Sensing Material

The sensing material selected was ITO. This metal oxide has a low selectivity towards VOCs [33]; this feature can be very useful if the sensor is included in a sensor array because it allows, with the use of post processing techniques such as principal component analysis (PCA) [34], the identification and the detection of VOCs' complex mixtures [35]. Furthermore, due to the high sensitivity of ITO towards VOCs added to the study that this paper proposes, it is possible to detect VOCs in small concentrations that range from ppm down to ppb [36].

2.3. Experimental Set Up

ITO thin film was deposited onto the head and into the walls of the MOF suspended-core sensors using a sputtering machine (Pulsed DC sputtering System, Nadetech Innovations, Pamplona, Spain). The construction parameters were configured as follows: a partial pressure of argon of 5×10^{-2} mb, a current of 160 mA, and a voltage of 190 V for 8 min. The distance between the target of ITO and the head of the sensors was set at 6 cm. The suspended-core MOF sensors were placed into the sputtering machine as perpendicular as possible to the ITO target in order to obtain a homogeneous ITO thin film.

Figure 2 shows the set up used during the construction process. It consists of a commercial optical interrogator for optical fiber sensors (Smartec SM 125, Lugano, Switzerland) and the sputtering machine that was described above. The optical interrogator was used to illuminate the MOF sensors and to record their reflected optical power; at the same time, their signals were processed with a computer using the commercial software Matlab® (Mathworks, MA, USA). Due to this set up, it was possible to verify in real time that the amplitudes of the reflected optical power from the sensors were high enough to characterize the sensor response.

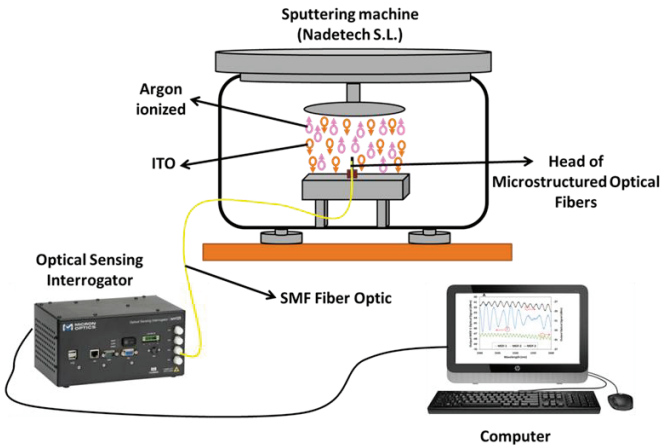

Figure 2. Experimental setup used to control the construction process of the different MOF sensors. ITO = indium tin oxide; SMF = single mode fiber.

The set up proposed to carry out the VOC measurements (see Figure 3) was an in-reflection one using the same commercial optical interrogator (Smartec SM 125). As explained at the beginning of the section, it was used both to illuminate the MOFs as well as to analyze the sensor responses; in this manner, it was possible to simultaneously measure the response of the three different sensors when they were exposed to VOCs with the same temperature and humidity values. These responses were performed placing the sensors in a hermetic metallic cell (avoiding any external contamination as, for example, external gases and ensuring constant humidity and temperature values during the measurement process). At this point, it is important to mention that all sensors used in this paper are sensitive to temperature as all of them were made of a MOF–FP cavity. Because of this reason, if the temperature varies during the exposure of the MOF sensors towards ethanol, it is necessary to use another sensor as a temperature reference in order to avoid the temperature crosstalk and its influence on the final sensor sensitivity, as Reference [37] proposes. Figure 4 shows the temperature characterization curves for the three sensors after the deposition process. Their sensitivities, when they were exposed towards temperature from 25 °C to 65 °C, were: MOF-1: 9.025 pm/°C; MOF-2: 10.1 pm/°C; MOF-3: 12.05 pm/°C.

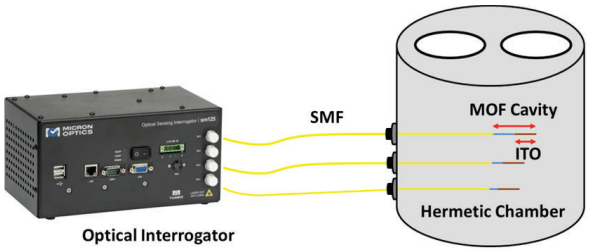

Figure 3. Experimental setup used to simultaneously analyze the response of the sensors towards saturated atmospheres of ethanol.

The volume of the hermetic chamber was calculated in order to inject a controlled volume of ethanol that saturated the atmosphere of the chamber. Ethanol was injected with a pipette through the hermetic chamber holes. After 10 min of exposure, the ethanol injected was evaporated and then, the door of the hermetic chamber was opened for a period of 400 s, with the aim of ensuring that ethanol was removed of the hermetic chamber by applying a nitrogen flow.

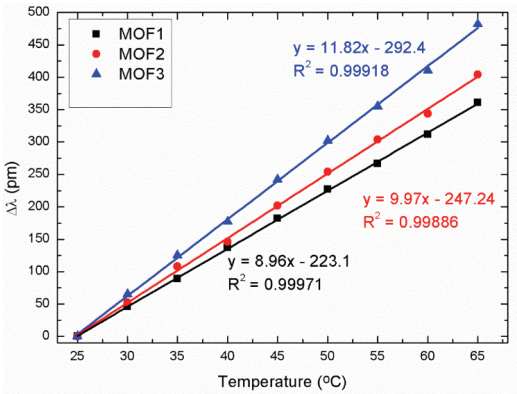

Figure 4. Characterization curves of the three different MOF sensors when they were exposed to temperatures from 25 °C to 65 °C.

2.4. Parameters and Software Used in the Theoretical Simulations

The finite element method (FEM) is the method selected to make the theoretical simulations of the different MOF structures. Each single structure was designed and computed with COMSOL© Multiphysics software and evaluated with COMSOL© Wave Optics Module. For every simulation, silica refractive index was set at 1.444 and air (holes inside the fiber) at 1. In this work, many high order modes have been calculated for all the studied structures, although only the fundamental mode, LP_{01} at 1550 nm is shown for the sake of simplicity of interpretation. This simplification is due to the power difference between the fundamental mode and the high order ones (one order of magnitude) that makes their influence negligible. All fibers are excited by the same Gaussian beam (corresponding to the LP_{01} of a SMF). These simulations were performed in a two-step analysis: firstly, the fundamental mode of the MOF was obtained and used as input in the second step. The second step was a propagation study where the maximum electric field values were obtained in order to compare the performance of the different structures presented. Analogously to an SMF optical fiber, LP_{01} is the lowest order propagated mode with the highest effective refractive index and which presents [38], in a symmetric SMF, a Gaussian optical power profile with a maximum in its center.

To study and verify the fibers' performance as optical waveguides and the effect of the ITO thin film in their behaviors, new field simulations were performed taking this new material into account. The complex refractive index of ITO thin film was measured using an ellipsometer (UVISEL 2, Horiba) and the result was 1.81103 + j0.051964 at 1550 nm (this exact value was used during the ITO simulations).

For these new simulations, symmetric and homogeneous fiber structures (in practice, they show slight variations due to the fabrication process) as well as thin films deposited by means of sputtering technique were implemented in order to achieve symmetric distributions of the LP_{01} fundamental mode.

3. Results and Discussions

3.1. Deposition ITO Procedure

To prepare the different MOF sensors, ITO nanofilms were deposited following the procedure explained in the Section 2.3. At this point, it is very important to remark that the goal of this paper was to improve the sensitivity of the MOF sensors only by means of its structures; the effect of other important factors on the MOF sensor sensitivity, such as the thickness of the nanofilm, will be studied in future papers. For this reason, and in order to obtain the same thickness for every sensor, sputtering technique was selected. This technique allows the final thin film thickness to be controlled with high accuracy and it can be considered a reproducible process [39], but the structure of the MOFs (core and bridges) do not always present the same dimensions (due to the custom fabrication process). The construction parameters were set based on previous studies with the intention of depositing a thickness which provides an optimal sensitivity. These parameters were the same for the three fibers (see Section 2.3), so that for a certain sputtering time, the final thickness was assumed to be similar in the three cases. Following these considerations, the film deposited onto MOF-3 was determined from images captured by a scanning electron microscope as follows: firstly, the width of each of the four bridges of MOF-3 was measured and averaged (1.158 ± 0.009 µm) prior to the coating deposition in order to minimize the possible error in this measurement; secondly, after the sputtering deposition, the average width of the four bridges was measured again (see Figure 5). To determine the real value of the MOF-3 ITO nanofilm thickness, both values were subtracted (average width before and after deposition); the result obtained was 500 ± 17 nm.

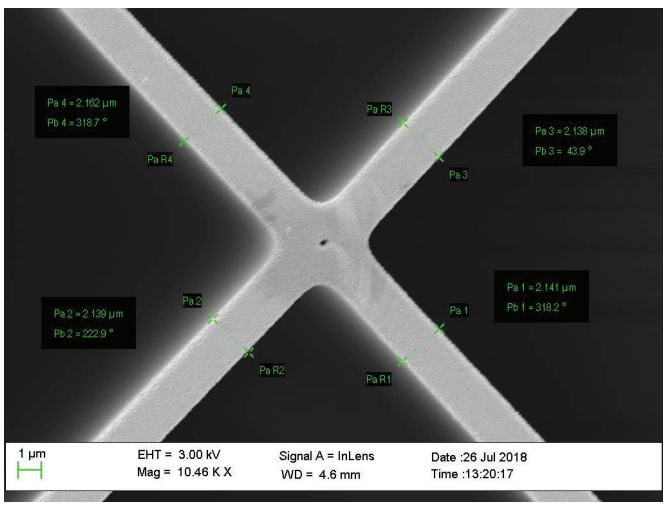

Figure 5. ITO nanofilm thickness measured for the MOF-3 using the SEM after 8 min of sputtering construction process.

3.2. Suspended-Core MOF Field Distribution Simulations

Theoretically, when the core of a suspended-core MOF is smaller, the interaction of the evanescent field with the surrounding external medium is stronger because the modes travel along the fiber less confined; on the other hand, although this structure magnifies this effect, the propagated optical power is lower when the core effective area is reduced. Therefore, there is a tradeoff between evanescent field interaction and coupled optical power.

With the purpose to study the effect of the suspended-core fiber geometry on the coupled optical power and on the evanescent guided field of light, mode field distributions were simulated for the three different types of fiber (without and with ITO nanofilm) as described in Section 2.4.

3.2.1. Theoretical Simulations without ITO Nanofilm Deposited

In this section, the results obtained for simulations without ITO nanofilm deposited are shown according to Section 2.4. Figure 6A shows the LP_{01} mode propagated through fiber MOF-1. Due to the reduced dimensions of MOF-1's core, on the one hand, low optical power is guided in the core showing maximum values of 50 V/m. On the other hand, this optical power has low confinement showing an evanescent field outside the core reaching values of 38 V/m. LP_{01} mode presents an effective refractive index of 1.344. As expected, the effective refractive index of the LP_{01} is affected by the guiding structure, and more precisely by the effective area of the core cross section; if this area is reduced, the value of the effective refractive index is decreased. Likewise, the fundamental mode field distribution was simulated for MOF-2 as Figure 6B illustrates. As it can be noticed, this particular fiber with its rectangular core presents bigger dimensions in comparison with MOF-1 and therefore, the coupled optical power is higher (reaching maximums of 340 V/m) and more confined in the core. Although, theoretically, the evanescent field should be weaker in MOF-2 than in MOF-1, due to this important difference in the guided optical power, a stronger evanescent field (100 V/m) is observed outside the core. The LP_{01} effective refractive index is higher in MOF-2 (1.418) than in MOF-1 due to the increase of the silica-core surface.

Finally, LP_{01} mode field distributions for MOF-3 are displayed in Figure 6C. This fiber presents almost similar dimensions as MOF-2 but it includes a small hole of 761 nm diameter located at the center of the silica core. The effect of this hole is clear: firstly, it produces a reduction of the optical power coupled to the MOF-3 core showing maximum values of 50 V/m (like MOF-1 values but 7 times less than MOF-2); secondly, it also produces an LP_{01} mode that travels along MOF-3 with less confinement producing an increase on its evanescent field values, reaching maximums of 33 V/m in the zone close to the hole. Moreover, an effective index decrease (1.394) can be noticed in relation to MOF-2 and this is due to the air hole inside the core which produces a reduction of the overall effective refractive index.

In brief, based on these simulations, the interaction between the evanescent field of the guided/coupled light along the MOFs and a material deposited into the MOF walls, as well as on the top of it, could be possible if a film in the range of a nanometer [38] is deposited. But this interaction does not occur in the same way for all the studied structures. MOF-2 presents the highest values in terms of coupled optical power and evanescent field but the part of the evanescent field that interacts with the nanofilm is very small and it can be a drawback. MOF-1 shows the lowest values of coupled optic power and evanescent field and for this reason, this structure does not look like the best option to develop the sensor. Finally, MOF-3 core hole produces a different distribution of the guided optical power making its use very interesting for the final purpose of the sensor. It is true that the MOF-3 evanescent field values are lower than MOF-2, but the part of the evanescent field that could interact with the nanofilm is increased due to the effect of the hole; this phenomenon could make the sensitivity of the sensor improve.

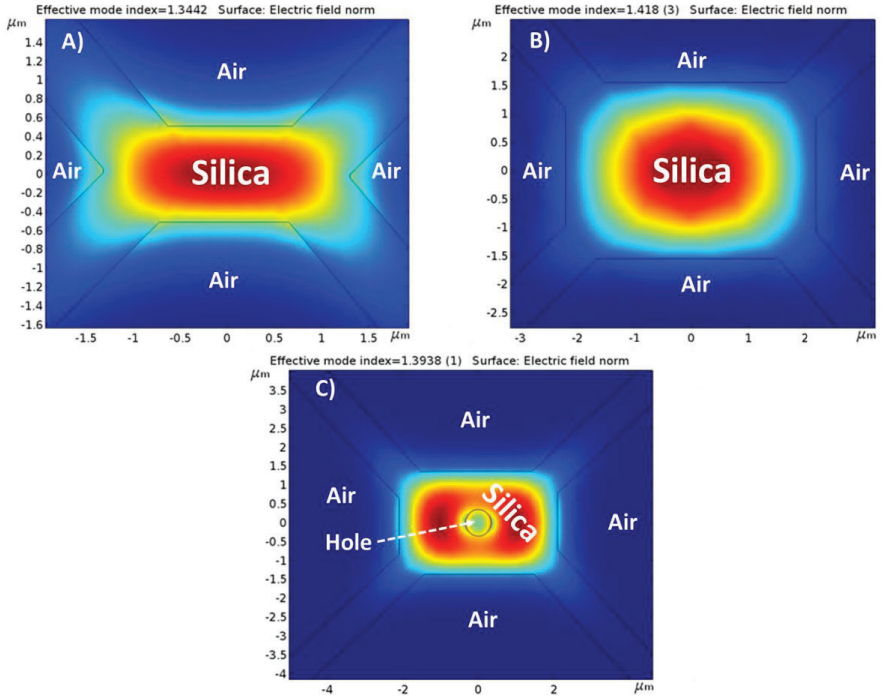

Figure 6. LP_{01} modal field distribution for fiber MOF-1 (**A**), MOF-2 (**B**), and MOF-3 (**C**).

3.2.2. Theoretical Simulations with an ITO Nanofilm

The results of the theoretical simulations when an ideal homogeneous ITO thin film of 500 nm is deposited are presented in this section following the steps explained in Section 2.4.

Figure 7 illustrates the new optical field mode distribution of MOF-1 with ITO nanofilm. As it can be directly inferred from Figure 7, the waveguide properties have been highly modified: the light is no more guided by the silica structure but the ITO thin film, becoming a one layer antirresonant optical waveguide (ARROW) [40]. Since ncore < ncladding (where core is made of silica and cladding of ITO), total internal reflection does not occur at the core–cladding interface, and therefore no guided modes can propagate in the low-index core. However, these structures would support leaky-mode propagation [41]. In addition to this, Figure 7 indicates that not only the fundamental LP_{01} (symmetric) mode is being propagated through the fiber in the shown cases but also the LP_{11} (asymmetric) mode; LP_{11} propagated mode presents an asymmetric distribution with orthogonal phases between maximums in the same location as LP_{01}. Generally, LP_{11} presents lower optical power (one order of magnitude) than LP_{01}, but in this case, due to the dimensions of the new propagating structure, both optical powers are closer to interfering significantly with each other. As expected in ARROW structures, LP_{01} and LP_{11} can present very similar effective refractive indices [42] and appear simultaneously interfering one with the other. This is due to the dimensions of the fiber and the presence of two guiding areas isolated through a non-guiding region (in this case the original silica core). Both regions propagate the LP_{01} and LP_{11} modes within the same effective refractive index and therefore, they appear simultaneously interfering with each other. As it can be noticed, the effective refractive index of the propagated modes has been significantly increased as expected due to the higher refractive index of the ITO waveguide thin film. Moreover, the optical power of the guided modes has also been increased up to values of 147 V/m with evanescent fields of 70 V/m regarding the MOF-1

values obtained without ITO thin film (see Figure 6A). The former evanescent field (MOF-1 without ITO deposition) couples inside the ITO nanofilm and is propagated along the deposition, forming the new ARROW waveguide.

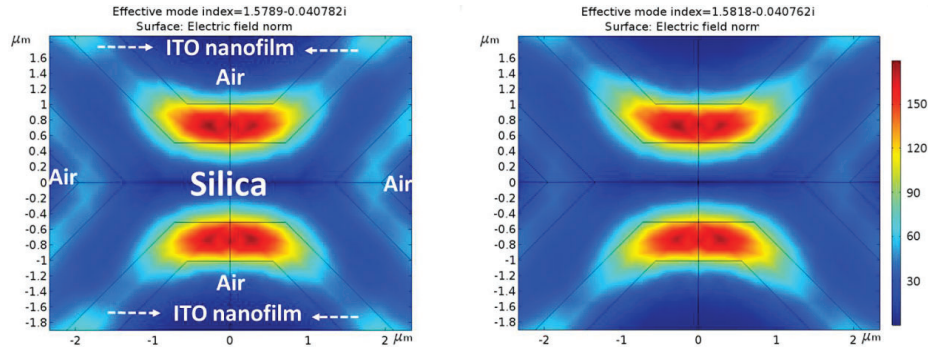

Figure 7. Mode field distribution for MOF-1 with ITO thin film. LP_{01} and LP_{11} are present simultaneously in each polarization.

MOF-2 also presents higher propagated optical power than MOF-1 (maximum of 181 V/m) when ITO thin film is deposited, as shown in Figure 8. This is due to the stronger field of the original MOF-2 structure (without ITO thin film deposited) despite its bigger core dimensions (Figure 6B). MOF-2 presents evanescent fields close to 90 V/m. It must be remarked, that in the particular case of MOF-2, the propagated optical power through the ITO thin film is lower than the original one (without ITO thin film). This is a result of the significant guiding effective area decrease: 3.1 μm by 4.4 μm for MOF-2 without ITO (dimensions of the core) and 0.5 μm (the thickness of the nanofilm) by 3 μm (the length of the bridges) for MOF-2 with ITO as now, the ITO thin film is the waveguide.

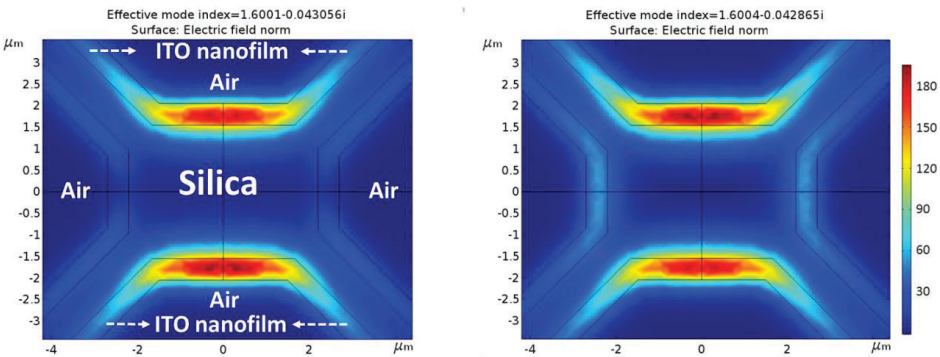

Figure 8. Mode field distribution for MOF-2 with ITO thin film. LP_{01} and LP_{11} are present simultaneously in each polarization.

Finally, when ITO thin film is deposited, MOF-3 presents the highest propagated optical power values (up to 340 V/m) and also the most powerful evanescent field reaching amplitudes of 200 V/m, as Figure 9 illustrates. In this case, the low confinement of the optical power (due to the air hole at the center of the silica core) in the original MOF-3 (without ITO thin film) allows higher optical values to be coupled into the ITO thin film waveguide.

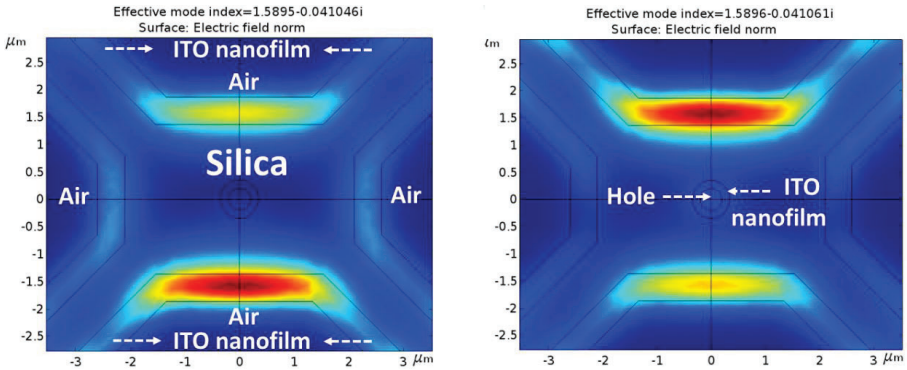

Figure 9. Mode field distribution for MOF-3 with ITO thin film. LP_{01} and LP_{11} are present simultaneously in each polarization.

In order to simplify the data obtained in every simulation, Table 1 shows the maximum values of coupled optical power and evanescent field obtained for the different MOF structures with and without ITO thin film deposited. It is important to clarify that the optical power coupled to the ITO thin films does not only depend on the evanescent field of the MOF structures without ITO, but also on the part of optic power that this structure can be coupled to the ITO thin film which is inversely related to the MOF structure confinement.

Based on this, when ITO thin film is deposited, MOF-3 is the structure with the best conditions to develop the final ethanol sensor due to the hole effects; this hole causes the light to travel in a less confined manner making it possible to couple more optical power into the ITO thin film in comparison with MOF-2 (see the values of MOF-2 and MOF-3, before and after ITO deposition). According with this fact, the value of MOF-3 evanescent field is also increased and in this manner, the sensitivity towards ethanol should also increase.

Table 1. Maximum values of confined optic power and evanescent field obtained for the different microstructured optical fiber (MOF) sensors with and without indium tin oxide (ITO) thin film deposited.

		Maximum Optical Field (V/M)	Maximum Evanescent Field (V/M)
MOF-1	WITHOUT ITO	50	38
	WITH ITO	147	70
MOF-2	WITHOUT ITO	340	100
	WITH ITO	181	90
MOF-3	WITHOUT ITO	63	40
	WITH ITO	340	200

3.3. Ethanol Measurements

The sensors were characterized toward saturated atmosphere of ethanol using the fast Fourier transform (FFT) [39]; it is possible to apply this technique because the output optical signals of the three MOFs obtained after ITO deposition process describe a periodic sinusoidal function (see Figure 10A). The distance between peaks in the interference pattern is very small (a few nanometers) and this fact makes it very difficult to use traditional techniques based on registering the wavelength shift of remarkable points of the interferometric spectral response, such as a transmission valley. As can be observed in Figure 10B, the FFTs of the three MOFs' optical spectrum present a principal component in the transformed domain, which corresponds to the main FP interference frequency.

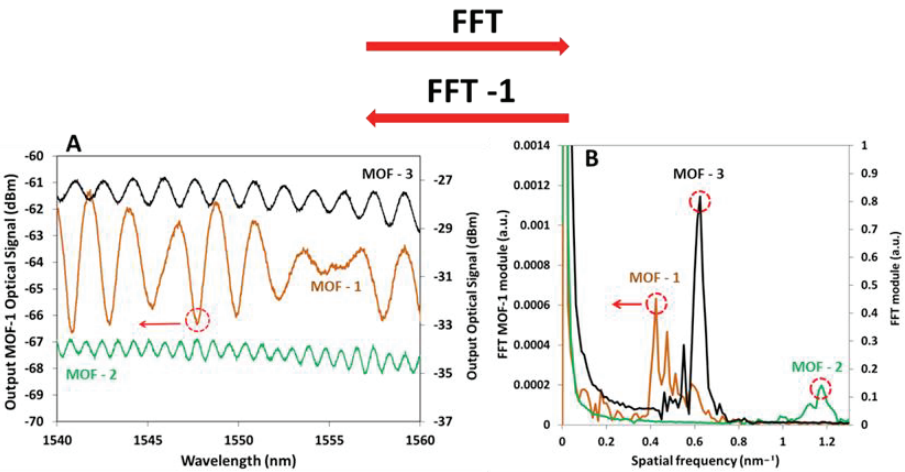

Figure 10. (**A**) Optical spectrum of MOFs and their fast Fourier transform (FFTs) after ITO deposition; (**B**) in both figures, the vertical left axis is applied for MOF-1 and the right axis for MOF-2 and MOF-3.

Saturated atmosphere of ethanol changes the refractive index of the sensing layer (due to the reduction and oxidation (chemisorption) reactions that occur between ITO, oxygen, and ethanol); when it happens, the optical path of the transmitted light changes and consequently, a phase shift occurs. Based on this fact, the sensor responses were analyzed monitoring the phase shifts of these components using the set up explained in Figure 4. In Figure 10B, these components are encircled with a red dotted line. Additional interference frequencies can also be noticed for each MOF, corresponding to interferences involving higher order modes that transport lower optical powers. Also using the FFT, the wavelength shifts in the optical spectrum can be monitored without the effects of the noise influence or signal amplitude variations that other techniques as wavelength shifts have.

Based on Reference [17], where the penetration depth of sputtering deposition (the length of the MOF with ITO) was 228 μm, and due to the smaller dimensions of the MOF holes used in this work, the authors assume that the penetration depth of the sputtering deposition is constant and FP cavities (MOF-1 350 μm, MOF-2 528 μm, and MOF-3 1 mm) are not completely covered in any of the cases by ITO; in this way, the different length of the FP cavities is a parameter which does not influence the sensor's sensitivity towards ethanol.

With the aim of confirming the ideas that are derived from previous theoretical studies, every sensor was exposed to saturated atmospheres of ethanol; the three MOF sensors showed different FFT phase spectral shift responses (see Figure 11). In the first case, MOF-1 showed a maximum variation of 0.685 radians, which implies the lowest sensitivity among the sensors. As previously mentioned, it is a consequence of the dimensions of the core; it has an original low evanescent field power which makes it difficult to couple light into the ITO thin film. Sensors fabricated with MOF-2 and MOF-3, with wider cores, showed higher sensitivities. Although the external dimensions of the cores of these last fibers are similar, the maxima phase shift obtained for MOF-3 (5 radians) is five times greater than the maxima phase shift obtained for MOF-2 (1 radian) and four times greater than previous papers published when MOFs are used to detect VOCs [43]. This result is in accordance with the results of the theoretical study performed in previous sections and reinforces the hypothesis that the increment in the sensor sensitivity is produced by the effect of the MOF-3 core hole. This hole produces a loss of light confinement and an increase in the evanescent field power (in comparison with the case of MOF-2). Due to this fact, when this power (the evanescent field power of MOF-3 without ITO thin film) is coupled to ITO thin film, the penetration depth of this evanescent field is increased and consequently,

its interaction with ethanol occurs in a more optimal way. Furthermore, the sensors' responses were repetitive, and every sensor always reached the baseline in a short period of time (below 100 s) after every exposure to ethanol.

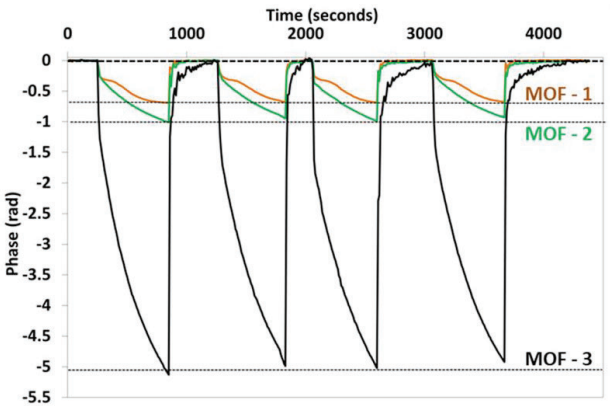

Figure 11. Phase responses of the three sensors for saturated atmospheres of ethanol.

4. Conclusions

In this paper, different optical sensing heads based on microstructured optical fibers (MOFs) have been designed and analyzed both theoretically and experimentally. The sensor heads were developed for VOC detection and tested in ethanol saturated atmospheres. It has been proved that there exists a tradeoff between the optical power guided by the original MOF (without ITO thin film depositions) and the mode distribution confinement. This tradeoff determines the optical power of the propagated modes in the MOF–ITO ARROW structure: geometries with small core dimensions lead to weaker core modes (less coupled optical power) but they show high evanescent field power because the light travels with less confinement; on the other hand, wider core structures lead to more powerful guided modes but having more confined distributions and lower evanescent field power.

It is important to comment that all the results inferred in this paper are not only based on the field amplitude results. These results are a strong support to the authors' proposal: the sensitivity of these kind of sensors can be improved by means of the substrate fiber structure. Additionally, there is another important factor that was not mentioned: the diffusion of the VOCs in the thin film layer. In the case of this paper, as the ITO thickness deposited on every sensor is similar, the influence of this parameter on the sensor sensitivity has not been studied. Still, the authors think that the nanofilm thickness of the sensing layer plays an important role on the sensor sensitivity and for this reason, in future works, the influence of this parameter will be analyzed in order to deposit a suitable thickness, improving in this manner the sensitivity obtained in this paper.

When an ITO thin film is deposited onto the MOFs, the guidance of the light is altered: the signal travels through the thin film deposited instead of the silica core of the fiber. This new optical power and its new evanescent field determine every sensor's sensitivity towards refractive index variations in the surrounding environment. Moreover, it has been demonstrated that the inclusion of a hole at the center of the fiber core (the structure of the MOF-3) makes the light travel in a less confined manner increasing the values of the new ITO-silica waveguide in terms of coupled optical power and evanescent field. Therefore, the sensitivity of this fiber, MOF-3, is also increased and in the case studied in this paper, the achieved sensitivity is enhanced by a factor of 5.

Author Contributions: D.L.-T. performed the experiments, analyzed the results, and wrote the paper; A.L.-A. participated in the experimental work, analyzed the results, and developed the splices between SMF and MOFs; C.E. participated in the experimental work and collaborated in the planning of the experiment; J.L.A., R.J., and P.R. designed and fabricated the different MOFs; M.L.-A. and F.J.A. conceived and designed the experiments and analyzed the results. All authors helped to draft the manuscript.

Funding: This research was funded by the financial support of MINECO (Spain) through TEC2016-79367-C2-2-R and TEC 2016-76021-C2-1-R as well as the FEDER funds and Public University of Navarre program PhD grants.

Conflicts of Interest: The authors declare no conflict of interest.

References

1. Chiuchiolo, A.; Bajas, H.; Bajko, M.; Bottura, L.; Consales, M.; Cusano, A.; Giordano, M.; Perez, J.C. Advances in Fiber Optic Sensors Technology Development for Temperature and Strain Measurements in Superconducting Magnets and Devices. *IEEE Trans. Appl. Superconduct.* **2016**, *26*, 1–5. [CrossRef]
2. Kersey, A.D. A review of recent developments in fiber optic sensor technology. *Opt. Fiber Technol.* **1996**, *2*, 291–317. [CrossRef]
3. Lin, W.; Zhang, C.; Li, L.; Liang, S. Review on Development and Applications of Fiber-Optic Sensors. In Proceedings of the 2012 Symposium on Photonics and Optoelectronics, Shanghai, China, 21–23 May 2012. [CrossRef]
4. Maute, M.; Raible, S.; Prins, F.; Kern, D.; Ulmer, H.; Weimar, U.; Göpel, W. Detection of volatile organic compounds (VOCs) with polymer-coated cantilevers. *Sens. Actuators B Chem.* **1999**, *58*, 505–511. [CrossRef]
5. Elosua, C.; Bariain, C.; Luquin, A.; Laguna, M.; Matias, I.R. Optimization of single mode fibre sensors to detect organic vapours. *Sens. Actuators B Chem.* **2011**, *157*, 388–394. [CrossRef]
6. Homayoonnia, S.; Zeinali, S. Design and fabrication of capacitive nanosensor based on MOF nanoparticles as sensing layer for VOCs detection. *Sens. Actuators B Chem.* **2016**, *237*, 776–786. [CrossRef]
7. Pinto, A.M.R.; Lopez-Amo, M. Photonic Crystal Fibers for Sensing Applications. *J. Sens.* **2012**, *2012*, 1–21. [CrossRef]
8. Liu, Z.; Tam, H.-Y.; Htein, L.; Tse, M.-L.V.; Lu, C. Microstructured Optical Fiber Sensors. *J. Lightwave Technol.* **2017**, *35*, 3425–3439. [CrossRef]
9. Villatoro, J.; Finazzi, V.; Badenes, G.; Pruneri, V. Highly sensitive sensors based on photonic crystal fiber modal interferometers. *J. Sens.* **2009**, *2009*, 747803. [CrossRef]
10. MacPherson, W.N.; Gander, M.J.; McBride, R.; Jones, J.D.C.; Blanchard, P.M.; Burnett, J.G.; Greenaway, A.H.; Mangan, B.; Birks, T.A.; Knight, J.C.; et al. Remotely addressed optical fibre curvature sensor using multicore photonic crystal fibre. *Opt. Commun.* **2001**, *193*, 97–104. [CrossRef]
11. Villatoro, J.; Finazzi, V.; Minkovich, V.P.; Pruneri, V.; Badenes, G. Temperature-insensitive photonic crystal fiber interferometer for absolute strain sensing. *Appl. Phys. Lett.* **2007**, *91*, 89–92. [CrossRef]
12. Shi, Q.; Lv, F.; Wang, Z.; Jin, L.; Hu, J.J.; Liu, Z.; Kai, G.; Dong, X. Environmentally Stable Fabry–Pérot-Type Strain Sensor Based On Hollow-Core Photonic Bandgap Fiber. *IEEE Photonics Technol. Lett.* **2008**, *20*, 2008–2010. [CrossRef]
13. Shinde, Y.S.; Kaur Gahir, H. Dynamic Pressure Sensing Study Using Photonic Crystal Fiber: Application to Tsunami Sensing. *IEEE Photonics Technol. Lett.* **2008**, *20*, 279–281. [CrossRef]
14. Martynkien, T.; Statkiewicz-Barabach, G.; Olszewski, J.; Wojcik, J.; Mergo, P.; Geernaert, T.; Sonnenfeld, C.; Anuszkiewicz, A.; Szczurowski, M.K.; Tarnowski, K.; et al. Highly birefringent microstructured fibers with enhanced sensitivity to hydrostatic pressure. *Opt. Express* **2010**, *18*, 15113–15121. [CrossRef] [PubMed]
15. Pinto, A.M.R.; Lopez-Amo, M.; Kobelke, J.; Schuster, K. Temperature Fiber laser sensor based on a hybrid cavity and a random mirror. *J. Lightwave Technol.* **2012**, *30*, 1168–1172. [CrossRef]
16. Martynkien, T.; Szpulak, M.; Urbanczyk, W. Modeling and measurement of temperature sensitivity in birefringent photonic crystal holey fibers. *Appl. Opt.* **2005**, *44*, 7780–7788. [CrossRef] [PubMed]
17. Lopez Aldaba, A.; Lopez-Torres, D.; Elosua, C.; Auguste, J.-L.; Jamier, R.; Roy, P.; Arregui, F.J.; Lopez-Amo, M. SnO_2-MOF-Fabry-Perot optical sensor for relative humidity measurements. *Sens. Actuators B Chem.* **2018**, *257*, 189–199. [CrossRef]
18. Lopez-torres, D.; Lopez-aldaba, A.; Elosua, C.; Ascorbe, J.; Rota, S.; Auguste, J.L.; Jamier, R.; Roy, P.; Lopez-Amo, M.; Arregui, F.J. Detection of Volatile Compounds with Ito Thin Films Deposited onto Suspended Core Optical Fiber. In Proceedings of the 16th IMCS, Jeju Island, Korea, 10–13 July 2016.

19. Elosua, C.; Arregui, F.J.; Zamarreño, C.R.; Bariain, C.; Luquin, A.; Laguna, M.; Matias, I.R. Volatile organic compounds optical fiber sensor based on lossy mode resonances. *Sens. Actuators B Chem.* **2012**, *173*, 523–529. [CrossRef]
20. Mirzaei, A.; Leonardi, S.G.; Neri, G. Detection of hazardous volatile organic compounds (VOCs) by metal oxide nanostructures-based gas sensors: A review. *Ceram. Int.* **2016**, *42*, 15119–15141. [CrossRef]
21. Elosua, C.; Arregui, F.J.; Del Villar, I.; Ruiz-Zamarreño, C.; Corres, J.M.; Bariain, C.; Goicoechea, J.; Hernaez, M.; Rivero, P.J.; Socorro, A.B.; et al. Micro and nanostructured materials for the development of optical fibre sensors. *Sensors (Switz.)* **2017**, *17*, 2312. [CrossRef] [PubMed]
22. Del Villar, I.; Arregui, F.J.; Corres, J.M.; Bariain, C.; Goicoechea, J.; Zamarreno, C.R.; Elosua, C.; Hernaez, M.; Rivero, P.J.; Socorro, A.B.; et al. Nanocoated optical fibre for lossy mode resonance (LMR) sensors and filters. In Proceedings of the 17th International Conference on Transparent Optical Networks (ICTON), Budapest, Hungary, 5–9 July 2015. [CrossRef]
23. Zubiate, P.; Zamarreño, C.R.; Del Villar, I.; Matias, I.R.; Arregui, F.J. High sensitive refractometers based on lossy mode resonances (LMRs) supported by ITO coated D-shaped optical fibers. *Opt. Express* **2015**, *23*, 8045. [CrossRef] [PubMed]
24. Leandro, D.; Bravo Acha, M.; Ortigosa, A.; Lopez-Amo, M. Real-time FFT analysis for interferometric sensors multiplexing. *J. Lightwave Technol.* **2015**, *33*, 354–360. [CrossRef]
25. Rota-Rodrigo, S.; López-Aldaba, A.; Pérez-Herrera, R.A.; Del Carmen López Bautista, M.; Esteban, O.; López-Amo, M. Simultaneous measurement of humidity and vibration based on a microwire sensor system using fast fourier transform technique. *J. Lightwave Technol.* **2016**, *34*, 4525–4530. [CrossRef]
26. Lopez-torres, D.; Elosua, C.; Villatoro, J.; Zubia, J.; Rothhardt, M.; Schuster, K.; Arregui, F.J. Enhancing sensitivity of photonic crystal fiber interferometric humidity sensor by the thickness of SnO_2 thin films. *Sens. Actuators B Chem.* **2017**, *251*, 1059–1067. [CrossRef]
27. Hodgkinson, J.; Tatam, R.P. Optical gas sensing: A review. *Meas. Sci. Technol.* **2013**, *24*, 012004. [CrossRef]
28. Xu, K.; Fu, C.; Gao, Z.; Wei, F.; Ying, Y.; Xu, C.; Fu, G. Nanomaterial-based gas sensors: A review. *Instrum. Sci. Technol.* **2017**, *9149*, 115–145. [CrossRef]
29. Timmer, B.; Olthuis, W.; Van Den Berg, A. Ammonia sensors and their applications—A review. *Sens. Actuators B Chem.* **2005**, *107*, 666–677. [CrossRef]
30. Cheng, J.P.; Wang, J.; Li, Q.Q.; Liu, H.G.; Li, Y. A review of recent developments in tin dioxide composites for gas sensing application. *J. Ind. Eng. Chem.* **2016**, *44*, 1–22. [CrossRef]
31. Del Villar, I.; Arregui, F.J.; Zamarreno, C.R.; Corres, J.M.; Bariain, C.; Goicoechea, J.; Elosua, C.; Hernaez, M.; Rivero, P.J.; Socorro, A.B.; et al. Optical sensors based on lossy-mode resonances. *Sens. Actuators B Chem.* **2017**, *240*, 174–185. [CrossRef]
32. Lopez-Aldaba, A.; Pinto, A.; Lopez-Amo, M.; Frazão, O.; Santos, J.; Baptista, J.; Baierl, H.; Auguste, J.-L.; Jamier, R.; Roy, P. Experimental and Numerical Characterization of a Hybrid Fabry-Pérot Cavity for Temperature Sensing. *Sensors* **2015**, *15*, 8042–8053. [CrossRef] [PubMed]
33. Vasanthi Pillay, V.; Goyal, S. Influence of Sputtering Power, Annealing on the Structural Properties of ITO Films, for Application in Ethanol Gas Sensor. *Mater. Today Proc.* **2015**, *2*, 4609–4619. [CrossRef]
34. Penza, M.; Cassano, G. Application of principal component analysis and artificial neural networks to recognize the individual VOCs of methanol/2-propanol in a binary mixture by SAW multi-sensor array. *Sens. Actuators B Chem.* **2003**, *89*, 269–284. [CrossRef]
35. Richard, E.; Mead, B.; Zlotnikov, E.; Park, H.; Us, N.J.; Haders, D.; Nj, S. Temperature and Humidity Compensation for Gas Detection Apparatus. U.S. Patent 4730479A, 23 June 1986.
36. Khan, M.R.R.; Kang, B.-H.; Lee, S.-W.; Kim, S.-H.; Yeom, S.-H.; Lee, S.-H.; Kang, S.-W. Fiber-optic multi-sensor array for detection of low concentration volatile organic compounds. *Opt. Express* **2013**, *21*, 20119–20130. [CrossRef] [PubMed]
37. Lopez-Aldaba, A.; Lopez-Torres, D.; Elosua, C.; Arregui, F.J.; Auguste, J.; Jamier, R.; Roy, P.; Lopez-Amo, M. Real time measuring system of multiple chemical parameters using microstructured optical fibers based sensors. *IEEE Sens. J.* **2018**, *18*, 5343–5351. [CrossRef]
38. Snyder, A.W.; Young, W.R. Modes of optical waveguides. *J. Opt. Soc. Am.* **1978**, *68*, 297–309. [CrossRef]
39. Lopez-Torres, D.; Elosua, C.; Villatoro, J.; Zubia, J.; Rothhardt, M.; Schuster, K.; Arregui, F.J. Photonic crystal fiber interferometer coated with a PAH/PAA nanolayer as humidity sensor. *Sens. Actuators B Chem.* **2017**, *242*, 1065–1072. [CrossRef]

40. Yin, D.; Schmidt, H.; Barber, J.; Hawkins, A. Integrated ARROW waveguides with hollow cores. *Opt. Express* **2004**, *12*, 2710–2715. [CrossRef] [PubMed]
41. Bise, R.; Windeler, R. Tunable photonic band gap fiber. In Proceedings of the Optical Fiber Communication Conference and Exhibit, Anaheim, CA, USA, 17–22 March 2002.
42. Lopez-amo, M.; Menendez-valdes, P.; Muriel, M.A. Depressed-Index Waveguides (DIW's) in Integrated Optics. *J. Lightwave Technol.* **1990**, *8*, 1779–1791. [CrossRef]
43. Kim, B.; Ahn, J.; Chung, P.; Chung, Y. Microstructured optical fiber-based micro-cavity sensor for chemical detection. *Proc. SPIE* **2014**, *8938*, 89380L. [CrossRef]

5.5. Conclusiones

Los óxidos metálicos son materiales que pueden ser utilizados para detectar diferentes gases. En este capítulo, se ha demostrado que son capaces de detectar amoniaco, etanol, oxígeno, monóxido de carbono y dióxido de carbono.

El software COMSOL© es una potente herramienta que ayuda a entender, gracias a los estudios teóricos, el comportamiento del campo eléctrico y magnético de la luz guiada a través de las diferentes estructuras de las MOFs. En particular, los estudios realizados con las diferentes fibras SSC concluyeron que en las fibras cuyos núcleos tienen dimensiones más pequeñas, el acople de la luz es inferior. Por tanto, la potencia óptica acoplada también es menor. Sin embargo, el haz de luz viajaba menos confinado, lo que provocaba que el porcentaje de campo evanescente que puede interactuar con la película depositada fuera mayor. En las fibras SSC donde las dimensiones de los núcleos son mayores, el efecto es el contrario. La potencia óptica que puede ser acoplada es mucho mayor y, por lo tanto, la magnitud del campo eléctrico, pero, por el contrario, la luz viajaba por la fibra más confinada y el porcentaje de campo evanescente que puede interactuar o acoplarse a la película depositada es menor. Por todo esto, para obtener una sensibilidad óptima, es necesario llegar a un compromiso entre potencia óptica acoplada a la fibra óptica y el campo evanescente que puede acoplar dicha potencia a una determinada película de material sensible depositada.

Cuando una película es depositada en los agujeros de una fibra SSC, la luz ya no se guía por la fibra óptica de manera convencional. En este caso, la película depositada pasa a ser la nueva guía. La luz se acopla a ella en mayor o menor medida dependiendo de las dimensiones de su núcleo y del espesor de la capa depositada: a mayor espesor, hasta llegar a un límite determinado mayor potencia óptica acoplada (aproximadamente 10 μm). Imperfecciones en los núcleos, como puede ser un agujero en su centro, favorecen este acople y consiguen por lo tanto una mayor potencia óptica guiada por esta nueva guía y, por consiguiente, mayor potencia óptica del campo evanescente.

La penetración de las moléculas del gas medido en la película del material sensible depositado, a través del fenómeno de la difusión, es otro parámetro a tener muy en cuenta a la hora de optimizar la sensibilidad final del sensor. A

mayores espesores depositados, las variaciones en el índice de refracción son menores y, por lo tanto, la sensibilidad es menor. Esto está en contraposición de la conclusión expuesta en el párrafo anterior. Por esta razón, para optimizar un sensor es necesario llegar a un compromiso entre la potencia que se acopla a la película depositada y la penetración de las moléculas del gas medido en dicha película.

Capítulo 6

Aplicaciones finales para los sensores desarrollados

En este capítulo quinto de la tesis, se plantea la implantación de los sensores desarrollados en aplicaciones reales, es decir, entornos donde el sensor tenga que trabajar baja condiciones no controladas. Además, se intenta sacar el máximo partido de las características que ofrecen los sensores. Por esta razón, se plantea la posibilidad de utilizar la multiplexación, ya que es una de las herramientas más potentes que ofrece la utilización de la fibra óptica; de esta forma, el coste total de una futura aplicación sería mucho más competitivo.

6.1. Introducción

Uno de los pasos más importantes, a la vez que complicado, en el campo de la investigación es intentar buscar una aplicación final para el dispositivo desarrollado. Para intentar lograr este objetivo, hay que aprovechar cada una de las ventajas que puedan ofrecer, mejorando de esta manera sistemas que anteriormente habían sido implantados. Este fue el objetivo principal de este capítulo. Una vez demostrado el buen comportamiento de los sensores frente a la humedad, gases y VOCs, el reto fue buscar una aplicación final en la que pudiera explotar todo su potencial o implantarlo en un sistema, el cual se viera mejorado por dicha inclusión.

6.2. Multiplexación

Una de las principales ventajas que ofrece el uso de la fibra óptica con respecto a otro tipo de sensores es la multiplexación. La multiplexación, en términos generales, se puede definir como la transmisión simultánea de varios canales por un camino/medio común. En el caso de la fibra óptica se pude redefinir como una red de sensores donde el número de fuentes de luz, canales o detectores es inferior al número resultante de estos elementos si cada uno de los sensores se implantara de una forma individual.

Uno de los mayores inconvenientes de los sensores de fibra óptica en comparación con otras tecnologías es su mayor coste económico, que, aunque está disminuyendo debido al desarrollo de los equipos ópticos, todavía sigue siendo relativamente alto. Pero si el sistema desarrollado permite la utilización de la multiplexación, el coste final se verá reducido en gran medida dado que los sensores pueden compartir la misma fuente de luz, detectores e incluso canal de transmisión. Este último escenario tiene una gran importancia, económicamente hablando, ya que hace que el sistema sea más competitivo.

Con el objetivo de aprovechar y utilizar las ventajas que ofrece esta técnica, se pensó en cómo se podían multiplexar los diferentes sensores desarrollados en esta tesis. Un tipo de multiplexación que podía encajar debido a las características de los sensores era la que se denomina multiplexación por división de frecuencia espacial, *"spatial frequency division multiplexing"* (SFDM, siglas en

inglés). En esta técnica, cada sensor se identifica por una determinada frecuencia espacial que se obtiene al aplicar la FFT. Como resultado, se pueden identificar en un mismo espectro, diferentes frecuencias espaciales correspondiente a diferentes sensores. Esta técnica es de especial interés para la monitorización de sensores basados en interferómetros, ya que generan un patrón de interferencia, generalmente periódico, en el espectro óptico. Dadas estas condiciones la aplicación de la FFT es inmediata y su identificación en el dominio de la frecuencia muy sencilla.

Una conclusión que se deriva de esta explicación es que, si se varía la frecuencia fundamental de un interferómetro, su patrón interferométrico no será el mismo y, por lo tanto, su frecuencia espacial al aplicar la FFT será distinta. Así que, una forma de multiplexar los sensores que se han desarrollado durante esta tesis es variando lo longitud de la cavidad FP. De esta manera, su patrón interferométrico será diferente y por consiguiente su frecuencia espacial, haciendo posible la monitorización de sus fases de una forma totalmente independiente. En el dominio del tiempo, la señal final será una suma de todos los patrones interferométricos difícilmente entendible, pero en el dominio de la frecuencia, cada uno de ellos quedará identificado debido a su frecuencia fundamental. En este sentido, el uso de la FFT como técnica de interrogación tiene una ventaja importante con respecto a otras: la independencia entre la fase de la FFT y la amplitud de la señal óptica en el dominio temporal. Por lo tanto, la fase se puede monitorizar de manera simple independientemente de la amplitud de la interferencia.

Un punto importante es saber el número de sensores que se pueden multiplexar. A mayor número de ellos, el coste final del sistema será más económico, pero existen limitaciones. Una de ellas es que, debido principalmente a que sólo se trabaja con una fuente óptica y esta tiene una potencia determinada (la cual se divide entre todos los sensores multiplexados), el número de sensores que pueden ser multiplexados depende en gran medida de ello.

Durante la realización de esta nueva contribución científica, 6 sensores fueron desarrollados con diferentes longitudes de su cavidad FP con el fin de satisfacer las condiciones necesarias para poder ser multiplexados en un sistema final. De esta forma, es posible optimizar los recursos del sistema para intentar que sea lo más competitivo posible. Además, se planteó la idea de que el sistema

final de sensores fuera capaz de detectar varios parámetros (temperatura, humedad y VOCs) manteniendo la independencia de cada uno. Todos los pasos que se dieron hasta llegar al sistema final, junto a los resultados expuestos, se detallaron en la siguiente contribución científica: *"Real Time Measuring System of Multiple Chemical Parameters Using Microstructured Optical Fibres Based Sensors"* la cual fue publicada en la revista *"IEEE Sensors"*.

Real Time Measuring System of Multiple Chemical Parameters Using Microstructured Optical Fibers Based Sensors

Aitor Lopez-Aldaba, Diego López-Torres, Cesar Elosúa Aguado, Francisco J. Arregui, *Member, IEEE*, Jean-Louis Auguste, Raphael Jamier, Philippe Roy, and Manuel López-Amo, *Senior Member, IEEE*

***Abstract*— In this paper, a multiplexing system for simultaneous interrogation of optical fiber sensors which measure different parameters is presented and validated. The whole system has been tested with six different sensing heads with different purposes: one temperature sensing head, two relative humidity sensors, and three VOCs leak sensors; all of them based on microstructured optical fibers. The interrogation system uses the fast Fourier transform technique to isolate each sensor's interference, enabling their simultaneous interrogation. The system interrogates all the sensors at frequencies up to 1 KHz, showing a good performance of each measurement without crosstalk between sensors. The developed system is independent of the sensors' purpose or of the multiplexing topology.**

***Index Terms*— Microstructured optical fiber, photonic crystal fiber, multiplexing, gas sensing.**

I. Introduction

MANY types of optical fibers have been used for sensing along the time: standard silica based, plastic, doped, and photonic crystal fibers are some examples. Since the first experiments with microstructured optical fibers (MOFs), they have shown relevant improved characteristics compared to conventional optical fibers as well as a great potential for sensing applications, overcoming some of the standard optical fiber handicaps [1]–[3]. Many geometries have been proposed for this kind of fibers. Among them, suspended-core MOFs present relatively large air holes surrounding a small core (typically a few microns diameter) resembling to be suspended along the fiber length but maintained by thin silica bridges. For instance, different pure silica suspended-core fibers have been used in temperature and curvature sensing [4], gas sensing [5]–[10] micro-displacement measurements [11], refractive index [12], mechanical deformation [13] or biochemical sensing [14]. One of the most important type of MOF sensors are the ones based on evanescent field. These sensors have been used for different applications: simultaneous measurement of humidity and mechanical vibration [15], detection of biomolecules in aqueous solutions [16] as well as organic pollutants [17]. MOFs based sensors have also been utilized for gas measurements, like hydrogen detection [18], [19], methane [7] or acetylene [20]. However, long pieces of MOFs fibers and a pump to control this interaction are usually used in order to obtain a good interaction between gas and light. This configuration limits the utilization of these sensors in practical applications [21], [22].

Fiber based optical Fabry-Pérot (FP) interferometers are a quite popular sensor configuration due to their compactness, simple configuration, flexibility in tuning sensitivity and dynamic range. FP cavities composed by MOFs are also common structures: a hybrid structure formed by a MOF as the guiding fiber in cascade with a hollow-core fiber and a single mode fiber (SMF), was demonstrated for high-temperature sensing [23] among others [24]. Nitrogen sensors [25], chitosan based ones for relative humidity (RH) [26], [26], magnetic field [27], refractive index [28] as well as strain, temperature and pressure FP devices [29], [30] have been reported. Other fiber based sensors were implemented by fusing a small length of PCF to the end of a cleaved SMF for relative humidity ranged 40%-95% RH [31] or by chemical deposition of polymers [32].

In order to develop short, fast, sensitive and versatile FP-MOF sensors we have deposited thin films of different materials inside the MOFS. Nanocoated based sensors have recently experienced a remarkable development [33]. Furthermore, deposition techniques such as sputtering [34]–[37], enable to control the morphology and thickness of the deposited coatings with high accuracy, and as a consequence, the final properties (sensitivity, kinetics) of the sensor.

Multiplexing interferometric sensors is a major target in the sensing field, allowing to perform multi-point and multi-parameter measurements within the scheme, and, therefore, reducing significantly the economic cost of the system. Multiplexing some Fabry-Pérot interferometric sensors without

Manuscript received March 12, 2018; accepted May 11, 2018. Date of publication May 16, 2018; date of current version June 12, 2018. This work was supported in part by the Spanish Comisión Interministerial de Ciencia y Tecnología within projects under Grant TEC2016-76021-C2-1-R, Grant TEC2016-78047-R, and Grant TEC2016-79367-C2-2-R, in part by the Cost Action MP1401, and in part by the FEDER funds from the European Union. The associate editor coordinating the review of this paper and approving it for publication was Dr. Marco Petrovich. *(Corresponding author: Aitor Lopez-Aldaba.)*

A. Lopez-Aldaba, D. Lopez-Torres, C. Elosúa Aguado, F. J. Arregui, and M. Lopez-Amo are with the Department of Electronic and Electronic Engineering and ISC, Universidad Pública de Navarra, 31006 Pamplona, Spain (e-mail: aitor.lopez@unavarra.es; diego.lopez@unavarra.es; cesar.elosua@unavarra.es; parregui@unavarra.es; mla@unavarra.es).

J.-L. Auguste, R. Jamier, and P. Roy are with the Fiber Photonics Department, UMR CNRS, University of Limoges, 87060 Limoges, France (e-mail: jean-louis.auguste@xlim.fr; raphael.jamier@xlim.fr; philippe.roy@xlim.fr).

Digital Object Identifier 10.1109/JSEN.2018.2837159

reflective layers present several difficulties due to their low reflectivity (4%) and their cavity length limitation (the number of multiplexed sensors depends on the cavity lengths chosen). Several approaches have been demonstrated during the last years: spatial-frequency-division multiplexing (SFDM) and coarse-wavelength-division multiplexing (CWDM) schemes [38], in-line FP cavities based on FBGs reflectometers [39], weak fiber Bragg gratings using frequency shifted interferometry [40], conventional graded-index multimode fibers in mode-multiplexed transmission [41], photonic crystal fibers in Sagnac interferometers [42] or polarization-division multiplexing [43]. These techniques present several handicaps such as complex setups with high economic cost or systems whose complexity increases exponentially with the number of multiplexed sensors.

In this paper, a multiplexing system with 6 FP-interferometric sensing heads for multiparameter monitoring is presented and characterized. In previous works, authors reported up to three sensors in a single optical channel for relative humidity measurements [44]. Using a commercial FBG interrogator with a MATLAB based software, six different RH sensors are simultaneously and independently measured within a single optical interrogator's channel. The scanning frequency of the commercial interrogator (from 1 Hz up to 1 KHz) allows real time measurements, avoiding the utilization of Optical Spectrum Analyzers and post-processing [45]. An experimental study of the sensors response and their crosstalk is presented by monitoring the Fast Fourier Transform (FFT) phase variations of the FP interference frequencies. This measuring method is independent of the signal amplitude and avoids the necessity of tracking the wavelength evolution in the spectrum, which becomes a problem when several interferometric contributions come up. Also, the multiplexing system is independent of the monitoring target of each interferometric sensor. Thus with the FFT method it is possible to multiplex sensors in real time for multiple purposes (even vibrations at frequencies higher than the scanning frequency of the interrogation system [15]) without crosstalk.

The sensors based on MOF-FP cavities had been reported previously by ourselves, but it is the very first time we report in a journal the multiplexing of these MOF-FP cavities for different chemical parameters' detection with different deposited materials with these promising results in terms of sensitivity and fast response time. This proof of concept validates the utilization of these sensors for applications such as electronic noses [46] or Toxic and Hazardous Gas Detection [47], [48].

II. Materials & Methods

In this work, 6 different sensors were fabricated and multiplexed within a single optical interrogator channel as shown in Fig. 1. To multiplex all the sensors, 3 optical couplers were used in cascade in order to achieve the required number of multiplexing channels. In this particular case, in a first stage, a 2 × 4 optical coupler was used to divide the optical interrogator's output in 4 identical optical paths. 2 of this paths were directly used with two sensors and the others were used as inputs in a second multiplexing stage where 2

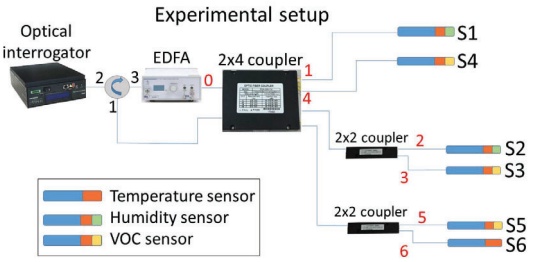

Fig. 1. Multiplexing experimental setup.

TABLE I
Optical Losses Between Optical Ports

Ports	Optical losses (dB)
0 → 1	6.55
0 → 2	10
0 → 3	10.87
0 → 4	7.15
0 → 5	11.15
0 → 6	10.6

2 × 2 optical couplers were installed. All the output channels of the 2 × 2 couplers were directly connected to their corresponding sensing head.

The sensor's distribution was chosen in relation with their optical insertion losses. Sensors S1 and S4 presented higher optical losses and therefore they were directly connected to the 2 × 4 optical interrogator's output. Sensors S2, S3, S5 and S6 were connected to the outputs of the 2 × 2 couplers.

The optical losses of the multiplexing system where measured before installing the sensors and results are shown in Table 1. Optical ports are highlighted in red color in Fig. 1, being port 0 the input port of the multiplexing system and port 1, 2, 3, 4, 5 and 6 the corresponding port of each sensing head.

As it can be remarked from Table 1, ports 1 and 4 were the most suitable ones for the sensing heads with higher optical losses.

Six Fabry-Perot based sensing heads were multiplexed and used as sensors in this work. These cavities were made from a microstructured optical fiber with particular characteristics. The MOF used was fabricated using the stack and draw process. It is formed by four large air holes divided by four bridges, presenting a suspended core of 6.5 μm by 806 nm exhibiting a double Y shape, as it was studied in [49]. The Fabry-Pérot cavities were made by splicing different lengths of MOF fiber to one side of a single mode fiber (Corning SMF-28). The splice was made with a Fitel S175 fusion splicer with a custom developed program for this MOF and manual operation for its alignment. This manual splice leads to different insertion losses in each sensing head that must be taken into account.

By splicing a piece of MOF to a SMF, two low-reflectivity mirrors are formed at both ends of the MOF: the first one in

the interface SMF-MOF due to the discontinuity in refractive index between both fibers; the second one is located at the interface MOF-air because this high discontinuity provides a Fresnel reflection (3.3%). As a result, a low-finesse Fabry-Pérot interferometer is created when a light beam reaches the cavity (MOF) and it is reflected between the two interfaces several times. Each beam has a certain phase difference with respect to the preceding one: this shift corresponds to the extra path length travelled inside the cavity. Due to the high loss of the MOF and the low reflectivity of the air-glass interface, high order reflections inside the cavity are neglected and therefore a low-finesse scenario is assumed, which approximates a two-beam Fabry-Perot [50]. Furthermore, and for the same reasons, high order modes influence is negligible as they propagate, presenting an optical power one order of magnitude lower compared with the fundamental one.

Assuming a two beam Fabry-Perot, the reflected signal obtained should follow equation (1), where $\Delta\lambda$ is the optical spectrum wavelength spacing, λ is the working wavelength, n is the refractive index (neff = 1.37 [49]) and d is the MOF cavity length.

$$\Delta\lambda = \lambda^2/2\text{nd} \tag{1}$$

Two commercial interrogators of optical fiber sensors (Smartec SM125 and Smartec Si155) were used to illuminate the network and also to analyze the spectra signals guided through the MOF sensors. The optical interrogators employed were originally commercialized for FBG sensors' monitoring and allow sensors to be interrogated with a scan frequency of 1 Hz and a 5 pm resolution for the SM125 and 1k Hz and 10pm for the Si155. Si155 optical interrogator allowed the system performance to be verified in high sampling frequency conditions being possible to take measures up to 1k Hz. FFT is computed in MATLAB also every sample, providing real-time information of the sensor system [51].

The FFT technique allows each sensor to be monitored independently avoiding the noise influence (high frequency components in the FFT module) or signal amplitude variations (variations in the power of the FFT module).

We want to remark that this interrogation method can be used in any of the usual topologies of optical fiber sensors multiplexing networks (star, tree, bus, mesh... [52]). These typical multiplexing networks prefer bus topologies in order to save cabling costs. However, these systems require complicated modulation/demodulation techniques and fiber delays to identify each interferometric sensor [53] or FBGs placed by the sensors to identify them [54]. Our interrogation method is also suitable for this kind of topology because the sensors' identification is achieved in the spatial frequency domain and not by their position inside the networks, as happens in time division multiplexing (TDM) modulated systems.

Due to the optical losses of the sensing heads and the multiplexing system, a pre-amplification stage was used. The objective of this amplification stage is to compensate all the induced losses and to allow long distance remote motorization (up to 75km with the sensors comprised in this work). This stage is composed of a 3 port optical circulator and an Erbium doped amplifier (EDFA). The optical circulator is needed in order to use the same optical interrogator's channel to send and collect the light into and from the multiplexing system.

In order to verify the performance of the multiplexing system and the polyvalence of its combination with this type of sensing heads, three kind of sensors were employed: one temperature sensor, two relative humidity sensors and three volatile organic compounds presence sensors.

Relative humidity sensors were developed by creating a thin film of SnO2 inside the holes of the MOF fiber through the sputtering process, as authors previously demonstrated in [55]. VOCs presence sensors were developed with the same technique but changing the sensing material to ITO [56]. Temperature sensor is the FP-MOF cavity without any deposited sensitive layer [49]. These thin film depositions do not vary the interference period of the sensing heads but reduce their amplitude depending on the deposition time.

Deposition time determines the sensor's performance (sensitivity and response time). In this work, the deposition time of each sensor has been selected in order to enable simultaneous measurement in the same atmosphere avoiding crosstalk between sensors. For this reason, their sensitivity is not maximal when compared with the results showed in [46], [55], and [56], as they were optimized.

The interaction between SnO_2/ITO and H_2O/VOCs molecules is due to a phenomena called chemisorption by means of the adsorption/desorption of these molecules [57].

S1 and S2 present a SnO_2 thin film sensitive layer as a result of a 2 minutes sputtering process. S3, S4 and S5 have an ITO thin film sensitive. This metallic oxide changes its refractive index in presence of different VOCs. Thus, an ITO thin film was deposited onto the head and into the walls of the MOF using a sputtering technique. The distance between the target of ITO and the head of the sensor was set at 5 cm. The main transduction mechanism which governs the behavior of this sensor [58] is the interaction between the evanescent field of the guided light along the MOF and the ITO thin film deposited into the walls of the MOF.S6 presents no sputtering deposition in order to keep it insensible to relative humidity nor VOCs variations.

External variations (in the example studied: temperature, relative humidity or VOCs presence for each kind of sensing head) produce a wavelength shift in the optical spectrum domain. In the FFT domain, this shift is translated into a variation of the FFT phase of the corresponding FFT module delta. By monitoring the FFT phase of each sensors' main component, optical wavelength variations can be unambiguously identified.

To perform the temperature and relative humidity measurements, sensors were inserted inside a climatic chamber (Binder KMF 115). VOC presence was tested by introducing the sensors in fully saturated methanol atmospheres.

III. Results and Discussion

A. Multiplexing System

The FFT technique allows to multiplex a number of sensors using the whole spectral range for each of them. Each sensor

TABLE II
CAVITY LENGTHS AND THEIR ASSOCIATED INTERFERENCE PERIODS

Sensor	MOF Cavity Length (mm)	$\Delta\lambda$ (nm)
S1	~1.25	0.7
S2	~0.8	1.1
S3	~0.4	2.2
S4	~1.4	0.63
S5	~0.7	1.28
S6	~0.65	1.35

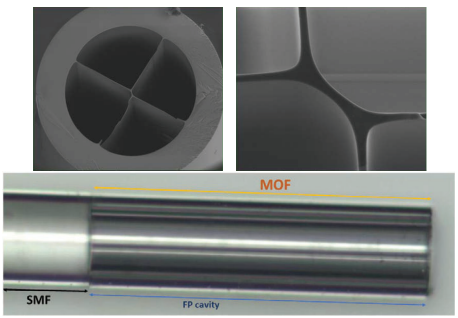

Fig. 2. MOF-4-Bridge cross section (SEM picture) and a resulting FP cavity (microscope picture).

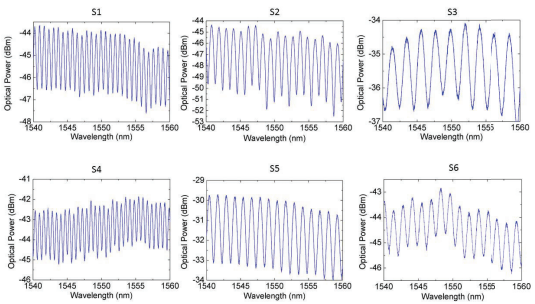

Fig. 3. Sensor's individual optical spectrum.

presents a sinusoidal interference pattern in the optical spectrum domain.

As can be seen in equation (1) the MOF cavity length determines its interference wavelength spacing period ($\Delta\lambda$). Different sensors were obtained varying this interference period, as shown in Table 2.

The individual optical spectra of the sensors mentioned above are shown in Fig. 3. These MOF cavity lengths were chosen in order to get examples of sensors in a wide spatial frequency range (0.4 – 1.5 nm^{-1}) and also to verify their performance when other sensors are located in a spatial frequency close to them.

Using the setup showed in Fig. 1, the resulting optical spectrum is shown in Fig. 4. This optical spectrum is the result

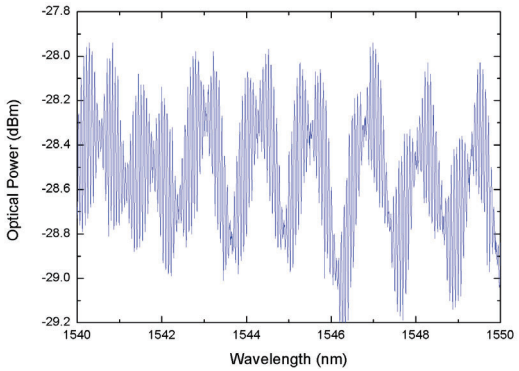

Fig. 4. Resulting multiplexed optical spectrum.

of the combination of all the sensor's interferences. As can be noticed, it becomes impossible to track the evolution of each interference independently and a wavelength shift in one of the interferences produces a wavelength variation of the whole multiplexed optical spectrum.

Typically, interferometric sensors have been multiplexed through wavelength division multiplexing devices (WDM) [59], [60] committing a certain wavelength range for each sensor. This technique allows a low number of sensors to be multiplexed, depending on the wavelength range committed to each sensor and the operating wavelength range of the devices employed (light source, analyzer and EDFA). Moreover, the interference period ($\Delta\lambda$) of each sensor and the wavelength range assigned to it determines the operating range of the device, leading to a tradeoff between operating range of the sensor and the number of sensors that can be multiplexed.

The FFT of each optical spectrum leads to a single peak (theoretically a single Dirac delta) in the FFT magnitude domain as can be seen in Fig. 5. The experimental FFT magnitude of each sensor is shown in Fig. 5. Table 2 show the theoretical frequencies that should be obtained just by applying equation (2), where x makes reference to any sensor.

$$\mathrm{Freq_x} = 1/\Delta\lambda x \tag{2}$$

As can be seen in Fig. 5 theoretical frequencies matches with experimental FFT results of each sensors. With this technique, the experimental multiplexed FFT magnitude is shown in Fig.6.

The FFT shows two single Dirac deltas in the FFT module domain (one in the negative part of the FFT spectrum and one in the positive part) due to the sinusoid optical spectrum resulting of each MOF-FP cavity. Experimentally, it is not a perfect Dirac delta but a broadened component because of the limited number of samples in each period of the optical interference the FFT. This is due to the FFT properties: the more samples are comprised within an optical spectrum interference period, the most defined will be the FFT delta. As a result, the higher the interference period is, the more number

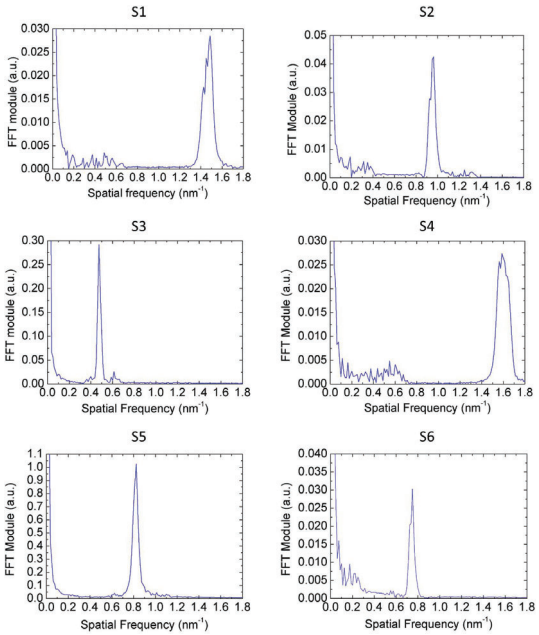

Fig. 5. Sensor's individual FFT magnitude.

TABLE III
FFT FREQUENCIES OF EACH SENSOR

Sensor	$\Delta\lambda$ (nm)	FFT frequency (nm^{-1})
S1	0.7	~1.43
S2	1.1	~0.9
S3	2.2	~0.45
S4	0.63	~1.59
S5	1.28	~0.78
S6	1.35	~0.74

of points are comprised within it and therefore the resulting FFT delta is more defined. As an example, S3 presents an interference period of 2.2 nm which means 440 samples (optical interrogator's resolution of 05pm) and then, S4 has an interference period of 0.63 nm which means 126 samples. This property involves a technical limit of the maximum number of sensors that can be multiplexed in a single channel.

B. Multiplexing System Validation

A scenario of 6 sensing heads for temperature, relative humidity and methanol presence was designed to test the performance of the multiplexing system and verify its capability to multiplex several sensors with independence of their sensing target. As presented in Fig. 1, S1 and S2 monitored temperature variations, S3, S4 and S5 were developed to

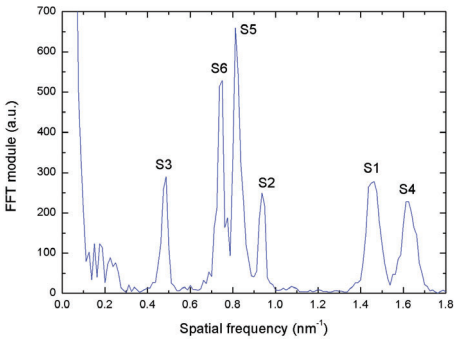

Fig. 6. Multiplexed FFT magnitude spectrum.

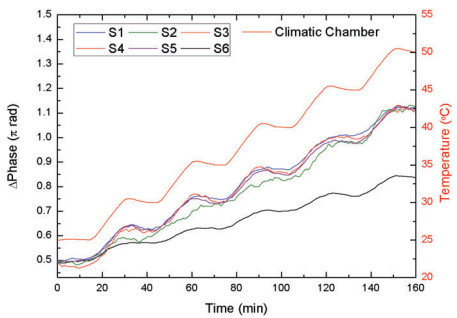

Fig. 7. Temperature characterization of all the sensors.

monitor methanol presence and S6 monitored temperature variations. The objective of the system is to be able to monitor each sensor independently of the others and without crosstalk between them.

1) Temperature Monitoring: FP-MOF based temperature sensors are fully described in [49].

In this case, all sensors are sensitive to temperature variations as all of them are made of a MOF-FP cavity [49]. In order to avoid this temperature crosstalk, a temperature characterization was carried out as shown in Fig. 7.

In order to avoid the temperature influence in sensors S1-S5, S6 is used as temperature reference. For these measurements, S6 was inserted inside the climatic chamber and the other were placed in a box outside. All the sensors were monitored simultaneously using the multiplexing setup. Temperature variations from 25°C to 50°C were applied to only S6 with 5°C steps as Fig. 8 illustrates.

As can be noticed, S6 works as temperature sensor showing a sensitivity of 0.015π rad/°C. S1, S2, S3, S4 and S5 are not affected by temperature variations inside the climatic chamber verifying the systems isolation capability. They show small variations due to room temperature variations of ± 0.4°C, but with no relation to the steps induced by the climatic chamber.

Knowing all sensors' temperature sensitivities and being S6 insensitive to relative humidity and to VOCs concentration

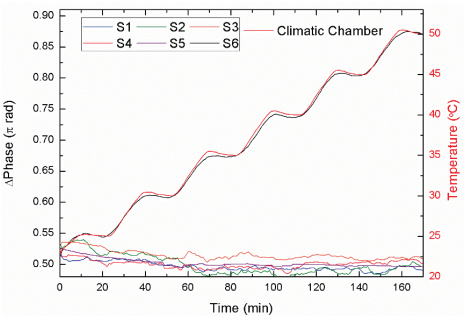

Fig. 8. S6 performance towards temperature variations.

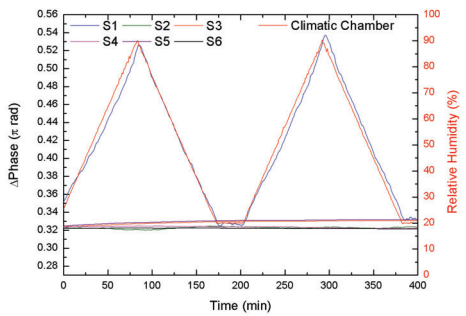

Fig. 9. S1 performance towards relative humidity variations.

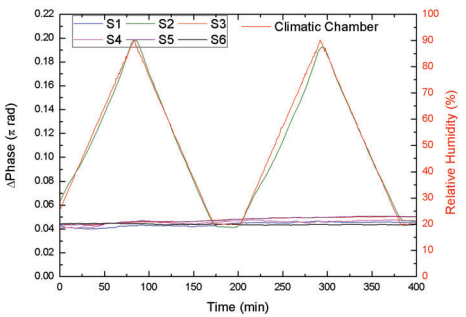

Fig. 10. S2 performance towards relative humidity variations.

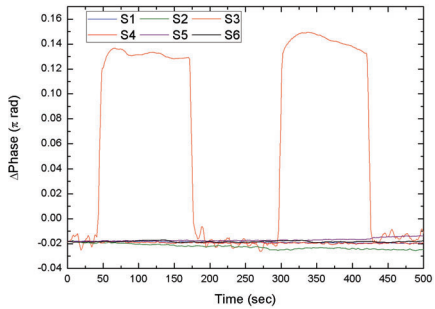

Fig. 11. S3 performance towards methanol fully saturated atmosphere.

variations, this last sensor is used as a temperature reference, making consequently the system independent from temperature variations by means of the suitable calibration algorithm.

2) Relative Humidity Monitoring: SnO_2-FP-MOF based relative humidity sensors are fully described in [49]. S1 and S2 were deposited with a ∼2 minutes SnO2 sputtering deposition. Firstly, S1 was inserted inside the climatic chamber while S2, S3, S4, S5 and S6 remained outside in an expanded polystyrene EPS box to avoid the room temperature variations influence. All sensors were monitored simultaneously. The results of this experiment are shown in Fig. 9. Secondly, S2 was placed inside the climatic chamber and S1, S3, S4, S5 and S6 inside the box. As previously all sensors were monitored at the same time which results are shown in Fig. 10.

Both sensors showed good agreement with climatic chamber's variations and presented no crosstalk with sensors outside it. A little hysteresis effect can be seen in S1: it might be caused by the carton substrate used to fix the sensors as it retains water molecules easily. S1 and S2 showed sensitivities of 0.003π rad/% RH and 0.0021π rad/% RH respectively. This sensitivity difference is due to the difference in the sensitive layers thickness. S3, S4 and S5 also showed low sensitivities towards humidity variations as ITO also reacts towards this parameter but their sensitivities are 10 times lower than S1 and S2. S6 is insensitive towards humidity variations.

Moreover, different approaches have been developed in order to make more selective this kind of sensors like the use of post process techniques as for example "principal component analysis" (PCA) [61], artificial neural networks [62] or making more selective the sensing layer using other metals or additives [63].

3) VOC (Methanol) Presence Monitoring: The sensing material selected was ITO because it has been previously used to successfully detect VOCs.

Fig. 11 shows all the system performance when S3 is exposed to fully saturated atmospheres of methanol. As in previous analysis, all sensors were monitored simultaneously. Fig. 12 and Fig. 13 illustrates the systems results when S4 and S5 respectively are exposed to methanol atmospheres.

As in previous results, the sensors exposed showed sensitivity to methanol presence and the others presented no crosstalk between them. With the deposition times presented, sensors showed maximal phase shifts of 0.15π rad, 0.16π rad and 0.31π rad respectively, making them suitable for escape detectors in gas bottles or containers applications.

Analogously, as it happened with humidity measurements, S1 and S2 presents low sensitivity towards methanol in comparison with S3, S4 and S5. S6 is insensitive towards methanol variations. Due to this important sensitivities difference, using one sensor as reference, this crosstalk influence can be reduced.

Taking into account all the results obtained during the experiments, the system can be used to multiplex interferometric sensors without crosstalk between them. Additionally,

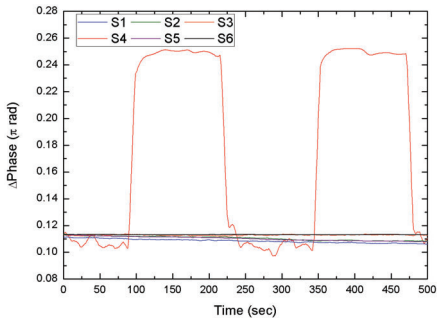

Fig. 12. S4 performance towards methanol fully saturated atmosphere.

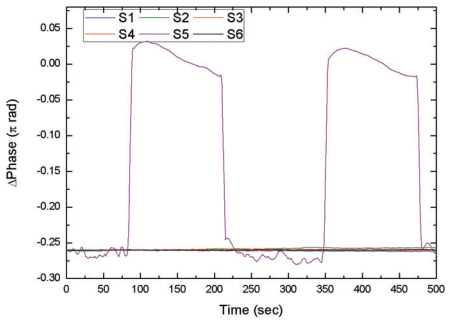

Fig. 13. S5 performance towards methanol fully saturated atmosphere.

a multipoint application to monitor temperature, relative humidity and VOCs escapes with 6 sensing heads has been presented and characterized. The multiplexing system can be used with any combination of sensors and applications and an example has just been presented.

IV. Conclusion

In summary, a multiplexing system for interferometric sensors based on the FFT has been presented and validated. Six sensing heads have been multiplexed and measured simultaneously within a single channel of an optical interrogator showing no crosstalk between sensors. The measurements have been carried out by measuring the phase of the FFT component of each sensor at a scanning frequency from 1 Hz up to 1 KHz. The number of multiplexed sensors depends on the Fabry-Perot cavity lengths chosen.

An application for temperature, relative humidity and Volatile Organic Compounds has been proposed and analyzed. Sensors sensitivity depends on the deposited thin film material and deposition time. One sensor is proposed for temperature measurements, two sensors for relative humidity (20-90%) and three sensors for methanol presence. All of them show great sensitivity to their parameter target and no crosstalk between sensors.

This multiplexing technique is independent of the measured parameter by the MOF based sensors and also of the topology of the multiplexing network.

References

[1] A. M. R. Pinto and M. Lopez-Amo, "Photonic crystal fibers for sensing applications," *J. Sensors*, vol. 2012, pp. 1–21, 2012.

[2] T. M. Monro *et al.*, "Sensing with suspended-core optical fibers," *Opt. Fiber Technol.*, vol. 16, no. 6, pp. 343–356, 2010.

[3] O. Frazão, J. L. Santos, F. M. Araújo, and L. A. Ferreira, "Optical sensing with photonic crystal fibers," *Lasers Photon. Rev.*, vol. 2, no. 6, pp. 449–459, 2008.

[4] O. Frazão *et al.*, "All fiber Mach–Zehnder interferometer based on suspended twin-core fiber," *IEEE Photon. Technol. Lett.*, vol. 22, no. 17, pp. 1300–1302, Sep. 1, 2010.

[5] A. S. Webb, "Suspended-core holey fiber for evanescent-field sensing," *Opt. Eng.*, vol. 46, no. 1, p. 010503, 2007.

[6] L. Niu *et al.*, "Photonic crystal fiber loop mirror-based chemical vapor sensor," *J. Lightw. Technol.*, vol. 32, no. 22, pp. 4416–4421, Nov. 15, 2014.

[7] Y. L. Hoo, S. Liu, H. L. Ho, and W. Jin, "Fast response microstructured optical fiber methane sensor with multiple side-openings," *IEEE Photon. Technol. Lett.*, vol. 22, no. 5, pp. 296–298, Mar. 1, 2010.

[8] V. P. Minkovich, D. Monzón-Hernández, J. Villatoro, and G. Badenes, "Microstructured optical fiber coated with thin films for gas and chemical sensing," *Opt. Express*, vol. 14, no. 18, pp. 8413–8418, Sep. 2006.

[9] J. Villatoro *et al.*, "Photonic crystal fiber interferometer for chemical vapor detection with high sensitivity," *Opt. Express*, vol. 17, no. 3, pp. 1447–1453, 2009.

[10] S. Olyaee, A. Naraghi, and V. Ahmadi, "High sensitivity evanescent-field gas sensor based on modified photonic crystal fiber for gas condensate and air pollution monitoring," *Optik-Int. J. Light Electron Opt.*, vol. 125, no. 1, pp. 596–600, 2014.

[11] M. Bravo, A. M. R. Pinto, M. López-Amo, J. Kobelke, and K. Schuster, "High precision micro-displacement fiber sensor through a suspended-core Sagnac interferometer," *Opt. Lett.*, vol. 37, no. 2, pp. 202–204, 2012.

[12] J. Tian, Z. Lu, M. Quan, Y. Jiao, and Y. Yao, "Fast response Fabry–Pérot interferometer microfluidic refractive index fiber sensor based on concave-core photonic crystal fiber," *Opt. Express*, vol. 24, no. 18, pp. 20132–20142, 2016.

[13] R.-M. Beiu, V. Beiu, and V.-F. Duma, "Fiber optic mechanical deformation sensors employing perpendicular photonic crystals," *Opt. Express*, vol. 25, no. 19, pp. 23388–23398, 2017.

[14] L. Rindorf, J. B. Jensen, M. Dufva, L. H. Pedersen, P. E. Høiby, and O. Bang, "Photonic crystal fiber long-period gratings for biochemical sensing," *Opt. Express*, vol. 14, no. 18, pp. 8224–8231, 2006.

[15] S. Rota-Rodrigo, A. López-Aldaba, R. A. Pérez-Herrera, M. Del Carmen López Bautista, Ó. Esteban, and M. López-Amo, "Simultaneous measurement of humidity and vibration based on a microwire sensor system using fast Fourier transform technique," *J. Lightw. Technol.*, vol. 34, no. 19, pp. 4525–4530, Oct. 1, 2016.

[16] J. B. Jensen *et al.*, "Photonic crystal fiber based evanescent-wave sensor for detection of biomolecules in aqueous solutions," *Opt. Lett.*, vol. 29, no. 17, pp. 1974–1976, 2004.

[17] J. Bürck, J.-P. Conzen, and H.-J. Ache, "A fiber optic evanescent field absorption sensor for monitoring organic contaminants in water," *Fresenius' J. Anal. Chem.*, vol. 342, nos. 4–5, pp. 394–400, 1992.

[18] M. Tabibazarp, B. Sutapun, R. Petrick, and A. Kazemi, "Highly sensitive hydrogen sensors using palladium-coated fiber optics with exposed cores and evanescent field interactions," *Microelectron. Struct. MEMS Opt. Process. IV*, vol. 3513, pp. 80–89, 1998.

[19] S. Sekimoto *et al.*, "A fiber-optic evanescent-wave hydrogen gas sensor using palladium-supported tungsten oxide," *Sens. Actuators B, Chem.*, vol. 66, nos. 1–3, pp. 142–145, 2000.

[20] G. Yan *et al.*, "Fiber-optic acetylene gas sensor based on microstructured optical fiber Bragg gratings," *IEEE Photon. Technol. Lett.*, vol. 23, no. 21, pp. 1588–1590, Nov. 1, 2011.

[21] M. Cubillas, M. Silva-López, J. M. Lazaro, O. M. Conde, M. N. Petrovich, and J. M. López-Higuera, "Methane detection at 1670-nm band using a hollow-core photonic bandgap fiber and a multiline algorithm," *Opt. Express*, vol. 15, no. 26, pp. 17570–17576, 2007.

[22] T. Ritari *et al.*, "Gas sensing using air-guiding photonic bandgap fibers," *Opt. Express*, vol. 12, no. 17, pp. 4080–4087, 2004.

[23] H. Y. Choi, K. S. Park, S. J. Park, U.-C. Paek, B. H. Lee, and E. S. Choi, "Miniature fiber-optic high temperature sensor based on a hybrid structured Fabry–Pérot interferometer," *Opt. Lett.*, vol. 33, no. 21, pp. 2455–2457, 2008.

[24] C. Wu, H. Y. Fu, K. K. Qureshi, B.-O. Guan, and H. Y. Tam, "High-pressure and high-temperature characteristics of a Fabry–Pérot interferometer based on photonic crystal fiber," *Opt. Lett.*, vol. 36, no. 3, pp. 412–414, 2011.

[25] G. Z. Xiao, A. Adnet, Z. Zhang, F. G. Sun, and C. P. Grover, "Monitoring changes in the refractive index of gases by means of a fiber optic Fabry–Pérot interferometer sensor," *Sens. Actuators A, Phys.*, vol. 118, no. 2, pp. 177–182, 2005.

[26] L. H. Chen *et al.*, "Chitosan based fiber-optic Fabry–Pérot humidity sensor," *Sens. Actuators B, Chem.*, vol. 169, pp. 167–172, Jul. 2012.

[27] Y. Zhao, R.-Q. Lv, Y. Ying, and Q. Wang, "Hollow-core photonic crystal fiber Fabry–Pérot sensor for magnetic field measurement based on magnetic fluid," *Opt. Laser Technol.*, vol. 44, no. 4, pp. 899–902, 2012.

[28] T. Wei, Y. Han, Y. Li, H.-L. Tsai, and H. Xiao, "Temperature-insensitive miniaturized fiber inline Fabry–Pérot interferometer for highly sensitive refractive index measurement," *Opt. Express*, vol. 16, no. 8, pp. 5764–5769, 2008.

[29] O. Frazão *et al.*, "Fabry–Pérot cavity based on a suspended-core fiber for strain and temperature measurement," *IEEE Photon. Technol. Lett.*, vol. 21, no. 17, pp. 1229–1231, Sep. 1, 2009.

[30] M. J. Gander *et al.*, "Embedded micromachined fiber-optic Fabry–Pérot pressure sensors in aerodynamics applications," *IEEE Sensors J.*, vol. 3, no. 1, pp. 102–107, Feb. 2003.

[31] J. Mathew, Y. Semenova, G. Rajan, and G. Farrell, "Humidity sensor based on photonic crystal fibre interferometer," *Electron. Lett.*, vol. 46, no. 19, pp. 1341–1343, Sep. 2010.

[32] M. Hernaez, D. López-Torres, C. Elosua, I. R. Matias, and F. J. Arregui, "Sensitivity enhancement of a humidity sensor based on poly(sodium phosphate) and poly(allylamine hydrochloride)," in *Proc. IEEE SENSORS*, Nov. 2013, pp. 1–4.

[33] G. Jiménez-Cadena, J. Riu, and F. X. Rius, "Gas sensors based on nanostructured materials," *Analyst*, vol. 132, no. 11, pp. 1083–1099, 2007.

[34] M. Stowell, J. Müller, M. Ruske, M. Lutz, and T. Linz, "RF-superimposed DC and pulsed DC sputtering for deposition of transparent conductive oxides," *Thin Solid Films*, vol. 515, no. 19, pp. 7654–7657, 2007.

[35] M. Śmietana *et al.*, "Optical monitoring of electrochemical processes with ITO-based lossy-mode resonance optical fiber sensor applied as an electrode," *J. Lightw. Technol.*, vol. 36, no. 4, pp. 954–960, Feb. 15, 2018.

[36] J. Ascorbe, J. M. Corres, F. J. Arregui, and I. R. Matias, "Humidity sensor based on Bragg gratings developed on the end facet of an optical fiber by sputtering of one single material," *Sensors*, vol. 17, no. 5, p. 991, 2017.

[37] C. Christopher, A. Subrahmanyam, and V. V. R. Sai, "Gold sputtered U-bent plastic optical fiber probes as SPR- and LSPR-based compact plasmonic sensors," *Plasmonics*, vol. 13, no. 2, pp. 493–502, 2018.

[38] Y.-J. Rao, "Recent progress in fiber-optic extrinsic Fabry–Pérot interferometric sensors," *Opt. Fiber Technol.*, vol. 12, no. 3, pp. 227–237, 2006.

[39] Z. Wang, F. Shen, L. Song, X. Wang, and A. Wang, "Multiplexed fiber Fabry–pérot interferometer sensors based on ultrashort Bragg gratings," *IEEE Photon. Technol. Lett.*, vol. 19, no. 8, pp. 622–624, Apr. 15, 2007.

[40] Y. Ou, C. Zhou, L. Qian, D. Fan, C. Cheng, and H. Guo, "Large-capacity multiplexing of near-identical weak fiber Bragg gratings using frequency-shifted interferometry," *Opt. Express*, vol. 23, no. 24, p. 31484, 2015.

[41] R. Ryf *et al.*, "Mode-multiplexed transmission over conventional graded-index multimode fibers," *Opt. Express*, vol. 23, no. 1, pp. 235–246, 2015.

[42] H. Y. Fu *et al.*, "Multiplexing of polarization-maintaining photonic crystal fiber based Sagnac interferometric sensors," *Opt. Express*, vol. 17, no. 21, pp. 18501–18512, 2009.

[43] J.-W. Goossens, M. I. Yousefi, Y. Jaouën, and H. Hafermann, "Polarization-division multiplexing based on the nonlinear Fourier transform," *Opt. Express*, vol. 25, no. 22, pp. 26437–26452, 2017.

[44] A. Lopez-Aldaba *et al.*, "Relative humidity multi-point optical sensors system based on fast Fourier multiplexing technique," in *Proc. 25th IEEE Opt. Fiber Sensors Conf. (OFS)*, 2017, pp. 1–4.

[45] Y. J. Rao, J. Jiang, and C. X. Zhou, "Spatial-frequency multiplexed fiber-optic Fizeau strain sensor system with optical amplification," *Sens. Actuators A, Phys.*, vol. 120, no. 2, pp. 354–359, 2005.

[46] A. D. Wilson and M. Baietto, "Applications and advances in electronic-nose technologies," *Sensors*, vol. 9, no. 7, pp. 5099–5148, Jan. 2009.

[47] K. Arshak, E. Moore, G. M. Lyons, J. Harris, and S. Clifford, "A review of gas sensors employed in electronic nose applications," *Sensor Rev.*, vol. 24, no. 2, pp. 181–198, 2004.

[48] C. Bariain, I. R. Matías, C. Fernández-Valdivielso, F. J. Arregui, M. L. Rodríguez-Méndez, and J. A. de Saja, "Optical fiber sensor based on lutetium bisphthalocyanine for the detection of gases using standard telecommunication wavelengths," *Sens. Actuators B, Chem.*, vol. 93, nos. 1–3, pp. 153–158, 2003.

[49] A. López-Aldaba *et al.*, "Experimental and numerical characterization of a hybrid Fabry–Pérot cavity for temperature sensing," *Sensors*, vol. 15, no. 4, pp. 8042–8053, 2015.

[50] J. L. Santos, A. P. Leite, and D. A. Jackson, "Optical fiber sensing with a low-finesse Fabry–Pérot cavity," *Appl. Opt.*, vol. 31, no. 34, pp. 7361–7366, 1992.

[51] D. Leandro, M. Bravo, A. Ortigosa, and M. López-Amo, "Real-time FFT analysis for interferometric sensors multiplexing," *J. Lightw. Technol.*, vol. 33, no. 2, pp. 354–360, Jan. 15, 2015.

[52] R. A. Perez-Herrera and M. López-Amo, "Fiber optic sensor networks," *Opt. Fiber Technol.*, vol. 19, no. 6, pp. 689–699, 2013.

[53] O. C. Akkaya, M. J. F. Digonnet, G. S. Kino, and O. Solgaard, "Time-division-multiplexed interferometric sensor arrays," *J. Lightw. Technol.*, vol. 31, no. 16, pp. 2701–2708, Aug. 15, 2013.

[54] R. Hernandez-Lorenzo, M. López-Amo, and P. Urquhart, "Single and double distributed optical amplifier fiber bus networks with wavelength division multiplexing for photonic sensors," *J. Lightw. Technol.*, vol. 16, no. 4, pp. 485–489, Apr. 1998.

[55] A. L. Aldaba *et al.*, "SnO_2-MOF-Fabry–Pérot optical sensor for relative humidity measurements," *Sens. Actuators B, Chem.*, vol. 257, pp. 189–199, Mar. 2018.

[56] N. G. Patel, P. D. Patel, and V. S. Vaishnav, "Indium tin oxide (ITO) thin film gas sensor for detection of methanol at room temperature," *Sens. Actuators B, Chem.*, vol. 96, no. 1, pp. 180–189, 2003.

[57] W. Schmid, "Consumption measurements on SnO_2 sensors in low and normal oxygen concentration," Ph.D. dissertation, Fakultät Che mie und Pharmazie., Eberhard-Karls-Univ. Tübingen, Tübingen, Germany, 2004.

[58] D. López-Torres *et al.*, "Enhancing sensitivity of photonic crystal fiber interferometric humidity sensor by the thickness of SnO_2 thin films," *Sens. Actuators B, Chem.*, vol. 251, pp. 1059–1067, Nov. 2017.

[59] M. Bravo, M. Fernández-Vallejo, M. Echapare, M. López-Amo, J. Kobelke, and K. Schuster, "Multiplexing of six micro-displacement suspended-core Sagnac interferometer sensors with a Raman–Erbium fiber laser," *Opt. Express*, vol. 21, no. 3, pp. 2971–2977, 2013.

[60] P. Childs, "An FBG sensing system utilizing both WDM and a novel harmonic division scheme," *J. Lightw. Technol.*, vol. 23, no. 1, pp. 348–354, Jan. 2005.

[61] J. Mizsei, "How can sensitive and selective semiconductor gas sensors be made?" *Sens. Actuators B, Chem.*, vol. 23, nos. 2–3, pp. 173–176, 1995.

[62] C. Delpha, M. Siadat, and M. Lumbreras, "Discrimination of a refrigerant gas in a humidity controlled atmosphere by using modelling parameters," *Sens. Actuators B, Chem.*, vol. 62, no. 3, pp. 226–232, 2000.

[63] X. Wang, N. Miura, and N. Yamazoe, "Study of WO_3-based sensing materials for NH_3 and NO detection," *Sens. Actuators B, Chem.*, vol. 66, nos. 1–3, pp. 74–76, 2000.

Aitor Lopez-Aldaba was born in Navarra, Spain, in 1988. He received the Degree in telecommunication engineering degree from the Universidad Pública de Navarra, Navarra, in 2014. In 2013, he joined the Optical Communications Group, Department of Electrical and Electronic Engineering, Universidad Pública de Navarra. His research interests include fiber optic lasers, optical amplifiers, optical fiber sensor networks, photonic crystal fibers, and chemical fiber optic sensors.

Diego López-Torres received the M.S. degree in electrical and electronic engineering and the master's degree in communications from the Universidad Pública de Navarra (UPNA), Pamplona, Spain, in 2013 and 2014, respectively. Since 2014, he has been a Researcher with UPNA. In 2015, he received a scholarship from UPNA. His research interests include optical fiber sensors, photonic crystal fiber, and nanostructured materials.

Cesar Elosúa Aguado received the M.S. degree in electrical and electronic engineering from the Universidad Pública de Navarra (UPNA), Pamplona, Spain, in 2004, and the Ph.D. degree in 2008. In 2014, he received a scholarship from the Science and Technology Spanish Ministry and he joined the Optical Fiber Sensor Group, UPNA. In 2008, he was a Visiting Ph.D. Student with the University of Limerick and with the City University of London. He became a Lecturer with the Electrical and Electronic Engineering Department in 2009. His research interests include optical fiber sensors and networks, organometallic chemistry, and data mining techniques.

Francisco J. Arregui (M'01) is a Full Professor with the Universidad Pública de Navarra, Pamplona, Spain. He was part of the team that fabricated the first optical fiber sensor by means of the Layer-by-Layer assembly method at Virginia Tech, Blacksburg, VA, USA, in 1998. He has authored around 300 scientific journal and conference publications. He has been an Associate Editor of the IEEE SENSORS JOURNAL, the *Journal of Sensors* (founded by Prof. Arregui, in 2007), and the *International Journal on Smart Sensing and Intelligent Systems*. He is also the Editor of the books entitled *Sensors Based on Nanostructured Materials* and *Optochemical Nanosensors*.

Jean-Louis Auguste received the Ph.D. degree in optical and high frequency of telecommunications from the University of Limoges, France, in 2001, and the HDR degree, highest diploma of the University and giving him the possibility to be the Research Director for Ph.D. students in 2010. During his thesis, the main areas of activity have been in theory, design and experimental investigation on optical fibers and more particularly on a design and fabrication of high negative chromatic dispersion fiber. Since 2000, he has been a CNRS Engineer with the Xlim Research Institute, where until 2012 he was in charge (Process Manager) of the research and development around fabrication of optical fibers–guide structure and materials for optical fibers with recent developments around glass synthesis thanks to a European project that he manages. He works in strong collaboration with researchers of the Fiber Group and is associated with ANR and other European Projects as a researcher from SPCTS (Ceramic Laboratory) to develop new topics mixing optical glass development and optical fibre applications. In this way in collaboration with researchers from SPCTS he manages a new research project at Xlim around original glasses for optical fiber applications. He has authored or co-authored 45 publications in international journals (with referees) and 43 papers in international conferences (with referees) including several invited papers, international seminars plus four patent applications. A part of his activity is dedicated to teaching and training students from the University and the School of Engineering.

Raphael Jamier was born in Périgueux, France, in 1981. He received the Ph.D. degree from the University of Limoges, France, in 2007. Since 2008, he has been an Assistant Professor with the XLIM Research Institute, University of Limoges, where he has been engaged in design, fabrication, and characterization of specialty optical fibers. He has been the Deputy Director of the Physics Department, University of Limoges, since 2012. He has authored or co-authored 27 articles in refereed journals, 58 papers in internationally recognized conferences with peer-review system, and two patents. His current research activities include the design, fabrication and characterization of photonic crystal fibers for high-power generation at unconventional spectral domains (in particular, in the mid-infrared wavelengths).

Philippe Roy was born in Bellac, France, in 1971. He received the Ph.D. degree in microwave electronics and optoelectronics (speciality photonics and electronics systems) from the University of Limoges in 1997. He is currently a Senior Researcher with CNRS and the Head of the Fiber Photonics Group, Xlim, which is a mixed laboratory of the University of Limoges and CNRS. Since 1998, he has been involved in design, fabrication, and characterization of photonic crystal fibers. More recently, he developed specialty and composite fibers mainly dedicated to advanced fiber sensor systems and to very high power fiber lasers. He develops rare earth doped fiber with complex structure based on an aperiodic design to reach higher power levels without modal instabilities and/or non-conventional emitted spectrum, from visible to THz domain.

Manuel López-Amo (M'91–SM'98) was born in Madrid, Spain, in 1960. He received the Degree in telecommunications engineering and the Ph.D. degree from the Universidad Politécnica de Madrid, Madrid, in 1985 and 1989, respectively. From 1985 to 1996, he was with the Photonic Technology Department, Universidad Politécnica de Madrid, where he became an Associate Professor in 1990. In 1996, he moved to the Electrical and Electronic Engineering Department, Universidad Pública de Navarra, Pamplona, Spain, where he became a Full Professor and is currently the Head of the Optical Communications Group. He has been the Chairman of the Optoelectronic Committee of Spain. He has been the leader more than 40 research projects and he has co-authored more than 250 works in international refereed journals and conferences related to fiber-optic networks, optical amplifiers, fiber-optic sensors, and integrated optics. He is a member of the technical committees of the International Conference on Fiber Optic Sensors and the European Workshop on Optical Fiber Sensors, among others. He is a member of the Optical Society of America.

6.3. Utilización de sensores para la medición de la humedad en suelos con diferentes tipos de tierra

Dada la sensibilidad obtenida y la resolución alcanzada por el sensor desarrollado en el capítulo 4 de la tesis frente a los distintos cambios de humedad (para recordar, dicho sensor se basaba en un interferómetro Fabry Pèrot con un película sensible de SnO_2 depositaba sobre una fibra SSC), se pensó que podía ser un buen candidato para realizar medidas en un escenario real. Las anteriores medidas se realizaron en el interior de una cámara climática, donde la temperatura y la humedad estaban bajo control, utilizando la FFT como herramienta para la interrogación del sensor. En esta ocasión se propuso utilizar dicho sensor para medir la humedad en suelos, con diferentes tipos de tierra, bajo condiciones climatológicas no controladas.

Se decidió medir la humedad del suelo porque este parámetro desempeña un papel clave en el ciclo hidrológico al controlar procesos, como la evapotranspiración, la escorrentía y la recarga de acuíferos. Por lo tanto, su medición es de vital importancia para muchos de los seres vivos que habitan en la naturaleza. Pero al querer medir la humedad de un suelo determinado, la estructura del sensor debía ser modificada para poder conseguir un correcto comportamiento en este nuevo entorno; este fue uno de los retos que tuvieron que ser superados en esta nueva publicación científica.

Uno de los problemas era la fragilidad de la punta del sensor. Además, era conveniente aislar la tierra del sensor para evitar el contacto directo entre ellos y reducir al máximo los posibles errores en la medición. Para solventar este inconveniente, se desarrolló un encapsulado de policloruro de vinilo (PVC) agujereado de forma periódica. De esta manera, se conseguía aislar al sensor de la influencia de la tierra y el polvo, pero se permitía el paso de la humedad a través de los agujeros. Para comprobar que el encapsulado no afectaba la respuesta del sensor, se realizó una prueba en cámara climática: el resultado verificó que el comportamiento del dispositivo no estaba comprometido.

Llegados a este punto, el sensor ya estaba listo para ser instalado en el escenario real propuesto, es decir, al aire libre y dentro de la tierra. Para estudiar sus características, se propuso comparar los resultados obtenidos con un sensor capacitivo comercial midiendo en dos tierras con propiedades distintas durante

dos semanas. Una vez analizadas y estudiadas las respuestas se concluyó que existía una buena concordancia entre las mediciones ópticas y capacitivas de ambos sensores en el rango de humedad comprendido entre 15-100%. Para humedades inferiores al 15%, la sensibilidad del sensor óptico disminuyó significativamente. Un punto a favor del sensor desarrollado en esta nueva contribución científica fue las ventajas que ofrece en comparación con los sensores capacitivos tradicionales: una de ellas, la inmunidad a las variaciones de temperatura (compensadas y explicadas en la contribución), siguiendo con la posibilidad de realizar mediciones en varios puntos concretos del suelo (en contra de las mediciones de área que ofrecen exclusivamente otro tipo de sensores) y la capacidad de multiplexación vista en el apartado anterior.

Todos los resultados obtenidos en este estudio fueron expuestos de una forma más detallada en la siguiente contribución científica: *"Comparison between Capacitive and Microstructured Optical Fibre Soil Moisture Sensors"* que fue publicado en la revista *"Applied Sciences"*.

Por último, es importante destacar el posible potencial que tiene fusionar la técnica de la multiplexación con una determinada aplicación final del sensor. Por ejemplo, se ha visto que el sensor presentado en este apartado de la tesis puede realizar medidas puntuales. Si varios sensores son multiplexados, pueden realizarse más medidas puntuales, obteniendo más información de otros puntos de la tierra que se está estudiando; basándonos en los resultados obtenidos, como mínimo, un total de 6 puntos distintos pueden llegar a ser medidos. Pero, además, debido a la versatilidad de los óxidos metálicos, los sensores multiplexados pueden ser utilizados con diferentes fines, no sólo para detectar cambios de humedad. Es decir, cada uno de los sensores multiplexados pueden detectar un parámetro determinado como, por ejemplo: contaminantes disueltos en el agua por el uso de pesticidas o insecticidas, VOCs, elementos sólidos ferromagnéticos o agentes químicos. De esta forma, el posible sistema final sería mucho más potente, interesante y el coste económico se reduciría sustancialmente.

applied sciences

MDPI

Article

Comparison between Capacitive and Microstructured Optical Fiber Soil Moisture Sensors

Aitor Lopez Aldaba [1,2,*], Diego Lopez-Torres [1], Miguel A. Campo-Bescós [3], José Javier López [2,3], David Yerro [3], César Elosua [1,2], Francisco J. Arregui [1,2], Jean-Louis Auguste [4], Raphael Jamier [4], Philippe Roy [4] and Manuel López-Amo [1,2]

1 Deptment of Electrical and Electronic Engineering, Universidad Pública de Navarra, Campus Arrosadia, 31006 Pamplona, Spain; diego.lopez@unavarra.es (D.L.-T.); cesar.elosua@unavarra.es (C.E.); parregui@unavarra.es (F.J.A.); mla@unavarra.es (M.L.-A.)
2 Institute of Smart Cities (ISC), and IDISNA, Campus Arrosadia, 31006 Pamplona, Spain; jjlr@unavarra.es
3 Department of Projects and Rural Engineering, IS-FOOD Institute (Innovation & Sustainable Development in Food Chain), Public University of Navarre, Campus de Arrosadía, 31006 Pamplona, Spain; miguel.campo@unavarra.es (M.A.C.-B.); davidyerro@gmail.com (D.Y.)
4 Institute de Recherche, Univ. Limoges, CNRS, XLIM, UMR 7252, F-87000 Limoges, France; jean-louis.auguste@xlim.fr (J.-L.A.); raphael.jamier@xlim.fr (R.J.); philippe.roy@xlim.fr (P.R.)
* Correspondence: aitor.lopez@unavarra.es; Tel.: +34-948-16-98-41

Received: 20 July 2018; Accepted: 27 August 2018; Published: 1 September 2018

Abstract: Soil moisture content has always been an important parameter to control because it is a deterministic factor for site-specific irrigation, seeding, transplanting, and compaction detection. In this work, a discrete sensor that is based on a SnO_2–FP (Fabry-Pérot) cavity is presented and characterized in real soil conditions. As far as authors know, it is the first time that a microstructured optical fiber is used for real soil moisture measurements. Its performance is compared with a commercial capacitive soil moisture sensor in two different soil scenarios for two weeks. The optical sensor shows a great agreement with capacitive sensor's response and gravimetric measurements, as well as a fast and reversible response; moreover, the interrogation technique allows for several sensors to be potentially multiplexed, which offers the possibility of local measurements instead of volumetric: it constitutes a great tool for real soil moisture monitoring.

Keywords: photonic crystal fiber; microstructured optical fiber; fiber sensor; humidity sensing; soil moisture

1. Introduction

Soil moisture plays a key role in the hydrological cycle by controlling processes, such as evapotranspiration, runoff, and recharge of aquifers, just to mention some of them [1–3]. Therefore, soil water content data are very useful for the application and evaluation of hydrological models that yield to irrigation programming and optimization [4]. Hydrological models are essential tools for estimating water resources and floods in the current situation, as well as in relation to different scenarios of global climate change and/or under different land uses [5].

Several methodologies have been developed to determinate soil moisture, both in the field and in the laboratory: gravimetric measurements, optical spectroscopy, continuous wave acoustics, electric resistance blocks, tensiometers, and neutron probes, among others [6–9]. Recently, the use of capacitive sensors has increased [10], since they offer a good cost-benefit in relationship when compared to other devices, like the ones that are based on reflectometry in the time domain, which was considered as one of the most accurate methods for estimating the water content of soils so far [11,12].

Optical fiber sensors have been used to measure many parameters, such as temperature, curvature, vibration, displacement, pressure, refractive index, electric field, magnetic field, relative humidity, and gases due to their ability to work as transducers [13]. There exist many different types of fibers that are suitable for sensing applications: silica optical fibers, plastic fibers, or photonic crystal fibers are some common ones.

Microstructured optical fibers (MOFs) present great sensing potential and they have shown improved properties over traditional optical fiber sensors overcoming some of their handicaps [14–16]. For example, several pure silica suspended-core fibers have been used in temperature and curvature sensing [17], gas sensing [18], or relative humidity (RH) sensing [19].

Fiber based optical Fabry–Pérot (FP) interferometers are a quite popular optical fiber sensor configuration due to their compactness, simple configuration, flexibility in tuning sensitivity, and dynamic range. This structure presents robustness and multiplexing capability. The FP cavity transfer function consists of an interference pattern that depends on the cavity length and of the refractive index of the cavity, or more precisely, the effective indices of the different modes that are supported by the fiber interferometer. Actually, FP cavities fabricated with MOFs are structures that are commonly used for sensing: a hybrid structure that used a MOF, a hollow-core fiber, and a single mode fiber (SMF) was developed for high-temperature sensing [20], whereas a chitosan FP cavity was fabricated for relative humidity (RH) measurements [21] and also compact FP cavities for humidity between 40% and 95% were reported [22].

Nanocoated based sensors have experienced a great development during the last decades [23]. Furthermore, new chemical deposition techniques, such as sputtering [24], enable precisely customizing the morphology and thickness of the deposited thin film coatings, and as a consequence, the final properties (sensitivity, kinetics) of the sensor. Sputtering depositions are commonly used to create a homogeneous layer on the surface of a pure silica optical fiber [25,26].

Finally, not many works have been reported up to date measuring real soil moisture with optical fibers: cascade fiber Bragg gratings (FBG) sensors were employed to monitor temperature and soil moisture simultaneously [27], hetero-core spliced optical fiber SPR sensor [28], and a summary of the most common techniques employed in humidity sensing [29] were reported.

In this work, an optical fiber sensor based on a sputtering deposition on a MOF is presented for real moisture measurements and compared simultaneously with a commercial capacitive sensor. The operation principle of the humidity optical sensor has been previously reported by authors [19] showing in detail the construction process of an optimized sensing head and its performance towards humidity variations. In the present paper, the authors propose, for the first time, a sensor that has been adapted and used for measurements in real soil conditions. Moreover, the authors also present a comparison between the performance of microstructured optical fiber sensors, a commercial capacitive sensor, and a comparison of both devices against gravimetric measurements, showing the pros and cons of every type of sensors (and remarking the advantages of fiber optic against commercial capacitive ones). It is worth remarking that the aim of this work is not to present the optical sensing head in detail, as it is fully described in [19], but to show a real comparison between commercial capacitive soil moisture sensors and the application of the optical sensing head for the same purpose.

2. Materials and Methods

A Decagon 10HS capacitive sensor (Meter Group Inc., Pullman, WA, USA) was used as reference for the soil moisture measurements. This capacitive device is a frequency domain reflectometry (FDR) based electrical sensor. Its operation principle consists of measuring the dielectric constant or permittivity of the soil to calculate its humidity content. It performs soil moisture measurements within a big volume of soil (~6.5 dm^3) with great moisture range and it is designed for any soil composition.

Its measurements have been compared with an optical fiber Fabry-Pérot interferometer that was fabricated by splicing a single mode fiber (SMF) to a cleaved four-bridge MOF, as shown in [19]. As shown in [19], the MOF–FP optical fiber core was used as the substrate in a SnO_2 coating-DC-Sputter

deposition process. SnO_2 can be deposited on the walls of the air holes of the short section of the MOF as well as on the top of the sensor head due to the particular structure of the MOF that is used. SnO_2 coating is highly sensitive to humidity changes of the surrounding environment [30].

The interaction between SnO_2 and H_2O molecules is due to the phenomena called physisorption by means of the adsorption/desorption of these molecules [31]. The molecules of water interact just with the surface of the deposited SnO_2 thin film.

The MOF cavity length determines the periodicity of the sensor optical spectrum interference obtained following (1). Where $\Delta\lambda$: optical spectrum wavelength spacing, λ: working wavelength, n: refractive index, and d: MOF cavity length [32].

$$\Delta\lambda = \lambda^2/2nd, \quad (1)$$

In this particular case, the MOF length used was ~700 μm showing an interference period of 1.24 nm, as Figure 1a shows (after a 10 min SnO_2 deposition).

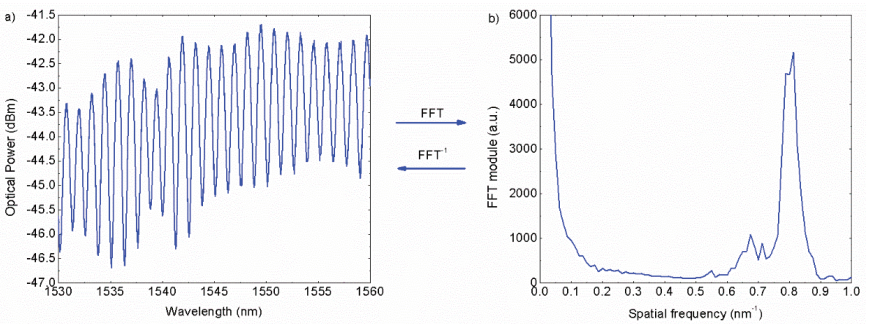

Figure 1. (**a**) Optical microstructured optical fiber-Fabry–Pérot (MOF-FP) sensor´s spectral transfer function and (**b**) its Fast Fourier Transform (FFT) module.

As it can be inferred, the sensing head is very fragile and, moreover, dust inside the MOF holes and in contact with the SnO_2 deposition could lead to measurement errors. In order to avoid this scenario, a protective cap was developed: it consists of a polyvinylchloride (PVC) tube with four arrays of drilled holes (1 mm of diameter) each 5 mm and a cap in one of its ends enabling the access of the optical fiber. Figure 2 shows the real pictures of the protective cap and the final sensor installed inside the cap.

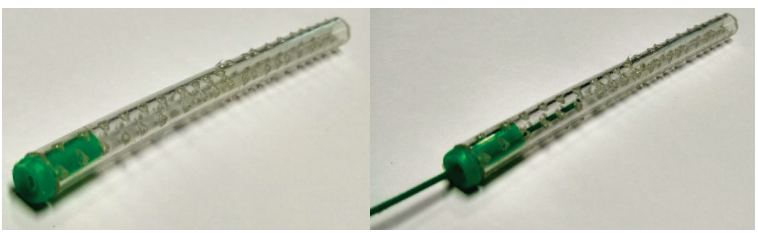

Figure 2. Optical sensor's polyvinylchloride (PVC) drilled protective cap.

This PVC protection prevents the optical sensor from any damage during installation as well as undesired elements polluting the sensing material, creating a cavity inside the tube permeable to humidity, so that it can be measured.

The influence of the protective cap was verified before the installation in the soil in order to verify the correct behavior of the sensing head. The protected sensing head was inserted in a climatic chamber where humidity ranges from 20% to 90% were applied at constant temperature of 25 °C. Results are shown in Figure 3.

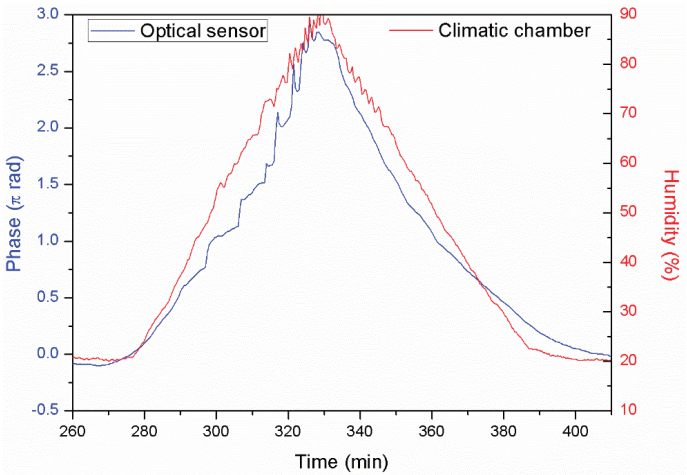

Figure 3. Calibration of the optical sensor.

These results show a correct performance of the sensing head towards humidity changes, but with a reduction of its sensitivity in comparison with the case where no protective cap is employed. The delay of the sensors in relation with the climatic chamber is due to the small hysteresis effect induced by the tube. This performance can be improved by optimizing the sputtering deposition time or through the design of a three-dimensional (3D) printed protective cap to achieve optimal results, as shown in [19].

A commercial FBG (sensitivity of 10 p.m./°C) was also monitored at the same time in order to measure the temperature variations inside the soil sample and compensate the optical sensor's deviations. Temperature variations affect directly on a FP cavity as they modify the cavity length due to the thermal expansion of the silica. These variations produce a wavelength shift or analogously a FFT phase shift. Once known the variation of temperature through the FBG and the sensitivity of the MOF sensing head to temperature variations it can be directly compensated by subtracting the wavelength shift–FFT phase shift to the MOF's results.

A commercial interrogator equipment for FBGs based sensors (SM125, SMARTEC, Lugano, Switzerland) was used to illuminate the network and also to analyze the spectra of the signals reflected from the sensors. The interrogating equipment has a sampling frequency of 1 Hz [33], four different channels, and is remotely controlled through a MATLAB software (MathWorks, Natick, MA, USA) that also executes a FFT real time analysis. This analysis consists of tracking the FFT phase corresponding to the FFT module main component located at 0.8 nm^{-1}, as shown in in Figure 1b. The main advantage of this technique is the negligible influence of noise (high frequency components) and signal amplitude undesired variations. Moreover, choosing correctly the MOF lengths, several FP sensors could be multiplexed within a single optical interrogators channel through common optical couplers, as it has been demonstrated by authors in [34,35]. The three sensors where buried in the soil, as Figure 4 illustrates.

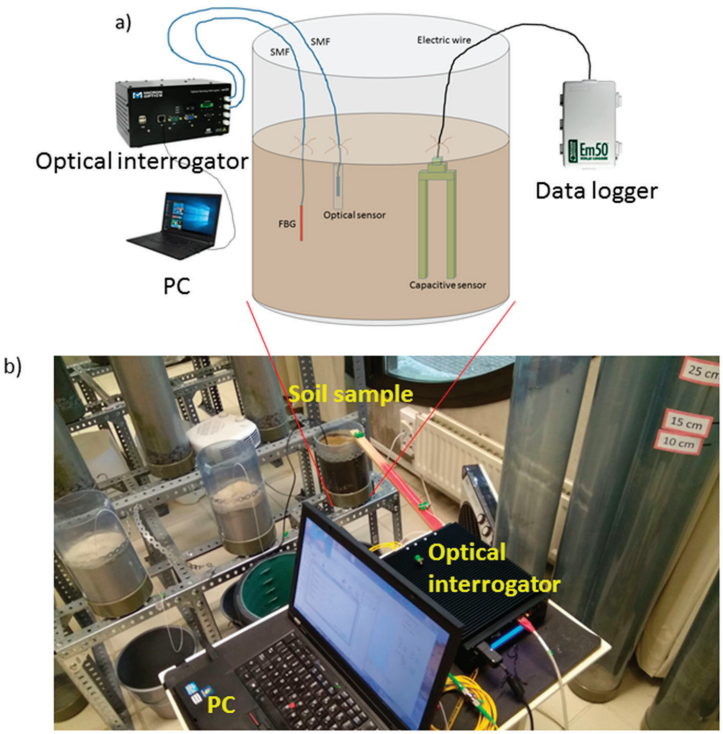

Figure 4. Experimental set up: (**a**) schematic set up and (**b**) real picture of the set up.

The optical sensors were placed at the same radial distance from the soil center as the capacitive sensor and buried ~10 cm deep (trying to be at the mid depth of the capacitive sensor). In this study, two different types of soil were tested in order to check the performance of the optical sensor in comparison with the capacitive one. The first porous media was a silica sand specified for use in pool filters, water purification, and sports fields. The soil texture was defined as sand [36], 100% sand. The second one was a mix of 50% weight of the silica sand and 50% weight of a contrasting natural soil texture classified as clay loam, 28% sand, 36% silt, and 36% clay [36].

3. Results

Different measurements were performed to compare the behavior of capacitive sensors against optical fiber sensors with the two types of soil samples that are described above. Moreover, gravimetric measurements were also performed to verify the results. Temperature variations affect directly on optical fiber sensors and therefore it was also monitored by a FBG.

3.1. Temperature Monitoring and Compensation

As it was previously mentioned, MOF-FP optical sensor is affected by temperature variations, leading to crosstalk between temperature and relative humidity measurements. Figure 5 shows the response of the MOF-FP sensor (calibration) towards temperature showing a linear response with sensitivity of 0.00377π rad/°C.

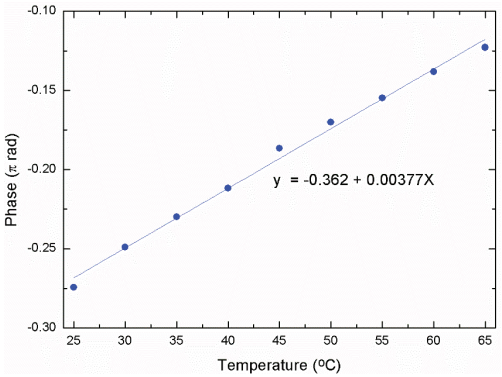

Figure 5. Optical sensor's response towards temperature variations.

To avoid this undesirable crosstalk a commercial FBG (sensitivity of 10 p.m./°C) was also buried in contact to the MOF-FP sensor and simultaneously monitored. This temperature reference showed the behavior illustrated in Figure 6 Measurements shown were taken during a week. As can be noticed in Figure 6, the FBG optical interrogator has a wavelength resolution of 5 p.m., which means a temperature resolution of 0.5 °C.

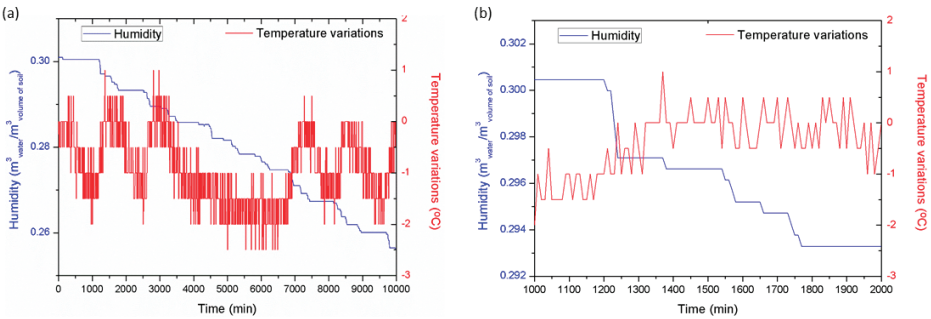

Figure 6. (**a**) Temperature and humidity measured during a week in Soil1 and (**b**) a detailed region.

Results shown in Figure 6 show a good agreement between the dynamics of humidity and temperature. Temperature shows oscillations of 2 °C depending on the time of the day. During day hours temperature rises and when sun sets (soil sample was at direct exposition of sun light) it decreases ~2 °C. Humidity results follows the same trend showing great variations (decreasing humidity) during the day and slower ones at night. These variations agree temporarily with temperature, showing bigger slopes during sunshine hours.

With a temperature reference and being the sensitivity of the optical sensor to temperature variations known, its influence can be cancelled. Thus, the FFT phase shift induced by temperature variations (deduced through the FBG sensor) can be directly subtracted to the MOF-FP sensor's results. This compensation can be made either in real time or by post processing. In this study, it was directly implemented in the acquisition software. Results that are shown in Figures 7–9 are already temperature compensated ones.

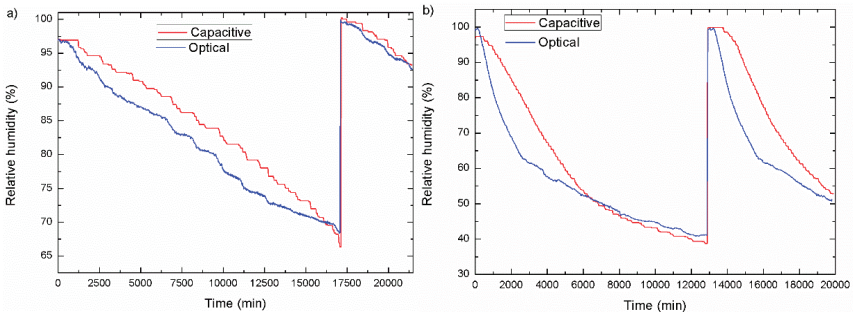

Figure 7. Capacitive and optical sensor's response towards soil humidity: (**a**) Soil1 and (**b**) Soil2.

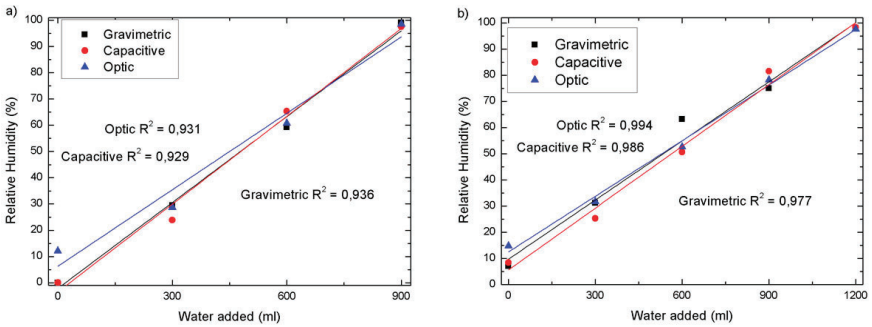

Figure 8. Capacitive and optical sensor's response towards soil humidity: (**a**) Soil1 and (**b**) Soil2.

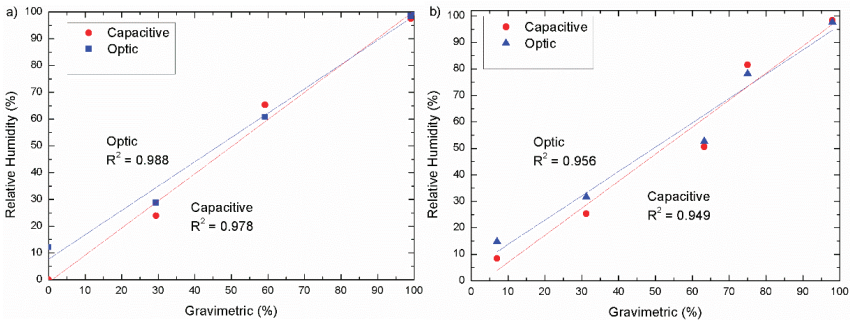

Figure 9. Capacitive and optical sensor's regression slopes: (**a**) Soil1 and (**b**) Soil2.

3.2. Dynamic Measurements

Long term measurements were performed in order to check the viability of the MOF-FP sensor. For this aim, the MOF-FP sensor was buried in the soil at ~5 cm deep, whereas the capacitive sensor was at ~20 cm, as it has been shown in Figure 4a. This difference must be underlined as it will affect directly on the results and it is produced due to the size difference of the sensors. On the one hand, MOF-FP sensor presents reduced dimensions, allowing for the moisture measurement within a small volume of soil while on the other hand, capacitive sensors need a significant soil volume (as it will be described) to work properly. After the sensor's installation, water was carefully added to the soil until saturation (water dropping at the bottom of the sample—Relative humidity = 100%). All of the sensors

were monitored every 10 min during ~14 days uninterruptedly showing the results shown in Figure 7. After ~12 days for Soil1 and ~9 days for Soil2, humidity was raised again until saturation to check the sensor's reversibility and adaptability to changing environments.

As can be seen in Figure 7, there is a discrepancy in terms of kinetics between both sensors. The optical sensing head measures the humidity directly in contact with it while capacitive sensors integrate the moisture in a volume of soil. As previously commented, due to the size, the principle of operation of each sensor, and their burial depth, the optical sensor is able to measure localized humidity variations, and therefore it measures moisture variations before the capacitive sensor.

3.3. Point Measurements

Point measurements were also performed in both soils to check and compare the precision of the sensors. For this kind of measurements, the results of both capacitive and optical sensors were compared with gravimetric measurements.

Soil samples of ~3 L were prepared for the test. The measuring initial point is with soil totally dried by an oven to get a ~0% humidity. At each sample, 300 mL of water were added to the soil until saturation was achieved. For the gravimetric measurements at each sample, just after performing the measures with both capacitive and optical sensors, a sample of soil was taken in a cylinder with a volume of 100.14 cm^3, weighed, dried in the oven, and weighed again to check the real weight of water (difference in weight before and after the drying process) and as a consequence the humidity contained in the sample. Results that are shown in Figures 8 and 9 illustrate the regression slopes for both experiments showing $R^2 = 0.988$ for the capacitive sensor and $R^2 = 0.978$ for the optical sensor in Soil1 and $R^2 = 0.956$ and $R^2 = 0.949$ respectively in Soil2.

Each value was measured five times with a lapse time of 30 s between measurements and the mean value is represented in Figures 8 and 9. The maximum error of the measured samples was 9% and the minimum 2%, being the mean error of point measurements of 4%.

An important aspect to comment is the difficulty to perform accurate gravimetric measurements. The operation principle of this technique is to take a known volumetric sample of wet soil, weigh it, dry the sample in the oven and weigh again to analyze the water weight evaporated. To perform accurate measurements the volume and compaction of the soil sample are critical. Although the volume is not a problem, to maintain the same compaction during the drying process of the soil is not obvious and it requires complex techniques and devices. This difficulty led to small discrepancies, as can be seen in Figures 8 and 9.

4. Discussion

Results shown in Section 3 in overall show an agreement between capacitive sensors, MOF–FP optical sensors, and gravimetric measurements in (two) different types of soil.

One of the main differences between capacitive and optical results can be seen in Figure 5. There, it can be noticed differences in the time response to humidity changes between both sensors. It is due to two important factors: devices size and type of measurements. On the one hand, capacitive sensors that are used in this study have dimensions of 14.5 cm × 3.3 cm × 0.7 cm and they give us volumetric measurements by measuring the dielectric constant of the soil, as shown in Figure 10. On the other hand, MOF-FP based sensors have very reduced dimensions (0.7 mm × 125 μm) without the protective cap. This cap is a cylinder 4 cm long having 0.8 cm of radius. The sensing head measures the humidity that is directly in contact with it. Therefore, it can be concluded that capacitive sensors are field sensors in opposition to point optical sensors. Due to this difference, the optical sensor is very sensitive to point humidity changes very close to the sensing head while capacitive measures all of the humidity comprised around it, being less sensitive to local variations.

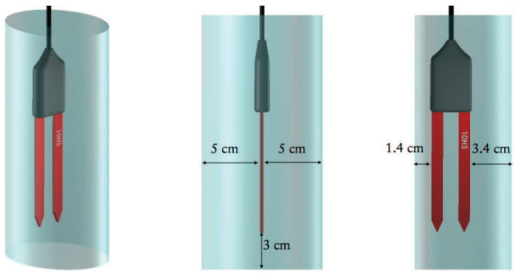

Figure 10. Idealized measurement volume of Decagon 10HS sensor.

Table 1 shows the measured errors between optical—capacitive sensors and optical sensor—gravimetric measurements. As previously commented, gravimetric measurements present great variations due to the employed technique and its variability depending on the measuring conditions. Therefore, the errors measured between optical or capacitive sensors and gravimetric in some points (i.e., in Figure 9b) at 63% RH in gravimetric measurements) are higher than expected, as can be seen in the case of the maximum error between optical sensor and gravimetric measurement.

Table 1. Summary of measured errors between sensors.

Comparison	Soil	Mean	Max
Optical—Capacitive Sensors	Soil1	3.5%	5%
	Soil2	3%	6%
Optical sensor—Gravimetric measurements	Soil1	1%	1.5%
	Soil2	3.5%	9%

Another difference shown in the results from capacitive and optical sensors in Figures 6 and 7 is a measuring error when humidity is close to 0%. This is due to the different nature of the sensors. On the one hand, capacitive sensors measure the dielectric constant of the soil and therefore the content of water in soil: moisture. On the other hand, optical sensors measure refractive index variations that are produced by the presence of soil moisture. Relative humidity can be described, as follows:

$$Relative\ humidity = \frac{Pw}{Pws} \times 100 \quad (2)$$

where Pw is the water vapor pressure and Pws is the water vapor pressure in saturation and it is a function of temperature [28].

The term humidity usually makes reference to the presence of water in gaseous form, but it is often used to refer to expressions that are related to water vapor characteristics and in the field of measurement, there are various terms associated with such water vapor measurements. In addition, the term moisture is frequently interchanged with humidity even though the actual definition of moisture refers to the water in liquid form that may be present in solid materials [37]. Since humidity is a measure of water in gaseous state present in the environment, water vapor found in a gas mixture behaves in accordance with the gas laws and the amount of pressure it exerts equates to the partial pressure of the water vapor components in the gas mixture, as defined by Dalton's law [37].

To set a reference between capacitive sensors and optical sensors when the soil is saturated, the air in holes inside the soil (and therefore the cavity created by the optical sensor) is saturated too, and as a conclusion, both of the sensors show 100% of humidity and relative humidity, respectively.

As can be seen in Figures 8 and 9, both of the sensors work similarly in high humidity scenarios. The difference arises when the soil approaches to 0% humidity. Due to the nature of the optical sensor

and its operation principle measuring the water present in air it becomes impossible to reach 0% of relative humidity while capacitive sensor can reach such low values. As a conclusion, the optical sensor is not suitable for environments of very low humidity (under 15%).

Additionally, as can be noticed in Figure 8, both of the graphs present different x-axe length. This is due to the fact that, Soil2, as a result of its composition, is able to retain more water than Soil1, and therefore, an additional 300 mL was needed to reach the saturation stage.

The last difference in the results can be seen in the X axis of Figure 7a,b. Figure 7a shows the results of the natural evaporation process in indoor conditions. As it can be seen, there is a very slow kinetic and humidity decreased ~30% in 12 days. To accelerate this process, for Soil2 measurements (Figure 7), two heating fans where placed close to the sample. Temperature variations were compensated as explained before. A significant difference can be seen as the humidity decreased ~60% in 9 days.

An important aspect to comment is the difficulty to perform accurate gravimetric measurements as they are very dependent on the experiment conditions. It has been demonstrated that the optical sensor can be used as a reference to measure moisture above 15%, avoiding imprecise gravimetric measurements. As previously commented, below this level, optical sensor decreases its sensitivity due to its measuring working principle.

As commented in Section 3.3, soil temperature close to the optical sensor location has been monitored. Results shown in Figure 6 show a good agreement between the dynamics of humidity and temperature. Temperature shows oscillations of 2 °C depending on the time of the day. During day hours temperature rises and when sun sets (soil sample was at direct exposition of sun light) it decreases ~2 °C. Humidity results follows the same trend, showing great variations (decreasing humidity) during the day and slower ones at night. These variations agree temporarily with temperature, showing bigger slopes during sunshine hours.

5. Conclusions

In this study, a fiber optical sensor based in a microstructured optical fiber has been proposed and demonstrated for first time for soil moisture measurements. The optical sensing head is based on a Fabry-Pérot cavity made of a microstructured optical fiber with a SnO_2 sputtering thin film acting as sensitive layer and it was temperature and humidity characterized in a climatic chamber before its installation in soil. A comparison between a commercial capacitive FDR and the optical sensor has been carried out in two different types of soils during two weeks. The optical interrogation of the MOF–FP sensing head was carried out through the FFT technique, which avoids noise and amplitude variations' influence and enables multiplex several sensors within a single optical interrogator's channel. Results show a good agreement between capacitive and optical measurements in the range 15–100% humidity and also match with gravimetric analysis. For humidity below 15%, the optical sensor's sensitivity decreases significantly. Soil moisture can be measured with MOF–FP sensors with the advantages that they offer in comparison with traditional capacitive sensors: immunity to temperature variations (compensated), point measurements (against field measurements), and high multiplexing capability.

These particular characteristics lead to a new set of local applications that capacitive sensors are unable to attend, such as monitoring the soil moisture distribution (radial distance) in a local irrigation point performing measurements each centimeter. Moreover, due to the versatility of the sensing heads to be customized depending on the target application, different sensing heads with different purposes (such as dissolved pollutants, volatile organic compounds, solid or dissolved ferromagnetic elements can be detected by the correctly selection of the deposited chemical agent) can be multiplexed within the same optical interrogator, reducing the relative economic cost of the system and leading to complex real time (also high sampling rate applications) multiparameter monitoring schemes.

Author Contributions: A.L.A. performed the experiments and wrote the paper; D.Y. performed the experiments; D.L.-T., C.E. and F.J.A. designed and deposited the SnO_2 sensitive layer; M.A.C.-B., J.J.L., and M.L.-A. conceived and designed the experiments and analyzed the results; R.J., J.-L.A. and P.R. designed and fabricated the MOF.

Funding: This work was supported by the Spanish Government projects TEC 2016-76021-C2-1-R, TEC2016-78047-R, TEC2016-79367-C2-2-R, Innocampus and the Cost Action MP 1401, as well as to the AEI/FEDER Funds.

Acknowledgments: The authors are grateful to D. Erro and R.A. Perez-Herrera. We also thank the Spanish Government projects TEC 2016-76021-C2-1-R, TEC2016-78047-R, TEC2016-79367-C2-2-R, Innocampus and the Cost Action MP 1401, as well as to the AEI/FEDER Funds. Also, the authors thank to the Agricultural Engineering School for sharing the Hydraulic Laboratory.

Conflicts of Interest: The authors declare no conflict of interest.

References

1. Rodríguez-Iturbe, I. Ecohydrology: A hydrologic perspective of climate-soil-vegetation dynamics. *Water Resour. Res.* **2000**, *36*, 3–9. [CrossRef]
2. Eagleson, P.S. *Ecohydrology*; Cambridge University Press: Cambridge, UK, 2002.
3. Bull, C.R. A review of sensing techniques which could be used to generate images of agricultural and food materials. *Comput. Electron. Agric.* **1993**, *8*, 1–29. [CrossRef]
4. Nolz, R.; Kammerer, G.; Cepuder, P. Calibrating soil water potential sensors integrated into a Wireless monitoring network. *Agric. Water Manag.* **2013**, *116*, 12–20. [CrossRef]
5. Loaiza-Usuga, J.C.; Pauwels, V.R.N. Utilización de sensores de humedad para la determinación del contenido de humedad del suelo: ecuaciones de calibración. *Suelos Ecuatoriales SCCS* **2008**, *38*, 24–33.
6. WMO. Guide to Hydrological Practices. Available online: http://www.whycos.org/hwrp/guide/chapters/english/original/WMO168_Ed2008_Vol_I_Ch4_Up2008_en.pdf (accessed on 14 April 2008).
7. Sharma, R.K.; Gupta, A.K. Continuous wave acoustic method for determination of moisture content in agricultural soil. *Comput. Electron. Agric.* **2010**, *73*, 105–111. [CrossRef]
8. Christy, C.D. Real-time measurement of soil attributes using on-the-go near infrared reflectance spectroscopy. *Comput. Electron. Agric.* **2008**, *61*, 10–19. [CrossRef]
9. Wang, Y.B.; Huang, T.Y.; Liu, J.; Lin, Z.L.; Li, S.H.; Wang, R.J.; Ge, Y.J. Soil pH value, organic matter and macronutrients contents prediction using optical diffuse reflectance spectroscopy. *Comput. Electron. Agric.* **2015**, *111*, 69–77. [CrossRef]
10. Visconti, F.; De Paz, J.M.; Martínez, D.; Molina, M.J. Laboratory and field assessment of the capacitance sensors Decagon10HS and 5TE for estimating the water content of irrigated soils. *Agric. Water Manag.* **2014**, *132*, 111–119. [CrossRef]
11. Topp, G.C. State of the art of measuring soil water content. *Hydrol. Processes* **2003**, *17*, 2993–2996. [CrossRef]
12. Dobriyal, P.; Qureshi, A.; Badola, R.; Hussain, S.A. A review of the methods available for estimating soil moisture and its implications for water resource management. *J. Hydrol.* **2012**, *458–459*, 110–117. [CrossRef]
13. Alwis, L.; Sun, T.; Grattan, K.T.V. Optical fibre-based sensor technology for humidity and moisture measurement: Review of recent progress. *Measurement* **2013**, *46*, 4052–4074. [CrossRef]
14. Pinto, A.M.R.; Lopez-Amo, M. Photonic crystal fibers for sensing applications. *J. Sens.* **2012**. [CrossRef]
15. Monro, T.M.; Warren-Smith, S.; Schartner, E.P.; François, A.; Heng, S.; Ebendorff-Heidepriem, H.; Afshar, S. Sensing with suspended-core optical fibers. *Opt. Fiber Technol.* **2010**, *16*, 343–356. [CrossRef]
16. Frazao, O.; Santos, J.L.; Araújo, F.M.; Ferreira, L.A. Optical sensing with photonic crystal fibers. *Laser Photonics Rev.* **2008**, *2*, 449–459. [CrossRef]
17. Frazao, O.; Silva, S.F.O.; Viegas, J.; Baptista, J.M.; Santos, J.L.; Kobelke, J.; Schuster, K. All fiber Mach–Zehnder interferometer based on suspended twin-core fiber. *IEEE Photonics Technol. Lett.* **2010**, *22*, 1300–1302. [CrossRef]
18. Webb, A.S.; Poletti, F.; Richardson, D.J.; Sahu, J.K. Suspended-core holey fiber for evanescent-field sensing. *Opt. Eng.* **2007**, *46*, 010503. [CrossRef]
19. Aldaba, A.L.; Lopez-Torres, D.; Elosua, C.; Auguste, J.L.; Jamier, R.; Roy, P.; Arregui, F.J.; Lopez-Amo, M. SnO_2-MOF-Fabry-Perot optical sensor for relative humidity measurements. *Sens. Actuators B* **2018**, *257*, 189–199. [CrossRef]
20. Choi, H.Y.; Park, K.S.; Park, S.J.; Paek, U.C.; Lee, B.H.; Choi, E.S. Miniature fiber-optic high temperature sensor based on a hybrid structured Fabry–Perot interferometer. *Opt. Lett.* **2008**, *33*, 2455–2457. [CrossRef] [PubMed]

21. Chen, L.H.; Li, T.; Chan, C.C.; Menon, R.; Balamurali, P.; Shaillender, M.; Neu, B.; Ang, X.M.; Zu, P.; Leong, K.C. Chitosan based fiber-optic Fabry–Perot humidity sensor. *Sens. Actuators B* **2012**, *169*, 167–172. [CrossRef]
22. Mathew, J.; Semenova, Y.; Rajan, G.; Farrell, G. Humidity sensor based on photonic crystal fibre interferometer. *Electron. Lett.* **2010**, *46*, 1341–1343. [CrossRef]
23. Arregui, F.J. *Sensors Based on Nanostructured Materials*; Springer: New York, NY, USA, 2009.
24. Stowell, M.; Müller, J.; Ruske, M.; Lutz, M.; Linz, T. RF-superimposed DC and pulsed DC sputtering for deposition of transparent conductive oxides. *Thin Solid Films* **2007**, *515*, 7654–7657. [CrossRef]
25. Ou, J.Z.; Yaacob, M.H.; Campbell, J.L.; Breedon, M.; Kalantar-Zadeh, K.; Wlodarski, W. H_2 sensing performance of optical fiber coated with nano-platelet WO_3 film. *Sens. Actuators B* **2012**, *166*, 1–6. [CrossRef]
26. Dai, J.; Yang, M.; Yu, X.; Lu, H. Optical hydrogen sensor based on etched fiber Bragg grating sputtered with P_d/Ag composite film. *Opt. Fiber Technol.* **2013**, *19*, 26–30. [CrossRef]
27. Laylor, H.M.; Calvert, S.; Taylor, T.; Schulz, W.; Lumsden, R.; Udd, E. Fiber optic grating moisture and humidity sensors. *Proc. SPIE* **2002**, *4694*, 210–217.
28. Goh, L.S.; Kumekawa, N.; Watanabe, K.; Shinomiya, N. Hetero-core spliced optical fiber SPR sensor system for soil gravity water monitoring in agricultural environments. *Comput. Electron. Agric.* **2014**, *101*, 110–117. [CrossRef]
29. Yeo, T.L.; Sun, T.; Grattan, K.T.V. Fibre-optic sensor technologies for humidity and moisture measurement. *Sens. Actuators A* **2008**, *144*, 280–295. [CrossRef]
30. Sanchez, P.; Zamarreño, C.R.; Hernaez, M.; Matias, I.R.; Arregui, F.J. Optical fiber refractometers based on Lossy Mode Resonances by means of SnO_2 sputtered coatings. *Sens. Actuators B* **2014**, *202*, 154–159. [CrossRef]
31. Schmid, W. Consumption Measurements on SnO_2 Sensors in Low and Normal Oxygen Concentration. Ph.D. Thesis, Universität Tübingen, Baden-wurttemberg state tubingen, Germany, March 2004.
32. Yoshino, T.; Kurosawa, K.; Itoh, K.; Ose, T. Fiber-optic Fabry-Perot interferometer and its sensor applications. *IEEE Trans. Microwave Theory Tech.* **1982**, *30*, 1612–1621. [CrossRef]
33. Leandro, D.; Bravo, M.; Ortigosa, A.; Lopez-Amo, M. Real-time FFT analysis for interferometric sensors multiplexing. *J. Lightwave Technol.* **2015**, *33*, 354–360. [CrossRef]
34. Lopez-Aldaba, A.; Auguste, J.L.; Jamier, R.; Roy, P.; Lopez-Amo, M. Simultaneous strain and temperature multipoint sensor based on microstructured optical fiber. *J. Lightwave Technol.* **2018**, *36*, 910–916. [CrossRef]
35. Aldaba, A.L.; Lopez-Torres, D.; Elosua, C.; Auguste, J.L.; Jamier, R.; Roy, P.; Arregui, F.J.; Lopez-Amo, M. Real Time Measuring System of Multiple Chemical Parameters Using Microstructured Optical Fibers Based Sensors. *IEEE Sens. J.* **2018**, *18*, 5343–5351. [CrossRef]
36. Soil Survey Staff. *Soil Taxonomy: A Basic System of Soil Classification for Making and Interpreting Soil Surveys*, 2nd ed.; Natural Resources Conservation Service. U.S. Department of Agriculture: Washington, DC, USA, 1999.
37. Wiederhold, P.R. *Water Vapor Measurement: Methods and Instrumentation*; CRC Press: Boca Raton, FL, USA, 1997.

6.4. Conclusiones

Gracias al patrón interferométrico con forma sinusoidal que se obtiene de la señal óptica reflejada del sensor Fabry Pèrot, es posible aplicar la técnica basada en la FFT para la caracterización e interrogación del sensor. De esta forma, variando la cavidad del interferómetro se pueden multiplexar sensores reduciendo el coste final del sistema.

Gracias a la baja selectividad de los óxidos metálicos depositados, se puede desarrollar un sistema compuesto por varios sensores capaces de detectar diferentes parámetros como por ejemplo humedad, temperatura, VOCs, gases… Todos estos sensores pueden ser multiplexados en un mismo canal, lo que hace que la aplicación final tenga un gran potencial en el mercado.

El comportamiento del sensor cuando es utilizado para medir la humedad de diferentes suelos puede ser comparado con los sensores capacitivos en un rango de humedad comprendido entre el 15% y el 100%. Además, gracias a la utilización de la FFT como técnica de interrogación del sensor, es posible multiplexar varios sensores para realizar medidas puntuales. Esto es una ventaja respecto a los sensores capacitivos, los cuales sólo pueden realizar medidas de área.

Dadas las sensibilidades obtenidas con los sensores desarrollados y una vez probada la posibilidad de ser multiplexados, el interés que pueden despertar los sistemas que son capaces de unir estas dos características es muy alto y abre una nueva línea de investigación futura muy atractiva y prometedora.

Capítulo 7

Conclusiones y posibles líneas futuras de trabajo

En este último capítulo, se presentan las principales conclusiones que se derivan de los trabajos y experimentos desarrollados durante esta tesis. Se expondrán las conclusiones más relevantes de cada uno de los capítulos, así como unas conclusiones generales que engloben todo el trabajo realizado. Por último, se describirán las posibles futuras líneas de investigación que pueden tener como punto de partida esta tesis, así como las posibles mejoras que se puedan aplicar a los sensores o montajes que aquí se presentan, con la idea de mejor sus características.

7.1. Conclusiones

Después del análisis presentado en el segundo capítulo de esta tesis doctoral sobre el estado del arte de los sensores de fibra óptica basados en fibras micro estructuradas para la detección de gases y VOCs, se observó que estas fibras ofrecían un enorme potencial para desarrollar este tipo de sensores debido a los siguientes factores. Su estructura agujereada (en el caso de las PCFs) o los agujeros de aire que rodean el núcleo (en el caso de las SSCs), podían ser utilizados de forma ventajosa para el sensado de gases o VOCs. Por ejemplo, las moléculas de los gases y VOCs, que se querían detectar, podían penetrar en la estructura interna de la fibra lo que favorecía la interacción con el campo evanescente de la luz guiada por la fibra; también, se podían realizar montajes, los cuales potenciaban que los modos de mayor orden viajaran por el revestimiento de la fibra, pudiendo detectar con mayor sensibilidad variaciones en el índice de refracción externo del medio que rodeaba a los sensores. De este estudio también se derivó una idea muy importante: una de estas estructuras era la formada por dos fibras SMFs empalmadas a una sección de SC-PCF, que fue la elegida como punto de partida de esta tesis.

Otra conclusión importante que se extrajo de los artículos científicos presentados en el segundo capítulo fue, la mejora que se obtenía en la sensibilidad del sensor, cuando una película de un material sensible era depositada para detectar un parámetro determinado (gases o VOCs). A su vez, otro factor determinante relacionado con la película de material sensible depositada era su espesor, siendo clave su estudio en el proceso de optimización de la sensibilidad del sensor.

En el tercer capítulo de la tesis, se demostró que era posible una mejora de la sensibilidad de los sensores previos, basados en un interferómetro MZ utilizando una SC-PCF, depositando una película polimérica (formada por PAH y PAA) o una película formada por óxidos metálicos (SnO_2). La elección de una técnica que permitiera controlar con exactitud el espesor de la película depositada fue clave para conseguir la optimización de sensibilidad final; las técnicas elegidas, *LbL y sputtering*, garantizaron esta condición. Además, el sensor, cuya película estaba formada por el óxido metálico SnO_2, mostró una mayor sensibilidad a los cambios de humedad relativa.

La sensibilidad del sensor previamente descrito fue mejorada, en el capítulo cuarto, gracias a la utilización de una nueva fibra micro estructurada (fibra SSC). Para estudiar únicamente la influencia de la estructura propuesta en la sensibilidad del sensor, una película compuesta por el mismo óxido metálico y con el mismo espesor que la del sensor del capítulo anterior, fue depositada en los agujeros de aire de la fibra SSC. La sensibilidad y respuesta dinámica del sensor mejoraron debido a dos factores: el primero, las estructuras basadas en fibras SSC consiguen un mayor acople de la señal óptica que viaja por el núcleo al campo evanescente; el segundo, gracias al tamaño de los agujeros de dichas fibras, existe una mayor superficie para que el campo evanescente pueda interactuar con las moléculas de agua. Además, al tener estos agujeros de la fibra un mayor tamaño, la difusión de dichas moléculas se lleva a cabo de una manera más rápida, lo que mejora los tiempos de respuesta y de recuperación del sensor.

Un estudio teórico del campo eléctrico y magnético de la luz guiada por diferentes estructuras de fibras SSC, como el presentado en el quinto capítulo de la tesis utilizando el software COMSOL©, es necesario realizarlo para obtener la mejor sensibilidad posible para el sensor. Gracias a este estudio se pudo concluir que, en las fibras cuyos núcleos tenían dimensiones más pequeñas, el acople de la luz era inferior. Por tanto, la potencia óptica acoplada también era menor. Sin embargo, el haz de luz viajaba menos confinado, lo que provocaba que el porcentaje de campo evanescente que podía interactuar con la película depositada fuera mayor. En las fibras SSC, donde las dimensiones de los núcleos eran mayores, el efecto fue el contrario. La conclusión que se obtuvo fue que, para obtener una sensibilidad óptima, era necesario llegar a un compromiso entre la potencia óptica acoplada a la fibra y el campo evanescente que podía generar dicha potencia acoplada. Otra importante idea que se derivó de este estudio fue que, cuando una película era depositada en los agujeros de una fibra SSC, la luz ya no se guiaba por la fibra óptica de manera convencional. En este caso, la película depositada pasaba a ser la nueva guía onda. Considerando todas estas conclusiones, se pudo optimizar la sensibilidad de dos sensores, uno para amoniaco y otro para etanol, con unos resultados muy prometedores.

Por último, en el capítulo sexto, se corroboró el buen comportamiento de los sensores desarrollados cuando fueron multiplexados gracias a la aplicación de la FFT para la caracterización e interrogación del sensor. De esta forma, variando únicamente la longitud de la cavidad del interferómetro, se pudieron

multiplexar diferentes sensores, reduciendo de esta manera el coste final del sistema. Además, la baja selectividad que ofrecían los óxidos metálicos fue también aprovechada para desarrollar sensores capaces de detectar diferentes parámetros como la humedad, la temperatura, los VOCs o los gases. Uniendo estas dos ideas, se consiguió desarrollar un sistema de multiplexación multiparamétrico. Por otro lado, la respuesta de dicho sensor se comparó con un sensor capacitivo exponiéndolo a cambios de humedad en diferentes tipos de suelos. Se concluyó que, en un rango comprendido entre un 15%-100%RH, el sensor desarrollado en esta tesis tenía un comportamiento análogo.

Resumiendo, esta tesis ha contribuido al desarrollo y a la mejora de los sensores y aplicaciones basadas en MOFs para la detección de gases y VOCs. Los resultados obtenidos de dichos sensores y aplicaciones, durante el desarrollo de esta tesis, sumados a los previamente publicados por la comunidad científica, permiten ser optimistas pensando que las MOFs pueden tener un futuro muy prometedor dentro del campo de los sensores de fibra óptica.

7.2. Líneas futuras de trabajo

Una vez que las conclusiones que se derivan de esta tesis han sido expuestas, se proponen algunas posibles líneas futuras de trabajo que pueden ser interesantes para futuros trabajos.

Debido a la importancia y efecto que tiene sobre la sensibilidad final del sensor, una posible línea futura de trabajo a explotar es el desarrollo de nuevas estructuras sensoras, pero en términos de la MOFs utilizada. Debido a la posibilidad de desarrollar una MOFs eligiendo las dimensiones de los agujeros de aire, la distancia existente entre ellos o las dimensiones del núcleo, estos parámetros pueden ser ajustados y seleccionados para mejorar las prestaciones y sensibilidades de los sensores previamente publicados. Además, nuevas estructuras híbridas formadas por interferómetros Fabry-Pèrot o Mach-Zehnder, fibras MOFs a las que se les realizan deformaciones en sus secciones (*tapers* o el colapso de sus agujeros de aire) pueden ser desarrollados con el objetivo de seguir mejorando la sensibilidad de los sensores. Previamente, debido a toda la información que puede aportar sobre la estructura, sería aconsejable realizar un

análisis teórico de la potencia guiada por la fibra y su campo evanescente (utilizando COMSOL©) para garantizar que pueda reportar buenos resultados.

Otra línea de investigación que se propone es la del estudio de nuevos materiales sensibles que puedan ser depositados en las MOFs. Al depositar estos materiales, existe la posibilidad de que la sensibilidad del sensor aumente o que incluso, nuevos parámetros puedan ser detectados, ampliando de esta manera el número de aplicaciones en las que pueden ser utilizados.

Otro aspecto que puede ser mejorado en el futuro es la selectividad de los óxidos metálicos. Existen ya ciertos estudios que, sin tener que trabajar con técnicas de post procesado, consiguen que los sensores sean selectivos por medio de la funcionalización de la película de material sensible. Esta idea podía ser muy interesante para el caso expuesto de los sensores multiplexados, ya que, se podría realizar una aplicación en la que cada sensor sólo fuera sensible a un parámetro en concreto, pudiendo trabajar además en tiempo real.

Relacionado con la capacidad que tienen los sensores desarrollados en esta tesis de ser multiplexados, reducir las pérdidas provocadas por los empalmes entre las fibras puede ser un punto muy interesante; si esto se consigue, la necesidad de introducir un amplificador óptico puede ser eliminada. De esta manera, el coste final del sistema se abarataría en gran medida. Otro parámetro que se puede estudiar para optimizar la multiplexación de los sensores, es el de realizar dispositivos con cavidades interferométricas de longitudes más próximas entre sí; de esta forma, se podrían multiplexar más sensores, manteniendo el mismo rango espectral de funcionamiento de la fuente óptica utilizada.

Chapter 7

Conclusions and future open research lines

In this last chapter, the main conclusions that are inferred from the works and experiments developed during this thesis are presented. The most relevant conclusions of every chapter will be presented, as well as some general conclusions that encompass all the work carried out. Finally, future open research lines will be also described.

7.1 Conclusions

After the analysis of the state of the art of the optical fibre sensors based on MOFs used to detect gases and VOCs, it was observed that this type of fibres could offer an enormous potential to develop this kind of sensors. Its holey structure (in the case of PCFs) or the air holes surrounding the core (in the case of SSCs), could be used advantageously for gas or VOCs sensing. For example, the molecules of the gases or VOCs could penetrate in the inner structure of the fibres encouraging the interaction with the evanescent field of the light guided through the optical fibre; moreover, it was possible to develop set ups, which enhanced that, the higher order modes travelled through the cladding of the fibre. Due to this, the shifts of the refractive index of the surrounding medium of the sensor could be detected with higher sensitivity. Two SMF fibres spliced to a section of SC-PCF formed one of these structures; this one was chosen as the starting point of this thesis.

Another important conclusion that can be inferred from the scientific papers presented in the second chapter of this thesis was the improvement of the sensor sensitivity when a thin film of a sensitive material was deposited in order to detect a certain parameter (in this case, gases or VOCs). In turn, another key factor that it should be taken into account was its thickness. The study of this parameter was a very important point in the process of the optimization of the sensor sensitivity.

In the third chapter of this thesis, it was presented the sensitivity optimization of two humidity sensors based on MZ interferometer using a SC-PCF. Two different thin films, one of them based on polymers (PAH/PAA) and the other one based on metallic oxides (SnO_2), were deposited along the section of the SC-PCF. The opportunity to select a technique that allowed controlling thickness of the nano film deposited accurately, was another important parameter to achieve an optimal sensor sensitivity; the chosen techniques, *LbL and sputtering*, guaranteed this condition. In addition, the sensor whose thin film was based on SnO_2 showed a higher sensitivity to relative humidity changes.

With the goal of improving the previous sensor sensitivity, in the fourth chapter of this thesis, a new sensor based on SSC fibre was proposed. In order to study only the influence of the structure on the sensor sensitivity, a nanofilm

with the same parameters in terms of thickness that the previous SC-PCF sensor, was deposited in and on the SSC section. This sensor showed a better sensitivity and dynamic response times due mainly two reasons: firstly, the structures based on SSC fibres, achieve a higher coupling of the optical signal that travels through the fibre to the evanescent field; secondly, thanks to the hole dimensions of SSC fibres, there is a greater surface area so that the evanescent field can interact with the water molecules. Furthermore, as the SSC holes have higher dimensions, the diffusion of water molecules is performed in a faster way, improving the response and recovery times of the sensor.

The theoretical study of the electric and magnetic field of light guided by different SSC fibre structures was analysed and presented in the fifth chapter of the thesis, using the COMSOL © software. Thanks to this tool, it was possible to conclude that in fibres with smaller core dimensions, the coupling of the light was lower; therefore, the value of the optical power coupled is also smaller. However, the light beam travelled less confined, which caused that a greater part of the evanescent field could interact with the deposited film. In SSC fibres, due to the dimensions of the core are higher, the effect is opposite. In view of the above, to obtain an optimal sensor sensitivity it is necessary to reach a trade-off between the optical power coupled into the optical fibre and the evanescent field that this optical power can generate. Another important conclusion that it is inferred from the theoretical study is that when a thin film is deposited into the holes of an SSC fibre, the optical fibre does not guide the light in a conventional manner; in this case, the deposited thin film is the new waveguide. Considering every conclusion obtained of the study, the sensitivity of two sensors, one for ammonia and the other one for ethanol, could be optimized with very promising results.

Finally, in the sixth chapter, it was confirmed the good behavior of the sensors developed when they were multiplexed thanks to the use of the FFT for the characterization and interrogation of the sensor. In this way, only varying the interferometer cavity, different sensors could be multiplexed reducing the final cost of the system. The low selectivity offered by metal oxides was also used to develop sensors capable of detecting different parameters such as humidity, temperature, VOCs or gases. Combining these two ideas, it was possible to develop a multiparameter system with multiplexed sensors. The behavior of this sensor was also studied to detect variations of the moisture of different soils. Its

performance was compared with a commercial capacitive soil moisture sensor concluding that, in a range between 15% -100%RH, the behavior of this sensor could be considered similar.

Briefly summarizing, this thesis has contributed to the development and improvement of sensors and applications based on MOFs for the detection of gases and VOCs. The sensors and applications results achieved, during the development of this thesis, allow to be optimistic thinking that MOFs may have a promising future within the field of fibre optics sensors.

7.2 Future open research lines

Once the main conclusions of this thesis have been exposed and analysed, some open research lines are suggested in the following paragraphs and should be considered for future works.

The first open research line proposed is the development of a new sensor structure, but in terms of the MOFs used, because of the importance and effect that it has on the final sensitivity of the sensor. Due to this it is possible to develop MOFs choosing the dimensions of the air holes, the distance between them and the dimensions of the core. These parameters can be selected and adjusted to develop a new device that improves the features and sensitivities of previously published sensors. Moreover, new hybrid structures based on cascaded Fabry-Pérot, Mach-Zehnder interferometers or MOFs with deformations in its structure as tapers or collapsed regions can lead to new interferometric devices with improved features. Previously, due to the information that it can be inferred about the structure, it would be advisable to carry out a theoretical analysis of the power guided by the fibre and its evanescent field (using COMSOL© software) in order to ensure the proper behavior of the sensor.

Another proposed line of research is the study of new sensitive materials that they can be deposited in MOFs. Depositing these materials, there is a possibility that the sensor sensitivity may increase or that even new parameters may be detected (different gases, for example).

Another aspect that can be improved in the future is the selectivity of metal oxides. Currently, there are several works in the bibliography that, avoiding the necessity to work with post-processing techniques, have achieved that the sensor is only sensitive to one parameter by means of the functionalization of the sensitive material thin film. This idea could be very interesting for the exposed case of multiplexed sensors because an application could be developed in such a way that the sensors were only sensitive to a particular parameter.

Regarding to the multiplexing capability of the studied sensors in this thesis, the improving of the sensors splice losses is of great interest in order to avoid the use of optical amplification reducing in this manner the final cost of the system. Finally, another parameter that could be studied to optimize the multiplexing features of the sensors is the length of the interferometric cavities. If theses lengths of the different sensors are very close, more sensors could be multiplexed, in the same frequency range.

Anexo I

Estudio de las propiedades de diferentes recubrimientos nano estructurados

Este anexo de la tesis ha sido utilizado para presentar el estudio y caracterización de una pareja de polímeros formada por el PSP y el PAH. La idea inicial fue depositar estos dos polímeros mediante la técnica LbL para fabricar una película capaz de detectar cambios de humedad, pero al estudiar sus características morfológicas (la rugosidad, ángulos de contacto o espesor, se descubrió) se observaron unos resultados que podían tener relevancia para la comunidad científica. Es por eso, por lo que esta vía se siguió estudiando y los resultados obtenidos se presentan en el siguiente anexo.

I.1 Introducción

Cabe recordar que uno de los primeros retos que se tuvieron que afrontar en esta tesis, fue la búsqueda de una pareja de polímeros higroscópicos que tuvieran una respuesta óptima a los cambios de humedad. Como bien se ha explicado en la contribución científica presentada en el capítulo 3, esta pareja fue la formada por el PSP y el PAA. Pero no fue la única estudiada.

El primer paso que se dio en la búsqueda de dicha pareja fue analizar, comprender y estudiar un artículo publicado por Gero Decher, Nejla Cini et al. [113]. En este artículo se exponía la idea de que dos determinados polímeros, poly(sodium phosphate) (PSP) y poly(allylamine hydrochloride) (PAH), tenían un comportamiento anómalo cuando se depositaban mediante la técnica *LbL*; con unas condiciones específicas, al aumentar el número de parejas de capas depositadas y en consecuencia, el espesor de la película que formaba esta pareja de polímeros, su rugosidad aumentaba. Este hecho hacía replantearse las reglas generales de la técnica *LbL* ya que, hasta ese momento, al aumentar el número de parejas de capas de una determinada película polimérica, su espesor aumentaba, pero la rugosidad final obtenida sufría el efecto contrario, disminuía. Por esta razón, se consideró que podía ser una buena opción estudiar su comportamiento frente a la humedad por el potencial e interés que suscitaba y ofrecía esta nueva característica. Hay que aclarar que, al aumentar la rugosidad de la película, las moléculas de agua pueden penetrar e interactuar con dicha película con mayor facilidad.

I.1.1 Estudio de la pareja de polímeros PSP/PAH frente a la humedad depositada mediante la técnica *LbL*

Para estudiar el comportamiento de la película formada por PSP/PAH frente a la humedad, se reprodujeron y construyeron, bajo las condiciones expuestas en [113], dos tandas distintas de sensores con las siguientes características siguiendo el método *LbL*:

- 20, 40, 60, 80 y 100 parejas de capas de PSP/PAH ajustando su molaridad a 10^{-3}.

- 20, 40, 60, 80 y 100 parejas de capas de PSP/PAH ajustando su molaridad a 10^{-4}.

Cada una de ellas se depositó sobre una fibra SC-PCF en cuyos extremos se habían empalmado dos SMF, es decir, sobre la misma estructura que se expuso en la primera contribución científica de la tesis. Los mejores resultados que se obtuvieron, en término de potencia óptica relativa reflejada, fueron para los casos de 80 parejas de capas cuando la molaridad de la pareja PSP/PAH fue ajustada a 10^{-4} M (ver Figura 6.1) y 40 parejas de capas para la tanda donde la molaridad se ajustó a 10^{-3} M (ver Figura 6.2). Como se aprecia en ambas figuras, la respuesta del sensor no puede ser considerada óptima debido a que no sigue los cambios de humedad de la cámara climática a lo largo del tiempo. Además, la línea base tiene una deriva al igual que el máximo de humedad en ambos casos. También hay que destacar que la señal es muy ruidosa.

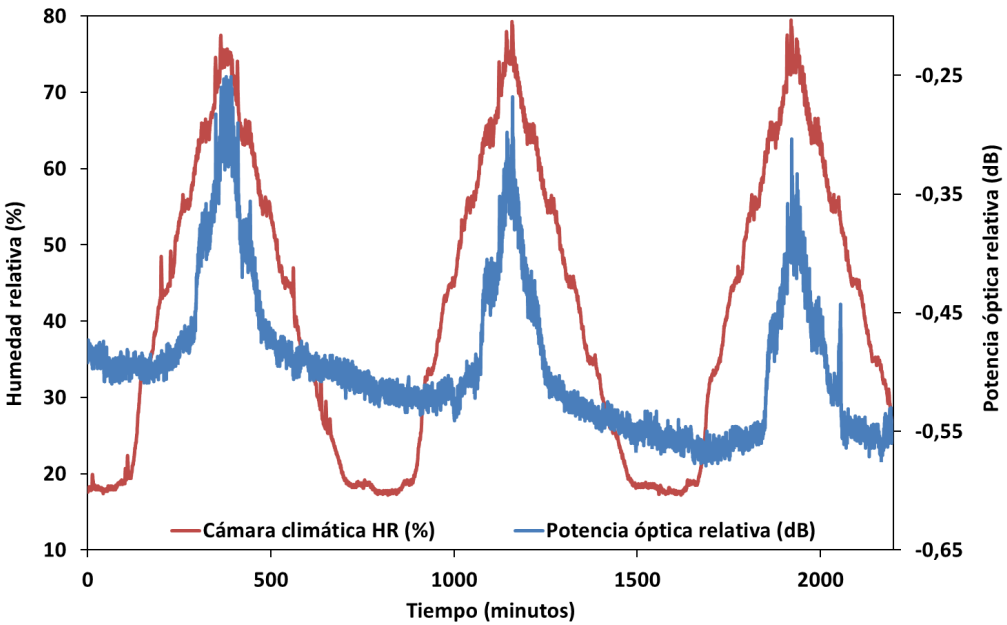

Figura Anexo I. 1 *Variaciones en la potencia óptica medida cuando una película de 80 parejas de capas fue depositada con una molaridad de 10^{-4}.*

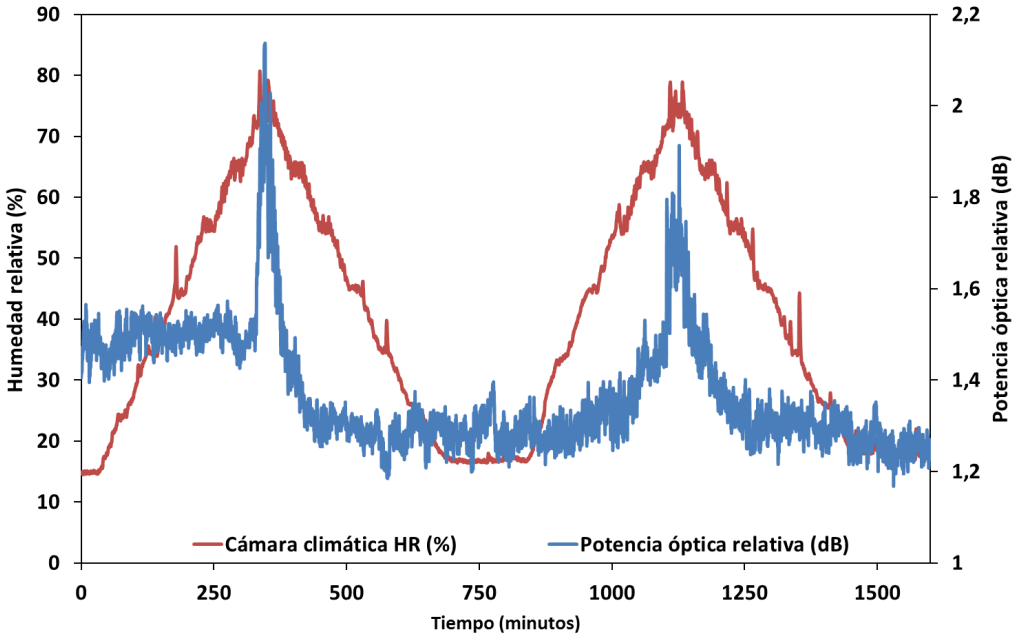

Figura Anexo I. 2 *Variaciones en la potencia óptica medida cuando una película de 40 parejas de capas fue depositada con una molaridad de* 10^{-3}.

Por todas estas razones, se desechó la opción de seguir trabajando con esta pareja de polímeros para desarrollar sensores de humedad. Pero se pensó que, debido al importante avance hallado por Decher en su artículo, se podía estudiar el comportamiento de esta curiosa pareja de polímeros cuando eran fabricadas con otras técnicas de deposición.

El primer paso que se dio fue intentar reproducir los resultados obtenidos por Decher, depositando películas de PSP/PAH sobre portaobjetos mediante la técnica spray *LbL* (pulverización *LbL*) que es la que se utilizó en el trabajo de referencia. La rugosidad y el espesor de las diferentes muestras fueron medidos con un microscopio de fuerza atómica (sus siglas en inglés son AFM) corroborando las conclusiones de Decher. Una vez llegados a este punto, se hizo un nuevo estudio comparativo entre la técnica *LbL* tradicional y la ya comentada técnica spray *LbL*. Para esta ocasión, se volvieron a construir otras dos nuevas tandas con idénticos parámetros a los expuestos anteriormente, con la salvedad del ya comentado cambio de técnica de deposición. Además, para completar y dar más rigor científico al estudio, se midió el ángulo de contacto de cada una de

las diferentes películas fabricadas para poder calificar si el recubrimiento era hidrofílico o hidrofóbico.

La conclusión más importante que se deriva de todo el estudio realizado fue que, utilizando la técnica de deposición *LbL*, con ambas molaridades, 10^{-3} y 10^{-4}, la rugosidad aumentaba conforme el espesor aumentaba. Se confirmaban de esta forma los resultados de Decher, pero extrapolándolos a otra técnica de deposición. Además, muchas de las películas estudiadas tenían la propiedad de ser superhidrofílicas, ya que sus ángulos de contacto medidos con una gota de agua eran cero, lo que quería decir que tenían una gran afinidad a las moléculas de H_2O.

Todo este estudio y los resultados que se derivan del mismo, quedaron reflejados y explicados de una forma más extensa y detallada en la contribución científica que lleva por nombre: *"Comparative study of layer-by-layer deposition techniques for poly(sodium phosphate) and poly(allylamine hydrochloride)"* que fue publicada en la revista *"Nanoscale Research Letters"* .

Nanoscale Research Letters
a SpringerOpen Journal

NANO EXPRESS Open Access

Comparative study of layer-by-layer deposition techniques for poly(sodium phosphate) and poly (allylamine hydrochloride)

Cesar Elosua*, Diego Lopez-Torres, Miguel Hernaez, Ignacio R Matias and Francisco J Arregui

Abstract

An inorganic short chain polymer, poly(sodium phosphate), PSP, together with poly(allylamine hydrochloride), PAH, is used to fabricate layer-by-layer (LbL) films. The thickness, roughness, contact angle, and optical transmittance of these films are studied depending on three parameters: the precursor solution concentrations (10^{-3} and 10^{-4} M), the number of bilayers deposited (20, 40, 60, 80, and 100 bilayers), and the specific technique used for the LbL fabrication (dipping or spraying). In most cases of this experimental study, the roughness of the nanofilms increases with the number of bilayers. This contradicts the basic observations made in standard LbL assemblies where the roughness decreases for thicker coatings. In fact, a wide range of thickness and roughness was achieved by means of adjusting the three parameters mentioned above. For instance, a roughness of 1.23 or 205 nm root mean square was measured for 100 bilayer coatings. Contact angles close to 0 were observed. Moreover, high optical transmittance is also reported, above 90%, for 80 bilayer films fabricated with the 10^{-4} M solutions. Therefore, these multilayer structures can be used to obtain transparent superhydrophilic surfaces.

Keywords: Layer-by-layer, Dipping and spray deposition, Inorganic polymer, Hydrophilic film, Functionalized surfaces

Background

Among different deposition techniques, the layer-by-layer (LbL) method has focused the attention of a large number of research groups. The pioneering work of Iler in 1966 [1] did not become public until it was rediscovered by Decher in the beginning of 1990s as a simple and automatable method to fabricate films at the nanometer scale [1,2]. Compared to LbL, other deposition techniques are limited to flat substrates and require expensive and delicate instrumentation [3]. On the contrary, LbL does not depend neither on the substrate shape or size and a wide range of different materials can be deposited on different substrates such as windows [4] or small optical fibers [5-7]. Additionally, this method can be also used to attach analytes of different chemical nature [8,9]. As a consequence of these features, LbL has been used to functionalize surfaces with different goals such as antibacterial applications [10], the fabrication of hydrophobic or hydrophilic films [11,12], or to develop sensors [13,14]. The main idea of LbL method consists of the assembly of oppositely electrically charged polyelectrolytes (polycation and polyanion respectively) which form a bilayer [15]; the process can be repeated as many times as the design requires. The chemical properties of the polyelectrolytes, such as the average molecular weight, the ionization degree, the concentration or the ionic strength [16,17], just to mention some of the most important ones, define the morphology of the final film and, hence, its features.

The polyelectrolytes that can be used are divided in two categories, the strong and weak ones: in the first group, the ionization degree is not adjustable, whereas in the second one, it is adjustable by the pH of the solution [18]. Depending on the ionization degree, the polymers get adsorbed on the substrate in a different manner: highly ionized solutions would yield to flat polyelectrolytes and very thin films; meanwhile, low ionization levels produce curled chains and rough layers [19]. As the pH can be used to set the ionization degree, typically at least one of

* Correspondence: cesar.elosua@unavarra.es
Nanostructured Optical Devices Laboratory, Electric and Electronic Engineering Department, Public University of Navarra, Edif. Los Tejos, Campus Arrosadía, Pamplona 31006, Spain

the polymers is weak, although in most times both of them belong to this category. In the case of polyelectrolytes whose ionization degree is not adjustable, the ionic strength of the solution can be varied by adding salts, and in this manner, altering the morphology of the polymer chains by electrostatical interactions [20]. Another important factors are temperature, which defines the kinetics of the process [21], as well as the way the substrates is exposed to the polyelectrolytes solutions, for example, by dipping or spray [22].

Some of the ideas that were established about LbL, as the ones mentioned above, have been set under consideration. It was supposed the Z potential of the last deposited layer should always show the opposite sign of the following one; on the other hand, the roughness of the film was accepted to be reduced as the films grows. A recent work

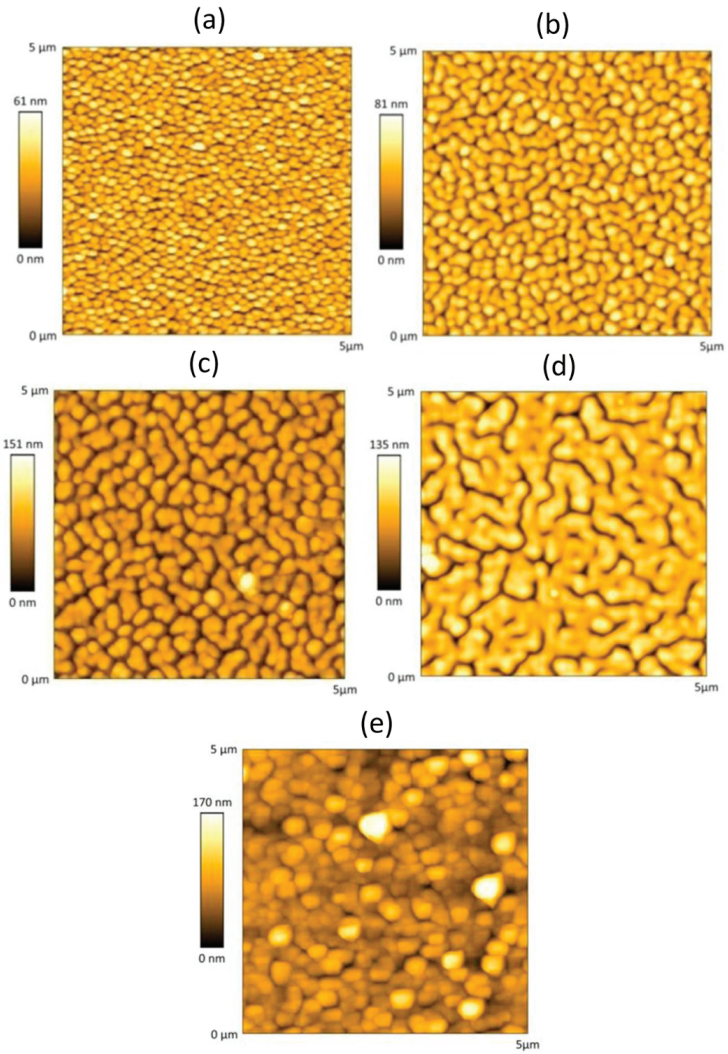

Figure 1 AFM images for the films obtained when the glass slides are dipped into the 10^{-4} M solutions. 20 bilayers **(a)**, 40 bilayers **(b)**, 60 bilayers **(c)**, 80 bilayers **(d)**, and 100 bilayers **(e)**.

has revealed that when using certain polymers, these rules are not satisfied [23]: With a 10^{-4} M concentration of poly (sodium phosphate) (PSP) and poly(allylamine hydrochloride) (PAH), the Z potential is not alternated between one layer and the next one; moreover, the roughness of the film increases with the number of bilayers when the substrate is sprayed with the polymeric solutions [23]. This behavior seems to be a consequence of using PSP, an inorganic short chain polymer with interesting properties; the use of this kind of polymers establishes a new researching line and raises again some questions about the fundamentals of LbL, taking into account other non-electrostatic interactions such as hydrogen bonds during the growing process of the film [24]. In the light of these results, some works have focused in the study of the key parameters of LbL in order to revise the effect

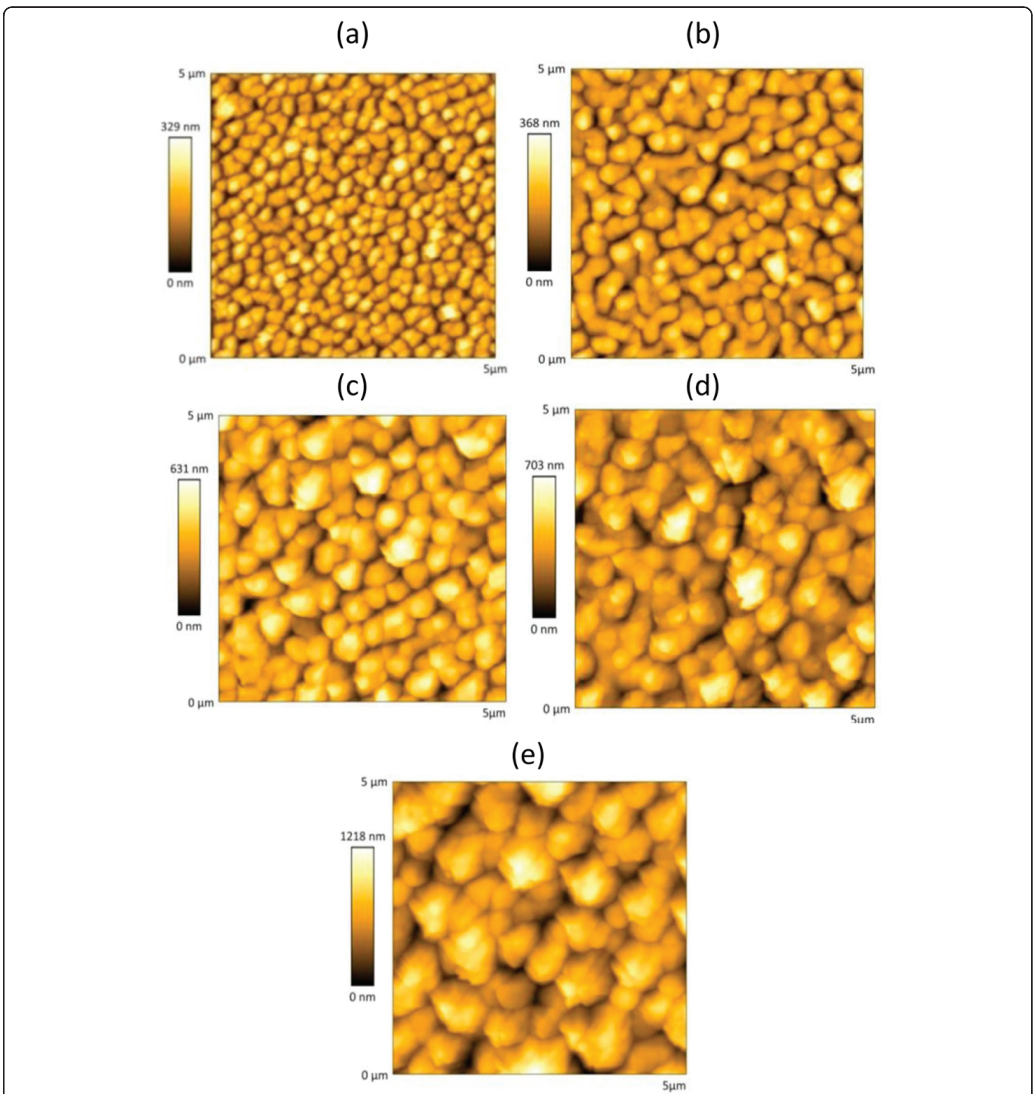

Figure 2 AFM images for the films obtained when the glass slides are dipped into the 10^{-3} M solutions. 20 bilayers **(a)**, 40 bilayers **(b)**, 60 bilayers **(c)**, 80 bilayers **(d)**, and 100 bilayers **(e)**.

of polymers as PSP in detail and redefine the rules of this technique [24].

In this work, nanofilms were prepared onto glass slides using PSP and PAH. Two different concentrations were used for the experiments, 10^{-3} and 10^{-4} M, because these are the same concentration values reported in the sprayed films studied by Decher et al. [23]. Moreover, the substrates were dipped or sprayed with the solutions to check also how these alternatives affect the features of the film. The growing process was evaluated by preparing substrates with different number of bilayers so that their thickness, roughness, contact angle, and optical transmittance spectra were measured. To our knowledge, this is the first time that a comparative study of the properties of PSP/PAH films fabricated by dip-coating LbL and spray-assisted LbL is presented in the literature.

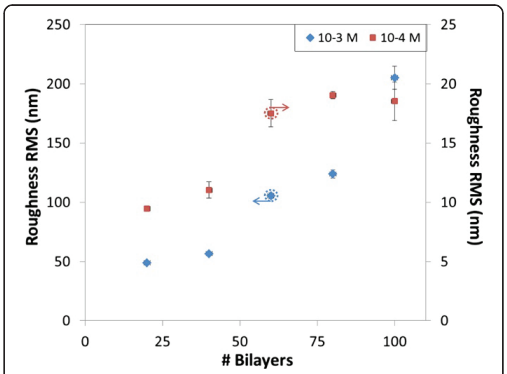

Figure 3 Roughness RMS registered for the dipped glass slides. The left vertical axe is applied for the 10^{-3} M solutions and the right vertical axe for the 10^{-4} M ones.

Methods

Materials

The polymers used were PAH ($M_w \sim 58{,}000$), PSP, P_2O_5 basis, and poly(ethylenimine) (PEI) ($M_w \sim 25{,}000$). All chemicals were purchased from Sigma-Aldrich (St. Louis, MO, USA) and used without further purification. All aqueous solutions were prepared using ultrapure water with a resistivity of 18.2 MΩ cm.

Construction of the nanofilms

The glass slides were treated in order to eliminate any organic remains and also to enhance the hydroxyl density onto their surface. To achieve it, the slide was immersed in a solution of water and detergent, sonicating it for 10 min; thereafter, the substrate was sonicated again for the same time in ultrapure water. Finally, it was dipped into a 1 M KOH aqueous solution for 10 min and sonicated once more in ultrapure water for the same time. Between each step, the glass slide was dried with nitrogen. In order to promote the initial growing of the nanofilms, an anchoring layer was deposited onto the slides by dipping them into a 2.5 mg/1 mL of PEI aqueous solution for 10 min; thereafter, the slide was rinsed with ultrapure water for 10 min and dried with nitrogen.

Solutions with concentrations of 10^{-3} and 10^{-4} M for PAH and PSP were prepared; in all cases, the mixtures had a 0.15 M NaCl to set the ionic strength. The pH of both solutions was adjusted to 6.37 with NaOH or HCl [23].

The nanofilms were developed by either dipping the substrate into the $10^{-3}/10^{-4}$ M solutions or by spraying the different solutions on the substrate. Therefore, up to four different growing conditions were studied (10^{-3} and 10^{-4} M of LbL dipping and 10^{-3} and 10^{-4} M of spray-assisted LbL). The anchoring layer of PEI led a positive superficial density charge onto the fiber so that each bilayer shows the structure PSP/PAH. Films with 20, 40, 60, 80, and 100 bilayers were prepared in each growing configuration in order to study the effects of the construction parameters.

In the case of the dipping process, each construction cycle was performed by immersing the slide into the PSP solution for 2 min and then rising it in ultrapure water for 1 min; thereafter, it was dipped into the PAH mixture for 2 min and rinsed again for 1 min in ultrapure water. This process was repeated as many times as required for the film. The steps were similar for the spray technique: the polymeric solutions and ultrapure water were sprayed for 10 s onto the slides. Both methods were automated by using a robotic arm (in the case of the dipping construction) and a spraying robot

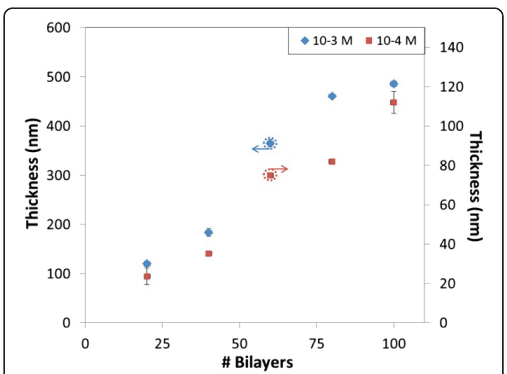

Figure 4 Thickness recorded for the dipped glass slides. The left vertical axe is applied for the 10^{-3} M solutions and the right vertical axe for the 10^{-4} M ones.

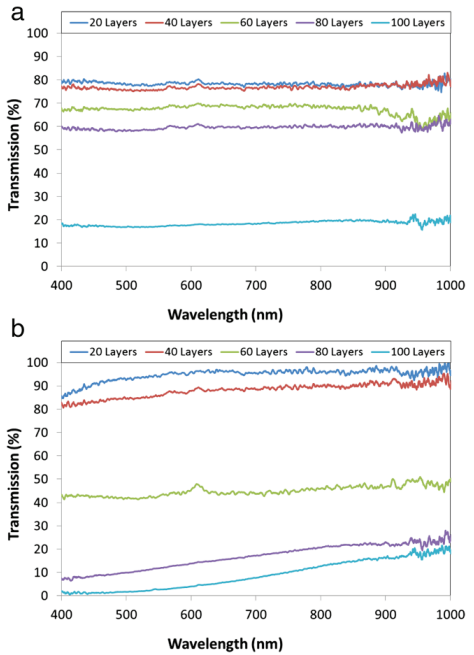

Figure 5 Transmission spectra of the films developed using dipping approach. Transmission spectra measured for the films developed using the dipping approach with the 10^{-4} M solutions **(a)** and the 10^{-3} M mixtures **(b)**.

(both of them acquired from Nadetech Innovations S.L., Sarriguren, Spain).

Characterization

The films prepared were characterized in order to study the growing process depending on the construction conditions. One of the key parameters, roughness, was measured by an atomic force microscope (AFM) (Veeco Innova, model 840-012-711; Veeco Instruments, Inc., Plainview, NJ, USA) in tapping mode; it was also used to register the thickness of the films by scratching the surface with a needle and scanning the cantilever perpendicularly to the scratch. For each sample, the AFM measurements were performed seven times in different zones to get the mean value and the standard deviation. AFM images were obtained by scanning 5 μm × 5 μm areas with 512 lines at a 0.1-Hz frequency. UV/Visible transmission spectra were recorded by a spectrometry transmission configuration, placing the glass slide under study in a holder between a white light source (HL2000; OceanOptics, Dunedin, FL, USA) and a spectrometer (USB2000XR1, OceanOptics). Finally, the contact angle was registered using a contact angle meter (KSV Instruments goniometer; Espoo, Finland) for each sample.

Results and discussion

As it was cited before, four sets of samples were prepared: 10^{-3} and 10^{-4} M of LbL dipping as well as 10^{-3} and 10^{-4} M of spray-assisted LbL. In each set, five slides were coated with different number of bilayers (20, 40, 60, 80, and 100). The information will be presented in the next two sections depending on the way the glass slides are exposed to the polyelectrolyte solutions; in each section, results with different polymer concentrations are also commented.

LbL dipping approach

A traditional assumption in LbL films is that the thickness of the film increases as the number of bilayers does, whereas the root mean square (RMS) roughness decreases [25]. In order to study this statement, the first set of slides was prepared with 10^{-4} M polymer solutions (0.15 M NaCl): the AFM images obtained for 20, 40, 60, 80, and 100 bilayer films are shown in Figure 1. It can be observed that the RMS roughness increases with the number of bilayers, from 9.47 up to 18.53 nm RMS for 20 and 100 bilayers, respectively. Although this surprising behavior was reported recently for sprayed-assisted LbL coatings [23], this is the first time that it is reported for PSP/PAH films fabricated by LbL dip coating. The morphology of the films looks islandlike for the 20 bilayer films: as the number of construction cycles grows, so does the size of the island, as well as the RMS

Table 1 Characterization of the films prepared using dipping approach

Number of bilayers	Roughness				Thickness				Contact angle			
	10^{-4} M		10^{-3} M		10^{-4} M		10^{-3} M		10^{-4} M		10^{-3} M	
	μ	σ	μ	σ	μ	σ	μ	σ	μ	σ	μ	σ
20	9.47	0.15	48.98	1.33	23.67	4.24	120.33	5.34	48.75	1.49	0.36	0.21
40	11.03	0.695	56.78	1.45	35.33	0.71	184.12	7.78	65.50	1.55	3.31	0.81
60	17.51	1.16	105.5	2.34	75.11	1.41	365.03	7.07	30.12	0.91	0	0
80	19.05	0.29	123.93	3.51	82.07	0.70	461.06	0.35	28.51	1.66	0	0
100	18.53	1.62	205.23	9.79	112.02	5.65	486.07	5.65	28.02	1.41	0	0

roughness. This behavior was observed in other work focused on nanostructures based on PSP [23]. The use of a short-chain inorganic polymer as PSP seems to alter the growth of the nanofilms, keeping the roughness increasing with the number of bilayers. In the case of the films prepared with 10^{-3} M solutions (Figure 2), the behavior is similar: the roughness goes from 48.98 up to 205.53 nm RMS for 20 and 100 bilayers, respectively. The morphology looks granulated in all cases, with a bigger granulate size as the number of bilayers increases. The values registered for the RMS roughness are much higher than the ones observed with 10^{-4} M solutions and also contradict what is expected from LbL films. Figure 3 shows a graph with the registered RMS roughness as a function of the

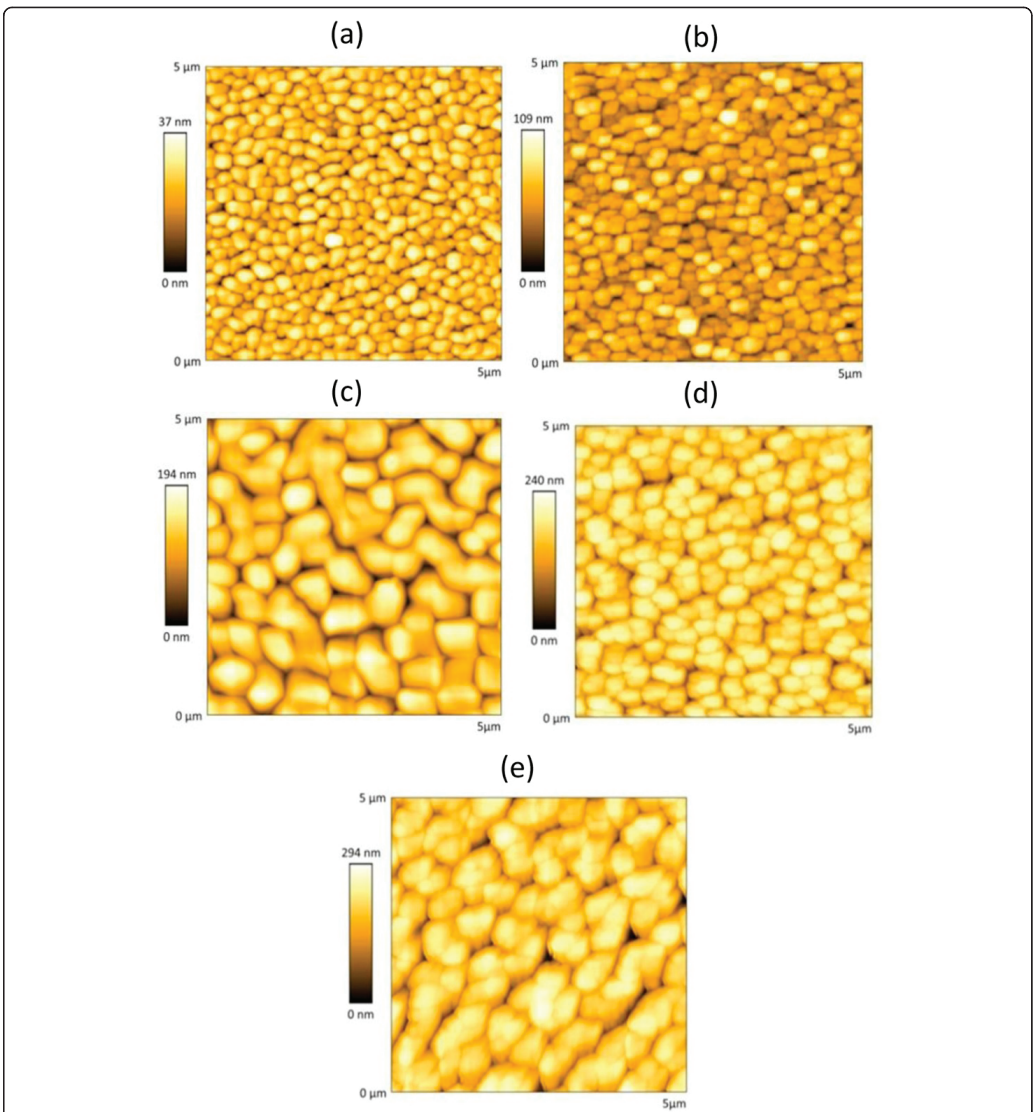

Figure 6 AFM images for the films obtained when the glass slides are sprayed into the 10^{-4} M solutions. 20 bilayers **(a)**, 40 bilayers **(b)**, 60 bilayers **(c)**, 80 bilayers **(d)**, and 100 bilayers **(e)**.

number of bilayers for the slides prepared for the two concentrations; although the scale is not the same, the increasing trend is similar in both cases, which highlights the fact that PSP alters the growing of LbL films.

On the other hand, the thickness of the fabricated films points that the growth increases with the number of bilayers, as it can be checked in Figure 4. The thickness values obtained for the more concentrated solution are around six times higher than for the nanoconstructions prepared with the 10^{-4} M mixtures; in both cases, the thickness grows monotonically [21].

Additionally, the contact angle of the samples was also measured to study the hydrophilicity of the films [26]. In the case of the films prepared with the 10^{-4} M solutions,

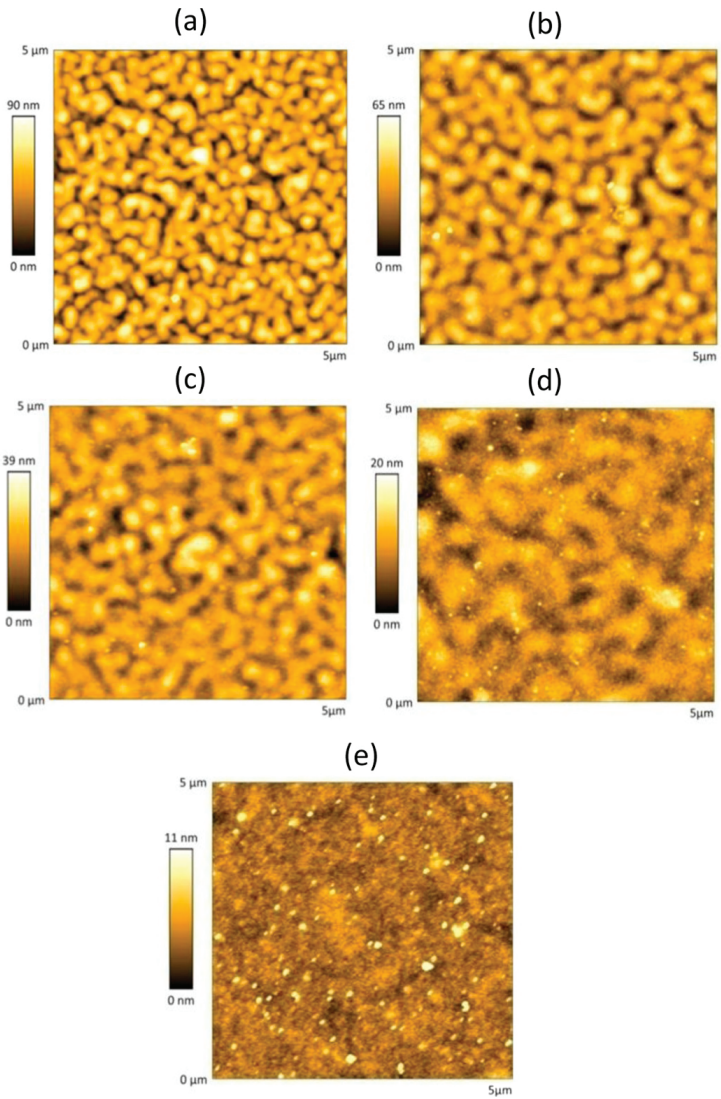

Figure 7 AFM images for the films obtained when the glass slides are sprayed into the 10^{-3} M solutions. 20 bilayers **(a)**, 40 bilayers **(b)**, 60 bilayers **(c)**, 80 bilayers **(d)**, and 100 bilayers **(e)**.

as a consequence of the increasing roughness with the number of bilayers, the contact angle lowers from 60° down to 28°; despite of this decrease, the films are far from being superhydrophilic. On the contrary, contact angles registered for the films prepared with the 10^{-3} M solutions are close to 0 even for 20 bilayers, which enables the utilization of these films in superhydrophilic applications [26]. Registered images of the contact angle are available in the Additional file 1.

Regarding to the transmittance spectra, the optical losses increased with the number of bilayers: in the case of 10^{-4} M prepared films, transmittance is about 80% for 20 and 40 bilayers, decreasing around 65% for 60 and 80 bilayers, and falling down to 20% in the case of the 100 bilayer films. For the other set of slides, the 10^{-3} M prepared films, the optical transmittance falls in the case of 60 bilayers and down to 15% when 100 bilayers are deposited. These results are a consequence of the increasing thickness, which is around 600 μm in the case of the film formed by 100 bilayers of the second set; the roughness could also contribute to the scattering of light, increasing the optical transmission losses. The spectra recorded are plotted in Figure 5. All the data registered are summarized in Table 1.

Spray-assisted LbL approach

Up to ten glass slides were coated by spray-assisted LbL to study the same parameters analyzed before for the LbL dip coating, five slides with 10^{-4} M solutions and the other ones with 10^{-3} M. The AFM images registered for the 10^{-4} M mixtures are shown in Figure 6. The films are also islandlike, showing an uniform pattern along the image in each case: the size of the island increases with the number of bilayers. Again, it denotes an increase of the roughness: actually, it goes from 4 nm RMS for 20

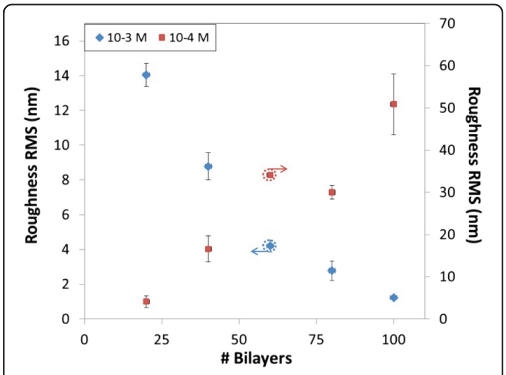

Figure 8 Roughness RMS registered for the sprayed glass slides. The left vertical axe is applied for the 10^{-3} M solutions and the right vertical axe for the 10^{-4} M ones.

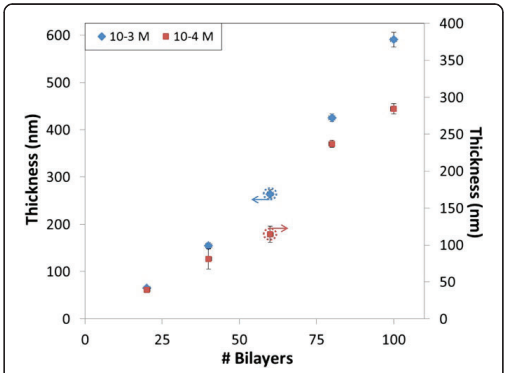

Figure 9 Thickness recorded for the sprayed glass slides. The left vertical axe is applied for the 10^{-3} M solutions and the right vertical axe for the 10^{-4} M ones.

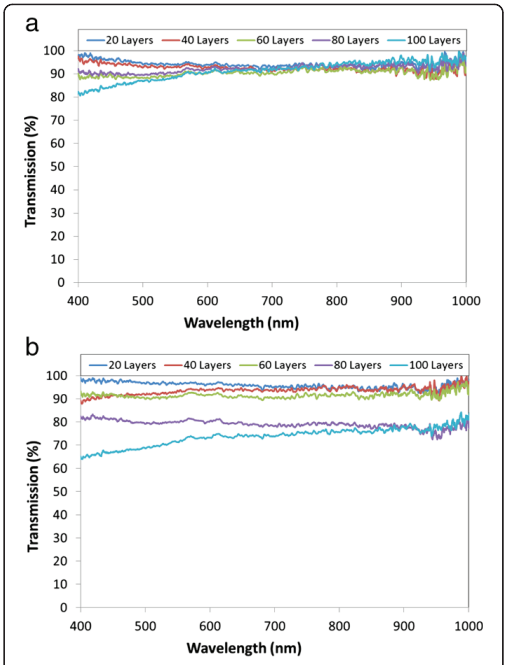

Figure 10 Transmission spectra of films developed by spraying approach. Transmission spectra measured for the films developed by spraying approach with the 10^{-4} M solutions **(a)** and the 10^{-3} M mixtures **(b)**.

bilayers up to 50 nm RMS when 100 bilayers are deposited. In the case of the 10^{-3} M solutions, the AFM images can be observed in Figure 7: for 20 bilayers, the surface looks granular, but contrarily to the phenomena observed for the other coatings (films prepared with 10^{-4} M solutions), now as the number of sprayed bilayers increases, this appearance gets diffused. As a consequence, the roughness of the films prepared by spray-assisted LbL with the 10^{-3} M solutions decreases as the nanofilm grows, which is expected from LbL depositions [25], down to 1.23 nm RMS when 100 bilayers are deposited. The roughness obtained for both concentrations is displayed in Figure 8: the results from the nanoconstructions prepared with 10^{-3} M remark the decreasing roughness as the film increases, whereas the 10^{-4} M films show a monotonically increasing growth, confirming the surprising results reported by Decher et al. [23]. The thickness of the films are plotted in Figure 9: the values obtained with 10^{-3} M approximately double the ones registered with 10^{-4} M due to the lower concentration.

The contact angle measured for the 10^{-4} M prepared films falls to near 0 with 60 bilayers or more, highlighting the effect of the increasing roughness; on the contrary, for the films prepared with 10^{-3} M solutions, the contact angle remains above 30°, so they cannot be considered superhydrophilic.

The transmittance spectra registered for the different cases are plotted in Figure 10. For the first set of films (10^{-4} M), the optical transmittance is around 90%; only in the case of the thickest film that this value falls below 90% from 400 to 600 nm. The other set of films also shows a high-transmission spectra, above 90% with 60 bilayers or less and higher than 65% for the other two cases. The lower transmittance is a consequence of the higher thickness produced by the more concentrated solutions.

Results reported in this section are summarized in Table 2.

Conclusions

In light of the results reported, both the polymeric concentrations and the deposition method (dipping or spraying) affect the growth of the nanofilms. The roughness obtained with the dipped slides is higher than the registered one with the sprayed substrates; on the other hand, the optical transmittance is lower as a consequence of the greater thickness obtained with the dipped slides. Moreover, in all cases but in the one with 10^{-3} M of sprayed solutions, the roughness is increased as the number of bilayers grows, which is an unexpected behavior in LbL films. It is also remarkable that the concentrations used here are lower than the ones typically studied in the literature, around 10^{-2} M [27]. The thickness and roughness observed using the dipping approach are higher than the ones registered with the sprayed slides: these differences have been observed in previous works [22]. The best results in terms of a superhydrophilic behavior are obtained with 10^{-3} M dipping solutions and with 10^{-4} M spraying mixtures. On the other hand, the high optical transmittance registered with the 10^{-4} M of sprayed solutions, even when 100 bilayers are deposited, points to its potential use in applications where superhydrophilic and transparent surface are required.

The use of inorganic short-chain polymers in LbL method shows that some assumed rules need to be redefined. In this work, it has been demonstrated that the roughness of nanofilms can increase as the growing process goes on, depending on the concentration of the polymers used and also on the way the slides are exposed to the solutions (dipped or sprayed). The highest roughness is obtained when the slides are dipped into the highest concentration solutions, which was supposed to produce the lowest roughness. The thickness of the resulting films falls in the nanometric range so they could be used in applications where surfaces have to be functionalized. Optical transmittance is above 90% for the films prepared with the 10^{-4} M of sprayed solutions, which highlights its potential used for preparing superhydrophilic transparent films. The use of PSP offers other important advantages: as it is an inorganic polymer, it can yield to surfaces whose degradation is lower than the ones prepared with organic polymers. Therefore, this work enforces to keep on studying the effect of this kind of polymers in LbL nanostructures.

Table 2 Characterization of the films prepared using spraying approach

Number of bilayers	Roughness				Thickness				Contact angle			
	10^{-4} M		10^{-3} M		10^{-4} M		10^{-3} M		10^{-4} M		10^{-3} M	
	μ	σ	μ	σ	μ	σ	μ	σ	μ	σ	μ	σ
20	4.07	1.38	14.05	0.66	39.23	2.58	64.6	0.14	21.6	1.41	32.48	8.05
40	16.58	3.12	8.78	0.79	81.23	13.55	155	6.36	8.15	0.97	91	5.89
60	34.13	0.58	4.2	0.34	114.39	10.92	264.33	8.14	0	0	45.45	3.67
80	30	1.56	2.78	0.56	236.97	4.73	425.33	8.49	0	0	59.45	6.92
100	50.87	7.17	1.23	0.05	284.6	7.31	590.67	15.56	0	0	37.03	4.78

Additional file

Additional file 1: Contact angles recorded for each film. Images of the contact angles. Four slides are available:1st slide, 10^{-4} M dipped films; 2nd slide, 10^{-3} M dipped films; 3rd slide, 10^{-4} M sprayed films; 4th slide, 10^{-3} M sprayed films.

Abbreviations

AFM: Atomic force microscope; LbL: Layer-by-layer; PAH: Poly(allylamine hydrochloride); PEI: Poly(ethylenimine); PSP: Poly(sodium phosphate).

Competing interests

The authors declare that they have no competing interests.

Authors' contributions

CE participated in the experimental work and carried out the AFM images. He also collaborated in the planning of the experiment; he prepared the drafting of the manuscript as well. DLT developed the films with the different number of bilayers and deposition approaches. He also contributed with the draft of the paper. MH participated in the experimental work registering AFM images and also contributed to the draft of the manuscript. IRM supervised the design of the study. FJA led the design of the study and helped to draft the manuscript. All authors read and approved the final manuscript.

Acknowledgements

This work was supported by the Spanish Economy and Competitiveness Ministry-FEDER TEC2010-17805. The authors would like to express their gratitude to Nadetech Inc. for the design, fabrication, and tune-up of the robot used for the deposition of the nanocoatings.

Received: 31 October 2013 Accepted: 4 December 2013
Published: 20 December 2013

References

1. Iler RK: **Multilayers of colloidal particles.** *J Colloid Interface Sci* 1966, **21**:569–594.
2. Decher G: **Fuzzy nanoassemblies: toward layered polymeric multicomposites.** *Science* 1997, **277**(5330):1232–1237.
3. Goto TE, Sakai A, Iost RM, Silva WC, Crespilho FN, Péresa LO, Caseli L: **Langmuir-Blodgett films based on poly(p-phenylene vinylene) and protein-stabilised palladium nanoparticles: implications in luminescent and conducting properties.** *Thin Solid Films* 2013, **540**:202–207.
4. Ishikawa R, Bando M, Wada H, Krokawa Y, Sandhu A, Konagai M: **Layer-by-layer assembled transparent conductive graphene films for silicon thin-film solar cells.** *Jpn J Appl Phys* 2012, **51**(11):11PF01-1–11PF01-4.
5. Elosua C, Arregui FJ, Zamarreño CR, Bariain C, Luquin A, Laguna M, Matias IR: **Volatile organic compounds optical fiber sensor based on lossy mode resonances.** *Sens Actuators B* 2013, **173**:523–529.
6. Mingjie Y, Quanfu A, Jinwen Q, Aping Z: **Preparation and application of fiber-optic sensors based on layer-by-layer self-assembly multilayers.** *Progress in Chemistry* 2011, **23**(12):2568–2575.
7. Goicoechea J, Zamarreño CR, Matías IR, Arregui FJ: **Optical fiber pH sensors based on layer-by-layer electrostatic self-assembled Neutral Red.** *Sens Actuators B* 2008, **132**(1):305–311.
8. Rivero PJ, Goicoechea J, Urrutia A, Matias IR, Arregui FJ: **Multicolor layer-by-layer films using weak polyelectrolyte-assisted synthesis of silver nanoparticles.** *Nanoscale Res Lett* 2013, **8**:438.
9. Elosua C, Bariain C, Luquin A, Laguna M, Matias IR: **Optimization of single mode fibre sensors to detect organic vapours.** *Sens Actuators B* 2011, **157**(2):388–394.
10. Liu X, Qi S, Li Y, Yang L, Cao B, Tang CY: **Synthesis and characterization of novel antibacterial silver nanocomposite nanofiltration and forward osmosis membranes based on layer-by-layer assembly.** *Water Res* 2013, **47**(9):3081–3092.
11. Corres JM, Matias IR, Hernaez M, Bravo J, Arregui FJ: **Optical fiber humidity sensors using nanostructured coatings of SiO_2 nanoparticles.** *IEEE Sensors J* 2008, **8**(3–4):281–285.
12. Bravo J, Zhai L, Wu ZZ, Cohen RE, Rubner MF: **Transparent superhydrophobic films based on silica nanoparticles.** *Langmuir* 2007, **23**(13):7293–7298.
13. Del Villar I, Hernaez M, Zamarreno CR, Sanchez P, Fernandez-Valdivielso C, Arregui FJ, Matias IR: **Design rules for lossy mode resonance based sensors.** *Appl Optics* 2012, **51**(19):4298–4307.
14. Elosua C, Bariain C, Luquin A, Laguna M, Matias IR: **Optical fiber sensors array to identify beverages by their odor.** *IEEE Sensors J* 2012, **12**(11):3156–3162.
15. Schaaf P, Voegel JC, Jierry L, Boulmedais F: **Spray-assisted polyelectrolyte multilayer buildup: from step-by-step to single-step polyelectrolyte film constructions.** *Adv Mater* 2012, **24**(8):1001–1016.
16. Halthur TJ, Claesson PM, Elofsson UM: **Stability of polypeptide multilayers as studied by in situ ellipsometry: effects of drying and post-buildup changes in temperature and pH.** *J Am Chem Soc* 2004, **126**(51):17009–17015.
17. Glinel K, Moussa A, Jonas AM, Laschewsky A: **Influence of polyelectrolyte charge density on the formation of multilayers of strong polyelectrolytes at low ionic strength.** *Langmuir* 2002, **18**:1408–1412.
18. Choi J, Rubner MF: **Influence of the degree of ionization on weak polyelectrolyte multilayer assembly.** *Macromolecules* 2005, **38**:124–166.
19. Yoo D, Shiratori SS, Rubner MF: **Controlling bilayer composition and surface wettability of sequentially adsorbed multilayers of weak polyelectrolytes.** *Macromolecules* 1998, **31**(13):4309–4318.
20. Apaydin K, Laachachi A, Bour J, Toniazzo V, Ruch D, Ball V: **Polyelectrolyte multilayer films made from polyallylamine and short polyphosphates: influence of the surface treatment, ionic strength and nature of the electrolyte solution.** *Colloids Surf A Physicochem Eng Asp* 2012, **415**:274–280.
21. Salomaki M, Vinokurov IA, Kankare J: **Effect of temperature on the buildup of polyelectrolyte multilayers.** *Langmuir* 2005, **21**(24):11232–11240.
22. Izquierdo A, Ono SS, Voegel JC, Schaaf P, Decher G: **Dipping versus spraying: exploring the deposition conditions for speeding up layer-by-layer assembly.** *Langmuir* 2005, **21**(6):7558–7567.
23. Cini N, Tulun T, Decher G, Ball V: **Step-by-step assembly of self-patterning polyelectrolyte films violating (almost) all rules of layer-by-layer deposition.** *J Am Chem Soc* 2010, **132**(24):8264–8265.
24. Kotov NA: **Layer-by-layer self-assembly: the contribution of hydrophobic interactions.** *Nanostruct Mater* 1999, **12**(5–8):789–796.
25. Seo J, Lutkenhaus JL, Kim J, Hammond PT, Char K: **Effect of the layer-by-layer (LbL) deposition method on the surface morphology and wetting behavior of hydrophobically modified PEO and PAA LbL films.** *Langmuir* 2008, **24**(15):7995–8000.
26. Tasaltin N, Sanli D, Jonas A, Kiraz A, Erkey C: **Preparation and characterization of superhydrophobic surfaces based on hexamethyldisilazane-modified nanoporous alumina.** *Nanoscale Res Lett* 2011, **6**:487.
27. Sanchez P, Zamarreno CR, Hernaez M, Del Villar I: **Considerations for lossy-mode resonance-based optical fiber sensor.** *IEEE Sensors J* 2013, **13**(4):1167–1171.

doi:10.1186/1556-276X-8-539
Cite this article as: Elosua *et al.*: Comparative study of layer-by-layer deposition techniques for poly(sodium phosphate) and poly(allylamine hydrochloride). *Nanoscale Research Letters* 2013 **8**:539.

I.1.2 Modificación de las características de la película polimérica formada por el PSP y el PAH

Analizando de una forma detallada las películas obtenidas para el caso de 10^{-3} M, se comprobó que todas ellas tenían unas características en común: una alta rugosidad desde los espesores más bajos (20 parejas de capas) y la propiedad de ser superhidrofílicas (en todas ellas el ángulo de contacto medido fue 0°). Estas dos propiedades tienen una gran importancia en la estructura de la película y pueden ser utilizadas para modificar sus propiedades y características dotándola de un mayor potencial de cara a desarrollar una aplicación final.

La propiedad que se pensó modificar fue la superhidrofilidad de las películas, intentando transformarlas en películas superhidrofóbica. De esta manera y habiendo logrado este cambio, podría ser utilizada en aplicaciones para repeler el agua, como por ejemplo en ventanas de viviendas, lunas y espejos de automóviles o recubrimientos cuyo objetivo sea evitar el paso del agua, ampliando así el rango de aplicaciones potenciales en las que podía ser utilizada. Además, otro dato muy importante era el punto de partida: la película superhidrofílica obtenida. En muchos de los trabajos previos, para poder obtener este tipo de superficies, con unos valores tan altos de rugosidad, es necesario emplear sofisticados procesos de funcionalización o altas temperaturas; en el caso que se expone en esta tesis, simplemente es necesario utilizar la técnica *LbL* a temperatura ambiente, lo que simplificó en gran manera todo el proceso.

Para el proceso de funcionalización, se pensó en realizar una silanización utilizando la técnica de deposición basada en vapores químicos (Chemical Vapor Deposition; en inglés sus siglas son CVD). Esta técnica consiste en introducir la película depositada en el portaobjetos dentro de un horno a una determinada temperatura (150° en este caso) junto al reactivo (H,1H,2H,2H-Perfluorodecyltriethoxsilane), el cual se va evaporando, y consecuentemente, depositando en la película conforme transcurre el tiempo. De nuevo, gracias a la técnica empleada, y a las características de la película, el proceso fue muy simple, y las temperaturas utilizadas no fueron excesivamente altas. Además, no fue necesaria la utilización de nano partículas durante la funcionalización.

Los resultados obtenidos fueron muy prometedores ya que con determinadas películas que se fabricaron se llegó a tener un incremento en el

ángulo de contacto de 165°. Este estudio, junto a los resultados que se derivaron de él, se presentaron en la revista *"Applied Surface Science"* la cual decidió aceptar la contribución científica. A continuación, se presenta el trabajo aceptado que llevó por título *"From superhydrophilic to superhydrophobic surfaces by means ofpolymeric Layer-by-Layer films"*, donde se explica todo el proceso de una forma más extensa y detallada.

Applied Surface Science 351 (2015) 1081–1086

Contents lists available at ScienceDirect

Applied Surface Science

journal homepage: www.elsevier.com/locate/apsusc

From superhydrophilic to superhydrophobic surfaces by means of polymeric Layer-by-Layer films

Diego Lopez-Torres*, Cesar Elosua, Miguel Hernaez, Javier Goicoechea, Francisco J. Arregui

Nanostructured Optical Devices Laboratory, Electric and Electronic Engineering Department, Public University of Navarra, Edif. Los Tejos, Campus Arrosadía, 31006, Pamplona, Spain

ARTICLE INFO

Article history:
Received 23 February 2015
Received in revised form 28 May 2015
Accepted 1 June 2015
Available online 9 June 2015

Keywords:
Layer-by-Layer
CVD technique
Hydrophilic and hydrophobic films
PSP-PAH
Functionalized surfaces

ABSTRACT

In this paper a nanocoating that shows a superhydrophilic behavior (with a contact angle close to 0°) is transformed into a superhydrophobic nanofilm (whose contact angle is 165°) following a procedure that needs no nanoparticles to generate the nano-roughness required for superhydrophobicity. The superhydrophilic nanocoating was fabricated using poly (allylamine hydrochloride) (PAH) and poly (sodium phosphate) (PSP) combined by means of the Layer-by-Layer (LbL) technique. Seven different nanocoatings were constructed with different number of bilayers (4, 8, 12, 16, 20, 30 and 40) being the concentration of both polymers 10^{-3} M. The analysis was conducted studying three different features: roughness, thickness and contact angle. The results show that initially, the contact angle of the nanofilms above 20 bilayers is close to 0°, that is, the minimum value for a superhydrophilic coating. These surfaces were functionalized using 1H,1H,2H,2H-Perfluorodecyltriethoxsilane to transform them into hydrophobic coatings by Chemical Vapor Disposition (CVD). Thereafter, the nanofilms showed a superhydrophobic behavior with a contact angle of 165° for the 40 bilayers films. The results of roughness and the images of AFM prove that the morphology of the nanocoating is preserved.

1. Introduction

In the last two decades the development of nanocoatings has been greatly improved [1]. Diverse surfaces can be functionalized to get relevant features such as hydrophilicity or hydrophobicity which has important implications in different fields such as the fabrication of anti-fog films, avoidance of ice formation [2], self-cleaning coatings [3], bio-fueling and its leakage prevention [4], oil–water separation [5,6], textiles [7], droplet generation or liquid manipulation in microfluidics [8] and other applications in the biomedical field [9], just to mention a few examples. In fact, nowadays, hydrophilicity and hydrophobicity are the most published topics about wet nanofilms construction techniques [10].

The concept of superhydrophilicity was proposed by Onda et al. [11,12] in 1996 and Fujishima et al. found out the superhydrophilicity effect on a glass slide film with TiO_2 one year later [13]. On the other hand, superhydrophobic surfaces are generally defined as surfaces with water contact angles above 140° or 150° [14,15]. The appropriate texturing and roughening of surfaces on the nano and microscale are used to obtain these extreme wetting characteristics. Many strategies to achieve these synthetic superhydrophobic behavior are based on functionalization of superhydrophilic surfaces: they show a significant roughness and therefore, a high volume–surface rate, so that chemical reagents with a superhydrophobic can be deposited onto them. When working with transparent substrates, such as glass, it is also required that the optical transmittance is preserved along the process. In the case of metallic surfaces, the roughness is increased with an oxidation treatment that requires temperatures of some hundreds of Celsius degrees [16] and thereafter, the substrate is coated with a superhydrophobic material such as polydimethylsiloxane (PDMS) [17]. Other methods to obtain the initial superhydrophilic surface employ carbon nanotubes: they can be organized in order to obtain high roughness surfaces, increasing the temperature up to 800 °C; then, they are functionalized with superhydrophilic molecules [18]. When working with glass substrates, the high affinity between superficial hydroxyl groups and water molecules define an initial hydrophilic behavior, in order to counteract it, the substrate is heated to high temperatures so that this interaction is reduced [19];

Abbreviations: LbL, Layer-by-Layer; PAH, poly (allylamine hydrochloride); PSP, poly (sodium phosphate); PEI, poly (ehylenimine); CVD, chemical vapor deposition; PDS, perfluorodecylsilane; AFM, Atomic Force Microscope; EDX, energy-dispersive X-ray spectroscopy.

* Corresponding author.
E-mail addresses: diego.lopez@unavarra.es (D. Lopez-Torres), cesar.elosua@unavarra.es (C. Elosua), miguel.hernaez@unavarra.es (M. Hernaez), javier.goico@unavarra.es (J. Goicoechea), parregui@unavarra.es (F.J. Arregui).

http://dx.doi.org/10.1016/j.apsusc.2015.06.004
0169-4332/

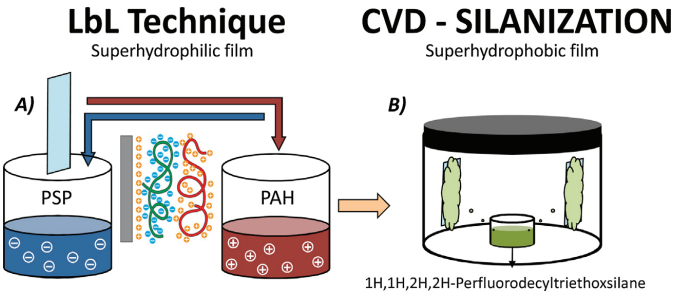

Fig. 1. Scheme of the techniques used to prepare the superhydrophilic film (A) and its transformation into a superhydrophobic one (B).

another option consists of the functionalization with hydrophobic molecules [20]. One of the most used methods to perform this final step is Chemical Vapor Deposition (CVD): briefly, the chemical reagent to be coated is evaporated, so that it interacts with the substrate, getting attached onto it [21]. Depending on the reagent, this process can be done at room temperature, but is come cases, it requires at high temperatures (700 °C) [18].

When working with glass substrates, the high affinity between superficial hydroxyl groups and water molecules define an initial hydrophilic behavior, in order to counteract it, the substrate is heated to high temperatures so that this interaction is reduced [19]; another option consists of the functionalization with hydrophobic molecules [20]. One of the most used methods to perform this final step is Chemical Vapor Deposition (CVD): briefly, the chemical reagent to be coated is evaporated, so that it interacts with the substrate, getting attached onto it [21]. Depending on the reagent, this process can be done at room temperature, but is come cases, it requires at high temperatures (700 °C) [18].

Among the different techniques proposed to achieve the initial specific high roughness, LbL technique was reported by Bravo, Rubner et al. in [22]. LbL is one of the most important procedures for the deposition of nanofilms. The method was proposed by Decher [23] at the beginning of 1990s as a simple and automatable method to fabricate films at the nanometer scale. LbL technique consists of the assembly of oppositely electrically charged polyelectrolytes (polycation and polyanion respectively) forming a bilayer [24]; the number of bilayers can be chosen by the designer because the process can be repeated as many times as desired. LbL procedure is not limited by the shape or the size of substrates and it does not require any expensive or delicate instrumentation [25]; another positive aspect comparing to other techniques is the wide range of different materials that can be deposited on distinct substrates such as windows, glass slides or optical fibers [26]. The procedure allows surfaces to be coated at nanometric scale in an automated and repetitive way. Furthermore, the properties of these surfaces can be altered by including in the process nanoparticules such as metal oxide or silica nanospheres [27]. Actually, in the above mentioned work (Bravo, Rubner et al.) it is described the controlled placement and level of aggregation of differently sized SiO_2 nanoparticles by means of LbL to optimize the level of surface roughness necessary to obtain superhydrophobic behavior. Additionally, the substrate is calcined to improve its features.

In the case of non LbL based techniques, high temperature is needed to enhance the roughness of the substrate (as referenced in the previous paragraph), so that it shows and superhydrophilic behavior; even for the superhydrophobic functionalization, sometimes high temperatures are also required. LbL procedure makes easier the initial high roughness functionalization (at room temperature), although SiO_2 are required to obtain the superhydrophobic coating, followed by a calcination. To the best of our knowledge, here we present for the first time a nanocoating that can achieve the required level of roughness to show superhydrophilic and superhydrophobic behavior by means of the LbL method without the need of using nanoparticles; the whole process is performed at room temperature and the optical properties of the film are preserved, keeping its transparency.

2. Materials and methods

2.1. Materials

Two different polymers have been used for the construction of the nanocoating: Poly (allylamine hydrochloride) (PAH) ($M_w \sim 58{,}000$) and Poly (sodium phosphate) (PSP, P_2O_5 basis). The cleaning and the induction of a superficial electrical charge onto the glass slide were performed by Potassium Hydroxide (KOH) whereas Poly (EhylenImine) (PEI) ($M_w \sim 25{,}000$) was used to prepare an anchoring layer. The acidity of the solution was adjusted by Hydrochloridric acid (HCl) and Sodium Hydroxide (NaOH); the ionic strength was set with sodium chloride (NaCl). Finally, 1H,1H,2H,2H-Perfluorodecyltriethoxsilane 97% was employed to functionalize the superhydrophilic surfaces. The entire set of reagents were supplied by Sigma–Aldrich and used without a further purification. All aqueous solutions were prepared using ultrapure water with a resistivity of 18.2 MΩ cm.

2.2. Construction of the functionalized nanofilms

The construction process can be divided in three parts: the preparation of the substrate (glass slide), the construction of the nanofilm and finally, its functionalization.

The first task consisted of three steps: cleaning the substrate, inducing a negative electrical charge onto its surface and lastly, depositing and anchoring layer of PEI [28]. The whole process is detailed in a previous work [29].

Table 1
Contact angles (°) measured before and after silanization.

#Bilayers	Contact angles (°) measured before and after silanization			
	Before CVD		After CVD	
	μ	σ	μ	σ
4	26	0.5	105	1.1
8	18	0.3	110	2.7
12	16	0.1	114	1.1
16	6	0.3	130	1.2
20	0	0	141	1.0
30	0	0	147	0.6
40	0	0	161	4.2

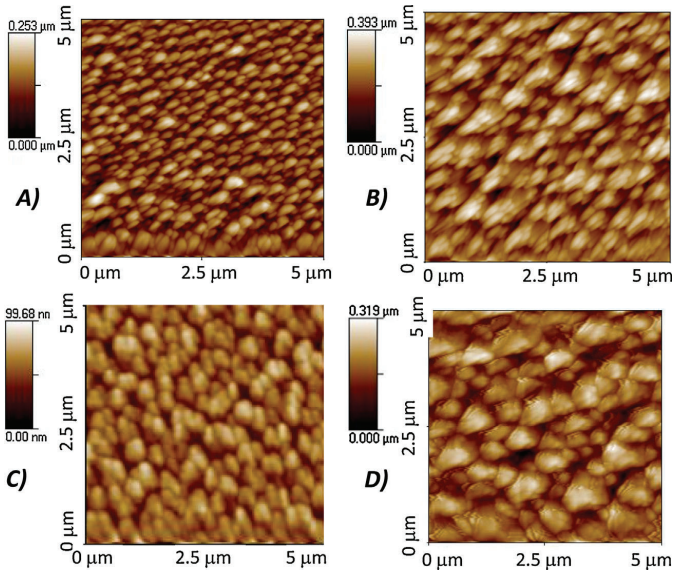

Fig. 2. AFM images for the superhydrophilic films prepared with 20 bilayers (A) and 40 bilayers (B); they can be compared with the images obtained after silanization 20 bilayers + silanization (H); 40 bilayers + silanization (I).

The film was constructed (second stage) using two polyelectrolyte solutions of PAH (polycation) and PSP (polyanion) with a 10^{-3} M concentration were prepared; the ionic strength of the mixtures was set with a 0.15 M NaCl concentration. The pH of the both solutions was adjusted to 6.4 by adding NaOH or HCl. The nanofilms were prepared following the LbL method (see Fig. 1A). The method was automated by using a robotic arm (acquired from Nadetech Innovations S.L.) [30], as it is described in [29]. Films with a different number of bilayers (specifically, 4, 8, 16, 20, 30 and 40) were prepared in order to study the effects of the nanolayers morphology over of the final deposition features.

There are different methods to convert superhydrophilic surfaces into superhydrophobic coatings such as chemically altered metal surfaces, carbon nanotubes, modified silica-based surfaces and Chemical Vapor Deposition (CVD) [31]. These techniques are combined with reagents such as Fluoroalkylsilane (FAS), Perfluorodecylsilane (PDS), Poly(tetrafluoroethalene) (PTFE), Alkyl–ketene dimers (AKDs) or Poly(alkylpyrrole) to improve the

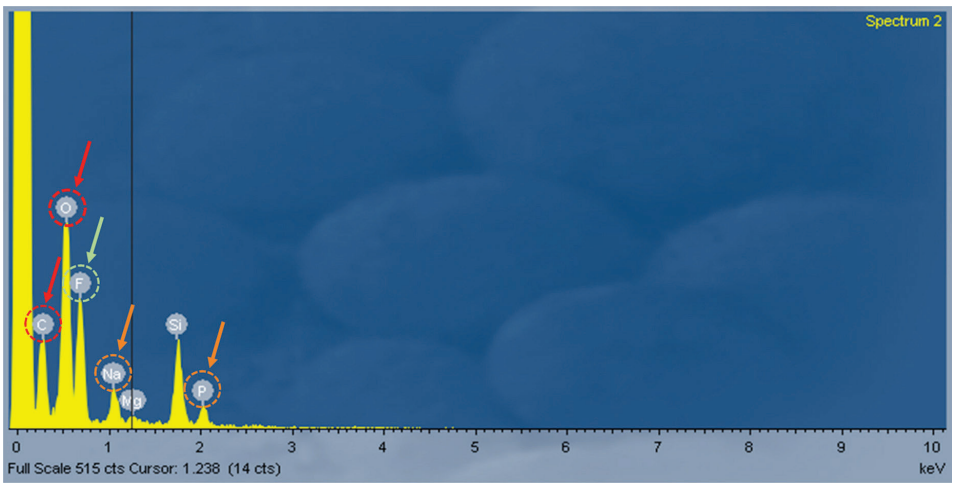

Fig. 3. EDX analysis results for the film obtained when 40 bilayers are deposited. The elements corresponding to PAH are highlighted in red (carbon and oxygen), for PSP in orange (phosphorous and sodium) and in green for the fluorine present in fluorosilane.

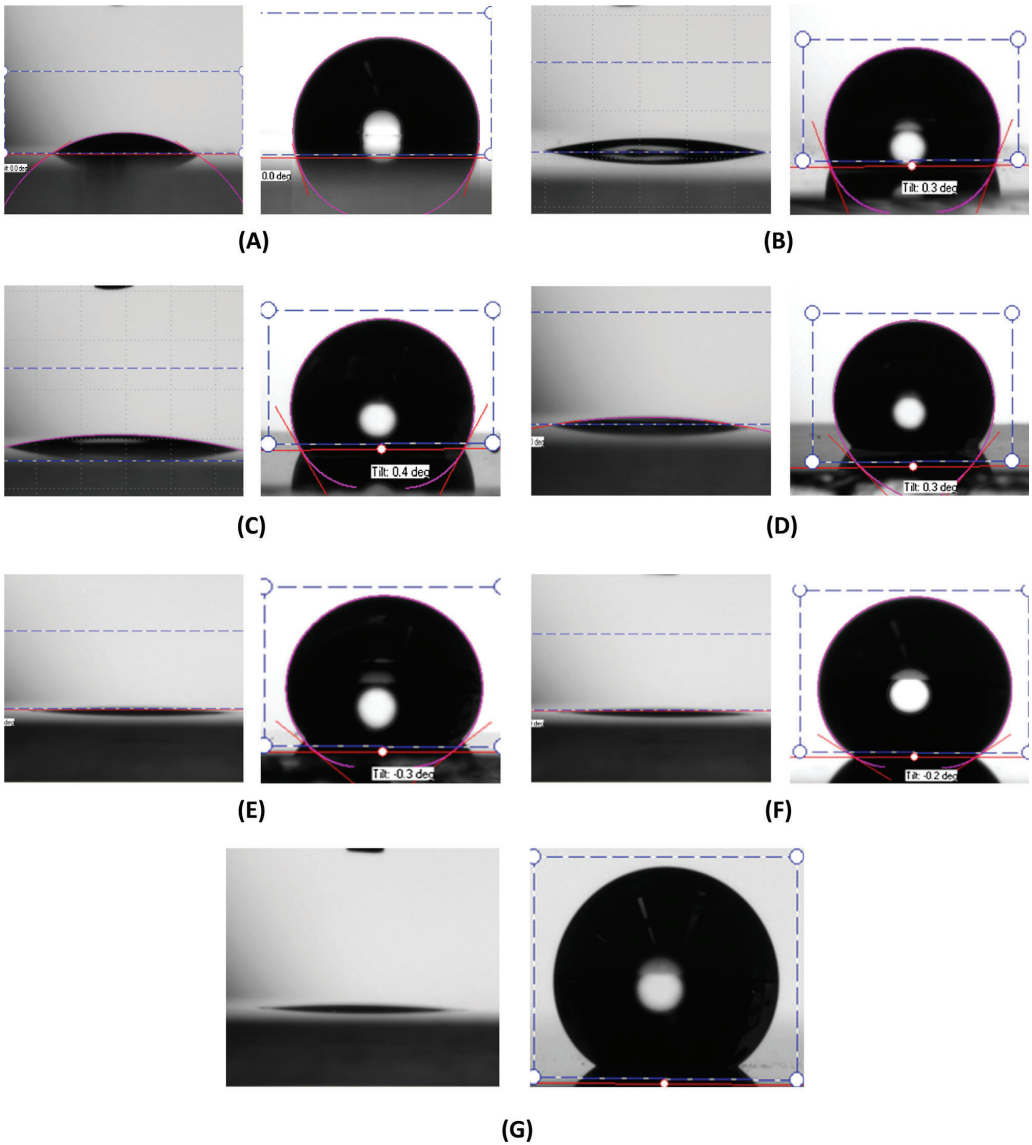

Fig. 4. Comparison between the contact angles images recorded for the films obtained when the glass slides are not silanizated versus when the ones that are functionalized with a different number of bilayers: 4 bilayers (A); 8 bilayers (B); 12 bilayers (C); 16 bilayers (D); 20 bilayers (E); 30 bilayers (F); 40 bilayers (G). In very case, left image is recorded before CVD and the right one after it to ease its comparison.

hydrophobicity. To produce this kind of surfaces, it is necessary to obtain a low energy of interaction with water [32]. Groups such as alkyl or fluorinated are very interesting for creating superhydrophobic surfaces because they satisfy this condition and water is very strongly repelled by these surfaces [33].

In our case, the prepared nanofilms were functionalized by the CVD of 1H,1H,2H,2H-Perfluorodecyltriethoxsilane 97%. To achieve it, each slide was introduced in a glass flask together with 200 μL of 1H,1H,2H,2H-Perfluorodecyltriethoxsilane 97%, sealing it hermetically. The recipient was introduced into an oven at 150 °C for 150 min to ease the silane evaporation as well as its reaction with the nanofilms, completing its silanization (Fig. 1B). Due to the silane nature of the reagent, this process is known as silanization.

2.3. Characterization

The studied features of the nanofilms were roughness, thickness and contact angle before and after the silanization. The roughness was measured by an Atomic Force Microscope (AFM) (Veeco

Innova, model 840-012-711) in tapping mode; it was also used to register the thickness of the films by scratching the surface with a needle and scanning the cantilever perpendicularly to the scratch [34]. For each sample, the AFM measurements were performed 7 times in different zones in order to obtain the mean value and the standard deviation. AFM images were obtained scanning 5 μm × 5 μm areas with 512 lines at a 0.2 Hz frequency. The contact angle was registered (performing five measurements for each slide) with a contact angle meter (CAM 100 KSV Instruments's products). Finally, the composition of the functionalized surfaces was studied by energy-dispersive X-ray spectroscopy (EDX).

3. Results and discussion

Glass slides were coated with different number of bilayers (4, 8, 12, 16, 20, 30 and 40 bilayers). The distinct morphology parameters were registered firstly before the silanization and then, compared to the ones obtained after the CVD process. Furthermore, the superhydrophilic/superhydrophobic behavior was compared in terms of the contact angles measured from the different slides.

3.1. Analysis of superhydrophilic nanofilms

For the LbL technique, a decrease in the roughness of the nanofilms has been assumed when the number of bilayers increases [35]. Nevertheless, some works have recently refuted this feature and have experimentally proven the existence of exceptions that apparently contradict the rules of Layer-by-Layer method and increase roughness when the number of bilayers increase for specific materials and under certain conditions for the spray-assisted Layer-by-Layer [36] and for the classic wet approach (Table 1).

The glass slides were prepared with 10^{-3} M polymer solutions (0.15 M NaCl) and AFM images were taken using 4, 8, 12, 16, 20, 30 and 40 bilayers. The morphology of these coatings is detailed in the supplementary material in terms of thickness, roughness and contact angle (the results agree with the ones reported in a previous work [23,29]). In our case, there is a tradeoff between roughness and optical transmittance: therefore, the highest number of bilayers is set at 40 because above this value, the transmittance is lowered significantly (transmittance of glass slides was measured with a spectrum analyser (JASCO) and was shown in Supplementary Material Fig. 03).

3.1.1. Analysis of the nanofilms after silanization (CVD)

The silanization was based on the chemical evaporation of 1H,1H,2H,2H-Perfluorodecyltriethoxsilane 97%, a reagent considered as a Perfluorodecylsilane (PDS). This type of molecules shows a highly hydrophobic tail and a hydrophilic head: in this case, the hydrophobic part of the molecule is the fluorinated tail, whereas the Si–O constitutes the hydrophilic head. This reagent cannot be directly used for formation of a hydrophobic surface because it has both hydrophobic and hydrophilic properties, so that it is handled as described in Section 2 in order to get the superhydrophobic surface. In this manner, the hydrophilic head of the molecule gets orientated towards the superhydrophilic surface of the nanocoating; as a consequence, the hydrophobic tail points the opposite direction, which inverts the behavior of the film. This change allows the surface energy of the drop to be distributed in a way that does not contact the coating [33]. Therefore, a superhydrophobic surface is obtained by combining the technique LbL with the CVD without using nanoparticles. A picture was taken to confirm the superhydrophobic behavior of the final coating; moreover, a video was recorded comparing the coatings prepared before and after CVD (both the picture and the video are available as supplementary material). Regarding to the optical properties, all the substrates shown an acceptable transmittance at the visible spectrum range

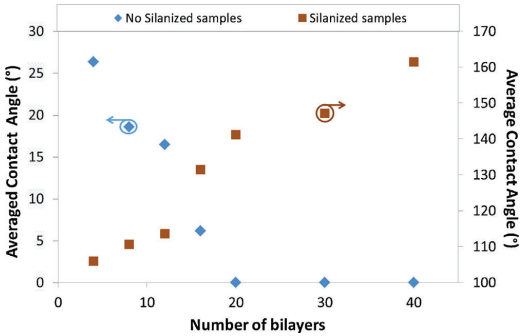

Fig. 5. Averaged of contact angles for the films obtained: left vertical axe is applied for the glass slides are no functionalized whereas the right vertical axe for the silanizated ones.

(as reported in [29]): performing a similar analysis, this parameter is kept after the silanization process.

The morphology of the nanocoating was analysed by AFM images obtained before and after the silanization process in order to quantify any parameter change. The difference between the nanocoatings with 20 bilayers before (Fig. 2A) and after the silanization (Fig. 2C) was only 7 nm RMS and in the case of 40 bilayers the difference was 9.03 nm RMS (comparing Fig. 2B and D). This decrease of the roughness can be a consequence of the bilayers compression when the temperature increases, as well as a smoothing effect produced by the deposited fluorosilane molecules. Likewise, an EDX analysis confirmed the presence of silicon and fluoride, which were not present in a similar test performed before the functionalization (Fig. 3).

In terms of the contact angle, the values obtained after the silanization change sharply compared to the previous ones: in Fig. 4 are shown the captures of a droplet (volume 500 μL) on substrates with different number of bilayers before (left) and after (right) the silanization. It is evident that, when the roughness increases, the pre-treated substrate gets more superhydrophilic, whereas in the case of the post treated one, the contact angle increases. These results are quantified in Fig. 5, where the inverse trend of the contact angle versus the number of bilayers (and therefore, roughness), before and after silanization can be checked. On the one hand, until bilayer 12 there is almost no increment in the contact angle but for higher number of bilayers deposited, the contact angle exhibits a much higher increase: it reaches the maximum value for bilayer 40,

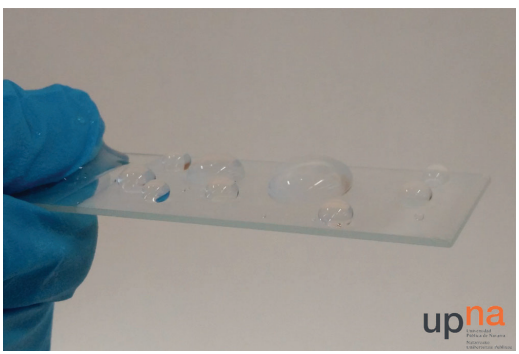

Fig. 6. Picture of the highest contact angle (161°) registered from the 40 bilayers functionalized film for droplets of different volume (from 100 μL up to 4 mL).

which is 161° (Fig. 6). All these data are detailed in Supplementary material Tables 1 and 2. It can be considered that the functionalized coating has become superhydrophobic [37].

4. Conclusions

A superhydrophilic nanocoating with the structure $[PSP/PAH]_n$ prepared with the LbL method is transformed into a superhydrophobic surface by CVD of fluorosilane molecules using only reagents. In this work, the creation of superhydrophobic surfaces does not imply the use of nanoparticles to generate the nanoroughness required in this type of surfaces making the process simpler than others presented in previous works. Furthermore, the contact angles vary from 0° before the silanization up to values above 160° after it. Before the functionalization, the nanofilms show an increasing roughness as the thickness grows: in terms of the hydrophilic behavior, expressed in contact angle, it is enhanced. This morphology easies the deposition of fluorosilane molecules by CVD, yielding to superhydrophobic surfaces: the change in the contact angle before and after the silanization is higher as the number of bilayers grows. Both processes, the preparation of the superhydrophilic nanocoating and its later functionalization, are easy to perform and also show a high reproducibility. Actually, it is not necessary to include nanoparticles along the LbL construction process to get the superhydrophobic behavior, which, to the best of our knowledge, has been achieved for the first time.

Competing interest

The authors declare that they have no competing interests.

Acknowledgments

This work was supported by the Spanish Economy and Competitivity Ministry-FEDER TEC2013-43679-R. The authors would like to express their gratitude to Nadetech Inc. for the design, fabrication and tune-up of the robot used for the deposition of the nanocoatings.

Appendix A. Supplementary data

Supplementary data associated with this article can be found, in the online version, at http://dx.doi.org/10.1016/j.apsusc.2015.06.004

References

[1] H. Teisala, M. Tuominen, M. Aromaa, J.M. Mäkelä, M. Stepien, J.J. Saarinen, M. Toivakka, J. Kuusipalo, Development of superhydrophobic coating on paperboard surface using the Liquid Flame Spray, Surf. Coat. Technol. 205 (2) (2010 Oct) 436–445.
[2] M. Nakamura, P.E.P. Cherry, F. Application, P. Data, United States Patent, vol. 2, no. 12, 2009.
[3] A. Nakajima, K. Hashimoto, T. Watanabe, Transparent Superhydrophobic Thin Films with Self-Cleaning Properties, no. 15, 2000, pp. 7044–7047.
[4] A. Marmur, Super-hydrophobicity fundamentals: implications to biofouling prevention, Biofouling 22 (2006) 107–115.
[5] Z. Xue, S. Wang, L. Lin, L. Chen, M. Liu, L. Feng, L. Jiang, A novel superhydrophilic and underwater superoleophobic hydrogel-coated mesh for oil/water separation, Adv. Mater. 23 (October (37)) (2011) 4270–4273.
[6] T. Darmanin, F. Guittard, Superoleophobic polymers with metal ion affinity toward materials with both oleophobic and hydrophilic properties, J. Colloid Interface Sci. 408 (2013) 101–106.
[7] B. Mahltig, F. Audenaert, H. Böttcher, Hydrophobic silica sol coatings on textiles-the influence of solvent and sol concentration, J. Sol-Gel Sci. Technol. 34 (2005) 103–109.
[8] T. Kobayashi, K. Shimizu, Y. Kaizuma, S. Konishi, Novel combination of hydrophilic/hydrophobic surface for large wettability difference and its application to liquid manipulation, Lab Chip 11 (4) (2011) 639–644.
[9] Z. Ma, Z. Mao, C. Gao, Surface modification and property analysis of biomedical polymers used for tissue engineering, Colloids Surf. B: Biointerfaces 60 (2007) 137–157.
[10] J. Drelich, E. Chibowski, D.D. Meng, K. Terpilowski, Hydrophilic and superhydrophilic surfaces and materials, Soft Matter 7 (21) (2011) 9804.
[11] T. Onda, S. Shibuichi, N. Satoh, K. Tsujii, Super-water-repellent fractal surfaces, Langmuir 12 (1996) 2125–2127.
[12] S. Shibuichi, T. Onda, N. Satoh, K. Tsujii, Super water-repellent surfaces resulting from fractal structure. II, J. Jpn. Oil Chem. Soc. 46 (713) (1997) 649–659.
[13] R. Wang, K. Hashimoto, A. Fujishima, M. Chikuni, E. Kojima, A. Kitamura, M. Shimohigoshi, T. Watanabe, Light-induced amphiphilic surfaces, Nature 388 (1997) 431–432.
[14] J. Drelich, E. Chibowski, Superhydrophilic and superwetting surfaces: definition and mechanisms of control, Langmuir 26 (December (24)) (2010) 18621–18623.
[15] G.J. Toes, K.W. Van Muiswinkel, W. Van Oeveren, A.J.H. Suurmeijer, W. Timens, I. Stokroos, J.J.A.M. Van Den Dungen, Superhydrophobic modification fails to improve the performance of small diameter expanded polytetrafluoroethylene vascular grafts, Biomaterials 23 (2002) 255–262.
[16] Z.G. Guo, W.M. Liu, B.L. Su, A stable lotus-leaf-like water-repellent copper, Appl. Phys. Lett. 92 (May 2015) (2008) 1–4.
[17] M. Jin, X. Feng, J. Xi, J. Zhai, K. Cho, L. Feng, L. Jiang, Super-hydrophobic PDMS surface with ultra-low adhesive force, Macromol. Rapid Commun. 26 (2005) 1805–1809.
[18] C.T. Wirth, S. Hofmann, J. Robertson, Surface properties of vertically aligned carbon nanotube arrays, Diam. Relat. Mater. 17 (2008) 1518–1524.
[19] B. Siboulet, B. Coasne, J.F. Dufrêche, P. Turq, Hydrophobic transition in porous amorphous silica, J. Phys. Chem. B 115 (2011) 7881–7886.
[20] X. Liu, J. He, One-step hydrothermal creation of hierarchical microstructures toward superhydrophilic and superhydrophobic surfaces, Langmuir 25 (35) (2009) 11822–11826.
[21] E.L. Decker, S. Garoff, Contact line structure and dynamics on surfaces with contact angle hysteresis 7463 (15) (1997) 6321–6332.
[22] J. Bravo, L. Zhai, Z. Wu, R.E. Cohen, M.F. Rubner, Transparent Superhydrophobic Films Based on Silica Nanoparticles, no. 28, 2007, pp. 7293–7298.
[23] N. Cini, T. Tulun, G. Decher, V. Ball, Step-by-step assembly of self-patterning polyelectrolyte films violating (almost) all rules of layer-by-layer deposition, J. Am. Chem. Soc. 132 (June (24)) (2010) 8264–8265.
[24] F. Surre, W.B. Lyons, T. Sun, K.T.V. Grattan, S. O'Keeffe, E. Lewis, C. Elosua, M. Hernaez, C. Barian, U-bend fibre optic pH sensors using layer-by-layer electrostatic self-assembly technique, J. Phys. Conf. Ser. 178 (July) (2009) 012046.
[25] F.J. Arregui, I.R. Matias, J.M. Corres, I. Del Villar, J. Goicoechea, C.R. Zamarreño, M. Hernáez, R.O. Claus, Optical fiber sensors based on Layer-by-Layer nanostructured films, Proc. Eng. 5 (January) (2010) 1087–1090.
[26] P. Zubiate, C.R. Zamarreño, I. Del Villar, I.R. Matias, F.J. Arregui, D-shape optical fiber refractometer based on TM and TE lossy mode resonances, 9157 (2014) 91577V–91577V–4.
[27] W. Wang, B. Gu, Self-Assembly of Two- and Three-Dimensional Particle Arrays by Manipulating the Hydrophobicity of Silica Nanospheres, 2008, pp. 22175–22180.
[28] N.A. Kotov, Layer-by-layer self-assembly: the contribution of hydrophobic interactions, Nanostruct. Mater. 12 (1999) 789–796.
[29] C. Elosua, D. Lopez-Torres, M. Hernaez, I.R. Matias, F.J. Arregui, Comparative study of layer-by-layer deposition techniques for poly(sodium phosphate) and poly(allylamine hydrochloride), Nanoscale Res. Lett. 8 (539) (2013).
[30] M. Hernaez, D. Lopez-Torres, C. Elosua, I.R. Matias, F.J. Arregui, Sensitivity enhancement of a humidity sensor based on poly(sodium phosphate) and poly(allylamine hydrochloride), 2013 IEEE Sens. (November) (2013) 1–4.
[31] V. Ball, A. Laachachi, V. Toniazzo, D. Ruch, Influence of the nature of the polycation on the adsorption kinetics and on exchange processes in polyelectrolyte multilayer films, J. Colloid Interface Sci. 366 (January (1)) (2012) 96–104.
[32] D. Popovici, a.I. Barzic, I. Stoica, M. Butnaru, G.E. Ioanid, S. Vlad, C. Hulubei, M. Bruma, Plasma modification of surface wettability and morphology for optimization of the interactions involved in blood constituents spreading on some novel copolyimide films, Plasma Chem. Plasma Process. 32 (2012) 781–799.
[33] M. Zhu, W. Zuo, H. Yu, W. Yang, Y. Chen, Superhydrophobic surface directly created by electrospinning based on hydrophilic material, J. Mater. Sci. 41 (April (12)) (2006) 3793–3797.
[34] A. Urrutia, P.J. Rivero, L. Ruete, J. Goicoechea, C. Fernández-Valdivieso, F.J. Arregui, I.R. Matías, An antibacterial surface coating composed of PAH/SiO_2 nanostructurated films by layer by layer, Phys. Status Solidi 7 (November (11–12)) (2010) 2774–2777.
[35] K. Apaydin, A. Laachachi, V. Ball, M. Jimenez, S. Bourbigot, V. Toniazzo, D. Ruch, Intumescent coating of (polyallylamine-polyphosphates) deposited on polyamide fabrics via layer-by-layer technique, Polym. Degrad. Stab. 106 (August) (2014) 158–164.
[36] J. Seo, J.L. Lutkenhaus, J. Kim, P.T. Hammond, Effect of the Layer-by-Layer (LbL) Deposition Method on the Surface Morphology and Wetting Behavior of Hydrophobically Modified PEO and PAA LbL Films, no. 16, 2008, pp. 7995–8000.
[37] T. Sun, G. Wang, L. Feng, B. Liu, Y. Ma, L. Jiang, D. Zhu, Reversible switching between superhydrophilicity and superhydrophobicity, Angew. Chem. Int. Ed. Engl. 43 (January (3)) (2004) 357–360.

I.2 Conclusiones

La película formada por los polímeros PSP y PAH no es una buena candidata para desarrollar sensores de humedad basados en fibras SC-PCF e interferómetros MZ.

Al aumentar el espesor de una película formada por los polímeros PSP y PAH, siendo depositada mediante la técnica *LbL* o spray *LbL* y bajo unas determinadas condiciones de molaridad, se consigue que la rugosidad de la película también aumente. Este es un resultado muy relevante ya que está en contra de las reglas generales de la técnica *LbL* y abre nuevas vías de investigación.

Gracias a este hecho, la morfología final de dicha película permite, en gran medida, la interacción con el agua. Debido a este comportamiento, los ángulos de contacto medidos son muy bajos pudiendo ser considerado como superhidrofílico el comportamiento de los recubrimientos.

Mediante una silanización de la superficie, utilizando la técnica CVD, se ha conseguido cambiar por completo la afinidad de la película polimérica formada por el PSP y el PAH pasando de ser superhidrofílica (0° su ángulo de contacto) a superhidrofóbica (165° su ángulo de contacto). El proceso se ha conseguido de una forma simple y utilizando temperaturas no excesivamente elevadas como necesitan otros métodos o técnicas.

Anexo II

Publicaciones

En este Anexo II de la tesis, se exponen las diferentes contribuciones científicas que se han obtenido durante el desarrollo de la misma. Se ha realizado un resumen de los diferentes artículos científicos publicados en revistas internacionales o nacionales, así como de la participación del autor en congresos, bien sean internacionales o nacionales, y de contribución realizada, posters o charlas.

II.1 Artículos científicos publicados en revistas internacionales relacionados directamente con el tema principal de la tesis

[1] D. Lopez-Torres, A. Lopez-Aldaba, C. Elosua, J. L. Auguste, R. Jamier, P. Roy, M. Lopez-Amo, and F. J. Arregui, "Comparison between different structures of suspended-core microstructured optical fibres for volatiles sensing," Sensors (Switzerland), vol. 18, no. 8, 2018.

[2] A. Lopez-Aldaba, D. Lopez-Torres, C. E. Aguado, F. J. Arregui, J. L. Auguste, R. Jamier, P. Roy, and M. Lopez-Amo, "Real time measuring system of multiple chemical parameters using microstructured optical fibres based sensors," IEEE Sens. J., vol. 18, no. 13, pp. 5343–5351, 2018.

[3] A. Lopez Aldaba, D. Lopez-Torres, M. Campo-Bescós, J. López, D. Yerro, C. Elosua, F. Arregui, J.-L. Auguste, R. Jamier, P. Roy, and M. López-Amo, "Comparison between Capacitive and Microstructured Optical Fibre Soil Moisture Sensors," Appl. Sci., vol. 8, no. 9, p. 1499, 2018.

[4] C. Elosua, D. Lopez-Torres, M. Hernaez, I. R. Matias, and F. J. Arregui, "Comparative study of layer-by-layer deposition techniques for poly(sodium phosphate) and poly(allylamine hydrochloride)," Nanoscale Res. Lett., vol. 8, no. 1, pp. 1–22, 2013.

[5] D. Lopez-Torres, C. Elosua, M. Hernaez, J. Goicoechea, and F. J. Arregui, "From superhydrophilic to superhydrophobic surfaces by means of polymeric Layer-by-Layer films," Appl. Surf. Sci., vol. 351, pp. 1081–1086, 2015.

[6] D. Lopez-Torres, A. Lopez-Aldaba, C. E. Aguado, J.-L. Auguste, R. Jamier, P. Roy, M. Lopez-Amo, and F. J. Arregui, "Sensitivity Optimization of a Microstructured Optical Fibre Ammonia Gas Sensor by means of Tuning the Thickness of a Metal Oxide nano-Coating," IEEE Sens. J., vol. 19, no. 13, pp. 1–1, 2019.

[7] A. Lopez Aldaba, D. Lopez-Torres, C. Elosua, J. L. Auguste, R. Jamier, P. Roy, F. J. Arregui, and M. Lopez-Amo, "SnO2-MOF-Fabry-Perot optical sensor for relative humidity measurements," Sensors Actuators, B Chem., vol. 257, pp. 189–199, 2018.

[8] D. Lopez-Torres, C. Elosua, J. Villatoro, J. Zubia, M. Rothhardt, K. Schuster, and F. J. Arregui, "Photonic crystal fibre interferometer coated with a PAH/PAA nanolayer as humidity sensor," Sensors Actuators, B Chem., vol. 242, pp. 1065–1072, 2016.

[9] D. Lopez-Torres, C. Elosua, J. Villatoro, J. Zubia, M. Rothhardt, K. Schuster, and F. J. Arregui, "Enhancing sensitivity of photonic crystal fibre interferometric humidity sensor by the thickness of SnO2 thin films," Sensors Actuators B Chem., 2017.

II.2 Otros artículos científicos publicados relacionados con el tema de la tesis

[1] C. Elosua, F. J. Arregui, I. Del Villar, C. Ruiz-Zamarreño, J. M. Corres, C. Bariain, J. Goicoechea, M. Hernaez, P. J. Rivero, A. B. Socorro, A. Urrutia, P. Sanchez, P. Zubiate, D. Lopez-Torres, N. De Acha, J. Ascorbe, A. Ozcariz, and I. R. Matias, "Micro and nanostructured materials for the development of optical fibre sensors," Sensors (Switzerland), vol. 17, no. 10, 2017.

[2] I. Del Villar, F. J. Arregui, C. R. Zamarreno, J. M. Corres, C. Bariain, J. Goicoechea, C. Elosua, M. Hernaez, P. J. Rivero, A. B. Socorro, A. Urrutia, P. Sanchez, P. Zubiate, D. Lopez, N. De Acha, J. Ascorbe, and I. R. Matias, "Optical sensors based on lossy-mode resonances," Sensors Actuators, B Chem., vol. 240, pp. 174–185, 2017.

II.3 Contribuciones orales en conferencias de congresos internacionales directamente relacionadas con el tema principal de la tesis

[1] "Enhancing Sensitivity of Photonic Crystal Fibre Interferometric Humidity Sensor with the Thickness of SnO_2 Thin Films", The 16th International Meeting on Chemical Sensors, 2016, Jeju Island, South Korea.

[2] C. Elosúa, D. López-Torres, N. de Acha, I. R. Matías, F.J. Arregui, "Functionalization of rough nanofilms deposited onto optical fibre to implement

gas and vapors sensors", The 16th International Meeting on Chemical Sensors, 2016, Jeju Island, South Korea.

[3] Greece Invited Talk: Micro and Nano structured Coatings for the Development of Optical Fibre, "IC-MAST 2016 6th International Conference on Materials and Applications for Sensors and Transducers."

II.4 Otras contribuciones orales en conferencias de congresos internacionales relacionadas con el tema de la tesis

[1] Fibre-Optic Lossy Mode Resonance Sensors, Francisco J. Arregui, Ignacio Del Villar, Jesus M. Corres, Javier Goicoechea, Carlos R. Zamarreño, Cesar Elosua, Miguel Hernaez, Pedro J. Rivero, Abian B. Socorro, Aitor Urrutia, Pedro Sanchez, Pablo Zubiate, Diego Lopez, Nerea De Acha, Ignacio R. Matias, XXVIII Eurosensors, 2014, Brescia, Italy doi:10.1016/j.proeng.2014.11.253

[2] Fibre optic sensors based on lossy mode resonances, Matias I. R., Arregui, F. J., Del Villar I., Corres J. M. Goicoechea J., Zamarreño Z. R., Elosúa C., Hernáez M., Rivero P. J., Socorro A. B. , Urrutia A., Sanchez P., Zubiate P., Lopez D., De Acha N., Latin America Optics and Photonics Conference, LAOP, 2014, Cancun, Mexico.

[3] Nanocoated Optical Fibre for Lossy Mode Resonance (LMR) Sensors and Filters, Ignacio Del Villar, Francisco J. Arregui, Jesus M. Corres, Candido Bariain, Javier Goicoechea, Carlos R. Zamarreño, Cesar Elosua, Miguel Hernaez, Pedro J. Rivero, Abian B. Socorro, Aitor Urrutia, Pedro Sanchez, Pablo Zubiate, Diego Lopez, Nerea De Acha, Joaquin Ascorbe, and Ignacio R. Matias, 17th International Conference on Transparent Optical Networks, ICTON, 2015, Budapest, Hungary http://dx.doi.org/10.1109/ICTON.2015.7193695

[4] Micro and Nano structured Coatings for the Development of Optical Fibre Sensors, C. Elosua, F. J. Arregui, I. Del Villar, C. R. Zamarreño, J. M. Corres, C. Bariain, J. Goicoechea, M. Hernaez, P. J. Rivero, A. B. Socorro, A. Urrutia, P. Sanchez, P. Zubiate, D. Lopez, N. De Acha, J. Ascorbe, A. Ozcariz, I. R. Matias, 6th International Conference on Materials and Applications for Sensors and Transducers, September 27-30, 2016, Athens, Greece.

[5] C. R. Zamarreño, P. Zubiate, A. Ozcariz, C. Elosua, A. B. Socorro, and A. Urrutia, "Optical Fibre Sensors Label-free optical fibre sensing platform based on Lossy Mode Resonances," 5th Int. Conf. Sensors Eng. Electron. Instrum. Adv., no. September, pp. 4–5, 2019.

II.5 Posters presentados en conferencias de congresos internacionales directamente relacionados con el tema principal de la tesis

[1] D. Lopez-Torres, A. Lopez-Aldaba, C. Elosua, J. L. Auguste, R. Jamier, P. Roy, M. Lopez-Amo, and F. J. Arregui, "Enhancement of the Sensitivity of a Volatile Organic Compounds MOF-Sensor by Means of Its Structure," Proc. Eurosensors, vol. 1, no. 4, p. 451, 2017.

[2] M. Hernaez, D. Lopez-Torres, C. Elosua, I. R. Matias, and F. J. Arregui, "Sensitivity enhancement of a humidity sensor based on poly(sodium phosphate) and poly(allylamine hydrochloride)," Proc. Ibernam, vol. 277, pp. 8264–8265, 2013.

[3] F. J. A. D. Lopez-Torres, N. De Acha, C. Elosua, "SnO2 humidity interferometric sensor based on photonic crystal optical fibre and Fast Fourier Transform," Proc. Ibernam, vol. 34, no. 5, p. 8724, 2016.

[4] I. R. M. and F. J. A. D. Lopez-Torres, C. Elosua, "Sensors based on Microstructured Optical Fibres for the detection of Volatile Organic Compounds, Gases and Humidity," Proc. Ibernam-CMC2, 2018.

[5] M. Hernaez, D. Lopez-Torres, C. Elosua, I. R. Matias, and F. J. Arregui, "Sensitivity enhancement of a humidity sensor based on poly(sodium phosphate) and poly(allylamine hydrochloride)," Proc. IEEE Sensors, pp. 1–4, 2013.

[6] A. Lopez-Aldaba, D. Lopez-Torres, J. Ascorbe, S. Rota-Rodrigo, C. Elosua, M. Lopez-Amo, F. J. Arregui, J. M. Corres, J.-L. Auguste, R. Jamier, and P. Roy, "SnO_2-MOF-Fabry-Pérot humidity optical sensor system based on fast Fourier transform technique," in Proceedings of SPIE - The International Society for Optical Engineering, 2016, vol. 9916.

[7] A. Lopez-Aldaba, D. Lopez-Torres, C. Elosua, J.-L. Auguste, R. Jamier, P. Roy, F.J. Arregui, and M. López-Amo, "Relative humidity multi-point optical sensors system based on Fast Fourier multiplexing technique," Proc. OFS, vol. 10323, pp. 1–4, 2017.

[8] A. L. Aldaba, D. Lopez-Torres, M. A. Campo-Bescós, J. J. López, D. Yerro, C. Elosua, F. J. Arregui, J.-L. Auguste, R. Jamier, P. Roy, and M. López-Amo, "Microstructured optical fibre sensor for soil moisture measurements," Proc. OFS26, p. WF41, 2018.

[9] A. Lopez Aldaba*, D. Lopez-Torres, M. A. Campo-Bescós, J. J. López, D. Yerro, C. Elosua, F. J. Arregui, J-L. Auguste, R. Jamier, P. Roy, and M. López-Amo, "Microstructured optical fibre sensor for soil moisture measurements," Proc. APOS, pp. 783–788, 2017.

II.6 Otros posters presentados en conferencias de congresos internacionales relacionados con el tema principal de la tesis

[1] F. J. A. Cesar Elosua*, Diego Lopez-Torres, Miguel Hernaez, Ignacio R. Matias, "SUPER-HYDROPHILIC BEHAVIOR O OF POLY(SODIUM PH HOSPHATE) BASED D LAYER- BY LAYER FILMS," in Layer-by-Layer Assemblies: Science and Technology, 2014.

[2] I. R. M. C. Elosua, F. J. Arregui1, I. Del Villar, C. R. Zamarreño, J. M. Corres, C. Bariain, P. J. Rivero, A. B. Socorro, P. Sanchez, P. Zubiate, D. Lopez, N. De Acha, J. Ascorbe, A. Ozcariz, "Optical fibre sensors for environmental and bio medical applications," in Metal and Water, 2017.

[3] C. Elosua, N. De Acha, D. Lopez-Torres, I. R. Matias, and F. J. Arregui, "Luminescent optical fibre oxygen sensor following layer-by-layer method," Procedia Eng., vol. 87, pp. 987–990, 2014.

[4] O. F. and G. D. C. Elosúa, D. López-Torres, F. J. Arregui, V. Ball, "Development of Highly Unusual Nanoscale Morphologies During the Alternating Exposure of Surfaces to Polyanions and Polycations," Proc. Nanyang Technol. Univ., 2018.

II.7 Premios obtenidos durante la tesis

Mejor presentación Póster en el congreso internacional: "IBERNAM-CMC2" que tuvo lugar en Tarragona en octubre de 2018.

REFERENCIAS

[1] S. P. Kumar and C. Y. Chong, "Sensor networks: Evolution, opportunities, and challenges," *Proc. IEEE*, vol. 91, no. 8, pp. 1247–1256, 2003.

[2] B. Gholamzadeh and H. Nabovati, "Fibre Optic Sensors," *World Acad. Sci. Eng. Technol.*, vol. 42, no. 6, pp. 297–307, 2011.

[3] K. O. Hill and G. Meltz, "Fibre Bragg grating technology fundamentals and overview," *J. Light. Technol.*, vol. 15, no. 8, pp. 1263–1276, 1997.

[4] V. Bhatia and A. M. Vengsarkar, "Optical fibre long-period grating sensors," *Opt. Lett.*, vol. 21, no. 9, p. 692, 1996.

[5] S. Tofighi, A. Bahrampour, N. Pishbin, and A. R. Bahrampour, "Interferometric fibre-optic sensors," *Opt. Fibre Sensors Adv. Tech. Appl.*, pp. 37–78, 2017.

[6] B. D. Gupta and R. K. Verma, "Surface Plasmon Resonance-Based Fibre Optic Sensors: Principle, Probe Designs, and Some Applications," *J. Sensors*, vol. 2009, pp. 1–12, 2009.

[7] Z. Liu, H.-Y. Tam, L. Htein, M.-L. V. Tse, and C. Lu, "Microstructured Optical Fibre Sensors," *J. Light. Technol.*, vol. 35, no. 16, pp. 3425–3439, 2017.

[8] J. Villatoro and J. Zubia, "New perspectives in photonic crystal fibre sensors," *Opt. Laser Technol.*, vol. 78, pp. 67–75, 2016.

[9] W. Jin, H. L. Ho, Y. C. Cao, J. Ju, and L. F. Qi, "Gas detection with micro- and nano-engineered optical fibres," *Opt. Fibre Technol.*, vol. 19, no. 6 PART B, pp. 741–759, 2013.

[10] C. Elosua, I. R. Matias, C. Bariain, and F. J. Arregui, "Volatile Organic Compound Optical Fibre Sensors: A Review," *Sensors*, vol. 6, no. 11, pp. 1440–1465, 2006.

[11] B. Lee, "Review of the present status of optical fibre sensors," *Opt. Fibre Technol.*, vol. 9, no. 2, pp. 57–79, 2003.

[12] X. D. Wang and O. S. Wolfbeis, "Fibre-Optic Chemical Sensors and Biosensors," *Anal. Chem.*, vol. 88, no. 1, pp. 203–227, 2016.

[13] J. I. Peterson and G. G. Vurek, "Fibre-optic sensors for biomedical applications," *Science (80-.).*, vol. 224, pp. 123–127, 1984.

[14] A. D. and A. D. Kersey, "Applications of Fibre-optic Sensors," *IEEE Trans. components, hybrids, Manuf. Technol.*, vol. 13, no. March, pp. 137–143, 1990.

[15] W. Morey, G. Meltz, and H. Glenn, "Fibre optic Bragg grating sensors," *Fibre Opt. Laser Sensors VII*, vol. 1169, pp. 98–107, 1989.

[16] F. J. Arregui, I. Del Villar, J. M. Corres, J. Goicoechea, C. R. Zamarreño, C. Elosua, M. Hernaez, P. J. Rivero, A. B. Socorro, A. Urrutia, P. Sanchez, P. Zubiate, D. Lopez, N. De Acha, and I. R. Matias, "Fibre-optic Lossy Mode Resonance Sensors," *Procedia Eng.*, vol. 87, pp. 3–8, 2014.

[17] C. Elosua, F. J. Arregui, I. Del Villar, C. Ruiz-Zamarreño, J. M. Corres, C. Bariain, J. Goicoechea, M. Hernaez, P. J. Rivero, A. B. Socorro, A. Urrutia, P. Sanchez, P. Zubiate, D. Lopez-Torres, N. De Acha, J. Ascorbe, A. Ozcariz, and I. R. Matias, "Micro and nanostructured materials for the development of optical fibre sensors," *Sensors (Switzerland)*, vol. 17, no. 10, 2017.

[18] R. A. Perez-Herrera and M. Lopez-Amo, "Fibre optic sensor networks," *Opt. Fibre Technol.*, vol. 19, no. 6 PART B, pp. 689–699, 2013.

[19] P. S. J. RUSSELL, "Photonic band gaps," *Phys. World*, vol. 5, no. 8, pp. 37–42, 1992.

[20] P. Kaiser and H. W. Astle, "Low-Loss Single-Material Fibres Made From Pure Fused Silica," *Bell Syst. Tech. J.*, vol. 53, no. 6, pp. 1021–1039, 1974.

[21] T. A. Birks, P. S. J. Russell, and J. C. Knight, "Endlessly single-mode photonic crystal fibre," *Opt. Lett.*, vol. 22, no. 13, p. 961, 1997.

[22] P. Russell, "Applied physics: Photonic crystal fibres," *Science (80-.).*, vol. 299, no. 5605, pp. 358–362, 2003.

[23] A. M. R. Pinto and M. Lopez-Amo, "Photonic Crystal Fibres for Sensing Applications," *J. Sensors*, vol. 2012, pp. 1–21, 2012.

[24] P. Lin, Y. Li, T. Cheng, T. Suzuki, and Y. Ohishi, "Coexistence of Photonic

Bandgap Guidance and Total Internal Reflection in Photonic Crystal Fibre Based on a High-Index Array With Internal Air Holes," *IEEE J. Sel. Top. Quantum Electron.*, vol. 22, no. 2, pp. 265–270, 2016.

[25] P. S. J. Russell, "Photonic-Crystal Fibres," vol. 24, no. 12, pp. 4729–4749, 2006.

[26] T. M. Monro, W. Belardi, K. Furusawa, J. C. Baggett, N. G. R. Broderick, and D. J. Richardson, "Sensing with microstructured optical fibres," *Meas. Sci. Technol.*, vol. 12, no. 7, pp. 854–858, 2001.

[27] T. M. Monro, S. Warren-Smith, E. P. Schartner, A. Franois, S. Heng, H. Ebendorff-Heidepriem, and S. Afshar, "Sensing with suspended-core optical fibres," *Opt. Fibre Technol.*, vol. 16, no. 6, pp. 343–356, 2010.

[28] O. Frazao, J. M. Baptista, J. L. Santos, and P. Roy, "Curvature sensor using a highly birefringent photonic crystal fibre with two asymmetric hole regions in a Sagnac interferometer," *Appl. Opt.*, vol. 47, no. 13, pp. 2520–2523, 2008.

[29] Q. S. Q. Shi, F. L. F. Lv, Z. W. Z. Wang, L. J. L. Jin, J. J. H. J. J. Hu, Z. L. Z. Liu, G. K. G. Kai, and X. D. X. Dong, "Environmentally Stable Fabry–Pérot-Type Strain Sensor Based On Hollow-Core Photonic Bandgap Fibre," *IEEE Photonics Technol. Lett.*, vol. 20, no. 4, pp. 2008–2010, 2008.

[30] J. Villatoro, V. P. Minkovich, and D. Monzón-Hernández, "Temperature-independent strain sensor made from tapered holey optical fibre," *Opt. Lett.*, vol. 31, no. 3, p. 305, 2006.

[31] S. Mathews, G. Farrell, and Y. Semenova, "Liquid crystal infiltrated photonic crystal fibres for electric field intensity measurements," *Appl. Opt.*, vol. 50, no. 17, p. 2628, 2011.

[32] Y. Zhao, R. Q. Lv, Y. Ying, and Q. Wang, "Hollow-core photonic crystal fibre FabryPerot sensor for magnetic field measurement based on magnetic fluid," *Opt. Laser Technol.*, vol. 44, no. 4, pp. 899–902, 2012.

[33] D. E. Ceballos-Herrera, I. Torres-Gomez, A. Martinez-Rios, L. Garcia, and J. J. Sanchez-Mondragon, "Torsion sensing characteristics of mechanically induced long-period holey fibre gratings," *IEEE Sens. J.*, vol. 10, no. 7, pp. 1200–1205, 2010.

[34] S. Silva, P. Roriz, and O. Frazão, "Refractive Index Measurement of Liquids Based on Microstructured Optical Fibres," *Photonics*, vol. 1, no. 4, pp. 516–529, 2014.

[35] K. Chah, N. Linze, C. Caucheteur, P. Mégret, P. Tihon, O. Verlinden, S. Sulejmani, T. Geernaert, F. Berghmans, H. Thienpont, and M. Wuilpart, "Temperature-insensitive polarimetric vibration sensor based on HiBi microstructured optical fibre," *Appl. Opt.*, vol. 51, no. 25, p. 6130, 2012.

[36] J. B. Jensen, L. H. Pedersen, P. E. Hoiby, L. B. Nielsen, T. P. Hansen, J. R. Folkenberg, J. Riishede, D. Noordegraaf, K. Nielsen, A. Carlsen, and A. Bjarklev, "Photonic crystal fibre based evanescent-wave sensor for detection of biomolecules in aqueous solutions," *Opt. Lett.*, vol. 29, no. 17, p. 1974, 2004.

[37] Y. Xu, P. Lu, L. Chen, and X. Bao, "Recent Developments in Micro-Structured Fibre Optic Sensors," *Fibres*, vol. 5, no. 1, p. 3, 2017.

[38] K. Ajani, "Triage; a literature review of key concepts," *J. Pak. Med. Assoc.*, vol. 62, no. 5, pp. 487–489, 2012.

[39] R. Thapa, K. Knabe, M. Faheem, A. Naweed, O. L. Weaver, and K. L. Corwin, "Saturated absorption spectroscopy of acetylene gas inside large-core photonic bandgap fibre," *Opt. Lett.*, vol. 31, no. 16, pp. 2489–2491, 2006.

[40] Y. L. Hoo, W. Jin, H. L. Ho, J. Ju, and D. N. Wang, "Gas diffusion measurement using hollow-core photonic bandgap fibre," *Sensors Actuators, B Chem.*, vol. 105, no. 2, pp. 183–186, 2005.

[41] Y. Tan, W. Jin, F. Yang, and H. L. Ho, "High finesse hollow-core fibre resonating cavity for high sensitivity gas sensing application," vol. 35, no. 14, p. 103230A, 2017.

[42] S. Li, S. Liu, Z. Song, Y. Han, T. Cheng, G. Zhou, and L. Hou, "Study of the sensitivity of gas sensing by use of index-guiding photonic crystal fibre," *Appl. Opt.*, vol. 46, no. 22, pp. 5183–5188, 2007.

[43] G. Pickrell, W. Peng, and A. Wang, "Random-hole optical fibre evanescent-wave gas sensing," *Opt. Lett.*, vol. 29, no. 13, p. 1476, 2004.

[44] Y. L. Hoo, "Evanescent-wave gas sensing using microstructure fibre," *Opt. Eng.*, vol. 41, no. 1, p. 8, 2002.

[45] G. F. Yan, A. P. Zhang, G. Y. Ma, B. H. Wang, B. Kim, J. Im, S. L. He, and Y. Chung, "Fibre-Optic Acetylene Gas Sensor Based on Microstructured Optical Fibre Bragg Gratings," *Ieee Photonics Technol. Lett.*, vol. 23, no. 21, pp. 1588–1590, 2011.

[46] E. Austin, A. van Brakel, M. N. Petrovich, and D. J. Richardson, "Fibre optical sensor for C2H2 gas using gas-filled photonic bandgap fibre reference cell," *Sensors Actuators, B Chem.*, vol. 139, no. 1, pp. 30–34, 2009.

[47] Y. L. Hoo, W. Jin, C. Shi, H. L. Ho, D. N. Wang, and S. C. Ruan, "Design and modeling of a photonic crystal fibre gas sensor," *Appl. Opt.*, vol. 42, no. 18, p. 3509, 2003.

[48] A. S. Webb, "Suspended-core holey fibre for evanescent-field sensing," *Opt. Eng.*, vol. 46, no. 1, p. 010503, 2007.

[49] S. H. Kassani, J. Park, Y. Jung, J. Kobelke, and K. Oh, "Fast response in-line gas sensor using C-type fibre and Ge-doped ring defect photonic crystal fibre," *Opt. Express*, vol. 21, no. 12, p. 14074, 2013.

[50] J. P. Parry, B. C. Griffiths, N. Gayraud, E. D. McNaghten, A. M. Parkes, W. N. MacPherson, and D. P. Hand, "Towards practical gas sensing with micro-structured fibres," *Meas. Sci. Technol.*, vol. 20, no. 7, 2009.

[51] A. M. Cubillas, M. Silva-Lopez, J. M. Lazaro, O. M. Conde, M. N. Petrovich, and J. M. Lopez-Higuera, "Methane sensing at 1300 nm band with hollow-core photonic bandgap fibre as gas cell," *Electron. Lett.*, vol. 44, no. 6, 2008.

[52] Y. L. Hoo, S. Liu, H. L. Ho, and W. Jin, "Fast response microstructured optical fibre methane sensor with multiple side-openings," *IEEE Photonics Technol. Lett.*, vol. 22, no. 5, pp. 296–298, 2010.

[53] A. M. Cubillas, M. Silva-Lopez, J. M. Lazaro, O. M. Conde, M. N. Petrovich, and J. M. Lopez-Higuera, "Methane detection at 1670-nm band using a hollow-core photonic bandgap fibre and a multiline algorithm.," *Opt. Express*, vol. 15, no. 26, pp. 17570–17576, 2007.

[54] M. R. Sardar and M. Faisal, "Gas sensor based on octagonal hollow core

photonic crystal Fibre," *2017 IEEE Int. Conf. Imaging, Vis. Pattern Recognition, icIVPR 2017*, pp. 2–5, 2017.

[55] I. Islam, B. K. Paul, K. Ahmed, R. Hasan, S. Chowdhury, S. Islam, S. Sen, A. N. Bahar, and S. Asaduzzaman, "Highly birefringent single mode spiral shape photonic crystal fibre based sensor for gas sensing applications," *Sens. Bio-Sensing Res.*, vol. 14, pp. 30–38, 2017.

[56] L. Kornaszewski, N. Gayraud, J. M. Stone, W. N. MacPherson, A. K. George, J. C. Knight, D. P. Hand, and D. T. Reid, "Mid-infrared methane detection in a photonic bandgap fibre using a broadband optical parametric oscillator," *Opt. Express*, vol. 15, no. 18, pp. 11219–11224, 2007.

[57] F. Yang and W. Jin, "All-fibre hydrogen sensor based on stimulated Raman gain spectroscopy with a 1550-nm hollow-core fibre," vol. 10323, p. 103233C, 2017.

[58] R. Pennetta, S. Xie, F. Lenahan, M. Mridha, D. Novoa, and P. S. J. Russell, "Fresnel-Reflection-Free Self-Aligning Nanospike Interface between a Step-Index Fibre and a Hollow-Core Photonic-Crystal-Fibre Gas Cell," *Phys. Rev. Appl.*, vol. 8, no. 1, pp. 1–5, 2017.

[59] V. P. Minkovich, D. Monzón-Hernández, J. Villatoro, and G. Badenes, "Microstructured optical fibre coated with thin films for gas and chemical sensing," *Opt. Express*, vol. 14, no. 18, p. 8413, 2006.

[60] M. P. Buric, K. P. Chen, J. Falk, and S. D. Woodruff, "Enhanced spontaneous Raman scattering and gas composition analysis using a photonic crystal fibre," *Appl. Opt.*, vol. 47, no. 23, p. 4255, 2008.

[61] M. P. Buric, K. P. Chen, J. Falk, and S. D. Woodruff, "Improved sensitivity gas detection by spontaneous Raman scattering," *Appl. Opt.*, vol. 48, no. 22, p. 4424, 2009.

[62] X. Yang, L. Peng, L. Yuan, P. Teng, F. Tian, L. Li, and S. Luo, "Oxygen gas optrode based on microstructured polymer optical fibre segment," *Opt. Commun.*, vol. 284, no. 13, pp. 3462–3466, 2011.

[63] H. Ding, X. Li, J. Cui, S. Dong, and L. Yang, "An all-fibre gas sensing system using hollow-core photonic bandgap fibre as gas cell," *Instrum. Sci. Technol.*, vol. 39, no. 1, pp. 78–87, 2011.

[64] J. Henningsen, J. Hald, and J. C. Petersen, "Saturated absorption in acetylene and hydrogen cyanide in hollow-core photonic bandgap fibre," vol. 13, no. 26, pp. 10475–10482, 2005.

[65] T. Ritari, J. Tuominen, H. Ludvigsen, J. C. Petersen, T. Sorensen, T. P. Hansen, and H. R. Simonsen, "Gas sensing using air-guiding photonic bandgap fibres," *Opt. Express*, vol. 12, no. 17, p. 4080, 2004.

[66] B. K. Paul, E. Rajesh, S. Asaduzzaman, M. S. Islam, K. Ahmed, I. S. Amiri, and R. Zakaria, "Design and analysis of slotted core photonic crystal fibre for gas sensing application," *Results Phys.*, vol. 11, no. September, pp. 643–650, 2018.

[67] Y. Hao and L. Xiao, "Exposed antiresonant nodeless hollow core photonic crystal fibre for fast-response gas sensing," *ICOCN 2017 - 16th Int. Conf. Opt. Commun. Networks*, vol. 2017–Janua, pp. 1–3, 2017.

[68] J. K. Ranka, R. S. Windeler, and A. J. Stentz, "Optical properties of high-delta air–silica microstructure optical fibres," *Opt. Lett.*, vol. 25, no. 11, p. 796, 2000.

[69] S. Asaduzzaman, B. K. Paul, and K. Ahmed, "Enhancement of sensitivity and birefringence of a gas sensor on micro-core based photonic crystal fibre," *2016 3rd Int. Conf. Electr. Eng. Inf. Commun. Technol. iCEEiCT 2016*, pp. 8–11, 2017.

[70] H. Lehmann, J. Kobelke, K. Schuster, R. Willsch, H. Bartelt, P. Materials, C. Down, and U. Kingdom, "Gas sensing with suspended core fibres and hollow core band gap fibres - a comparative study," *Response*, vol. 7503, pp. 1–4, 2009.

[71] H. Liu, M. Wang, Q. Wang, H. Li, Y. Ding, and C. Zhu, "Simultaneous measurement of hydrogen and methane based on PCF-SPR structure with compound film-coated side-holes," *Opt. Fibre Technol.*, vol. 45, no. April, pp. 1–7, 2018.

[72] Z. Shao, X. Qiao, and Q. Rong, "Highly Sensitive Intensity-Interrogated Gas Refractometer Using Slotted Photonic Crystal Fibre," *IEEE Sens. J.*, vol. 18, no. 22, pp. 9263–9270, 2018.

[73] A. M. Shrivastav, G. Sharma, A. S. Rathore, and R. Jha, "Hypersensitive and Selective Interferometric Nose for Ultratrace Ammonia Detection with

Fast Response Utilizing PANI@SnO2 Nanocomposite," *ACS Photonics*, 2018.

[74] J. Mathew, Y. Semenova, and G. Farrell, "Photonic crystal fibre interferometer for dew detection," *J. Light. Technol.*, vol. 30, no. 8, pp. 1150–1155, 2012.

[75] M. Y. Mohd Noor, N. M. Kassim, A. S. M. Supaat, M. H. Ibrahim, A. I. Azmi, A. S. Abdullah, and G. D. Peng, "Temperature-insensitive photonic crystal fibre interferometer for relative humidity sensing without hygroscopic coating," *Meas. Sci. Technol.*, vol. 24, no. 10, 2013.

[76] T. Li, X. Dong, C. C. Chan, K. Ni, S. Zhang, and P. P. Shum, "Humidity sensor with a PVA-coated photonic crystal fibre interferometer," *IEEE Sens. J.*, vol. 13, no. 6, pp. 2214–2216, 2013.

[77] P. Wang, K. Ni, B. Wang, Q. Ma, and W. Tian, "A methylcellulose coated humidity sensor based on Mach-Zehnder interferometer with photonic crystal fibre," *ICOCN 2017 - 16th Int. Conf. Opt. Commun. Networks*, vol. 2017–Janua, pp. 16–18, 2017.

[78] S. Zhang, X. Dong, T. Li, C. C. Chan, and P. P. Shum, "Simultaneous measurement of relative humidity and temperature with PCF-MZI cascaded by fibre Bragg grating," *Opt. Commun.*, vol. 303, pp. 42–45, 2013.

[79] J. Mathew, Y. Semenova, and G. Farrell, "Experimental demonstration of a high-sensitivity humidity sensor based on an Agarose-coated transmission-type photonic crystal fibre interferometer," *Appl. Opt.*, vol. 52, no. 16, pp. 3884–3890, 2013.

[80] J. Mathew, Y. Semenova, and G. Farrell, "A high sensitivity humidity sensor based on an Agarose coated photonic crystal fibre interferometer," *OFS2012 22nd Int. Conf. Opt. Fibre Sensors*, vol. 8421, no. 842177, 2012.

[81] P. Zhang, H. Yang, K.-S. Lim, H. Ahmad, Q. Rong, Q. Tian, and X. Ding, "Temperature-independent hygrometry using micromachined photonic crystal fibre," *Appl. Opt.*, vol. 57, no. 15, p. 4237, 2018.

[82] R. Gao, Y. Jiang, and W. Ding, "Agarose gel filled temperature-insensitive photonic crystal fibres humidity sensor based on the tunable coupling ratio," *Sensors Actuators, B Chem.*, vol. 195, pp. 313–319, 2014.

[83] R. jie Tong, Y. Zhao, M. qing Chen, and Y. Peng, "Relative humidity sensor based on small up-tapered photonic crystal fibre Mach–Zehnder interferometer," *Sensors Actuators, A Phys.*, vol. 280, pp. 24–30, 2018.

[84] J. Mathew, Y. Semenova, and G. Farrell, "Effect of coating thickness on the sensitivity of a humidity sensor based on an Agarose coated photonic crystal fibre interferometer.," *Opt. Express*, vol. 21, no. 5, pp. 6313–20, Mar. 2013.

[85] S. S. Hindal and H. J. Taher, "Repeatability and Reversibility of the Humidity Sensor Based on Photonic Crystal Fibre Interferometer," *J. Phys. Conf. Ser.*, vol. 1003, no. 1, 2018.

[86] J. Mathew, Y. Semenova, G. Rajan, and G. Farrell, "Humidity sensor based on photonic crystal fibre interferometer," *Electron. Lett.*, vol. 46, no. 19, p. 1341, 2010.

[87] J. Mathew, Y. Semenova, and G. Farrell, "Relative Humidity Sensor Based on an Agarose-Infiltrated Photonic Crystal Fibre Interferometer," *IEEE J. Sel. Top. Quantum Electron.*, vol. 18, no. 5, pp. 1553–1559, Sep. 2012.

[88] J. Mathew, Y. Semenova, and G. Farrell, "Fibre optic hybrid device for simultaneous measurement of humidity and temperature," *IEEE Sens. J.*, vol. 13, no. 5, pp. 1632–1636, 2013.

[89] J. Villatoro, V. Finazzi, and V. Pruneri, "Functional photonic crystal fibre sensing devices," *Commun. Photonics Conf. Exhib. 2011. ACP. Asia*, vol. 8307, pp. 1–6, 2011.

[90] M. Y. M. Noor, G. Rajan, and G. D. Peng, "Microstructured fibre sealed-void interferometric humidity sensor," *IEEE Sens. J.*, vol. 14, no. 4, pp. 1154–1159, 2014.

[91] W. C. Wong, C. C. Chan, L. H. Chen, T. Li, K. X. Lee, and K. C. Leong, "Polyvinyl alcohol coated photonic crystal optical fibre sensor for humidity measurement," *Sensors Actuators, B Chem.*, vol. 174, pp. 563–569, 2012.

[92] W. C. Wong, C. C. Chan, T. Li, L. H. Chen, J. L. Boo, K. X. Lee, and K. C. Leong, "Miniature photonic crystal optical fibre humidity sensor based on polyvinyl alcohol," vol. 8421, p. 84216C–84216C–4, 2012.

[93] F. C. Favero, J. Villatoro, and V. Pruneri, "Microstructured optical fibre interferometric breathing sensor," *J. Biomed. Opt.*, vol. 17, no. 3, p. 037006, 2012.

[94] S. Zheng, Y. Zhu, and S. Krishnaswamy, "Nanofilm-coated photonic crystal fibre long-period gratings with modal transition for high chemical sensitivity and selectivity," *Smart Sens. Phenomena, Technol. Networks, Syst. Integr. Proc SPIE*, vol. 8346, 2012.

[95] S. Zheng, Y. Zhu, and S. Krishnaswamy, "Fibre humidity sensors with high sensitivity and selectivity based on interior nanofilm-coated photonic crystal fibre long-period gratings," *Sensors Actuators B Chem.*, vol. 176, pp. 264–274, 2013.

[96] H. Sun, X. Zhang, L. Yuan, L. Zhou, X. Qiao, and M. Hu, "An Optical Fibre Fabry-Perot Interferometer Sensor for Simultaneous Measurement of Relative Humidity and Temperature," *IEEE Sens. J.*, vol. 15, no. 5, pp. 2891–2897, 2015.

[97] X. Liu, M. Jiang, Q. Sui, and X. Geng, "Optical fibre Fabry–Perot relative humidity sensor based on HCPCF and chitosan film," *J. Mod. Opt.*, vol. 63, no. 17, pp. 1668–1674, 2016.

[98] Q. M. Sui, M. S. Jiang, Z. W. Jin, F. Y. Zhang, Y. Q. Cao, and L. Jia, "Optical Fibre Relative Humidity Sensor Based on Fabry-Perot Interferometer Coated with Sodium-p-styrenesulfonate/Allyamine Hydrochloride Films," *Sensors Mater.*, vol. 26, no. 5, pp. 291–298, 2014.

[99] Y. Zhao, R. jie Tong, M. qing Chen, and Y. Peng, "Relative humidity sensor based on Vernier effect with GQDs-PVA un-fully filled in hollow core fibre," *Sensors Actuators, A Phys.*, vol. 285, pp. 329–337, 2019.

[100] T. Li, C. L. Zhao, X. Dong, W. Qian, Y. Jin, and S. Jin, "Relative humidity sensor based on photonic crystal fibre with tapered and filled in polymer," *2010 Asia Commun. Photonics Conf. Exhib. ACP 2010*, pp. 288–289, 2010.

[101] C. Wang, G. Yan, Z. Lian, X. Chen, S. Wu, and S. He, "Hybrid-cavity fabry-perot interferometer for multi-point relative humidity and temperature sensing," *Sensors Actuators, B Chem.*, vol. 255, pp. 1937–1944, 2018.

[102] M. Y. Mohd Noor, N. Khalili, I. Skinner, and G. D. Peng, "Optical relative

humidity sensor based on a hollow core-photonic bandgap fibre," *Meas. Sci. Technol.*, vol. 23, no. 8, 2012.

[103] M. Y. M. Noor, N. Khalili, I. Skinner, and G. D. Peng, "Optical humidity sensor based on air guided photonic crystal fibre," *Photonic Sensors*, vol. 2, no. 3, pp. 277–282, 2012.

[104] J. Villatoro, M. P. Kreuzer, R. Jha, V. P. Minkovich, V. Finazzi, G. Badenes, and V. Pruneri, "High-sensitivity photonic crystal fibre interferometer for chemical vapors detection.," *Opt. Express*, vol. 17, no. 3, pp. 1447–53, 2009.

[105] J. Villatoro, M. P. Kreuzer, R. Jha, V. P. Minkovich, V. Finazzi, G. Badenes, and V. Pruneri, "Photonic crystal fibre interferometer for chemical vapor detection with high sensitivity," *Opt. Express*, vol. 17, no. 3, p. 1447, Jan. 2009.

[106] B. Kim, J.-C. Ahn, P.-S. Chung, and Y. Chung, "Microstructured optical fibre-based micro-cavity sensor for chemical detection," vol. 8938, p. 89380L, 2014.

[107] L. Niu, C.-L. Zhao, J. Kang, and M.-P. Ye, "Modal interferometer based on volatile organic compounds diffused in a simplified hollow-core photonic crystal fibre," vol. 9044, p. 904411, 2013.

[108] J. M. Kriesel, C. N. Makarem, M. C. Phillips, J. J. Moran, M. L. Coleman, L. E. Christensen, and J. F. Kelly, "Versatile, ultra-low sample volume gas analyzer using a rapid, broad-tuning ECQCL and a hollow fibre gas cell," vol. 10210, p. 1021003, 2017.

[109] C. Charlton, B. Temelkuran, G. Dellemann, and B. Mizaikoff, "Midinfrared sensors meet nanotechnology: Trace gas sensing with quantum cascade lasers inside photonic band-gap hollow waveguides," *Appl. Phys. Lett.*, vol. 86, no. 19, pp. 1–3, 2005.

[110] J. Ascorbe, J. M. Corres, F. J. Arregui, and I. R. Matias, "Recent developments in fibre optics humidity sensors," *Sensors (Switzerland)*, vol. 17, no. 4, pp. 1–23, 2017.

[111] I. S. Hwang, J. K. Choi, S. J. Kim, K. Y. Dong, J. H. Kwon, B. K. Ju, and J. H. Lee, "Enhanced H2S sensing characteristics of SnO2 nanowires functionalized with CuO," *Sensors Actuators, B Chem.*, vol. 142, no. 1, pp. 105–110, 2009.

[112] A. Kolmakov, D. O. Klenov, Y. Lilach, S. Stemmer, and M. Moskovitst, "Enhanced gas sensing by individual SnO 2 nanowires and nanobelts functionalized with Pd catalyst particles," *Nano Lett.*, vol. 5, no. 4, pp. 667–673, 2005.

[113] N. Cini, T. Tulun, G. Decher, and V. Ball, "Step-by-step assembly of self-patterning polyelectrolyte films violating (Almost) all rules of layer-by-layer deposition," *J. Am. Chem. Soc.*, vol. 132, no. 24, pp. 8264–8265, 2010.

LISTA DE ACRÓNIMOS

OFSs: Sensores de fibra óptica

RH: Humedad relativa

OFHS: Sensores de fibra óptica para detectar humedad

SMF: Fibra monomodo estándar

MMF: Fibra multimodo estándar

TIR: Reflexión total interna

PBG: Intervalo de banda fotónica

ADN: Ácido desoxirribonucleico

VOCs: Compuestos orgánicos volátiles

FFT: Transformada Rápida de Fourier

NEA: Ruido equivalente del coeficiente de absorción

ppm / ppb / ppt: Partes por millón/billón/trillón

ppmv: Partes por millón por volumen

FEM: Microscopio de efecto de campo

SPR: Resonancia de plasmón superficial

LMR: Resonancia de modo con pérdidas

LbL: Técnica de deposición bicapa a bicapa

PVA: Acetato de polivinilo

FBG: Fibras con rejilla de Bragg

LPG: Fibras con rejilla de largo periodo

GQDs: Puntos cuánticos de grafeno

SFDM: Multiplexación de división de frecuencia espacial